Contributions to the Continuum Modelling of Strong Discontinuities in Two-Dimensional Solids

E. Samaniego
X. Oliver
A. Huespe

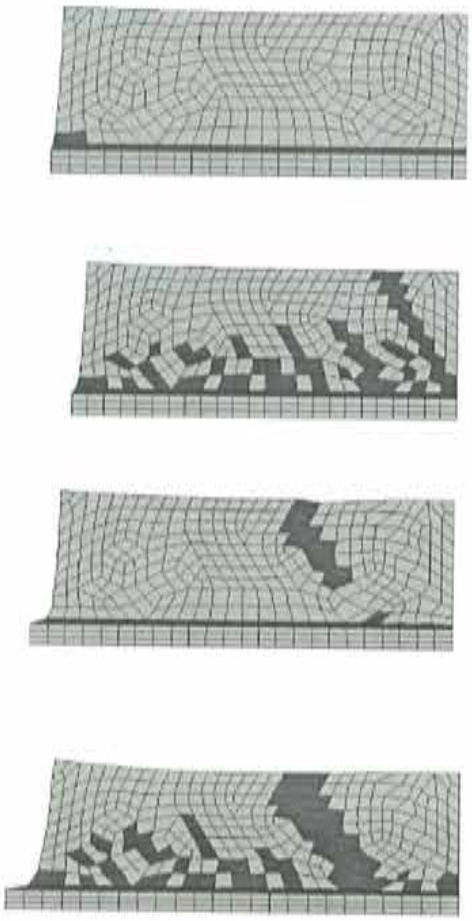

Monograph CIMNE Nº-72, March 2003

Contributions to the Continuum Modelling of Strong Discontinuities in Two-Dimensional Solids

E. Samaniego
X. Oliver
A. Huespe

Monograph CIMNE Nº-72, March 2003

INTERNATIONAL CENTER FOR NUMERICAL METHODS IN ENGINEERING
Gran Capitán s/n, 08034 Barcelona, Spain

INTERNACIONAL CENTER FOR NUMERICAL METHODS IN ENGINEERING
Edificio C1, Campus Norte UPC
Gran Capitán s/n
08034 Barcelona, Spain
www.cimne.upc.es

First edition: March 2003

CONTRIBUTIONS TO THE CONTINUUM MODELLING OF STRONG DISCONTINUITIES IN TWO-DIMENSIONAL SOLIDS
Monograph CIMNE M72

ISBN: 84-95999-20-X

Depósito legal: B-13720-2003

Contents

Figures

Chapter 1

Introduction

Computational Failure Mechanics has attracted increasing interest over the past years. However, there are still many aspects of this science that remain as open tasks. The study of the postcritical behavior of solids is by no means trivial and involves problems that range from finding an appropriate physical conception of the phenomenon to formulating correct and efficient mathematical and numerical models to describe it.

From the Continuum Mechanics point of view, failure is tightly related to *strain localization*, which can be defined as a material instability characterized by the presence of modes of intense deformation restricted to narrow regions in a solid. This general definition includes phenomena such as slip-lines in metals, shear bands in soils, and cracking in quasibrittle materials.

Perhaps, the most remarkable characteristic of localization is that it can occur without the presence of special boundary conditions (it can occur even in homogeneous fields). In light of this feature, strain localization, as a material phenomenon, is related to constitutive models with strain softening or with non-associative flow rules. From the mathematical point of view, when dealing with inviscid materials, the governing equations change of type when localization appears, rendering the Initial Boundary Value Problem (IBVP) ill-posed. The absence of an internal length scale leaves the width of the localization band undefined, which makes the mathematical description of the problem become meaningless. As a consequence, the corresponding numerical model may undergo pathological behavior if no precaution is taken. For instance, when a standard Finite Element formulation is used, a spurious strong dependence on the mesh size is observed. This manifold nature of strain localization has resulted in the appearance of a variety of approaches to study it.

The remaining of this chapter is organized as follows. Some approaches to Failure Mechanics are briefly reviewed in Section 1.1. In Section 1.2, the approach adopted

in this monograph is laid out. The objectives of this study are stated in Section 1.3. Section 1.4 gives an outline of the structure of this work.

1.1 Review of some approaches to failure mechanics

As said above, many ways of approaching the study of failure and strain localization have been proposed. A precise and exhaustive account of all of them goes beyond the scope of this monograph. However, here we try to classify them into general groups. The boundaries between these groups are not completely clear and they are likely to overlap each other.

1.1.1 Discrete Approaches.

These approaches are also known as *cohesive crack models*. For a deeper review of this type of models, the reader is referred to [Elices et al., 2002]. They were introduced in the early sixties by [Dugdale, 1960] and [Barenblatt, 1962]. The extension to the study of failure in concrete can be found in [Hillerborg et al., 1976]. The basic idea is to introduce a discontinuity interface governed by a traction-separation law within the solid when certain failure criterion is fulfilled. Discrete crack models have been related to the use of interface elements that allow the introduction of the discontinuity interface in Finite Element simulations (see, e.g., [Steinmann, 1999]). This entails that the placement of the discontinuity has to be known in advance or the necessity of using remeshing techniques in order to follow the discontinuity path, which can represent a major drawback from the computational cost point of view. However, the appearance of the so-called embedded elements ([Dvorkin et al., 1990],[Klisinski et al., 1991]), which introduce the discontinuity within the domain of an element, has been a crucial ingredient for the increasing popularity of cohesive crack models. More recently the use of enrichment based on the partition of unity concept (the resulting method has some times been termed Extended Finite Elements, X-Fem, [Belytschko et al., 2001]) has also been used in the context of discrete approaches ([Wells and Sluys, 2001]).

1.1.2 Approaches based on Classical Continuum

Classical Continuum Approaches to failure are based on the introduction of *strain softening* via the so-called *smeared crack models* ([Rashid, 1968]). In classical continuum, this leads to the above mentioned ill-posedness of the governing equations and the subsequent lack of objectivity of the corresponding spatial discretization.

To overcome these difficulties several strategies have been proposed. Among them, one can find approaches like the *crack band models* ([Bazant, 1983]). The idea here is to spread the energy release along the width of the localization band, so that it be objective. One way to do this is by using the Fracture Energy concept. The width of the band is computed in such a way that the dissipated energy is the correct one. This introduces a length parameter ([Oliver, 1989]) that depends on the size of the elements of the mesh used.

1.1.3 Enriched Continua

Enriched continua are based on introducing modifications to the classical continuum or on making use of more general continua in order to regularize the underlying governing equations. Usually they introduce a length scale, which determines the width of the localization band.

One example of a generalized continuum is the *Cosserat continuum*. It is part of the more general micro-polar theory and consists in augmenting the translational degrees of freedom by rotational degrees of freedom. It makes this approach specially suitable for the study of granular materials ([Vardoulakis, 1989]). However, the inclusion of additional degrees of freedom and the necessity of remeshing to improve the resolution of the localization band are important drawbacks that have diminished its use.

A way of enriching the continuum is by adding higher order spatial derivatives in quantities involved in the constitutive models ([de Borst and Mulhaus, 1992]). These strategies have some common features with the so-called *non-local* models ([Pjaudier-Cabot and Bazant, 1997]). For them, the stress at a given material point depends not only on the strain (and internal variables) at that point but also on the strain (and internal variables) in the neighborhood of that point or on some type of average strain (or average of some internal variable) of the neighborhood. This kind of approaches have a smoothing effect in the high displacement gradients that appear in the localization band. One of its drawbacks is the need of refinement to capture the behavior in the localization band properly.

Although the use of viscous regularization cannot be considered, in strict sense, as an enrichment of the Classical Continuum, we include it in this group of approaches due to some of its characteristics. An internal length scale is introduced and the governing equations remain well posed when localization appears. Besides, it can be interpreted as adding higher order time derivatives as pointed out in [Sluys, 1992]. Again remeshing is needed in the localization band.

1.1.4 Fundamental approaches

The microstructure (in the case of materials such as metals) or the mesostructure (in materials such as concrete) of the material is modelled in order to account for the micro(meso)mechanical changes that trigger the appearance of failure in solids. A very interesting approach is the one based on the so-called quasi-continuum method which bridges the continuum and the atomistic realms ([Knap and Ortiz, 2001]). This type of approaches are certainly appealing; however they are still in a developing phase that make them unaffordable in most of the cases.

1.2 Approach Adopted

The approach adopted in this work is the so-called *continuum strong discontinuity approach (CSDA)*. The CSDA remains within the general framework of classical continuum mechanics. It is based on the inclusion of jumps in the displacement field. Thus, the localization zone is modelled as having null width, i.e., as a surface in three dimensions or as a curve in two dimensions. This approach was first proposed in the pioneering work by [Simo et al., 1993]. Whereas classically strain localization had been treated as a *weak discontinuity*, i.e., as a discontinuity in the strain field, the use of strong discontinuities was justified by the results obtained in the context of functional analysis indicating that the proper space for classical inviscid plasticity was the so-called *space of bounded deformations (BD(Ω))* (see [Temam, 1983]). This space admits discontinuous solutions whose corresponding strains are bounded measures, which include Dirac delta (generalized) functions.

Though, as mentioned above, this approach remains within the realm of the classical continuum, its relationship with discrete approaches (or cohesive models) has been pointed out by [Oliver, 2000]. Cohesive traction-separation laws can be seen as "projections" of the original continuum stress-strain laws into the discontinuity interface.

Although the continuum strong discontinuity approach is, in principle, independent of the numerical model used, it has been tightly related to the use of Finite Elements with embedded discontinuities. In this work this kind of finite elements are adopted for the numerical simulation of strong discontinuities in solids.

1.3 Objectives

Based on the continuum strong discontinuity approach proposed in [Simo et al., 1993] and more deeply explained and developed in [Oliver, 1996a] and [Oliver, 1996b], the present study has the following as its objectives:

- To review the state of the art of the continuum strong discontinuity approach, aiming at contributing to its development for the simulation of complex problems.
- To compare and analyze the existing families of finite elements with embedded discontinuities within a general framework.
- To explore the possibility of devising a finite element with embedded discontinuities that captures the appearance of strong discontinuities in solids properly.
- To propose a strategy that allows to manage the propagation of several discontinuity interfaces in a solid.
- To improve the robustness of the algorithms currently used to simulate strong discontinuities in solids, so that complex problems, specially those involving multiple discontinuities, can be tackled.

These objectives are oriented to getting an efficient and robust computational tool that allows the simulation of complex problems in which strain localization appears. All this relying on a mathematical model consistent from the classical continuum mechanics point of view.

1.4 Outline

The remaining of this monograph will be organized as follows. In Chapter 2, a review of some fundamental concepts about the mathematical conditions for the appearance of strain localization is made. The relationship between strain localization and constitutive models with strain softening is explained. A representative isotropic continuum damage model is studied within the context of classical discontinuous bifurcation analysis. The methodology to obtain the conditions for the inception of a localization band in a solid and the propagation direction of the discontinuity are explained and applied to the above mentioned continuum damage model. Chapter 3 will be devoted to the theoretical aspects of the continuum strong discontinuity approach. The strong discontinuity kinematics will be introduced. The regularized version of that kinematics is presented in such a format that it can represent both weak and strong discontinuities. The so-called *strong discontinuity analysis* is explained and then applied to a representative isotropic continuum damage model. The formulation of finite elements with embedded discontinuities will be addressed in Chapter 4. A general framework based on the multi-field statement of the governing equations is presented. From that general

framework, the formulation of various finite elements with embedded discontinuities is tackled. The peculiarities of those formulations are analyzed. The locking effect observed in the so-called statically optimal symmetric element is studied and some remedies to this pathological behavior are proposed. The limitations of this type of elements are pointed out. Chapter 5 is devoted to studying some strategies to manage the simulation of the propagation of discontinuities when finite elements with embedded discontinuities are used. The concepts of "local" and "global" tracking algorithms are explained. Then a global tracking algorithm based on solving a heat-conduction-like boundary value problem is proposed. Its advantages in managing the propagation of multiple discontinuity paths are pointed out. Motivated by the complexity that the appearance of several discontinuity paths entails, Chapter 6 deals with some issues related with stability and uniqueness that can lead to the lack of robustness of the numerical model. An strategy based on adding an artificial regularizing damping is proposed. In Chapter 7, the concepts developed throughout this monograph are applied to the resolution of some numerical examples specially chosen due to its complexity. Finally, Chapter 8 presents the conclusions of this work and proposes some possible lines of future research.

Chapter 2

Strain localization

Failure in solids is related to the appearance of regions in which high gradients of the displacement field are observed. When these intense modes of deformation are concentrated in narrow bands, the solid is said to undergo *strain localization*. As mentioned in Chapter 1, it is a material instability related with constitutive models either equipped with strain softening or having non-associative flow rules. The material character of this type of instability becomes clear when one considers that, even in the presence of homogeneous stress states, the use of constitutive models including strain softening can lead to the appearance of strain localization. An illustrative one-dimensional example of this can be found in [Oliver et al., 1998].

The modelling of failure in solids requires information about the time at which a material point becomes part of a localization band and the direction in which that band evolves. In a context fully consistent with classical continuum mechanics, this information comes from the so called *discontinuous bifurcation analysis* ([Runesson et al., 1991]).

In this chapter, the mathematical conditions for the appearance of strain localization are studied within the framework of the discontinuous bifurcation analysis. The analysis is limited to infinitesimal strain and to rate independent materials and follows the guidelines of classical studies about strain localization for quasistatic problems such as the ones presented in [Rice and Rudnicki, 1980] and [Ottosen and Runesson, 1991].

In Section 2.1 the fundamentals of the discontinuous bifurcation analysis are laid out. Section 2.2 presents a representative continuum damage model. The discontinuous bifurcation analysis is applied to this model in section 2.3.

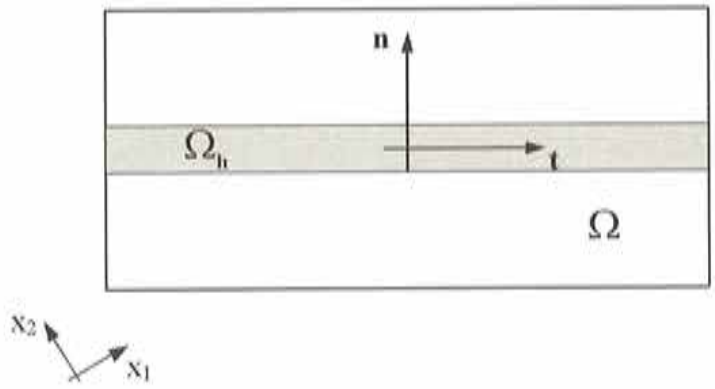

Figure 2.1: Continuum with a localization band.

2.1 Discontinuous bifurcation analysis

The problem of finding the conditions for the appearance of strain localization can be stated as follows:

Consider a homogeneous domain Ω undergoing uniform strains at a given time. Then, find the conditions under which the strain rate, $\dot{\boldsymbol{\varepsilon}}$, may become nonuniform, varying in a planar band $\Omega_h \subset \Omega$ bounded by two parallel planes (as shown in Fig. (2.1)), and remaining uniform outside that band.

To establish these conditions precisely, consider an orthonormal basis $\{\mathbf{n}, \mathbf{t}, \mathbf{p}\}$, where $\mathbf{n}$ is the normal to the middle plane of the band Ω_h, and $\mathbf{t}$ and $\mathbf{p}$ are two vectors lying on that plane. The directional derivatives of the velocity (displacement rate) field $\dot{\mathbf{u}}$ in the direction of $\mathbf{p}$ and $\mathbf{t}$ are assumed to be uniform, so we have that

$$[\![\partial_p \dot{\mathbf{u}}]\!]=[\![(\dot{\mathbf{u}} \otimes \boldsymbol{\nabla}) \cdot \mathbf{p}]\!]=[\![\dot{\mathbf{u}} \otimes \boldsymbol{\nabla}]\!]\cdot\mathbf{p} = 0 \tag{2.1}$$

$$[\![\partial_t \dot{\mathbf{u}}]\!]=[\![(\dot{\mathbf{u}} \otimes \boldsymbol{\nabla}) \cdot \mathbf{t}]\!]=[\![\dot{\mathbf{u}} \otimes \boldsymbol{\nabla}]\!]\cdot\mathbf{t} = 0 \tag{2.2}$$

where $[\![\bullet]\!]$ denotes the difference between the values of $(\bullet)$ in Ω_h and $\Omega \backslash \Omega_h$, $\partial_p(\bullet)$ and $\partial_t(\bullet)$ are the directional derivatives of $(\bullet)$ in the direction of $\mathbf{p}$ and $\mathbf{t}$, respectively. From (2.1) and (2.2) (see them as orthogonality conditions), it follows that

$$[\![\dot{\mathbf{u}} \otimes \boldsymbol{\nabla}]\!]= \boldsymbol{\beta} \otimes \mathbf{n}$$

where $\boldsymbol{\beta}$ is an arbitrary vector.

As a consequence the strain rate has to fulfill the following condition:

$$[\![\dot{\varepsilon}]\!]=[\![\nabla^s \dot{\mathbf{u}}]\!]=(\boldsymbol{\beta}\otimes\mathbf{n})^s \tag{2.3}$$

where $(\bullet)^s$ stands for the symmetric part of $(\bullet)$. Equation (2.3) is the so-called Maxwell's kinematical compatibility condition.

Besides this kinematical condition, equilibrium of the traction vector rate between Ω_h and $\Omega\backslash\Omega_h$ must hold[1]:

$$[\![\dot{T}]\!]=[\![\dot{\boldsymbol{\sigma}}\cdot\mathbf{n}]\!]=[\![\dot{\boldsymbol{\sigma}}]\!]\cdot\mathbf{n}=0 \tag{2.4}$$

Suppose that we are dealing with an incrementally linear material (which is the case of classical inviscid materials), then we can write the following incremental constitutive relation:

$$\dot{\boldsymbol{\sigma}}=\mathbf{C}^i:\dot{\varepsilon} \tag{2.5}$$

where $\mathbf{C}^i$ is the fourth order tangent constitutive tensor (also called incremental or tangent constitutive operator). Then two bifurcation scenarios, depending on the material behavior outside and inside the band, can be considered.

In the first scenario the tangent operator is the same inside the band as outside the band. From (2.5) and (2.3), we have that

$$[\![\dot{\boldsymbol{\sigma}}]\!]=\mathbf{C}^i:[\![\dot{\varepsilon}]\!]=\mathbf{C}^i:(\boldsymbol{\beta}\otimes\mathbf{n})^s \tag{2.6}$$

Substituting (2.6) into (2.4) and considering the symmetry of $\dot{\boldsymbol{\sigma}}$, we obtain

$$[\![\dot{\boldsymbol{\sigma}}]\!]\cdot\mathbf{n}=(\mathbf{n}\cdot\mathbf{C}^i\cdot\mathbf{n})\cdot\boldsymbol{\beta}=0$$

Knowing that $\mathbf{Q}(\mathbf{n})=\mathbf{n}\cdot\mathbf{C}^i\cdot\mathbf{n}$, which is the so called *Localization Tensor*, we have that

$$\mathbf{Q}(\mathbf{n})\cdot\boldsymbol{\beta}=0 \tag{2.7}$$

The trivial solution of (2.7), $\boldsymbol{\beta}=\mathbf{0}$, will entail $[\![\dot{\varepsilon}]\!]=0$. As a consequence, strain localization will take place only if $\mathbf{Q}$ is singular. Then, a necessary condition for strain localization to take place is that for some $\mathbf{n}$

[1]This condition will be studied more deeply in Chapters 3 and 4.

$$\det[\mathbf{Q}(\mathbf{n})] = 0 \tag{2.8}$$

An alternative scenario is the one in which the tangent operator inside the band is different from the tangent operator outside the band. Let $\dot{\bar{\varepsilon}}$ be the strain rate in $\Omega \backslash \Omega_h$, then we have that

$$\begin{aligned} [\![\dot{\boldsymbol{\sigma}}]\!] &= \mathbf{C}^i_{\Omega_h} : (\dot{\bar{\varepsilon}} + [\![\dot{\boldsymbol{\varepsilon}}]\!]) - \mathbf{C}^i_{\Omega \backslash \Omega_h} : \dot{\bar{\varepsilon}} \\ &= \mathbf{C}^i_{\Omega_h} : [\dot{\bar{\varepsilon}} + (\boldsymbol{\beta} \otimes \mathbf{n})^s] - \mathbf{C}^i_{\Omega \backslash \Omega_h} : \dot{\bar{\varepsilon}} \end{aligned} \tag{2.9}$$

where $\mathbf{C}^i_{\Omega_h}$ and $\mathbf{C}^i_{\Omega \backslash \Omega_h}$ are the tangent operator inside and outside the band, respectively. Replacing (2.9) in (2.4), we obtain

$$(\mathbf{n} \cdot \mathbf{C}^i_{\Omega_h} \cdot \mathbf{n}) \cdot \boldsymbol{\beta} + \mathbf{n} \cdot [\![\mathbf{C}^i]\!] : \dot{\bar{\varepsilon}} = 0$$

Defining $\mathbf{Q}_{\Omega_h} := (\mathbf{n} \cdot \mathbf{C}^i_{\Omega_h} \cdot \mathbf{n})$, we obtain

$$\mathbf{Q}_{\Omega_h} \cdot \boldsymbol{\beta} = -\mathbf{n} \cdot [\![\mathbf{C}^i]\!] : \dot{\bar{\varepsilon}}$$

Remark 1 *With regard to the two bifurcation scenarios studied, it is important to mention that in [Rice and Rudnicki, 1980] and [Ottosen and Runesson, 1991], it was pointed out that the case in which the tangent operator is the same inside and outside the band is a limit case (the most unfavorable) of the scenario with different tangent operators. So, according to this result, condition (2.7) is the critical one and bifurcation will be ruled by it.*

Remark 2 *As mentioned above, the results presented in this section are derived within the context of quasistatic problems. For the dynamical case, the appearance of strain localization has been analyzed in classical works such as [Hill, 1962]. There, the study of acceleration waves is used and localization corresponds to "stationary waves". The resulting condition for the appearance of strain localization is the singularity of the so called Acoustic Tensor, whose expression is the same as the one of the Localization Tensor. Moreover, this same condition coincides with the loss of strong ellipticity (see [Ogden, 1984] for a discussion on the concept of strong ellipticity) of the incremental constitutive relation.*

2.2 A representative continuum damage model

Continuum damage models are intended to describe the degradation of the mechanical properties of a solid prior to the formation of macrocracks[2]. Extensive information about Continuum Damage Mechanics can be found in [Lemaitre, 1996]. Here we will present an isotropic continuum damage model based on the ideas presented in [Oliver et al., 1990].

2.2.1 Ingredients of the model

The expression of the Helmholtz free energy density of the model is the following:

$$\psi(\boldsymbol{\varepsilon},r) = [1 - d(r)]\psi_0 \tag{2.10}$$

where $d \in [0,1]$ is the so-called *damage variable* (this variable determines the amount of loss of stiffness of the material point considered), r is a strain-like internal variable and ψ_0 is the elastic free energy, whose definition is

$$\psi_0(\boldsymbol{\varepsilon}) = \frac{1}{2}(\boldsymbol{\varepsilon} : \mathbf{C} : \boldsymbol{\varepsilon}) \tag{2.11}$$

where $\mathbf{C}$ is the elastic fourth order constitutive tensor, defined by $\mathbf{C} = \hat{\lambda}\mathbf{1} \otimes \mathbf{1} + 2\mu\mathbf{I}$, with $\mathbf{1}$ and $\mathbf{I}$ being the second and fourth order unit tensors, respectively, and $\hat{\lambda}$ and μ the Lamé parameters.

From the definition of the free energy made in (2.10), the following constitutive equation is derived:

$$\boldsymbol{\sigma} = \partial_{\boldsymbol{\varepsilon}}\psi(\boldsymbol{\varepsilon},r) = (1 - d)\mathbf{C} : \boldsymbol{\varepsilon} \tag{2.12}$$

The damage variable, d, is defined in terms of r:

$$d = 1 - \frac{q(r)}{r} \tag{2.13}$$

where q is a stress-like internal variable.

The internal variable r has the following evolution law:

[2]Later on in this thesis, we will see how a continuum constitutive model plus the inclusion of the so-called Strong Discontinuity Kinematics can be used for modelling macrocracks

$$\dot{r} = \lambda \tag{2.14}$$

with $r \in [r_0, \infty)$ and $r_0 \equiv r|_{t=0} = \sigma_u/\sqrt{E}$ (σ_u is the peak stress and E is the Young modulus).

The damage function (in stress space) used is

$$f(\boldsymbol{\sigma}, q) := \tau_\sigma - q \tag{2.15}$$

where $\tau_\sigma = \|\boldsymbol{\sigma}\|_{\mathbf{C}^{-1}} = \sqrt{\boldsymbol{\sigma} : \mathbf{C}^{-1} : \boldsymbol{\sigma}}$. The symbol $\|\bullet\|_{\mathbf{C}^{-1}}$ denotes the norm of $(\bullet)$ in the Riemannian metric defined by $\mathbf{C}^{-1}$. This metric is such that the damage surface

$$\partial \mathbf{E}_\sigma := \{\boldsymbol{\sigma} \mid f(\boldsymbol{\sigma}, q) := \tau_\sigma - q = 0\} \tag{2.16}$$

is an ellipsoid in the principal stress space.

To these ingredients one must add the loading/unloading conditions:

$$f \leq 0; \quad \lambda \geq 0; \quad \lambda f = 0 \tag{2.17}$$

and the consistency condition:

$$\lambda \dot{f} = 0 \tag{2.18}$$

Schematically the behavior of this model regarding loading and unloading is the following:

$$\begin{cases} f < 0 \implies \lambda = 0 \implies \dot{r} = 0 \quad \text{(damage does not evolve)} \\ f = 0 \begin{cases} \dot{f} < 0 \implies \lambda = 0 \implies \dot{r} = 0 \quad \text{(unloading)} \\ \dot{f} = 0 \implies \begin{cases} \lambda = 0 \implies \dot{r} = 0 \quad \text{(neutral loading)} \\ \lambda > 0 \implies \dot{r} > 0 \quad \text{(loading)} \end{cases} \end{cases} \end{cases} \tag{2.19}$$

Only the definition of q remains to be made. It will depend on the type of hardening/softening rule used. Here we write the incremental expression of it:

$$\dot{q} = \mathcal{H}(r)\dot{r} \tag{2.20}$$

where $\mathcal{H}$ is the hardening/softening incremental parameter. In addition $q_0 \equiv q|_{t=0} = r_0$.

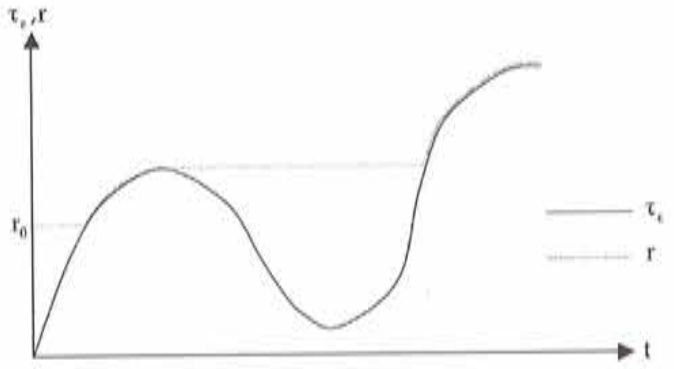

Figure 2.2: Integration of the damage internal variable in time.

2.2.2 Time integration of the evolution law

One of the most interesting features of this model is that (2.14) can be integrated in (pseudo)time in closed form. Here we find the resulting expression.

Let us define

$$\tau_\varepsilon = \|\varepsilon\|_{\mathbf{C}} = \sqrt{\varepsilon : \mathbf{C} : \varepsilon} \tag{2.21}$$

It can be easily proven that

$$\tau_\sigma = (1-d)\tau_\varepsilon \tag{2.22}$$

Then, it follows that

$$f(\sigma,q) := \tau_\sigma - q = 0 \Leftrightarrow f_r(\varepsilon,r) := \tau_\varepsilon - r = 0 \tag{2.23}$$

Thus the damage criterion can be posed in strain space [Simo and Ju, 1987], obtaining, as in the stress space formulation, a damage surface with the form of an ellipsoid in the principal strain space.

Consider the case of inelastic loading, then $\lambda = \dot{r} > 0$. Therefore, in light of (2.17), $f = 0$ and $r = \tau_\varepsilon$. Now, notice that, from (2.17) and (2.18), r grows in loading and does not change in unloading, but never decreases. Thus, the expression, in closed form, for r at a given (pseudo)time is

$$r(l) \equiv r_l = \max_{s\in[0,l]} \{r_0, \tau_\varepsilon(s)\} \tag{2.24}$$

Since the hardening/softening law is supposed to be given, then the whole constitutive model can be solved in closed form. A schematic picture of the evolution of r along time can be seen in Fig. 2.2.

2.2.3 Incremental constitutive relation

For the discontinuous bifurcation analysis that will be performed in the next section, it is important to have the expression of the incremental constitutive law. In the elastic regime this relation is

$$\dot{\boldsymbol{\sigma}} = \mathbf{C} : \dot{\boldsymbol{\varepsilon}}$$

$\mathbf{C}$ being the elastic fourth order constitutive tensor; whereas in damage regime

$$\dot{\boldsymbol{\sigma}} = \mathbf{C}^d : \dot{\boldsymbol{\varepsilon}} \tag{2.25}$$

where

$$\mathbf{C}^d = (1-d)\mathbf{C} - \frac{q - \mathcal{H}r}{q^2 r}\boldsymbol{\sigma} \otimes \boldsymbol{\sigma} \tag{2.26}$$

is the damage tangent operator.

2.3 Discontinuous bifurcation in continuum damage

In this section, the discontinuous bifurcation analysis is applied to the above continuum damage model. First, the general three-dimensional problem is tackled. Then the analysis is restricted to plane strain and plane stress.

2.3.1 The general 3-D problem

As stated in (2.7), a necessary condition for the appearance of localization is the singularity of the Localization tensor, regarded as a function of the unit normal to the surface of localization, $\mathbf{n}$, and of the hardening/softening parameter, $\mathcal{H}$. That is to say,

$$\det[\mathbf{Q}(\mathcal{H}, \mathbf{n})] = 0 \tag{2.27}$$

After defining the so-called effective stress $\bar{\boldsymbol{\sigma}} = \mathbf{C} : \boldsymbol{\varepsilon}$, and using (2.12) and (2.13), we can rewrite (2.26):

$$\mathbf{C}^d = \frac{q}{r}\mathbf{C} - \frac{q - \mathcal{H}r}{r^3}\bar{\boldsymbol{\sigma}} \otimes \bar{\boldsymbol{\sigma}} \tag{2.28}$$

Hence,

$$\mathbf{Q}^d = \frac{q}{r}(\mathbf{n} \cdot \mathbf{C} \cdot \mathbf{n}) - \frac{q - \mathcal{H}r}{r^3}(\mathbf{n} \cdot \bar{\boldsymbol{\sigma}} \otimes \bar{\boldsymbol{\sigma}} \cdot \mathbf{n}) \tag{2.29}$$

where $\mathbf{Q}^d$ is the Localization Tensor for damage. Let us now define the elastic acoustic-like tensor as $\mathbf{Q}^e = \mathbf{n} \cdot \mathbf{C} \cdot \mathbf{n}$ and the "effective" traction vector as $\bar{T}(\mathbf{n}) = \bar{\boldsymbol{\sigma}} \cdot \mathbf{n}$. So we have that

$$\mathbf{Q}^d = \frac{q}{r}\mathbf{Q}^e - \frac{q - \mathcal{H}r}{r^3}(\bar{T} \otimes \bar{T}) \tag{2.30}$$

Then, considering the symmetry of $\mathbf{Q}^e$, we arrive to the following expression of the localization tensor:

$$\mathbf{Q}^d = \frac{q}{r}\mathbf{Q}^e \cdot \left\{ \mathbf{1} - \frac{q - \mathcal{H}r}{qr^2}\left[\bar{T} \cdot (\mathbf{Q}^e)^{-1}\right] \otimes \bar{T} \right\}$$

Hence,

$$\det(\mathbf{Q}^d) = \frac{q}{r}\det(\mathbf{Q}^e)\det\left\{ \mathbf{1} - \frac{q - \mathcal{H}r}{qr^2}\left[\bar{T} \cdot (\mathbf{Q}^e)^{-1}\right] \otimes \bar{T} \right\} \tag{2.31}$$

Since we know that r, q, and $\det(\mathbf{Q}^e)$ are always positive, the condition (2.27) reduces to

$$\det\left\{ \mathbf{1} - \frac{q - \mathcal{H}r}{qr^2}\left[\bar{T} \cdot (\mathbf{Q}^e)^{-1}\right] \otimes \bar{T} \right\} = 0 \tag{2.32}$$

Which yields[3]

[3]The following identities are to be used:
1) $\det(\mathbf{A} \cdot \mathbf{B}) = \det(\mathbf{A})\det(\mathbf{B})$; $\mathbf{A}$ and $\mathbf{B}$ being two arbitrary second order tensors.
2) $\det(\mathbf{1} - \mathbf{a} \otimes \mathbf{b}) = 1 - \mathbf{a} \cdot \mathbf{b}$; $\mathbf{a}$ and $\mathbf{b}$ being two arbitrary vectors.

$$1 - \frac{q - \mathcal{H}r}{qr^2}\left[\underbrace{\bar{\mathcal{T}} \cdot (\mathbf{Q}^e)^{-1} \cdot \bar{\mathcal{T}}}_{\tau_{\mathcal{T}}^2}\right] = 0 \tag{2.33}$$

where $\tau_{\mathcal{T}} := \left\|\bar{\mathcal{T}}\right\|_{(\mathbf{Q}^e)^{-1}} = \sqrt{\bar{\mathcal{T}} \cdot (\mathbf{Q}^e)^{-1} \cdot \bar{\mathcal{T}}}$.

Based on (2.33), we arrive to an expression for the values of the softening parameter, $\mathcal{H}$, for which the bifurcation condition (2.27) would be satisfied for a given stress state in terms of arbitrary values of the unit normal, $\hat{\mathbf{n}}$:

$$\check{\mathcal{H}}(\hat{\mathbf{n}}) = \frac{q}{r}\left[1 - \frac{r^2}{\tau_{\mathcal{T}}^2(\hat{\mathbf{n}})}\right] \tag{2.34}$$

2.3.2 Determination of the critical values of $\mathcal{H}$ and $\mathbf{n}$

Now, let us define $\mathbb{G}$ as the set of values $\check{\mathcal{H}}(\hat{\mathbf{n}})$ obtained from (2.34) for all the possible $\hat{\mathbf{n}}$ at a given time and at a given material point of a solid. Formally,

$$\mathbb{G} := \left\{\check{\mathcal{H}}(\hat{\mathbf{n}}) \in \mathbb{R} \mid \exists \hat{\mathbf{n}} \in \mathbb{R}^{n_{\text{dim}}}, \|\hat{\mathbf{n}}\| = 1, \check{\mathcal{H}} = \frac{q}{r}\left[1 - \frac{r^2}{\left[\tau_{\mathcal{T}}(\hat{\mathbf{n}})\right]^2}\right]\right\} \tag{2.35}$$

where n_{dim} is the number of dimensions of the problem and $\|\bullet\|$ is the Euclidean norm of $(\bullet)$.

Therefore, the problem of finding the critical value of the softening parameter $\mathcal{H}$ at a given time and at a given material point can be stated as a maximization problem:

$$\mathcal{H}^{crit} = \max_{\check{\mathcal{H}}(\hat{\mathbf{n}}) \in \mathbb{G}} \check{\mathcal{H}}(\hat{\mathbf{n}}) \tag{2.36}$$

The corresponding critical value of $\mathbf{n}$ has the following definition

$$\mathbf{n}^{crit} := \hat{\mathbf{n}} \text{ such that } \check{\mathcal{H}}(\hat{\mathbf{n}}) = \mathcal{H}^{crit} \tag{2.37}$$

Hence, the bifurcation time, t_b, for a material point, $\mathbf{x}$, can be defined as the time at which the hardening/softening parameter $\mathcal{H}$ equals $\mathcal{H}^{crit}$, i.e.,

$$t_b := t \in \mathbb{R}_+ \text{ such that } \mathcal{H}(t) = \mathcal{H}^{crit} \tag{2.38}$$

Remark 3 *The determination of $\mathcal{H}^{crit}$ and $\mathbf{n}^{crit}$ is crucial for the inception and propagation of a localization band. In Chapter 5 the importance of this information in the context of tracking algorithms for managing crack propagation is remarked.*

2.3.3 Two-dimensional settings

Explicit expressions for $\mathcal{H}^{crit}$ and $\mathbf{n}^{crit}$ in the context of plane stress and plane stress are derived here.

Plane Strain

For the analysis the vectors and tensors involved are expressed in the orthonormal basis $\{\mathbf{n},\mathbf{t},\mathbf{p}\}$, where $\mathbf{n}$ is the unit normal to the localization line, $\mathbf{t}$ is the tangent to that localization line, and $\mathbf{p}$ is the normal to the plane in which the localization line lies. Then we have that

$$[\mathbf{n}] = \left\{ \begin{array}{c} 1 \\ 0 \\ 0 \end{array} \right\}; \quad [\boldsymbol{\varepsilon}] = \left[\begin{array}{ccc} \varepsilon_{nn} & \varepsilon_{nt} & 0 \\ \varepsilon_{nt} & \varepsilon_{tt} & 0 \\ 0 & 0 & 0 \end{array} \right]; \qquad [\bar{\boldsymbol{\sigma}}] = \left[\begin{array}{ccc} \bar{\sigma}_{nn} & \bar{\sigma}_{nt} & 0 \\ \bar{\sigma}_{nt} & \bar{\sigma}_{tt} & 0 \\ 0 & 0 & \bar{\sigma}_{pp} \end{array} \right] \tag{2.39}$$

Thus, the expression of $\mathbf{Q}^e = (\hat{\lambda} + \mu)\mathbf{n} \otimes \mathbf{n} + \mu\mathbf{1}$ in this basis is

$$[\mathbf{Q}^e] = \left[\begin{array}{ccc} \hat{\lambda} + 2\mu & 0 & 0 \\ 0 & \mu & 0 \\ 0 & 0 & \mu \end{array} \right] \tag{2.40}$$

Hence,

$$[(\mathbf{Q}^e)^{-1}] = \left[\begin{array}{ccc} 1/(\hat{\lambda} + 2\mu) & 0 & 0 \\ 0 & 1/\mu & 0 \\ 0 & 0 & 1/\mu \end{array} \right] \tag{2.41}$$

and the expression of the effective traction vector is

$$[\bar{T}] = \left\{ \begin{array}{c} \bar{\sigma}_{nn} \\ \bar{\sigma}_{nt} \\ 0 \end{array} \right\} \tag{2.42}$$

Hence,

$$\tau_T^2 = \bar{T} \cdot (\mathbf{Q}^e)^{-1} \cdot \bar{T} = \frac{1}{\hat{\lambda} + 2\mu} \bar{\sigma}_{nn}^2 + \frac{1}{\mu} \bar{\sigma}_{nt}^2 \tag{2.43}$$

Considering the definition of effective stress, $\bar{\boldsymbol{\sigma}} = \mathbf{C} : \boldsymbol{\varepsilon}$, the definition of the norm τ_ε (2.21), and that, in loading, $r = \tau_\varepsilon$, we can write

$$r^2 = \bar{\boldsymbol{\sigma}} : \mathbf{C}^{-1} : \bar{\boldsymbol{\sigma}} \tag{2.44}$$

with

$$\mathbf{C}^{-1} = -\frac{\hat{\lambda}}{2\mu(3\hat{\lambda} + 2\mu)} \mathbf{1} \otimes \mathbf{1} + \frac{1}{2\mu} \mathbf{I} \tag{2.45}$$

Hence,

$$r^2 = -\frac{\hat{\lambda}}{2\mu(3\hat{\lambda} + 2\mu)} Tr^2(\bar{\boldsymbol{\sigma}}) + \frac{1}{2\mu} \|\bar{\boldsymbol{\sigma}}\|^2 \tag{2.46}$$

where $Tr(\bullet)$ denotes the trace of $(\bullet)$.

Equations (2.43) and (2.46) can be rephrased using, as the elastic material parameters, the Young modulus and the Poisson's ratio as follows:

$$\tau_T^2 = -\frac{(1+\nu)(1-2\nu)}{(1-\nu)E} \bar{\sigma}_{nn}^2 + \frac{2(1+\nu)}{E} \bar{\sigma}_{nt}^2 \tag{2.47}$$

$$r^2 = -\frac{\nu}{E} (\bar{\sigma}_{nn} + \bar{\sigma}_{tt} + \bar{\sigma}_{pp})^2 + \frac{(1+\nu)}{E} (\bar{\sigma}_{nn}^2 + \bar{\sigma}_{tt}^2 + \bar{\sigma}_{pp}^2 + 2\bar{\sigma}_{nt}^2) \tag{2.48}$$

Then it can be proven that the following identity holds:

$$r^2 - \tau_T^2 = \frac{E}{1-\nu^2} \varepsilon_{tt}^2 \tag{2.49}$$

Let us now consider the orthonormal basis $\{\hat{\mathbf{e}}_1, \hat{\mathbf{e}}_2, \mathbf{p}\}$, coinciding with the principal strains directions. Vector $\hat{\mathbf{e}}_1$ corresponds to the direction of the maximum principal strain. Let θ be the angle of $\mathbf{n}$ with respect to $\hat{\mathbf{e}}_1$, such that $\mathbf{n} = \cos\theta \hat{\mathbf{e}}_1 + \sin\theta \hat{\mathbf{e}}_2$. Then ε_{tt} can be expressed as follows:

$$\varepsilon_{tt}(\theta) = (\varepsilon_1 - \varepsilon_2)\sin^2\theta + \varepsilon_2 \tag{2.50}$$

where ε_1 and ε_2 are the principal strains, with $\varepsilon_1 \geq \varepsilon_2$

Considering the fact that for two-dimensional cases the normal $\mathbf{n}$ is defined by θ, problem (2.36) can be stated as follows:

$$\mathcal{H}^{crit} = \max_{\theta\in[-\pi,\pi]} \tilde{\mathcal{H}}(\theta) \tag{2.51}$$

with

$$\tilde{\mathcal{H}}(\theta) = \frac{q}{r}\left[1 - \frac{r^2}{r^2 - \frac{E}{1-\nu^2}\varepsilon_{tt}^2(\theta)}\right] \tag{2.52}$$

where identity (2.49) and (2.34) have been used.

In light of (2.52), it follows that (2.51) reduces to minimizing ε_{tt}^2 for $\theta \in [-\pi, \pi]$.

The condition for an optimal point is

$$\frac{\partial(\varepsilon_{tt}^2)}{\partial(\sin^2\theta)} = 2[(\varepsilon_1 - \varepsilon_2)\sin^2\theta + \varepsilon_2](\varepsilon_1 - \varepsilon_2) = 0 \tag{2.53}$$

which yields

$$\sin^2\theta = -\frac{\varepsilon_2}{(\varepsilon_1 - \varepsilon_2)} \tag{2.54}$$

Considering that

$$\frac{\partial^2(\varepsilon_{tt}^2)}{\partial(\sin^2\theta)^2} = 2(\varepsilon_1 - \varepsilon_2)^2 \geq 0 \tag{2.55}$$

then, condition (2.53) gives us a minimum. Since, $\sin^2\theta \in [0, 1]$, we have

$$\sin^2\theta^{crit} = \begin{cases} -\frac{\varepsilon_2}{(\varepsilon_1-\varepsilon_2)} & \text{if } 0 \leq -\frac{\varepsilon_2}{(\varepsilon_1-\varepsilon_2)} \leq 1 \\ 1 & \text{if } -\frac{\varepsilon_2}{(\varepsilon_1-\varepsilon_2)} > 1 \\ 0 & \text{if } -\frac{\varepsilon_2}{(\varepsilon_1-\varepsilon_2)} < 0 \end{cases} \tag{2.56}$$

By replacing θ^{crit}, obtained by (2.56), in (2.50) and then in (2.52), we obtain $\mathcal{H}^{crit}$.

Plane stress

For the plane stress analysis, the components of the vectors and tensors corresponding to the direction outside the plane are not involved. Thus, we can make use of basis $\{\mathbf{n},\mathbf{t}\}$, where $\mathbf{n}$ is the unit normal to the localization line and $\mathbf{t}$ is the tangent to that localization line. Then we have

$$[\mathbf{n}] = \left\{ \begin{array}{c} 1 \\ 0 \end{array} \right\}; \quad [\bar{\boldsymbol{\sigma}}] = \left[\begin{array}{cc} \bar{\sigma}_{nn} & \bar{\sigma}_{nt} \\ \bar{\sigma}_{nt} & \bar{\sigma}_{tt} \end{array} \right] \tag{2.57}$$

Considering that, for plane stress, the expression of the elastic tensor is

$$\mathbf{C} = \frac{E}{1-\nu^2}\left[\nu \mathbf{1} \otimes \mathbf{1} + (1-\nu)\mathbf{I}\right] \tag{2.58}$$

we obtain

$$\mathbf{Q}^e = \frac{E}{1-\nu^2}\left[\frac{(1+\nu)}{2}\mathbf{n} \otimes \mathbf{n} + \frac{(1-\nu)}{2}\mathbf{1}\right] \tag{2.59}$$

Hence,

$$[(\mathbf{Q}^e)^{-1}] = \frac{1-\nu^2}{E}\left[\begin{array}{cc} 1 & 0 \\ 0 & \frac{2}{(1-\nu)} \end{array} \right] \tag{2.60}$$

The expression of the effective traction vector is

$$[\bar{T}] = \left\{ \begin{array}{c} \bar{\sigma}_{nn} \\ \bar{\sigma}_{nt} \end{array} \right\} \tag{2.61}$$

Thus,

$$\tau_{\bar{T}}^2 = \frac{1-\nu^2}{E}\bar{\sigma}_{nn}^2 + \frac{2(1+\nu)}{E}\bar{\sigma}_{nt}^2 \tag{2.62}$$

From (2.46), we have

$$r^2 = -\frac{\nu}{E}(\bar{\sigma}_{nn} + \bar{\sigma}_{tt})^2 + \frac{(1+\nu)}{E}(\bar{\sigma}_{nn}^2 + \bar{\sigma}_{tt}^2 + 2\bar{\sigma}_{nt}^2) \tag{2.63}$$

By using (2.62) and (2.63), after some algebra, we obtain the following identity:

$$r^2 - r_T^2 = E\varepsilon_{tt}^2 \tag{2.64}$$

Analogously to the plain strain case, let us consider the orthonormal basis $\{\hat{\mathbf{e}}_1, \hat{\mathbf{e}}_2\}$ with $\hat{\mathbf{e}}_1$ and $\hat{\mathbf{e}}_2$ corresponding to the principal strains directions. Vector $\hat{\mathbf{e}}_1$ corresponds to the direction of the maximum principal strain. Let θ be the angle of $\mathbf{n}$ with respect to $\hat{\mathbf{e}}_1$, such that $\mathbf{n} = \cos\theta\hat{\mathbf{e}}_1 + \sin\theta\hat{\mathbf{e}}_2$. Then we can write:

$$\varepsilon_{tt}(\theta) = (\varepsilon_1 - \varepsilon_2)\sin^2\theta + \varepsilon_2 \tag{2.65}$$

where ε_1 and ε_2 are the principal strains, with $\varepsilon_1 \geq \varepsilon_2$

Considering again that for two-dimensional cases the normal $\mathbf{n}$ is defined by θ, problem (2.36) can be stated as written in (2.51), with

$$\check{\mathcal{H}}(\theta) = \frac{q}{r}\left[1 - \frac{r^2}{r^2 - E\varepsilon_{tt}^2(\theta)}\right] \tag{2.66}$$

where identity (2.64) and (2.34) have been used.

Problem (2.51) reduces, as in the plain strain case, to minimizing ε_{tt}^2 for $\theta \in [-\pi, \pi]$. Hence, the value of θ^{crit} can be computed using the same expressions as in plane strain.

Remark 4 *Notice that, in both (2.52) and (2.66), $\check{\mathcal{H}}(\theta)$ can only take negative values, which implies that bifurcation cannot take place in hardening.*

Chapter 3

The continuum strong discontinuity approach

In Chapter 2, the study of strain localization was tackled. It was based on determining the necessary conditions for the appearance of a band in which the strain field becomes discontinuous. These discontinuities in the strain field are termed *weak discontinuities*. Their use has been classical in modelling strain localization. However, due to the absence of an internal length scale, the width of the localization band remains undetermined in the classical continuum context. In light of this, the limiting case in which the band of localization collapses into a surface of zero thickness emerges as a natural option. Then, the displacement field is discontinuous across this surface. This new type of discontinuities are referred to as *strong discontinuities*.

In the pioneering work by [Simo et al., 1993], the issue of modelling strain localization by means of strong discontinuities was dealt with. The space of bounded deformations $BD(\Omega)$ (see [Temam, 1983]), developed in the context of classical perfect plasticity, was adopted as the appropriate functional framework. Thus, the displacement field may be discontinuous and the corresponding strains are bounded measures, which include the Dirac delta. However, the stresses were assumed to be regular, which led to the necessity of reinterpreting the softening parameter in a distributional sense. A very interesting consequence of this interpretation is that dissipation can occur in a region of (Lebesgue) measure zero. The dissipation taking place in the discontinuity surface can then be related to the concept of fracture energy (which is energy per unit area) in a straightforward manner. Thus the spurious dependence of the energy released with respect to the width of the localization band is overcome (see [Oliver et al., 1998]).

The regularized version of the strong discontinuity kinematics was taken advantage of in [Oliver et al., 1997] to propose a transition between the weak and strong

discontinuity regimes. The issue of the conditions that must be fulfilled to allow the inclusion of strong discontinuities was analyzed. Later, in [Oliver, 2000], the same framework was used in order to show how the discrete (cohesive) constitutive models can be regarded as "projections" onto the discontinuity surface of continuum constitutive models when the strong discontinuity kinematics is adopted. The extension of the so-called *Strong Discontinuity Analysis* to large deformation settings has been tackled in [Oliver et al., 2002b]. Important contributions to the modelling of strong discontinuities in finite strain settings can be found in [Armero and Garikipati, 1996] and [Larsson et al., 1999], among others.

Throughout this chapter, the use of strong discontinuities and its implications are explored within the context of continuous constitutive modelling. However, modelling strong discontinuities in solids can be tackled from other standpoints. In [Oliver et al., 2002b] a classification of the possible ways of undertaking this task was presented and three main groups were identified:

Discrete approaches (e.g. [Alfaiate et al., 2002]): the adoption and introduction of the discrete constitutive model at the interface is done without resorting to the continuum one. Their connection with the strong discontinuity kinematics is limited to numerical aspects, mainly to the use of some kind of enriched elements to capture discontinuities.

Discrete-continuum approaches (e.g. [Steinmann, 1999]): the discrete model is derived from a continuum one and then introduced in the discontinuity interface regardless the fulfillment of the necessary conditions for the inception of a strong discontinuity[1].

Continuum approaches: the discrete constitutive model is fully consistent with the continuum one. In fact, the former does not need to be explicitly introduced, but it is induced from the adoption of the latter.

The last approach is the one adopted in this study and will be called, from now on, *Continuum Strong Discontinuity Approach (CSDA)*.

The governing equations of the boundary value problem are stated in Section 3.1. Section 3.2 is devoted to presenting the kinematics of discontinuous media. First the strong discontinuity kinematics is presented. Later the weak discontinuity kinematics is laid out. Then the regularized version of the strong discontinuity kinematics is presented as a limit case of the weak discontinuity kinematics when the width of the discontinuity band tends to zero. In Section 3.3 the implications of the adoption of the strong discontinuity kinematics in continuum constitutive models are studied. Finally, in Section 3.4 a relationship between the strong discontinuity approach and the concept of fracture energy is established.

[1]These are the so-called strong discontinuity conditions (see [Oliver et al., 1997])

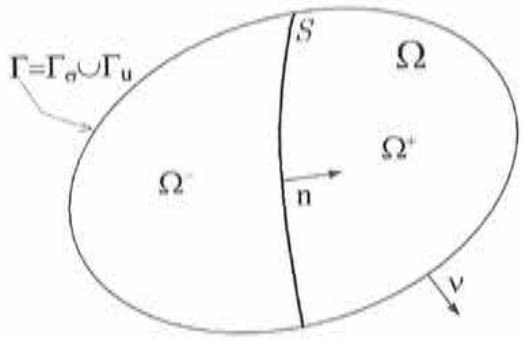

Figure 3.1: Solid with an internal boundary.

3.1 The Boundary Value Problem

Consider the open domain Ω, with elements $\mathbf{x}$ (called material points), whose boundary is Γ (see Fig. 3.1). The boundary is composed of the open sets Γ_u and Γ_σ such that $\Gamma_u \cap \Gamma_\sigma = \emptyset$ and $\overline{\Gamma_u \cup \Gamma_\sigma} = \Gamma$. The prescribed rate of displacements, $\dot{\mathbf{u}}$, is imposed on Γ_u, whereas the prescribed rate of tractions is imposed on Γ_σ. Consider, also, the internal boundary $\mathcal{S}$[2], which partitions Ω into Ω^+ and Ω^- (see Fig. 3.1). Then, the equilibrium equations[3] and boundary conditions in rates format are

$$\begin{array}{lll} \nabla \cdot \dot{\boldsymbol{\sigma}} + \dot{\mathbf{b}} = 0 & \text{in } \Omega \backslash \mathcal{S} & \text{(equilibrium equation)} \\ \dot{\boldsymbol{\sigma}}_{\mathcal{S}} \cdot \mathbf{n} = \dot{\boldsymbol{\sigma}}_{\Omega \backslash \mathcal{S}} \cdot \mathbf{n} & \text{on } \mathcal{S} & \text{(inner traction continuity)} \end{array}$$

$$\left\{ \begin{array}{ll} \dot{\mathbf{u}} = \dot{\mathbf{u}}^* & \text{on } \Gamma_u \\ \dot{\boldsymbol{\sigma}} \cdot \boldsymbol{\nu} = \dot{\mathbf{t}}^* & \text{on } \Gamma_\sigma \end{array} \right. \quad \text{(boundary conditions)} \tag{3.1}$$

where $\dot{\boldsymbol{\sigma}}$ is the Cauchy stress tensor rate, $\dot{\mathbf{b}}$ is the body force density rate, $\mathbf{n}$ is the unit normal to $\mathcal{S}$ pointing to Ω^+, and $\boldsymbol{\nu}$ is the unit outward normal to Γ (see Fig. 3.1).

The hypothesis of small strains is adopted throughout this monograph, then the kinematics equation is

$$\dot{\boldsymbol{\varepsilon}} = \nabla^s \dot{\mathbf{u}} \quad \text{in } \Omega \quad \text{(kinematics equation)} \tag{3.2}$$

The relationship between the stress, $\boldsymbol{\sigma}$, and the strain, $\boldsymbol{\varepsilon}$, fields is given by some constitutive model, for instance, the one presented in Section 2.2.

[2]Using Continuum Mechanics terminology, $\mathcal{S}$ is a material surface.

[3]The inner traction continuity is characteristic of problems involving discontinuous kinematics.

3.2 Strong and weak discontinuity kinematics

The kinematics of a continuum undergoing discontinuities is analyzed in this section. As a result the link between weak and strong discontinuities is established.

3.2.1 Strong discontinuity kinematics

Consider now that Ω is split by $\mathcal{S}$ (called discontinuity interface[4]) into Ω^+(pointed by the unit normal $\mathbf{n}$) and Ω^- (see Fig. 3.2-a), then the following structure for the rate of displacement field, $\dot{\mathbf{u}} : \Omega \times \mathbb{R}_+ \rightarrow \mathbb{R}^{n_{\text{dim}}}$ (n_{dim} is the number of the dimensions of the problem), is proposed:

$$\dot{\mathbf{u}}(\mathbf{x}, t) = \dot{\hat{\mathbf{u}}}(\mathbf{x}, t) + H_{\mathcal{S}}\, [\![\dot{\mathbf{u}}]\!](\mathbf{x},\ t) \tag{3.3}$$

where $H_{\mathcal{S}}$ is the Heaviside function acting on $\mathcal{S}$ ($H_{\mathcal{S}} = 1\ \forall \mathbf{x} \in \Omega^+$ and $H_{\mathcal{S}} = 0$ $\forall \mathbf{x} \in \Omega^-$) and $[\![\dot{\mathbf{u}}]\!] : \Omega \times \mathbb{R}_+ \rightarrow \mathbb{R}^{n_{\text{dim}}}$ is the rate of displacement jump function. Functions $\dot{\hat{\mathbf{u}}}$ and $[\![\dot{\mathbf{u}}]\!]$ are considered to be smooth[5]. From (3.3) and (3.2), we obtain the following expression for the strain rate field:

$$\dot{\boldsymbol{\varepsilon}}\,(\mathbf{x}, t) = \boldsymbol{\nabla}^s \dot{\mathbf{u}} = \underbrace{\boldsymbol{\nabla}^s \dot{\hat{\mathbf{u}}} + H_{\mathcal{S}}\, \boldsymbol{\nabla}^s [\![\dot{\mathbf{u}}]\!]}_{\dot{\boldsymbol{\varepsilon}}\ \text{(regular)}} + \underbrace{\delta_{\mathcal{S}}\, ([\![\dot{\mathbf{u}}]\!] \otimes \mathbf{n})^s}_{[\![\dot{\boldsymbol{\varepsilon}}]\!]\ \text{(singular)}} \tag{3.4}$$

where $\delta_{\mathcal{S}}$ is the Dirac delta function acting on $\mathcal{S}$.

Remark 5 *The structure of the strain tensor can be expressed as the sum of a term including only regular distributions and a term which includes a singular distribution (the term containing the Dirac delta)*[6].

Remark 6 *Notice that the restriction of function* $[\![\dot{\mathbf{u}}]\!]$ *to the discontinuity interface* $\mathcal{S}$ *(i.e.,* $[\![\dot{\mathbf{u}}]\!]_{\mathcal{S}}$*) defines the "jump" in the rate of displacement field,* $\dot{\mathbf{u}}$*, across* $\mathcal{S}$*, and hence the symbol used to denote it.*

[4]Discontinuity surface in 3-D and discontinuity line in 2-D.

[5]The issue of the smoothness of the fields involved in the strong discontinuity kinematis is tackled in chapter 4. For the moment, a smooth function can be understood as a function whose first derivatives are not singular distributions.

[6]A regular distribution is a distribution that can be generated by a (Lebesgue) locally integrable function (see [Reddy, 1998]), whereas a singular distribution cannot. Roughly speaking, regular distributions correspond to "normal" functions, while singular distributions correspond to "special" functions like the Dirac delta.

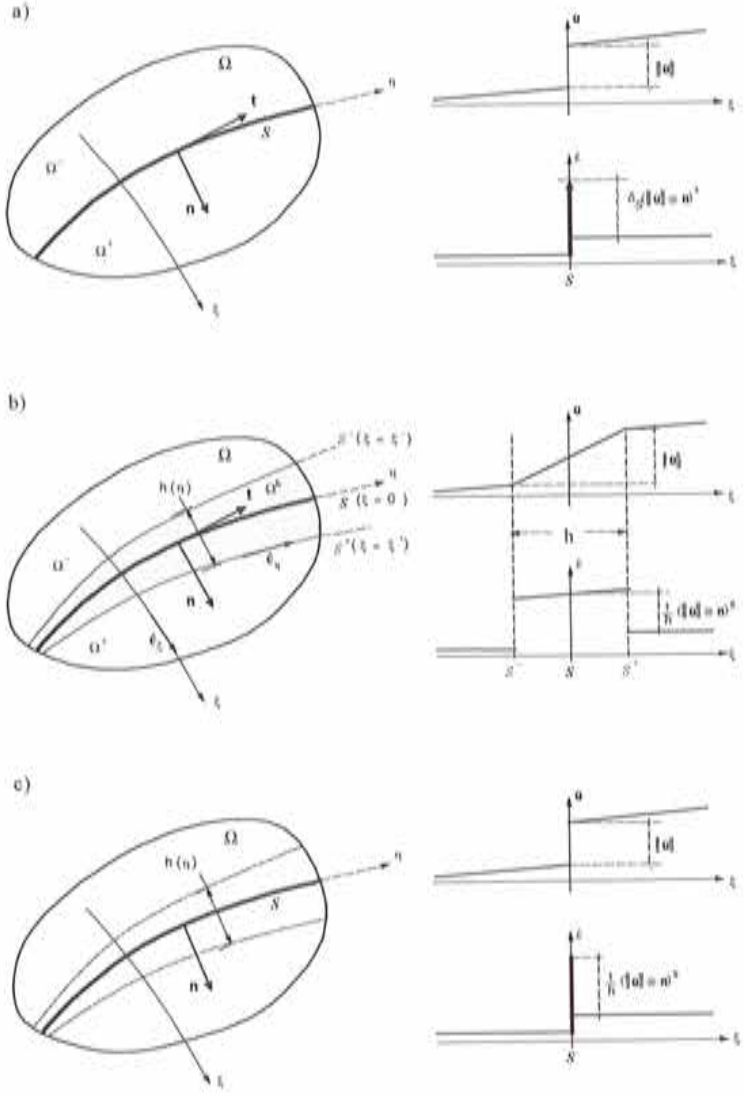

Figure 3.2: Discontinuous kinematics: a) strong discontinuity, b) weak discontinuity, c) regularized strong discontinuity.

3.2.2 Weak discontinuity kinematics

The definition of the weak discontinuity kinematics [Oliver et al., 1997] is made only for the two-dimensional case. Extension to three dimensions is straightforward.

Let $\{\xi,\eta\}$ be a curvilinear coordinate system such that $\mathcal{S}$ coincides with the coordinate line η (see Fig. 3.2-b), i.e.,

$$\mathcal{S} = \{\mathbf{x}(\xi,\eta) \mid \xi = 0\}$$

Then, let $\{\hat{\mathbf{e}}_\xi,\hat{\mathbf{e}}_\eta)$ be the orthonormal basis associated with the above coordinate system and let $r_\xi(\xi,\eta)$ and $r_\eta(\xi,\eta)$ be the corresponding scale factors, such that $ds_\xi = r_\xi d\xi$ and $ds_\eta = r_\eta d\eta$, where ds_ξ and ds_η are, respectively, the differential arc length along the coordinate lines ξ and η. Consider now the lines $\mathcal{S}^+$ and $\mathcal{S}^-$ which coincide with the coordinate lines $\xi = \xi^+$ and $\xi = \xi^-$, respectively, and define the limits of the discontinuity band $\Omega^h := \left\{\mathbf{x}(\xi,\eta) \mid \xi \in \left[\xi^-,\xi^+\right]\right\}$, whose representative width $h(\eta)$, from now on called *bandwidth*, is defined as $h(\eta) := r_\xi(0,\eta)(\xi^+ - \xi^-)$.

Consider, then, the following description of the rate of displacement field in Ω:

$$\dot{\mathbf{u}}(\mathbf{x},t) = \dot{\bar{\mathbf{u}}}(\mathbf{x},t) + H_{\Omega^h}(\xi,t)\,[\![\dot{\mathbf{u}}]\!](\eta,\ t) \tag{3.5}$$

where $H_{\Omega^h}(\xi,t)$ denotes the ramp function, defined by

$$H_{\Omega^h} = \begin{cases} 0 & \mathbf{x} \in \Omega^-\backslash\Omega^h\ (\xi \le \xi^-) \\ 1 & \mathbf{x} \in \Omega^+\backslash\Omega^h\ (\xi \ge \xi^+) \\ \frac{\xi-\xi^-}{\xi^+-\xi^-} & \mathbf{x} \in \Omega^h\ (\xi^- < \xi < \xi^+) \end{cases} \tag{3.6}$$

It is easy to see that H_{Ω^h} exhibits a unit jump, i.e., the difference of its values at $\mathcal{S}^+$ and $\mathcal{S}^-$ for the same coordinate line ξ is equal to one ($[\![H_{\Omega^h}]\!] = H_{\Omega^h}(\xi^+,t) - H_{\Omega^h}(\xi^-,t) = 1\ \forall\eta$). Hence, the corresponding gradient is

$$\begin{aligned} \nabla H_{\Omega^h} &= \frac{1}{r_\xi}\frac{\partial H_{\Omega^h}}{\partial\xi}\hat{\mathbf{e}}_\xi + \frac{1}{r_\eta}\frac{\partial H_{\Omega^h}}{\partial\eta}\hat{\mathbf{e}}_\eta = \mu_{\Omega^h}\frac{1}{h_\xi}\hat{\mathbf{e}}_\xi \\ h_\xi(\xi,\eta) &= r_\xi(\xi,\eta)\,(\xi^+ - \xi^-) \\ h_\xi(0,\eta) &= r_\xi(0,\eta)\,(\xi^+ - \xi^-) = h(\eta) \end{aligned} \tag{3.7}$$

where μ_{Ω^h} is a collocation function placed on Ω^h ($\mu_{\Omega^h} = 1$ if $\mathbf{x} \in \Omega^h$ and $\mu_{\Omega^h} = 0$ if $\mathbf{x} \notin \Omega^h$). From (3.2), (3.5), and (3.7), we obtain

$$\dot{\boldsymbol{\varepsilon}}(\mathbf{x},t) = \nabla^s\dot{\mathbf{u}} = \underbrace{\nabla^s\dot{\bar{\mathbf{u}}} + H_{\Omega^h}\,\nabla^s[\![\dot{\mathbf{u}}]\!]}_{\dot{\boldsymbol{\varepsilon}}\ \text{(continuous)}} + \underbrace{\mu_{\Omega^h}\frac{1}{h_\xi}([\![\dot{\mathbf{u}}]\!]\otimes\hat{\mathbf{e}}_\xi)^s}_{[\![\dot{\boldsymbol{\varepsilon}}]\!]\ \text{(discontinuous)}} \tag{3.8}$$

Remark 7 *The strain tensor corresponding to the weak discontinuity kinematics is expressed as the sum of a continuous term, $\dot{\tilde{\boldsymbol{\varepsilon}}}$, plus a discontinuous one, $[\![\dot{\boldsymbol{\varepsilon}}]\!]$. No singular term is present.*

3.2.3 Regularized strong discontinuity kinematics

Now, we define the regularized version of the strong discontinuity kinematics as the limit case of the weak discontinuity kinematics when $h(\eta)$ tends to zero (see Fig. 3.2-c). Thus, the expression of the displacement rate is the following:

$$\dot{\mathbf{u}}(\mathbf{x},t) \;=\; \dot{\tilde{\mathbf{u}}}(\mathbf{x},t) \;+ H_S\; [\![\dot{\mathbf{u}}]\!](\mathbf{x},\; t) \tag{3.9}$$

On the basis of (3.8), the corresponding strains rate is assumed to be

$$\dot{\boldsymbol{\varepsilon}}\,(\mathbf{x},t) = \underbrace{\boldsymbol{\nabla}^s\dot{\tilde{\mathbf{u}}} + H_S\;\boldsymbol{\nabla}^s[\![\dot{\mathbf{u}}]\!]}_{\dot{\boldsymbol{\varepsilon}}\text{ (bounded)}} + \underbrace{\mu_S\frac{1}{h(\eta)}([\![\dot{\mathbf{u}}]\!]\otimes\mathbf{n})^s}_{[\![\dot{\boldsymbol{\varepsilon}}]\!]\text{(unbounded when } h(\eta)\to 0)} \tag{3.10}$$

where μ_S is a collocation function placed on $\mathcal{S}$ ($\mu_S = 1$ if $\mathbf{x}\in\mathcal{S}$ and $\mu_S = 0$ if $\mathbf{x}\notin\mathcal{S}$)

Remark 8 *When the bandwidth, $h(\eta)$, tends to zero, $\left(\mu_S\frac{1}{h(\eta)}\right)\to\delta_S$. Thus, the kinematics defined by (3.9) and (3.10) becomes equivalent to that defined by (3.3) and (3.4).*

Remark 9 *Notice that $h(\eta)=h_\xi(0,\eta)$ and that $\mathbf{n}=\hat{\mathbf{e}}_\xi$ at $\mathcal{S}$. This means that (3.5) and (3.8) tend to be equivalent to (3.9) and (3.10), respectively, as the discontinuity band collapses into surface $\mathcal{S}$.*

Remark 10 *From remarks (8) and (9), one can conclude that the kinematics described by (3.9) and (3.10) are representative of both the weak discontinuity kinematics and the strong discontinuity kinematics for $h(\eta)$ relatively small in comparison with the dimensions of the solid.*

Remark 11 *The rate of strain field (3.10) is not kinematically compatible with the rate of displacement field (3.9) in the sense that $\dot{\boldsymbol{\varepsilon}}\neq\boldsymbol{\nabla}^s\dot{\mathbf{u}}$, since $\boldsymbol{\nabla}H=\delta_S\,\mathbf{n}\neq\mu_S[1/h(\eta)]\mathbf{n}$. Compatibility is only attained when $h(\eta)\to 0$.*

3.2.4 A variable bandwidth model

In [Oliver et al., 1997], the fact that discontinuous bifurcation was a necessary but not sufficient condition for the inception of a strong discontinuity was pointed out. Then specific conditions for the appearance of strong discontinuities were derived (the so-called *Strong Discontinuity Conditions*[7]). In order to reach the necessary conditions for the appearance of strong discontinuities, a transition from weak to strong discontinuities was devised. Thus, the formation of a strong discontinuity at a material point $\mathbf{x}$ can be modelled as a weak discontinuity at a certain time of the deformation process. At the bifurcation time, t_b, the stress and strain fields bifurcate according to the kinematics presented in (3.10), with $[\![\dot{\mathbf{u}}]\!] \neq 0$, and with $h_b = h(\eta)$ of finite width if the strong discontinuity conditions are not met. In such a case, for the subsequent states, the bandwidth decreases ruled by a certain bandwidth evolution law (which is regarded as a material property) until $h(\eta) \equiv k \to 0$ at time $t = t_{SD}$[8].

In light of this, time integration of (3.10) for $t \geq t_{SD}$ yields

$$\begin{aligned} \boldsymbol{\varepsilon}(\mathbf{x},t)|_{t\geq t_{SD}} &= \underbrace{\int_0^t \dot{\bar{\boldsymbol{\varepsilon}}}\,dt + \mu_S \int_0^{t_{SD}} \frac{1}{h}([\![\dot{\mathbf{u}}]\!]\otimes\mathbf{n})^s dt}_{\bar{\boldsymbol{\varepsilon}}} + \mu_S \int_{t_{SD}}^t \frac{1}{h}([\![\dot{\mathbf{u}}]\!]\otimes\mathbf{n})^s dt \\ &= \underbrace{\bar{\boldsymbol{\varepsilon}}}_{\text{(bounded for } h\equiv k\to 0)} + \underbrace{\mu_S \frac{1}{h}(\Delta[\![\mathbf{u}]\!]\otimes\mathbf{n})^s}_{\text{(unbounded for } h\equiv k\to 0)} \end{aligned} \tag{3.11}$$

where $\Delta[\![\mathbf{u}]\!] := [\![\mathbf{u}]\!](\mathbf{x},t) - [\![\mathbf{u}]\!](\mathbf{x},t_{SD})$ is the *incremental jump*.

Remark 12 *The material character of $\mathcal{S}$ (which implies $\dot{\mathbf{n}} = 0$) has been taken into account in the above derivation.*

Remark 13 *In (3.11) and in all the derivations related with the strong discontinuity analysis, the general case in which the strong discontinuity regime is preceded by a weak discontinuity regime is considered.*

3.3 Strong discontinuity analysis

A crucial issue that arises when the strong discontinuity approach is adopted is that of the compatibility of the strong discontinuity kinematics with continuum

[7] These conditions will be discussed later on in this thesis.

[8] In its computational implementation k is as small as allowed by the machine precision.

constitutive modelling. The strong discontinuity analysis [Oliver, 2000] aims at identifying the conditions that make that compatibility possible. The point of departure of the analysis is the inner traction continuity stated in (3.1). From this, the mathematical conditions that make a continuum constitutive model consistent with the inclusion of discontinuities in the displacement field are derived.

Let us state the inner traction continuity and the inner traction rate continuity[9]:

$$\left.\begin{array}{l} \mathcal{T}(\mathbf{x},t) = \boldsymbol{\sigma}_{\mathcal{S}}(\mathbf{x},t)\cdot\mathbf{n}(\mathbf{x}) = \boldsymbol{\sigma}_{\Omega\backslash\mathcal{S}}(\mathbf{x},t)\cdot\mathbf{n}(\mathbf{x}) \\ \dot{\mathcal{T}}(\mathbf{x},t) = \dot{\boldsymbol{\sigma}}_{\mathcal{S}}(\mathbf{x},t)\cdot\mathbf{n}(\mathbf{x}) = \dot{\boldsymbol{\sigma}}_{\Omega\backslash\mathcal{S}}(\mathbf{x},t)\cdot\mathbf{n}(\mathbf{x}) \end{array}\right\} \forall \mathbf{x} \in \mathcal{S}, \quad \forall t \in \mathbb{R}_+ \tag{3.12}$$

where $\mathcal{T}$ denotes the traction vector, $\boldsymbol{\sigma}_{\mathcal{S}}$ is the stress tensor of the material point $\mathcal{P} \in \mathcal{S}$, and $\boldsymbol{\sigma}_{\Omega\backslash\mathcal{S}}$ is the stress tensor of a material point in $\Omega\backslash\mathcal{S}$ belonging to the neighborhood of $\mathcal{P}$.

Hence, the following consequences can be inferred:

Since the strain tensor is bounded in $\Omega\backslash\mathcal{S}$ ($\boldsymbol{\varepsilon} = \bar{\boldsymbol{\varepsilon}}$), the stresses $\boldsymbol{\sigma}_{\Omega\backslash\mathcal{S}}$ are also bounded. Therefore, $\mathcal{T}(\mathbf{x},t) = \boldsymbol{\sigma}_{\Omega\backslash\mathcal{S}}\cdot\mathbf{n}$ is bounded. We also have that $\mathcal{T}(\mathbf{x},t) = \boldsymbol{\sigma}_{\mathcal{S}}\cdot\mathbf{n}$. Let us now express $\mathcal{T}(\mathbf{x},t)$ in the basis formed by the principal directions of $\boldsymbol{\sigma}_{\mathcal{S}}$:

$$\begin{array}{ll} \mathcal{T}_1 = \sigma_1 n_1 & \text{(bounded)} \\ \mathcal{T}_2 = \sigma_2 n_2 & \text{(bounded)} \\ \mathcal{T}_3 = \sigma_3 n_3 & \text{(bounded)} \end{array} \tag{3.13}$$

where σ_1, σ_2, σ_3 are the eigenvalues of $\boldsymbol{\sigma}_{\mathcal{S}}$. Since n_1, n_2, n_3 are bounded by definition ($\|\mathbf{n}\| = 1$), then σ_1, σ_2, σ_3 are also bounded[10], and so is the stress tensor $\boldsymbol{\sigma}_{\mathcal{S}}$. Analogous arguments can be used to prove the boundedness of $\dot{\boldsymbol{\sigma}}_{\mathcal{S}}$.

Remark 14 *The boundedness of the stress tensor $\boldsymbol{\sigma}_{\mathcal{S}}$, despite the unboundedness of $\boldsymbol{\varepsilon}_{\mathcal{S}}$, is a key result of the strong discontinuity analysis.*

3.3.1 A representative continuum damage model

Before proceeding with the strong discontinuity analysis, we present a summary of the isotropic continuum damage model laid out in Section 2.2.

[9] Although the inner traction continuity is treated as an assumption here, it can be derived, in a variational context, from the moment balance plus the adoption of the strong discontinuity kinematics, as done in [Simo and Oliver, 1994].

[10] This argument is not general, since n_i for some $i \in \{1,2,3\}$ could be zero . However, even in this case, the boundedness of $\boldsymbol{\sigma}_{\mathcal{S}}$ can be proven using alternative reasonings.

$$\text{Free Energy} \quad \psi(\boldsymbol{\varepsilon},r) = [1-d(r)]\psi_0; \;\; \psi_0(\boldsymbol{\varepsilon}) = \frac{1}{2}(\boldsymbol{\varepsilon} : \mathbf{C} : \boldsymbol{\varepsilon}) \tag{3.14}$$

$$\text{Constitutive Eq.} \quad \boldsymbol{\sigma} = \partial_{\boldsymbol{\varepsilon}}\psi(\boldsymbol{\varepsilon},r) = (1-d)\mathbf{C} : \boldsymbol{\varepsilon} \tag{3.15}$$

$$\text{Damage variable} \quad d = 1 - q(r)/r \quad d \in [0,1] \tag{3.16}$$

$$\text{Evolution law} \quad \dot{r} = \lambda; \quad r \in [r_0, \infty) \quad r_0 = \sigma_u/\sqrt{E} \tag{3.17}$$

$$\text{Damage Criterion} \quad f(\boldsymbol{\sigma},q) := \tau_\sigma - q; \;\; \tau_\sigma = \sqrt{\boldsymbol{\sigma} : \mathbf{C}^{-1} : \boldsymbol{\sigma}} \tag{3.18}$$

$$\text{L/U conditions} \quad f \leq 0; \;\; \lambda \geq 0; \;\; \lambda f = 0; \;\; \underbrace{\lambda \dot{f} = 0}_{\text{consistency}} \tag{3.19}$$

$$\text{Softening Rule} \quad \dot{q} = \mathcal{H}(r)\dot{r}; \quad q \in [0, r_0]; \;\; q|_{t=0} = r_0 \tag{3.20}$$

In the remaining of this section the strong discontinuity analysis is applied to the above constitutive model.

3.3.2 Discrete constitutive equation

Now we can resume the strong discontinuity analysis, applying it to the constitutive model sketched in Subsection 3.3.1. We have that, from the boundedness of $\boldsymbol{\sigma}_S$, the boundedness of $\tau_\sigma = \sqrt{\boldsymbol{\sigma} : \mathbf{C}^{-1} : \boldsymbol{\sigma}}$ follows immediately. Moreover, $\dot{\tau}_\sigma = [(1/\tau_\sigma)(\boldsymbol{\sigma} : \mathbf{C}^{-1} : \dot{\boldsymbol{\sigma}})]$ is also bounded. In light of (3.20) and (3.19), $\dot{q} \neq 0$ only in loading ($\dot{r} = \lambda > 0$). We also have that, from the consistency condition, $\dot{f} = 0$. Then, $\dot{q} = \dot{\tau}_\sigma$. Hence, $\dot{q}$ is bounded.

Let us now consider, for a given material point belonging to $\mathcal{S}$, the expression of the stresses given by (3.15) and use the structure of the strains stated in (3.11):

$$\boldsymbol{\sigma}_S = (1-d)\mathbf{C} : \boldsymbol{\varepsilon}_S = \frac{q}{r}\mathbf{C} : \left[\bar{\boldsymbol{\varepsilon}} + \frac{1}{h}(\Delta[\![\mathbf{u}]\!]_S \otimes \mathbf{n})^s\right]$$

Suppose that for that material point $t > t_{SD}$ (which implies $h \to 0$), then

$$
\begin{aligned}
\mathcal{T} &= \boldsymbol{\sigma}_{\mathcal{S}}\cdot\mathbf{n} = \lim_{h\to 0}\frac{q_{\mathcal{S}}}{r_{\mathcal{S}}}\mathbf{n}\cdot\mathbf{C}:\left[\bar{\boldsymbol{\varepsilon}}+\frac{1}{h}(\Delta[\![\dot{\mathbf{u}}]\!]_{\mathcal{S}}\otimes\mathbf{n})^{s}\right] \\
&= \lim_{h\to 0}\frac{1}{hr_{\mathcal{S}}}q_{\mathcal{S}}\mathbf{n}\cdot\mathbf{C}:[h\bar{\boldsymbol{\varepsilon}}+(\Delta[\![\dot{\mathbf{u}}]\!]_{\mathcal{S}}\otimes\mathbf{n})^{s}] \\
&= \lim_{h\to 0}\frac{1}{hr_{\mathcal{S}}}q_{\mathcal{S}}\mathbf{n}\cdot\mathbf{C}:(\Delta[\![\dot{\mathbf{u}}]\!]_{\mathcal{S}}\otimes\mathbf{n})^{s} \\
&= \lim_{h\to 0}\frac{1}{hr_{\mathcal{S}}}q_{\mathcal{S}}(\underbrace{\mathbf{n}\cdot\mathbf{C}\cdot\mathbf{n}}_{\mathbf{Q}^{e}})\cdot\Delta[\![\dot{\mathbf{u}}]\!]_{\mathcal{S}} \\
&= \lim_{h\to 0}\left(\frac{1}{hr_{\mathcal{S}}}\right)q_{\mathcal{S}}\mathbf{Q}^{e}\cdot\Delta[\![\dot{\mathbf{u}}]\!]_{\mathcal{S}} \qquad (3.21)
\end{aligned}
$$

Since $\mathbf{Q}^{e}$ is positive definite and, therefore, non-singular, $\mathbf{Q}^{e}\cdot\Delta[\![\dot{\mathbf{u}}]\!]_{\mathcal{S}} \neq \mathbf{0}$ unless $\Delta[\![\dot{\mathbf{u}}]\!]_{\mathcal{S}} = \mathbf{0}$, but that would contradict the assumption of $t > t_{SD}$. Hence $q_{\mathcal{S}}\mathbf{Q}^{e}\cdot\Delta[\![\dot{\mathbf{u}}]\!]_{\mathcal{S}}$ is bounded and different from zero. Thus the following must hold:

$$
\lim_{h\to 0} hr_{\mathcal{S}} \neq 0 \quad \text{if} \quad \Delta[\![\dot{\mathbf{u}}]\!]_{\mathcal{S}} \neq 0 \qquad (3.22)
$$

Let us consider the following structure for $\dot{r}_{\mathcal{S}}$:

$$
\dot{r}_{\mathcal{S}} = \frac{1}{h}\dot{\bar{\alpha}} \qquad \forall t \geq t_{WD} \qquad (3.23)
$$

with $\bar{\alpha}|_{t=t_{WD}} = 0$, t_{WD} being the time of the inception of the weak discontinuity regime and $\bar{\alpha}$ the *discrete internal variable*. The rate of the discrete internal variable, $\dot{\bar{\alpha}}$, is imposed to be bounded and different from zero for $t > t_{SD}$.

Now (3.23) can be integrated for $t \geq t_{SD}$, yielding

$$
\begin{aligned}
r_{\mathcal{S}} &= \int_{o}^{t}\dot{r}_{\mathcal{S}}dt \\
&= \underbrace{r_{WD}+\int_{t_{WD}}^{t_{SD}}\frac{1}{h(\tau)}\dot{\bar{\alpha}}(\tau)d\tau}_{:=r_{SD}} + \int_{t_{SD}}^{t}\underbrace{\frac{1}{h(\tau)}}_{h\equiv k}\dot{\bar{\alpha}}(\tau)d\tau \\
&= r_{SD}+\frac{1}{k}\int_{t_{SD}}^{t}\dot{\bar{\alpha}}(\tau)d\tau = r_{SD}+\frac{1}{k}\Delta\bar{\alpha} \qquad (3.24)
\end{aligned}
$$

where $\Delta\bar{\alpha}_{t} := \bar{\alpha}_{t} - \bar{\alpha}_{SD}$ and $r_{WD} = r_{\mathcal{S}}|_{t=t_{WD}}$. Thus, we have that, for $t \geq t_{SD}$,

$$\begin{aligned}\lim_{h\to 0} hr_{SD} &= \lim_{k\to 0} kr_{SD} \\ &= \lim_{k\to 0}\left[kr_{WD} + \int_{t_{WD}}^{t_{SD}} \frac{k}{h(\tau)}\dot{\bar{\alpha}}(\tau)d\tau\right] = 0 \end{aligned} \tag{3.25}$$

Then, replacing (3.25) in (3.24) and then in (3.22), it yields

$$\begin{aligned}\lim_{h\to 0} hr_{\mathcal{S}} &= \lim_{h\to 0}\left(hr_{SD} + \Delta\bar{\alpha}\right) \\ &= \Delta\bar{\alpha}\end{aligned} \tag{3.26}$$

By the definition of $\bar{\alpha}$, $\Delta\bar{\alpha} \neq 0\ \forall t > t_{SD}$. Therefore, (3.23) is compatible with condition (3.22) and ensures the consistency of (3.21) for $\Delta[\![\dot{\mathbf{u}}]\!]_{\mathcal{S}} \neq \mathbf{0}$.

Substituting (3.26) in (3.21), we obtain

$$\mathcal{T} = \frac{q_{\mathcal{S}}}{\Delta\bar{\alpha}}\mathbf{Q}^e \cdot \Delta[\![\mathbf{u}]\!]_{\mathcal{S}} \quad \forall t > t_{SD} \tag{3.27}$$

which is a constitutive equation of the discrete type relating the traction vector, $\mathcal{T}$, with the differential jump, $\Delta[\![\dot{\mathbf{u}}]\!]_{\mathcal{S}}$.

Replacing (3.23) in the softening rule (3.20), it yields

$$\dot{q} = \mathcal{H}(r)\dot{r} = \mathcal{H}(r)\frac{1}{h}\dot{\bar{\alpha}} \tag{3.28}$$

Since $\dot{q}$ and $\dot{\bar{\alpha}}$ are bounded, $\lim_{h\to 0}(\mathcal{H}/h)$ must also be bounded. In order to fulfill this requirement the following structure for the softening parameter is proposed:

$$\mathcal{H} = h(t)\bar{\mathcal{H}} \quad \forall t > t_{WD} \tag{3.29}$$

where $\bar{\mathcal{H}} < 0$ is defined to be bounded and will be named *discrete or intrinsic softening parameter.*

Remark 15 *When $h \to 0$, $\mathcal{H} = h\bar{\mathcal{H}}$ is equivalent to the distributional structure of the softening parameter proposed by [Simo et al., 1993]. The fact that in (3.29) this structure is stated in a regularized way allows for its extension to the weak discontinuity regime.*

Now, by substituting (3.29) in (3.28), the following relationship emerges

$$\dot{q} = \bar{\mathcal{H}}\dot{\bar{\alpha}}; \quad q \in [0, r_0] \qquad \forall t \geq t_{SD} \tag{3.30}$$

which is the discrete counterpart of the softening law stated in (3.20). It can be integrated in time as follows:

$$q_S = q_{SD} + \int_{t_{SD}}^{t} \bar{\mathcal{H}}\dot{\bar{\alpha}}(\tau)d\tau \tag{3.31}$$

where $q_{SD} = q_S|_{t=t_{SD}}$.

Consider for instance the case of a constant $\bar{\mathcal{H}}$, then (3.31) reduces to

$$q_S = q_{SD} + \bar{\mathcal{H}}\Delta\bar{\alpha} \tag{3.32}$$

Equation (3.32) illustrates the dependence of q_S on $\Delta\bar{\alpha}$ for a linear softening law, but this can be generalized to laws of nonlinear type.

Let us now define

$$\omega(\Delta\bar{\alpha}) = 1 - \frac{q(\Delta\bar{\alpha})}{\Delta\bar{\alpha}} \tag{3.33}$$

with $\omega(\Delta\bar{\alpha}) \in (-\infty, 1]$ and $\Delta\bar{\alpha} \in [0, \infty)$. The variable $\omega(\Delta\bar{\alpha})$ can be regarded as the *discrete damage variable* (whose continuum counterpart is d). Now the discrete constitutive equation (3.27) can be rewritten in a more convenient format:

$$T = (1 - \omega)\mathbf{Q}^e \cdot \Delta[\![\mathbf{u}]\!]_S \tag{3.34}$$

Thus, the analogy between the expressions of the continuum damage constitutive equation (3.15) and the discrete damage constitutive equation (3.34) is clear. Furthermore, the correspondence between the variables involved in (3.15) and (3.34) is evident:

Continuum	$\boldsymbol{\sigma}$	$\boldsymbol{\varepsilon}$	$\mathbf{C}$	d	r	$q(r)$
Discrete	T	$\Delta[\![\mathbf{u}]\!]_S$	$\mathbf{Q}^e$	ω	$\Delta\bar{\alpha}$	ω

(3.35)

Remark 16 *The discrete constitutive equation can be regarded as a 'projection' of the continuum constitutive equation on the discontinuity interface.*

Consider now the basis $\{\mathbf{n}, \mathbf{t}, \mathbf{p}\}$, where $\mathbf{n}$ is the unit normal to the discontinuity interface $\mathcal{S}$ at a given material point and $\mathbf{t}$ and $\mathbf{p}$ are two vectors lying on the tangential plane to $\mathcal{S}$ at that material point. The matrix expression of the elastic acoustic tensor is

$$[\mathbf{Q}^e] = \begin{bmatrix} \hat{\lambda} + 2\mu & 0 & 0 \\ 0 & \mu & 0 \\ 0 & 0 & \mu \end{bmatrix}$$

Then, the expression of discrete constitutive equation (3.34) in components reads

$$\begin{aligned} \mathcal{T}_n &= (1-\omega)(\hat{\lambda} + 2\mu)\Delta[\![u]\!]_1 \\ \mathcal{T}_t &= (1-\omega)\mu\Delta[\![u]\!]_2 \\ \mathcal{T}_p &= (1-\omega)\mu\Delta[\![u]\!]_3 \end{aligned} \tag{3.36}$$

3.3.3 Discrete free energy

Within the context of thermodynamically consistent constitutive modelling, the definition of *continuum free energy density functions* (as the one in (3.14) is a key task. For isothermal processes and under the assumption of small strains a *free energy density function* ψ is formulated in terms of the strains, $\boldsymbol{\varepsilon}$, (acting as the free variable) and a set of internal variables, Ξ. Based on thermodynamical arguments, the stresses can be obtained from $\psi(\boldsymbol{\varepsilon}, \Xi)$:

$$\boldsymbol{\sigma} = \partial_{\boldsymbol{\varepsilon}} \psi(\boldsymbol{\varepsilon}, \Xi) \tag{3.37}$$

Thus the continuum free energy density can be regarded as a potential for the stress field $\boldsymbol{\sigma}$.

Consider the discontinuity interface $\mathcal{S}$ and assume that a free energy function per unit area of that surface exists, which will be called *discrete free energy function* and will be denoted by $\bar{\psi}$ from now on, then, in the context of the regularized strong discontinuity analysis, it can intuitively be seen as

$$\bar{\psi} = \left(\frac{\text{free energy}}{\text{unit surface}}\right) = \underbrace{\left(\frac{\text{free energy}}{\text{unit volume}}\right)}_{\psi}\underbrace{\left(\frac{\text{unit volume}}{\text{unit surface}}\right)}_{h} = \lim_{h\to 0} h\psi_{\mathcal{S}} \tag{3.38}$$

where $\psi_{\mathcal{S}} \equiv \psi|_{\mathcal{S}}$. Thus, considering the regularized strong discontinuity kinematics presented in (3.11), we can define

$$\bar{\psi}(\bar{\varepsilon}, \Delta[\![\mathbf{u}]\!]_{\mathcal{S}}, \Xi) := \lim_{h\to 0} h\psi_{\mathcal{S}}(\varepsilon(\bar{\varepsilon}, \Delta[\![\mathbf{u}]\!]), \Xi) \tag{3.39}$$

Hence,

$$\begin{aligned} \partial_{\Delta[\![\mathbf{u}]\!]_{\mathcal{S}}}\bar{\psi} &= \lim_{h\to 0} h \underbrace{\partial_{\varepsilon}\psi_{\mathcal{S}}(\varepsilon, \Xi)}_{\sigma_{\mathcal{S}}} : \underbrace{\partial_{\Delta[\![\mathbf{u}]\!]}\varepsilon}_{\frac{1}{h}(\mathbf{n}\otimes\mathbf{1})^s} \\ &= \boldsymbol{\sigma}_{\mathcal{S}}\cdot\mathbf{n} = \mathcal{T} \end{aligned} \tag{3.40}$$

where $[(\mathbf{n}\otimes\mathbf{1})^s]_{ijk} = \frac{1}{2}(\delta_{ik}n_j + \delta_{jk}n_i)$.

Therefore, the discrete free energy is a potential from which the traction vector field on $\mathcal{S}$ is derived, i.e.,

$$\mathcal{T} = \partial_{\Delta[\![\mathbf{u}]\!]_{\mathcal{S}}}\bar{\psi} \tag{3.41}$$

Consider now the expression of the free energy density in (3.14), then, from (3.39),

$$\bar{\psi} = \lim_{h\to 0} h\psi = \lim_{h\to 0} \frac{hq}{r_{\mathcal{S}}} \left[\frac{1}{2}(\boldsymbol{\varepsilon}_{\mathcal{S}} : \mathbf{C} : \boldsymbol{\varepsilon}_{\mathcal{S}})\right] \tag{3.42}$$

Replacing (3.11) and (3.24) in (3.42) and after some algebra, we obtain

$$\begin{cases} \bar{\psi}(\Delta[\![\mathbf{u}]\!]_{\mathcal{S}}, \omega) = (1-\omega)\bar{\psi}_0(\Delta[\![\mathbf{u}]\!]_{\mathcal{S}}) \\ \bar{\psi}_0(\Delta[\![\mathbf{u}]\!]_{\mathcal{S}}) = \frac{1}{2}\Delta[\![\mathbf{u}]\!]_{\mathcal{S}}\cdot\mathbf{Q}^e\cdot\Delta[\![\mathbf{u}]\!]_{\mathcal{S}} \end{cases} \tag{3.43}$$

Remark 17 *The discrete free energy density in (3.43) and the free energy density of the continuum parent model (3.14) have analogous formats in terms of the corresponding variables in (3.35).*

3.3.4 Strong discontinuity conditions

The issue of the necessary conditions for the appearance of strong discontinuities is tackled here. The existence of this conditions justifies the necessity of the variable bandwidth model explained in Section 3.2.4, since bifurcation might not coincide with the inception of the strong discontinuity regime, as said before.

Let us consider the stress field $\boldsymbol{\sigma}_S$ in the discontinuity interface given by (3.15) in combination with the expression of the strain field presented in (3.11), then we can write:

$$\begin{aligned}
\boldsymbol{\sigma}_S &= \frac{q}{r_S}\mathbf{C} : \boldsymbol{\varepsilon}_S \\
&= \lim_{h\to 0}\frac{q}{r_{SD}+\frac{1}{h}\Delta\bar{\alpha}}\mathbf{C} : \left[\bar{\boldsymbol{\varepsilon}}+\frac{1}{h}(\Delta[\![\mathbf{u}]\!]_S \otimes \mathbf{n})^s\right] \\
&= \lim_{h\to 0}\frac{q}{hr_{SD}+\Delta\bar{\alpha}}\mathbf{C} : [h\bar{\boldsymbol{\varepsilon}}+(\Delta[\![\mathbf{u}]\!]_S \otimes \mathbf{n})^s] \\
&= \frac{q}{\Delta\bar{\alpha}}\mathbf{C} : (\Delta[\![\mathbf{u}]\!]_S \otimes \mathbf{n})^s
\end{aligned} \tag{3.44}$$

where the expressions (3.16) and (3.24) have been used. Hence,

$$(\Delta[\![\mathbf{u}]\!]_S \otimes \mathbf{n})^s = \frac{\Delta\bar{\alpha}}{q}\mathbf{C}^{-1} : \boldsymbol{\sigma}_S = \frac{\Delta\bar{\alpha}}{q}\boldsymbol{\varepsilon}_S^e \tag{3.45}$$

where $\boldsymbol{\varepsilon}_S^{eff} := \mathbf{C}^{-1} : \boldsymbol{\sigma}_S = (1-d)\boldsymbol{\varepsilon}$ is the so called *effective strain field*. Due to the boundedness of $\boldsymbol{\sigma}_S$, $\boldsymbol{\varepsilon}_S^{eff}$ is also bounded.

Equation (3.45) is the so called *strong discontinuity equation* [Oliver, 2000]. Let us now write its matrix expression in the orthonormal basis $\{\mathbf{n}, \mathbf{t}, \mathbf{p}\}$:

$$\begin{bmatrix} \Delta[\![u]\!]_n & \frac{1}{2}\Delta[\![u]\!]_t & \frac{1}{2}\Delta[\![u]\!]_p \\ \frac{1}{2}\Delta[\![u]\!]_t & 0 & 0 \\ \frac{1}{2}\Delta[\![u]\!]_p & 0 & 0 \end{bmatrix} = \frac{\Delta\bar{\alpha}}{q}\begin{bmatrix} \varepsilon_{nn}^{eff} & \varepsilon_{nt}^{eff} & \varepsilon_{np}^{eff} \\ \varepsilon_{nt}^{eff} & \varepsilon_{tt}^{eff} & \varepsilon_{tp}^{eff} \\ \varepsilon_{np}^{eff} & \varepsilon_{tp}^{eff} & \varepsilon_{pp}^{eff} \end{bmatrix} \tag{3.46}$$

Equality (3.46) represents a system of six equations with six unknowns. It can be proven that three of them furnish the expressions for the components of the displacement jump and are equivalent to (3.36), whereas the remaining three are conditions that must be satisfied in the strong discontinuity regime. These are the so-called strong discontinuity conditions and read

$$\varepsilon_{tt}^{eff} = \varepsilon_{tp}^{eff} = \varepsilon_{pp}^{eff} = 0 \tag{3.47}$$

Remark 18 *The strong discontinuity conditions are restrictions on the stress state for a strong discontinuity to develop. This means that the bifurcation time not necessarily coincides with the time of inception of the strong discontinuity regime. Therefore, a transition from weak to strong discontinuities, as the one proposed in [Oliver et al., 1997] and [Oliver et al., 1999], becomes necessary.*

Two-dimensional settings

Remember the definition of the effective strain, $\varepsilon_S^{eff} = (1-d)\boldsymbol{\varepsilon}$, then

$$\begin{aligned}\varepsilon_{tt}^{eff} &= (1-d)\varepsilon_{tt}\\ \varepsilon_{tp}^{eff} &= (1-d)\varepsilon_{tp}\\ \varepsilon_{pp}^{eff} &= (1-d)\varepsilon_{pp}\end{aligned}$$

Consider now the orthonormal basis $\{\mathbf{n}, \mathbf{t}, \mathbf{p}\}$, where $\mathbf{n}$ and $\mathbf{t}$ are vectors coplanar with the discontinuity line $\mathcal{S}$, the former being the normal to $\mathcal{S}$ at a given material point and the latter being tangent to $\mathcal{S}$ at that same material point. Vector $\mathbf{p}$ is a vector normal to the plane in which the discontinuity line lies. In the case of plane strain $\varepsilon_{pp} = 0$ and $\varepsilon_{tp} = 0$. Hence, the strong discontinuity conditions (3.47) reduce, for the case of plane strain, to

$$\varepsilon_{tt} = 0 \tag{3.48}$$

It is easy to see that the same condition holds for plane stress.

Remark 19 *For the isotropic continuum damage model described in (3.14) to (3.20), the strong discontinuity condition (3.48) is the same for plane strain as for plane stress.*

3.3.5 Discrete Damage Criteria

The elastic limit of damage models such as the one that we have been analyzing throughout this section is determined by damage functions based on the definition of *energy norms* [Simo and Ju, 1987]. One of such energy norms is the one used in (3.18). Here we examine the effects of the strong discontinuity kinematics on those norms and on the damage criteria through the representative damage model stated in (3.14) to (3.20).

From (3.44) and (3.45), we obtain

$$\begin{aligned}\tau_{\sigma_S} &= \sqrt{\boldsymbol{\sigma}_S \colon \mathbf{C}^{-1} : \boldsymbol{\sigma}_S}\\ &= \left[\left(\frac{q}{\Delta\bar{\alpha}}\right)^2 (\Delta[\![\mathbf{u}]\!]_S \otimes \mathbf{n})^s : \mathbf{C} : (\Delta[\![\mathbf{u}]\!]_S \otimes \mathbf{n})^s\right]^{1/2}\\ &= \frac{q}{\Delta\bar{\alpha}}(\Delta[\![\mathbf{u}]\!]_S \cdot \underbrace{[\mathbf{n}\cdot\mathbf{C}\cdot\mathbf{n}]}_{\mathbf{Q}^e} \cdot \Delta[\![\mathbf{u}]\!]_S)^{1/2}\\ &= \frac{q}{\Delta\bar{\alpha}}\sqrt{\Delta[\![\mathbf{u}]\!]_S \cdot \mathbf{Q}^e \cdot \Delta[\![\mathbf{u}]\!]_S}\end{aligned} \tag{3.49}$$

Now, replacing the discrete constitutive equation (3.27) in (3.49), it yields

$$\tau_{\sigma_S} = \tau_T := \|T\|_{(\mathbf{Q}^e)^{-1}} = \sqrt{T \cdot (\mathbf{Q}^e)^{-1} \cdot T} \tag{3.50}$$

Thus, a *discrete energy norm* is naturally induced at the discontinuity interface $\mathcal{S}$.

Remark 20 *Observe that the correspondence between the variables involved in the continuum model and the discrete one stated in (3.35) also holds for the continuum and the discrete norms.*

Let us now define the following norm in $\mathcal{S}$:

$$\tau_{\Delta[\mathbf{u}]} := \|\Delta[\![\mathbf{u}]\!]_S\|_{\mathbf{Q}^e} = \sqrt{\Delta[\![\mathbf{u}]\!]_S \cdot \mathbf{Q}^e \cdot \Delta[\![\mathbf{u}]\!]_S} \tag{3.51}$$

From (3.51), (3.50), and (3.34), the following relationship between the discrete norm of the displacement jump and the discrete norm of the traction vector is obtained:

$$\tau_T = (1 - \omega)\tau_{\Delta[\mathbf{u}]} \tag{3.52}$$

which is analogous to the relationship between the continuum norms of the stress and the strain, respectively. Thus, the damage function can be rephrased as follows:

$$f(\boldsymbol{\sigma}_S, q) := \tau_{\sigma_S} - q \equiv f(T, q) := \tau_T - q \tag{3.53}$$

Finally, let us furnish the *continuum damage multiplier* λ with the following structure based on (3.23):

$$\lambda_S := \frac{1}{h}\bar{\lambda} = \dot{r} = \frac{1}{h}\dot{\bar{\alpha}} \tag{3.54}$$

Now we can state the loading/unloading conditions in discrete format:

$$f \leq 0; \quad \bar{\lambda} \geq 0; \quad \bar{\lambda} f = 0; \quad \underbrace{\bar{\lambda}\dot{f} = 0}_{\text{consistency}} \tag{3.55}$$

3.3.6 The discrete damage constitutive model

By applying the strong discontinuity analysis to the isotropic continuum damage model sketched in (3.14) to (3.20) a set of definitions, relationships and equations that constitute a discrete damage model have been derived. Now a summary of the ingredients that define this model is presented.

Free energy

$$\begin{aligned} \bar{\psi}(\Delta[\![\mathbf{u}]\!]_S,\omega) &= (1-\omega)\bar{\psi}_0(\Delta[\![\mathbf{u}]\!]_S) \\ \bar{\psi}_0(\Delta[\![\mathbf{u}]\!]_S) &= \frac{1}{2}\Delta[\![\mathbf{u}]\!]_S\cdot\mathbf{Q}^e\cdot\Delta[\![\mathbf{u}]\!]_S \end{aligned} \tag{3.56}$$

Constitutive equation

$$\begin{aligned} T &= \partial_{\Delta[\![\mathbf{u}]\!]_S}\bar{\psi} \\ T &= (1-\omega)\mathbf{Q}^e\cdot\Delta[\![\mathbf{u}]\!]_S \end{aligned} \tag{3.57}$$

Damage Variable

$$\omega = 1 - \frac{q(\Delta\bar{\alpha})}{\Delta\bar{\alpha}} \tag{3.58}$$

with $\omega \in (-\infty, 1]$

Evolution law

$$\partial_t(\Delta\bar{\alpha}) = \dot{\bar{\alpha}} = \bar{\lambda} \tag{3.59}$$

with $\Delta\bar{\alpha} \in [0, \infty)$

Damage Criterion

$$\begin{aligned} f(T,q) &: = \tau_T - q \\ \tau_T &: = \|T\|_{(\mathbf{Q}^e)^{-1}} = \sqrt{T\cdot(\mathbf{Q}^e)^{-1}\cdot T} \end{aligned} \tag{3.60}$$

Loading/unloading conditions

$$\begin{aligned} f &\leq 0;\ \bar{\lambda} \geq 0;\ \bar{\lambda} f = 0 \\ &\underbrace{\bar{\lambda}\dot{f} = 0}_{\text{consistency}} \end{aligned} \tag{3.61}$$

Softening rule

$$\begin{aligned} \dot{q} &= \bar{\mathcal{H}}\dot{\bar{\alpha}} \\ \bar{\mathcal{H}} &= \frac{1}{h}\mathcal{H} \end{aligned} \tag{3.62}$$

for $q \in [0, q_{SD}]$ and $q_{SD} := q|_{t=t_{SD}}$

Remark 21 *The discrete damage model presented here is characterized by the discrete damage variable ω and by the* discrete secant constitutive modulus $\mathbf{Q}^s = (1-\omega)\mathbf{Q}^e$. *Due to the initial value of $\omega = -\infty$, the initial secant constitutive modulus is $\mathbf{Q}^s = +\infty\mathbf{Q}^e$; therefore the model can be classified as a discrete rigid-damage model as pointed out by [Oliver, 2000].*

3.4 Expended power in SD. Fracture energy

In the previous section, the strong discontinuity analysis was applied to an isotropic continuum damage model. The main result obtained was a discrete constitutive model induced in the discontinuity interface. The dissipative process related with this model is, therefore, concentrated on a surface[11], which entails energy release per unit area. Thus, the existence of a relationship between the energy released in the strong discontinuity regime at a discontinuity interface and the concept of fracture energy seems natural [Oliver, 1996a]. This relationship is established in this section. One of the most interesting results of this derivation is an expression which relates the intrinsic softening parameter to the fracture energy.

According to the Theorem of Power Expended [Gurtin, 1981] for quasistatic problems, in which the kinetic energy can be neglected, the power expended in a solid Ω by the surface and body forces ($\mathbf{t}^*$ and $\mathbf{b}$, respectively) is equal to the stress power, i.e.,

[11] More generally in a manifold of dimension $n-1$, where n is the dimension of the ambient space.

$$\int_{\Omega} \mathbf{b} \cdot \dot{\mathbf{u}} d\Omega + \int_{\Gamma} \mathbf{t}^* \cdot \dot{\mathbf{u}} d\Gamma = \int_{\Omega} \boldsymbol{\sigma} : \dot{\boldsymbol{\varepsilon}} d\Omega \tag{3.63}$$

Let us focus on the strong discontinuity regime and use the expression of the strain field given by (3.4) for the right hand side of (3.63):

$$\begin{aligned} \int_{\Omega} \boldsymbol{\sigma} : \dot{\boldsymbol{\varepsilon}} d\Omega &= \int_{\Omega} \boldsymbol{\sigma} : \left[\dot{\bar{\boldsymbol{\varepsilon}}} + \delta_{\mathcal{S}} \left([\![\dot{\mathbf{u}}]\!] \otimes \mathbf{n} \right)^s \right] d\Omega \\ \int_{\Omega} \boldsymbol{\sigma} : \dot{\boldsymbol{\varepsilon}} d\Omega &= \int_{\Omega \setminus \mathcal{S}} \boldsymbol{\sigma} : \dot{\bar{\boldsymbol{\varepsilon}}} d\Omega + \underbrace{\int_{\mathcal{S}} \boldsymbol{\sigma}_{\mathcal{S}} : \left([\![\dot{\mathbf{u}}]\!]_{\mathcal{S}} \otimes \mathbf{n} \right)^s d\mathcal{S}}_{\mathcal{P}_{\mathcal{S}}} \end{aligned} \tag{3.64}$$

where $\mathcal{P}_{\mathcal{S}}$ is the power expended in the development of the displacement jump in $\mathcal{S}$. Then, the total energy expended in the development of the strong discontinuity is given by

$$\mathcal{W}_{\mathcal{S}} = \int_{t_{SD}}^{t_\infty} \mathcal{P}_{\mathcal{S}} dt \tag{3.65}$$

where t_∞ stands for the time at which the displacement jump is fully developed

Moreover, from (3.64), we have that

$$\begin{aligned} \mathcal{P}_{\mathcal{S}} &= \int_{\mathcal{S}} \boldsymbol{\sigma}_{\mathcal{S}} : \left([\![\dot{\mathbf{u}}]\!]_{\mathcal{S}} \otimes \mathbf{n} \right)^s d\mathcal{S} \\ &= \int_{\mathcal{S}} \mathcal{T} \cdot [\![\dot{\mathbf{u}}]\!]_{\mathcal{S}} d\mathcal{S} \end{aligned} \tag{3.66}$$

Then, replacing (3.66) in (3.65) yields

$$\begin{aligned} \mathcal{W}_{\mathcal{S}} &= \int_{t_{SD}}^{t_\infty} \int_{\mathcal{S}} \mathcal{T} \cdot [\![\dot{\mathbf{u}}]\!]_{\mathcal{S}} d\mathcal{S} dt \\ &= \int_{\mathcal{S}} \underbrace{\int_{t_{SD}}^{t_\infty} \mathcal{T} \cdot [\![\dot{\mathbf{u}}]\!]_{\mathcal{S}} dt}_{G_{SD}} d\mathcal{S} \end{aligned} \tag{3.67}$$

where G_{SD} is the energy released on $\mathcal{S}$ per unit area in the strong discontinuity regime. If we assume that the energy released during the transition between the

bifurcation time and the inception of the strong discontinuity regime is small with respect to G_{SD}, we can readily identify G_{SD} with the fracture energy G_f.

Let us now find a more convenient expression of the kernel of (3.66) for the discrete damage model described in (3.56) to (3.62).

From (3.51) and considering that $t > t_{SD}$,

$$\begin{aligned} \dot{\tau}_{\Delta[\![\mathbf{u}]\!]} &= \frac{\partial}{\partial t}\left(\sqrt{\Delta[\![\mathbf{u}]\!]_S \cdot \mathbf{Q}^e \cdot \Delta[\![\mathbf{u}]\!]_S}\right) \\ &= \frac{\Delta[\![\mathbf{u}]\!]_S \cdot \mathbf{Q}^e \cdot [\![\dot{\mathbf{u}}]\!]_S}{\tau_{\Delta[\![\mathbf{u}]\!]}} \end{aligned} \tag{3.68}$$

Hence,

$$\Delta[\![\mathbf{u}]\!]_S \cdot \mathbf{Q}^e \cdot [\![\dot{\mathbf{u}}]\!]_S = \dot{\tau}_{\Delta[\![\mathbf{u}]\!]} \tau_{\Delta[\![\mathbf{u}]\!]}$$

Thus, in light of the discrete constitutive equation (3.57), the following equality holds:

$$\mathcal{T} \cdot [\![\dot{\mathbf{u}}]\!]_S = \underbrace{\left(\frac{q}{\Delta\bar{\alpha}} \Delta[\![\mathbf{u}]\!]_S \cdot \mathbf{Q}^e\right)}_{\mathcal{T}} \cdot [\![\dot{\mathbf{u}}]\!]_S = \frac{q}{\Delta\bar{\alpha}} (\dot{\tau}_{\Delta[\![\mathbf{u}]\!]} \tau_{\Delta[\![\mathbf{u}]\!]}) \tag{3.69}$$

By using the relation (3.52) and (3.58), we can prove that, for inelastic loading,

$$f(\mathcal{T}, q) := \tau_{\mathcal{T}} - q = 0 \Longleftrightarrow f_{\Delta[\![\mathbf{u}]\!]}(\Delta[\![\mathbf{u}]\!], \Delta\bar{\alpha}) := \tau_{\Delta[\![\mathbf{u}]\!]} - \Delta\bar{\alpha} = 0 \tag{3.70}$$

and that

$$\dot{f}_{\Delta[\![\mathbf{u}]\!]}(\Delta[\![\mathbf{u}]\!]_S, \Delta\bar{\alpha}) = \dot{\tau}_{\Delta[\![\mathbf{u}]\!]} - \dot{\bar{\alpha}} \tag{3.71}$$

From (3.61) we have that for loading $f(\mathcal{T}, q) = \dot{f}(\mathcal{T}, q) = 0$. Then from (3.70) and (3.71), equation (3.69) can be rewritten as

$$\mathcal{T} \cdot [\![\dot{\mathbf{u}}]\!]_S = q\dot{\bar{\alpha}} \tag{3.72}$$

By replacing (3.72) in the expression of G_{SD} in (3.67), we obtain

$$G_{SD} = \int_{t_{SD}}^{t_\infty} q\dot{\alpha}dt = \int_{t_{SD}}^{t_\infty} q\frac{\dot{q}}{\bar{\mathcal{H}}}dt$$
$$= \int_{q_{SD}}^{q_\infty} q\frac{1}{\bar{\mathcal{H}}}dq \tag{3.73}$$

where the discrete softening law (3.62) has been used. Now, noticing that $q_\infty = 0$ and considering the case of $\bar{\mathcal{H}}$ constant, equation (3.73) yields

$$G_{SD} = -\frac{q_{SD}^2}{2\bar{\mathcal{H}}} \tag{3.74}$$

For the case of $G_{SD} \approx G_f$, $q_{SD} \approx q_0 = r_0$. Since $r_0 = \sigma_u/\sqrt{E}$, then the following equality can be obtained from (3.74):

$$\bar{\mathcal{H}} = -\frac{\sigma_u^2}{2EG_f} \tag{3.75}$$

Remark 22 *Expression (3.75) reveals that the intrinsic softening modulus is endowed with the character of a material property.*

Chapter 4

Finite elements with embedded discontinuities: elemental enrichment

The numerical modelling of strong discontinuities in solids requires the use of non-standard formulations to enable the sharp resolution of jumps in the displacement field. Here, we study some of them within the context of the finite element method. However, it is important to mention that the strong discontinuity approach described in the preceding chapter was developed without any reference to some specific numerical method and can, therefore, be used as the underlying mathematical model to develop, in principle, numerical models based on any numerical method. In general, some type of enrichment of the standard finite element approximation is necessary to include discontinuities within an element domain. Multiple frameworks have been employed for attaining this goal. In [Simo and Oliver, 1994], the *assumed enhanced strain method* [Simo and Rifai, 1990] was used in order to model strong discontinuities. The *variational multiscale method* [Hughes, 1995] has also been used in [Garikipati and Hughes, 2000] to include discontinuities within an element domain. Lately, the partition of unit concept has been exploited for the inclusion of strong discontinuities, first in the context of Linear Fracture Mechanics [Belytschko et al., 2001], and then in the context of cohesive models [Wells and Sluys, 2001]. Applications of *multifield variational principles*[1] to embed discontinuities inside an element can be found in [Oliver et al., 2003] and [Spencer, 2002].

Although, as mentioned above, the strong discontinuity approach is independent of the numerical method used, it has classically been related to the use of

[1] As a matter of fact, the assumed enhanced strain method itself is based on a multifield variational principle.

the so-called *finite elements with embedded discontinuities*[2]. One of such elements was proposed for the first time in [Ortiz et al., 1987] to capture weak discontinuities. The inclusion of strong discontinuities was tackled in [Dvorkin et al., 1990] for quadrilaterals and in [Klisinski et al., 1991] for linear triangles. A general framework for the development of finite elements with embedded strong discontinuities regardless of the parent element was sketched in [Simo et al., 1993] and extensively explained in [Oliver, 1996b].

In [Jirasek, 2000a] a fairly comprehensive study of this type of elements can be found. There, they were classified into three groups:

- *Statically optimal symmetric elements*: the traction vector continuity is explicitly enforced at element level. Nevertheless, the symmetry of the formulation entails that the discontinuous kinematics does not guarantee free rigid motions of the two parts in which the element is split up by the discontinuity.

- *Kinematically optimal symmetric elements*: the kinematics allows to capture the free rigid motions of the two parts of an element crossed by a discontinuity line. However, because of the symmetric character of these elements, the traction vector continuity is not enforced at element level.

- *Kinematically and statically optimal non-symmetric elements*: both the kinematics that allows for rigid body relative motions and the enforcement of the traction continuity are introduced at element level. As a consequence, the resulting formulation is non-symmetric.

Based on this classification and using the multifield variational statement of the boundary value problem, [Oliver et al., 2003] studied the first and the third families of elements. The statically optimal symmetric formulation was shown to exhibit stress locking behavior. Then, the possibility of devising a statically optimal symmetric element not suffering from this pathological behavior was explored. This was motivated by the fact that, even though the kinematically and statically optimal non-symmetric formulation has shown the best performance, its optimal implementation entails the use of an algorithm for tracking the discontinuity[3]. These algorithms can become very cumbersome when the inception and propagation of multiple discontinuities has to be managed. Statically optimal symmetric elements seem not to need a tracking algorithm and would have, in principle, a self-propagating behavior, which could be exploited for simulating multiple discontinuities.

[2]The term *finite elements with embedded discontinuities* is reserved in the literature for formulations based on the *elemental enrichment* of the standard finite element approximation. In this chapter, we follow this convention. However, the term also seems adequate to refer to *nodal (partition of unity based) enrichment* (see Appendix B).

[3]Chapter 5 is devoted to studying such algorithms.

This chapter presents a study on finite elements with embedded discontinuities. In Section 4.1 the boundary value problem (BVP) is stated in a very general multifield format. Then the non-symmetric formulation is studied in Section 4.2. Its continuous and discrete[4] versions are stated. Section 4.3 presents a symmetric formulation consistent with the strong discontinuity kinematics (the *kinematically optimal symmetric element*), again in both its continuous and discrete version. Something similar is done in Section 4.4 for a symmetric element based on the assumed enhanced strain method (the *statically optimal symmetric element*). The question of the possibility of a self-propagating element is posed in Section 4.5. While exploring whether the statically optimal symmetric element is one of such elements, the problem of the stress locking effect arises and is illustrated through a representative numerical test. In Section 4.6. a mixed approach is proposed as a remedy for this stress locking, whereas in Section 4.7 an assumed re-enhanced strain strategy is presented with the same goal. The assessment of the performance of these elements is done in Section 4.8

4.1 The boundary value problem. Multifield format

Here, we reformulate the boundary value problem presented in chapter 3 as a multifield problem.

Consider the open domain Ω, with elements $\mathbf{x}$ (called material points), whose boundary is Γ. The boundary is composed of the open sets Γ_u and Γ_σ such that $\Gamma_u \cap \Gamma_\sigma = \emptyset$ and $\overline{\Gamma_u \cup \Gamma_\sigma} = \Gamma$. Prescribed displacement rates, $\hat{\dot{\mathbf{u}}}$, are imposed on Γ_u, and prescribed traction rates are imposed on Γ_σ. The material line $\mathcal{S}$ crosses Ω splitting it up into Ω^+ and Ω^- (as shown in Fig. 4.1).

In Chapter 3, the structure of the displacement field for the strong discontinuity kinematics has been presented:

$$\dot{\mathbf{u}}(\mathbf{x}, t) = \mathring{\dot{\mathbf{u}}}(\mathbf{x}, t) + H_{\mathcal{S}}\, [\![\dot{\mathbf{u}}]\!](\mathbf{x}, t) \tag{4.1}$$

Consider, now, the following vector-valued function $\mathring{\dot{\mathbf{u}}} : \Omega \times \mathbb{R}_+ \to \mathbb{R}^{n_{\text{dim}}}$ (n_{dim} is the number of dimensions of the problem), defined as

$$\mathring{\dot{\mathbf{u}}}(\mathbf{x}, t) := \mathring{\dot{\mathbf{u}}}(\mathbf{x}, t) + [\![\dot{\mathbf{u}}]\!](\mathbf{x}, t)\varphi(\mathbf{x}) \tag{4.2}$$

[4] In this chapter the term discrete refers, hereafter, to the finite element (discretized) version of a boundary value problem and not to a discrete (cohesive) constitutive model as in the preceding chapter.

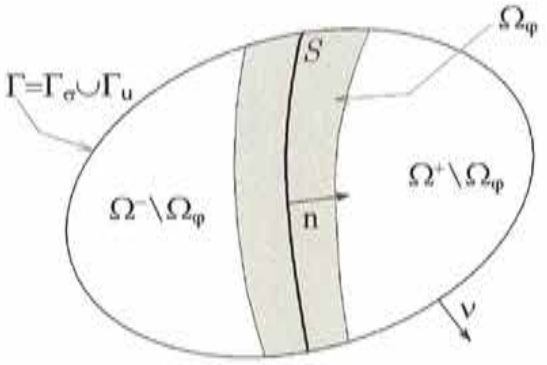

Figure 4.1: Solid with a strong discontinuity interface.

where φ is some smooth function fulfilling the following conditions:

$$\varphi(\mathbf{x}) = \begin{cases} 1 & \forall \mathbf{x} \in \Omega^+ \setminus \Omega_\varphi \\ 0 & \forall \mathbf{x} \in \Omega^- \setminus \Omega_h \end{cases} \tag{4.3}$$

with Ω_φ denoting a compact domain such that $\Omega_\varphi \subset \Omega$ and $\mathcal{S} \subset \Omega_\varphi$ in such way that Ω_φ is partitioned by $\mathcal{S}$.

Now 4.1 can be rewritten as

$$\dot{\mathbf{u}}(\mathbf{x}, t) = \dot{\hat{\mathbf{u}}}(\mathbf{x}, t) + \mathcal{M}_\mathcal{S}(\mathbf{x})\, [\![\dot{\mathbf{u}}]\!](\mathbf{x}, t) \tag{4.4}$$

where $\mathcal{M}_\mathcal{S}(\mathbf{x}) := H_\mathcal{S} - \varphi(\mathbf{x})$.

Remark 23 *Function $\mathcal{M}_\mathcal{S}$ has Ω_φ as its support, i.e., $\mathcal{M}_\mathcal{S}(\mathbf{x}) = 0\ \forall \mathbf{x} \in \Omega \setminus \Omega_\varphi$. This entails that, for a convenient choice of Ω_φ, the Dirichlet boundary conditions need to be prescribed only for $\dot{\hat{\mathbf{u}}}$ and not for $[\![\dot{\mathbf{u}}]\!]$ and that $\dot{\mathbf{u}}(\mathbf{x}, t) = \dot{\hat{\mathbf{u}}}(\mathbf{x}, t)\ \forall \mathbf{x} \in \Omega \setminus \Omega_\varphi$.*

Let us define $\mathbb{S}$ as the space of second order symmetric tensors. Consider, for a given time $t \in \mathbb{R}_+$, the following, in principle, independent fields: the displacement rate field $\dot{\mathbf{u}}(\bullet, t)$:$\Omega \to \mathbb{R}^{n_{\text{dim}}}$, the stress rate field, $\dot{\boldsymbol{\sigma}}(\bullet, t)$:$\Omega \to \mathbb{S}$, and the strain rate field, $\dot{\boldsymbol{\varepsilon}}(\bullet, t)$:$\Omega \to \mathbb{S}$. Then, the following incremental three field quasistatic boundary value problem can be stated in strong form:

$$FIND: \left\{ \begin{array}{l} \dot{\mathbf{u}} \\ \dot{\boldsymbol{\varepsilon}} \\ \dot{\boldsymbol{\sigma}} \end{array} \right. \text{ satisfying}$$

$$\begin{array}{lllll}
\nabla \cdot \dot{\boldsymbol{\sigma}} + \dot{\mathbf{b}} = 0 & in\ \Omega \backslash \mathcal{S} & \text{(internal equilibrium)} & (a) & \\
\dot{\boldsymbol{\varepsilon}} - \nabla^S \dot{\mathbf{u}} = 0 & in\ \Omega & \text{(kinematical compatibility)} & (b) & \\
\dot{\boldsymbol{\sigma}} - \dot{\Sigma}(\boldsymbol{\varepsilon}) = 0 & in\ \Omega & \text{(constitutive compatibility)} & (c) & (4.5) \\
\dot{\boldsymbol{\sigma}} \cdot \boldsymbol{\nu} = \dot{\mathbf{t}}^* & on\ \Gamma_\sigma & \text{(external equilibrim)} & (d) & \\
\underbrace{\dot{\boldsymbol{\sigma}}_{\Omega^+} \cdot \mathbf{n} - \dot{\boldsymbol{\sigma}}_{\Omega^-} \cdot \mathbf{n}}_{=: [\![\dot{\boldsymbol{\sigma}}]\!]_{\Omega \backslash \mathcal{S}} \cdot \mathbf{n}} = 0 & on\ \mathcal{S} & \text{(outer traction continuity} & (e) & \\
\underbrace{\dot{\boldsymbol{\sigma}}_{\Omega^+} \cdot \mathbf{n} - \dot{\boldsymbol{\sigma}}_{\mathcal{S}} \cdot \mathbf{n}}_{=: [\![\dot{\boldsymbol{\sigma}}]\!]_{\mathcal{S}} \cdot \mathbf{n}} = 0 & on\ \mathcal{S} & \text{(inner traction continuity)} & (f) &
\end{array}$$

where $\dot{\mathbf{b}}$ is the body force density rate, $\dot{\mathbf{t}}^*$ is the traction rate prescribed on Γ_σ, $\mathbf{n}$ is the unit normal to $\mathcal{S}$ pointing to Ω^+, $\boldsymbol{\nu}$ is the unit outward normal to Γ, and $\dot{\Sigma}$ stands for the time derivative of the constitutive function Σ, which returns the stresses, $\Sigma(\boldsymbol{\varepsilon})$, for some given strains[5], $\boldsymbol{\varepsilon}$.

Remark 24 *The function spaces for* $\dot{\mathbf{u}}$, $\dot{\boldsymbol{\varepsilon}}$, *and* $\dot{\boldsymbol{\sigma}}$ *are assumed to be defined in such a way that the Dirichlet type boundary conditions are automatically fulfilled.*

Remark 25 *The above very general statement of a quasistatic boundary value problem furnishes a framework that allows to consider other possible statements as particular cases of 4.5.*

Remark 26 *The inner traction continuity stated in (4.5-f) is non-standard in Solid Mechanics problems and is tightly related to the strong discontinuity kinematics.*

One of the possible simplifications of the above BVP statement is assuming that (4.5-c) is imposed explicitly. Then the following two field, $\dot{\mathbf{u}} - \dot{\boldsymbol{\varepsilon}}$, problem can be stated:

[5]For instance, Σ could be the stresses obtained by means of the continuum damage constitutive model described in section 2.2.

$$
\begin{array}{lllll}
FIND: \left\{ \begin{array}{l} \dot{\mathbf{u}} \\ \dot{\varepsilon} \end{array} \right. \text{ satisfying} & & & & \\
\nabla \cdot \dot{\Sigma} + \dot{\mathbf{b}} = 0 & in & \Omega \backslash \mathcal{S} & \text{(internal equilibrium)} & (a) \\
\dot{\varepsilon} - \boldsymbol{\nabla}^S \dot{\mathbf{u}} = 0 & in & \Omega & \text{(kinematical compatibility)} & (b) \\
\dot{\Sigma} \cdot \boldsymbol{\nu} = \dot{\mathbf{t}}^* & on & \Gamma_\sigma & \text{(external equilibrim)} & (c) \\
\underbrace{\dot{\Sigma}_{\Omega^+} \cdot \mathbf{n} - \dot{\Sigma}_{\Omega^-} \cdot \mathbf{n}}_{=: [\![\dot{\Sigma}]\!]_{\Omega \backslash \mathcal{S}} \cdot \mathbf{n}} = 0 & on & \mathcal{S} & \text{(outer traction continuity} & (d) \\
\underbrace{\dot{\Sigma}_{\Omega^+} \cdot \mathbf{n} - \dot{\Sigma}_{\mathcal{S}} \cdot \mathbf{n}}_{=: [\![\dot{\Sigma}]\!]_{\mathcal{S}} \cdot \mathbf{n}} = 0 & on & \mathcal{S} & \text{(inner traction continuity)} & (e)
\end{array}
\tag{4.6}
$$

4.2 Non-symmetric formulation

Based on (4.6), a convenient weak form is devised in this section. First of all, let us work with the displacement field stated in (4.4). In light of that kinematics, let us define the space of the displacement rate as follows:

$$\mathcal{V}_{\mathbf{u}} := \mathcal{V}_{\hat{\mathbf{u}}} \oplus \mathcal{V}_{\mathbf{u}'} \tag{4.7}$$

with

$$\mathcal{V}_{\hat{\mathbf{u}}} := \left\{ \hat{\boldsymbol{\eta}} \in [\mathsf{H}^1(\Omega)]^{n_{\text{dim}}} \quad ; \quad \hat{\boldsymbol{\eta}}|_{\Gamma_u} = \dot{\mathbf{u}}^* \right\} \tag{4.8}$$

where $\dot{\mathbf{u}}^*$ stands for the essential boundary conditions prescribed on Γ_u and $\mathsf{H}^1(\Omega)$ is the space of square integrable functions defined in Ω whose first derivatives are also square integrable[6], and

$$\mathcal{V}_{\mathbf{u}'} := \{ \boldsymbol{\eta}' = \mathcal{M}_{\mathcal{S}}\, \boldsymbol{\alpha} \; ; \boldsymbol{\alpha}_{\mathcal{S}} \equiv \boldsymbol{\alpha}|_{\mathcal{S}} \in \mathcal{V}_{\alpha} \} \tag{4.9}$$

where

$$\mathcal{V}_{\alpha} := [\mathsf{L}_2(\mathcal{S})]^{n_{\text{dim}}} \tag{4.10}$$

$\mathsf{L}_2(\mathcal{S})$ stands for the space of square integrable functions defined on $\mathcal{S}$.

[6] In one dimension the functions in $\mathsf{H}^1(\Omega)$ are continuous.

Remark 27 *Expression (4.7) can be understood within the framework of the variational multiscale method [Hughes, 1995] as the additive decomposition of the displacement field into a* coarse scale *and a* fine scale*, the latter resolves the jumps in the displacement field.*

Let us, now, define the space of admissible displacement rate variations, $\mathcal{V}_{\bar{\boldsymbol{\eta}}}$, as

$$\mathcal{V}_{\bar{\boldsymbol{\eta}}} := \left\{ \bar{\boldsymbol{\eta}} \in [\mathrm{H}^1(\Omega)]^{n_{\mathrm{dim}}} \quad ; \quad \bar{\boldsymbol{\eta}}|_{\Gamma_u} = \mathbf{0} \right\} \tag{4.11}$$

4.2.1 Continuum Problem

Assuming the kinematical compatibility (4.6-b) as explicitly imposed, then, with the above definitions in hand, let us state the following problem:

FIND

$$\dot{\mathbf{u}} \in \mathcal{V}_{\mathbf{u}} \Leftrightarrow \left\{ \begin{array}{c} \dot{\mathbf{u}} \in \mathcal{V}_{\dot{\mathbf{u}}} \\ \mathbf{u}' \in \mathcal{V}_{\mathbf{u}'} \end{array} \right.$$

SUCH THAT

$$\begin{array}{lll} \displaystyle\int_{\Omega\backslash\mathcal{S}} \dot{\Sigma}(\nabla^S \mathbf{u}) : \nabla^S \bar{\boldsymbol{\eta}}\, d\Omega - G_{ext}(\bar{\boldsymbol{\eta}}) = 0 & \forall \bar{\boldsymbol{\eta}} \in \mathcal{V}_{\bar{\boldsymbol{\eta}}} & (a) \\ \displaystyle\int_{\mathcal{S}} \boldsymbol{\alpha}_{\mathcal{S}} \cdot [\![\dot{\Sigma}]\!]_{\mathcal{S}} \cdot \mathbf{n}\, d\mathcal{S} = 0 & \forall \boldsymbol{\alpha}_{\mathcal{S}} \in \mathcal{V}_{\boldsymbol{\alpha}} & (b) \end{array} \tag{4.12}$$

where $G_{ext}(\bar{\boldsymbol{\eta}}) := \int_{\Omega\backslash\mathcal{S}} \dot{\mathbf{b}} \cdot \bar{\boldsymbol{\eta}}\, d\Omega + \int_{\Gamma_\sigma} \dot{\mathbf{t}}^* \cdot \bar{\boldsymbol{\eta}}\, d\Gamma$

By using standard arguments, one can prove that the strong form of (4.12-a) is

$$\begin{array}{ll} \nabla \cdot \dot{\Sigma}(\nabla^S \mathbf{u}) + \dot{\mathbf{b}} = \mathbf{0} & in\ \Omega\backslash\mathcal{S} \\ \dot{\Sigma} \cdot \boldsymbol{\nu} = \dot{\mathbf{t}}^* & on\ \Gamma_\sigma \\ [\![\dot{\Sigma}]\!]_{\Omega\backslash\mathcal{S}} \cdot \mathbf{n} = \mathbf{0} & on\ \mathcal{S} \end{array}$$

whereas the strong form of (4.12-b) is

$$[\![\dot{\Sigma}]\!]_{\mathcal{S}} \cdot \mathbf{n} = \mathbf{0} \quad on\ \mathcal{S}$$

Remark 28 *The choice of the spaces $\mathcal{V}_{\mathbf{u}}$ and $\mathcal{V}_{\bar{\boldsymbol{\eta}}}$ and the particular way of imposing the inner traction continuity in (4.12-b) are determinant for the nonsymmetric character of this formulation.*

Remark 29 *For the expression (4.12-b) to make sense, $[\![\dot{\Sigma}_{\mathcal{S}}]\!] \in \mathsf{L}_2(\mathcal{S};\mathbb{S})$ must hold. This smoothness of $[\![\dot{\Sigma}_{\mathcal{S}}]\!]$ can be guaranteed on the basis of the results obtained, by means of the strong discontinuity analysis, in the preceding chapter stating the bounded character of the stresses, despite the unbounded character of the strains in $\mathcal{S}$.*

4.2.2 Finite element discretization

With regard to the discretized versions of the problems presented in this chapter, only the two-dimensional case is treated. Thus, consider a two-dimensional domain Ω discretized into a finite element mesh with n_{elem} four-noded elements[7] and n_{node} nodes and crossed by the interface $\mathcal{S}$. Then, assume that some tracking algorithm determines the set $\mathcal{J}$ of elements crossed by the discontinuity interface at a given time t, i.e.,

$$\mathcal{J} := \{e \mid \Omega_e \cap \mathcal{S} \neq \emptyset\} \tag{4.13}$$

Let us also define

$$\mathcal{I} := \{1, ..., n_{elem}\} \tag{4.14}$$

The above mentioned tracking algorithm also provides the position of the elemental discontinuity $\mathcal{S}_e$ of length l_e within an element domain, Ω_e, which defines the domains $\Omega_e^+ := \Omega^+ \cap \Omega_e$ and $\Omega_e^- := \Omega^- \cap \Omega_e$ and the nodes $i^+ \in \overline{\Omega}^+$ and $i^- \in \overline{\Omega}^-$. With this in hand, the finite element approximation for the displacement rate field, $\dot{\mathbf{u}}$, proposed in [Oliver, 1996b], is adopted:

$$\dot{\mathbf{u}}^{h^{(e)}}(\mathbf{x},t) = \underbrace{\Sigma_{i=1}^{i=4}\, N_i^{(e)}(\mathbf{x})\dot{\mathbf{d}}_i(t)}_{\dot{\mathbf{u}}^{h^{(e)}}} + \underbrace{\mathcal{M}_S^{(e)}(\mathbf{x})\,[[\dot{\mathbf{u}}]]_e(t)}_{\dot{\mathbf{u}}'^{,h^{(e)}}} \tag{4.15}$$

where $\dot{\mathbf{u}}^{h^{(e)}}$ is the standard $\mathcal{C}^0$ elemental approximation of the rate of displacement field, interpolated by the bilinear element shape functions, $N_1^{(e)}$, $N_2^{(e)}$, $N_3^{(e)}$, $N_4^{(e)}$, and parametrized by the nodal values of the displacement rate $\dot{\mathbf{d}}_i(t)$, for $i \in \{1,..,4\}$. The term $\dot{\mathbf{u}}'^{,h^{(e)}}$ resolves the jumps in the rate of displacement field in terms of the

[7] Only four-noded quadrilaterals are considered as parent elements in this chapter. However, the application of the ideas presented here to formulations having linear triangles as parent elements is straightforward.

elemental displacement rate jump $[\![\dot{\mathbf{u}}]\!]_e$, which is element-wise constant, with $\mathcal{M}_S^{(e)}$ defined as follows:

$$\mathcal{M}_S^{(e)}(\mathbf{x}) = \left\{ \begin{array}{c} 0 \\ H_S^{(e)}(\mathbf{x}) - \varphi^{(e)} \\ (\varphi^{(e)} = \Sigma_{i^+=1}^{n_e^+} N_{i^+}) \end{array} \right\} \quad \begin{array}{l} \forall\, e \notin \mathcal{J} \\ \forall\, e \in \mathcal{J} \end{array} \tag{4.16}$$

n_e^+ stands for the number of nodes of element e that belong to $\overline{\Omega}^+$, and $H_S^{(e)}$ is the step function acting on $\mathcal{S}_e$.

From (4.6-b), (4.15), and (4.16) the discrete strain rate field at element level reads

$$[\dot{\boldsymbol{\varepsilon}}^h]^{(e)} = \Sigma_{i=1}^{i=4} \left(\nabla N_i^{(e)} \otimes \dot{\mathbf{d}}_i\right)^S - \left(\boldsymbol{\nabla}\varphi^{(e)} \otimes [\![\dot{\mathbf{u}}]\!]_e\right)^S + \mu_S^{(e)} \frac{1}{k} \left([\![\dot{\mathbf{u}}]\!]_e \otimes \mathbf{n}\right)^S \tag{4.17}$$

where for numerical purposes, the regularized version of the Dirac delta, δ_S, has been adopted:

$$\delta_S^{(e)} \approx \mu_S^{(e)} \frac{1}{k} \tag{4.18}$$

with $\mu_S^{(e)}$ being a collocation function whose support is a band $\mathcal{S}_e^k$ of thickness k having $\mathcal{S}_e$ as its middle line. This collocation function is defined as

$$\begin{array}{ll} \mu_S^{(e)}(\mathbf{x}) = 1 & \forall\, \mathbf{x} \in \mathcal{S}_e^k \\ \mu_S^{(e)}(\mathbf{x}) = 0 & \forall\, \mathbf{x} \notin \mathcal{S}_e^k \end{array} \tag{4.19}$$

Remark 30 *The regularization parameter k does not depend on the dimensions of the element and can be as small as allowed by the machine precision.*

Moreover, the element is furnished with an additional sampling point, named SSP (singular sampling point) and placed at the centroid of the element, that represents the material points in $\mathcal{S}_e^k$ and whose associated area is

$$meas(\mathcal{S}_e^k) = k l_e \tag{4.20}$$

A sampling point representing the stress state of the material points in $\Omega \backslash \mathcal{S}_e^k$, named RSP (regular sampling point) and placed at the centroid of the element as

well, is also added. The discontinuous bifurcation analysis studied in Chapter 2 is performed in RSP. This entails the normal, $\mathbf{n}$, being element-wise constant.

Now, based on the finite element approximation of the displacement rate field presented in (4.15), we can define the following function spaces:

$$\mathcal{V}_{\mathbf{u}}^h = \mathcal{V}_{\hat{\mathbf{u}}}^h \oplus \mathcal{V}_{\mathbf{u}'}^h \tag{4.21}$$

where

$$\begin{array}{l} \mathcal{V}_{\alpha}^h := \left\{ \boldsymbol{\alpha}^h;\ \boldsymbol{\alpha}^h(\mathbf{x}) = \boldsymbol{\alpha}_e\ \forall e \in \mathcal{J};\ \ \boldsymbol{\alpha}^h(\mathbf{x}) = 0\ \ \forall e \notin \mathcal{J} \right\} \\ \mathcal{V}_{\hat{\mathbf{u}}}^h := \left\{ \hat{\boldsymbol{\eta}}^h;\ \hat{\boldsymbol{\eta}}^h(\mathbf{x}) = \Sigma_{i=1}^{i=n_{node}} N_i(\mathbf{x})\, \hat{\boldsymbol{\eta}}_i;\ \hat{\boldsymbol{\eta}}_i|_{\Gamma_u} = \dot{\mathbf{u}}^* \right\} \\ \mathcal{V}_{\mathbf{u}'}^h := \left\{ \boldsymbol{\eta}'^h;\ \boldsymbol{\eta}'^h(\mathbf{x}) = \Sigma_{e\in\mathcal{J}}\, \mathcal{M}_{\mathcal{S}}^{(e)}(\mathbf{x})\boldsymbol{\alpha}_e \right\} \end{array} \tag{4.22}$$

with $\boldsymbol{\alpha}_e, \boldsymbol{\eta}_i \in \mathbb{R}^2$, and

$$\mathcal{V}_{\bar{\eta}}^h := \left\{ \bar{\boldsymbol{\eta}}^h;\ \bar{\boldsymbol{\eta}}^h(\mathbf{x}) = \Sigma_{i=1}^{i=n_{node}}\ N_i(\mathbf{x})\, \bar{\boldsymbol{\eta}}_i \quad ;\ \bar{\boldsymbol{\eta}}_i|_{\Gamma_u} = 0 \right\} \tag{4.23}$$

where $\bar{\boldsymbol{\eta}}_i \in \mathbb{R}^2$.

4.2.3 Discrete non-symmetric problem

Now the following discrete problem can be stated:

FIND:

$$\dot{\mathbf{u}}^h \in \mathcal{V}_{\mathbf{u}}^h \Leftrightarrow \left\{ \begin{array}{c} \dot{\hat{\mathbf{u}}}^h \in \mathcal{V}_{\hat{\mathbf{u}}}^h \\ [\![\dot{\mathbf{u}}]\!]^h \in \mathcal{V}_{\alpha}^h \end{array} \right. \tag{4.24}$$

SUCH THAT:

$$\begin{array}{ll} \Sigma_{e=1}^{e=n_{elem}} \displaystyle\int_{\Omega_e} \nabla^S \bar{\boldsymbol{\eta}}^h : \dot{\Sigma}(\boldsymbol{\varepsilon}^h) d\Omega\ - G_{ext}(\bar{\boldsymbol{\eta}}^h) = 0 & \forall \bar{\boldsymbol{\eta}}^h \in \mathcal{V}_{\bar{\eta}}^h \\ \Sigma_{e\in\mathcal{J}} \displaystyle\int_{S_e} \boldsymbol{\alpha}^h \cdot [\![\dot{\Sigma}]\!]_S \cdot \mathbf{n} dS = 0 & \forall \boldsymbol{\alpha}^h\ \in \mathcal{V}_{\alpha}^h \end{array} \tag{4.25}$$

4.2.4 Matrix representation

Using the standard *B-format* [Hughes, 1987], the matrix representation of the discrete strain rate field (4.17) reads

$$\{\dot{\varepsilon}\}^{(e)} = \mathbf{B}^{(e)}\dot{\mathbf{d}}^{(e)} + \left(\mu_S^{(e)}\frac{1}{k}\,[\mathbf{n}]^{(e)} - \left[\nabla\varphi^{(e)}\right]\right)[\![\dot{\mathbf{u}}]\!]_e \tag{4.26}$$

where

$$\dot{\mathbf{d}}^{(e)} = \left[\ \dot{\mathbf{d}}_1^T,\ \ \dot{\mathbf{d}}_2^T,\ \ \dot{\mathbf{d}}_3^T,\ \ \dot{\mathbf{d}}_4^T\ \right]^T \tag{4.27}$$

with $(\bullet)^T$ denoting the transpose of $(\bullet)$,

$$\begin{aligned} \mathbf{B}^{(e)} &= \left[\ \mathbf{B}_1^{(e)},\ \ \mathbf{B}_2^{(e)},\ \ \mathbf{B}_3^{(e)},\ \ \mathbf{B}_4^{(e)}\ \right] \\ \mathbf{B}_i^{(e)} &= \begin{bmatrix} \partial_x N_i^{(e)} & 0 \\ 0 & \partial_y N_i^{(e)} \\ \partial_y N_i^{(e)} & \partial_x N_i^{(e)} \end{bmatrix} \end{aligned} \tag{4.28}$$

and

$$[\boldsymbol{\nabla}\varphi]^{(e)} = \begin{bmatrix} \partial_x\varphi^{(e)} & 0 \\ 0 & \partial_y\varphi^{(e)} \\ \partial_y\varphi^{(e)} & \partial_x\varphi^{(e)} \end{bmatrix}; \qquad [\mathbf{n}]^{(e)} = \begin{bmatrix} n_x & 0 \\ 0 & n_y \\ n_y & n_x \end{bmatrix} \tag{4.29}$$

We also have that, in matrix form,

$$\{\nabla^S\bar{\boldsymbol{\eta}}\} = \mathbf{B}^{(e)}\{\bar{\boldsymbol{\eta}}\}^{(e)} \tag{4.30}$$

with

$$\{\bar{\boldsymbol{\eta}}\}^{(e)} = \left[\ \bar{\boldsymbol{\eta}}_1^T,\ \ \bar{\boldsymbol{\eta}}_2^T,\ \ \bar{\boldsymbol{\eta}}_3^T,\ \ \bar{\boldsymbol{\eta}}_4^T\ \right]^T \tag{4.31}$$

Now, we can write the expression of the element level incremental residual forces corresponding to (4.25):

$$\begin{aligned} \dot{\mathbf{R}}^{(e)} &:= \int_{\Omega_e} \mathbf{B}^{(e)^T}\ \{\dot{\Sigma}\}^{(e)}\ d\Omega - \dot{\mathbf{F}}_{ext}^{(e)} && (a) \\ \dot{\mathbf{r}}^{(e)} &:= \int_{\mathcal{S}_e} [\mathbf{n}]^{(e)^T}\ \left[\{\dot{\Sigma}_{\mathcal{S}_e}\}^{(e)} - \{\dot{\Sigma}_{\Omega^+}\}^{(e)}\right] d\mathcal{S} && (b) \end{aligned} \tag{4.32}$$

where $\dot{\mathbf{F}}_{ext}^{(e)}$ is the vector of incremental external forces at element level.

Assume that the constitutive function rate (which in this formulation coincides with the stress rate field), $\dot{\Sigma}$, can be expressed in matrix form as

$$\{\dot{\Sigma}\}^{(e)} = \mathbf{D}\{\dot{e}\}^{(e)} \tag{4.33}$$

with $\mathbf{D}$ being the matrix representation of the constitutive tangent operator, assumed to be symmetric.

Now, let us approximate the stresses in Ω_e^+ belonging to the neighborhood of $\mathcal{S}_e$ by

$$\frac{1}{l_e}\int_{\mathcal{S}_e}\{\dot{\Sigma}_{\Omega^+}\}^{(e)}d\mathcal{S} \approx \frac{1}{\Omega_e}\int_{\Omega_e}\{\dot{\Sigma}_{\Omega^+}\}^{(e)}d\Omega \tag{4.34}$$

where $\Omega_e := \int_{\Omega_e} d\Omega$ and $l_e = \int_{\mathcal{S}_e} d\mathcal{S}$. Hence, the second term of (4.32-b) can be rewritten:

$$\begin{aligned}\int_{\mathcal{S}_e}[\mathbf{n}]^{(e)^T}\ \{\dot{\Sigma}_{\Omega^+}\}^{(e)}d\mathcal{S} &= \frac{l_e}{\Omega_e}\int_{\Omega_e}[\mathbf{n}]^{(e)T}\{\dot{\Sigma}_{\Omega^+}\}^{(e)}d\Omega \\ &= \int_{\Omega_e}\frac{l_e}{\Omega_e}[\mathbf{n}]^{(e)T}\{\dot{\Sigma}_{\Omega^+}\}^{(e)}d\Omega \end{aligned}\tag{4.35}$$

where the fact of $[\mathbf{n}]^{(e)}$ being element-wise constant has been considered.

Remark 31 *In case of element-wise constant $\{\dot{\Sigma}_{\Omega^+}\}^{(e)}$, (4.34) is not an approximation but an identity.*

Notice that the first term of (4.32-b) can be expressed as follows:

$$\int_{\mathcal{S}_e}[\mathbf{n}]^{(e)^T}\ \{\dot{\Sigma}_{\mathcal{S}_e}\}^{(e)}d\mathcal{S} = \int_{\mathcal{S}_e^k}\frac{1}{k}[\mathbf{n}]^{(e)^T}\ \{\dot{\Sigma}_{\mathcal{S}_e}\}^{(e)}d\mathcal{S}^k \tag{4.36}$$

where $d\mathcal{S}^k = kd\mathcal{S}$ (k is the regularization parameter).

Remark 32 *Expression (4.36) is convenient for numerical purposes and is compatible with the character of the singular sampling point, SSP, whose associated area was defined in (4.20).*

Let us define the following matrices:

$$\mathbf{G}^{*(e)} := (\mu_S^{(e)} \frac{1}{k} - \frac{l_e}{\Omega_e}) \, [\mathbf{n}]^{(e)^T} \tag{4.37}$$

and

$$\mathbf{G}^{(e)} := \mu_S^{(e)} \frac{1}{k} \, [\mathbf{n}]^{(e)} - \left[\nabla \varphi^{(e)}\right] \tag{4.38}$$

Then, in light of (4.26), (4.33), (4.35), and (4.36), and considering definitions (4.37) and (4.38), the elemental residual forces (4.32) can be rephrased as

$$\begin{bmatrix} \mathbf{K}_{dd}^{(e)} & \mathbf{K}_{d\alpha}^{(e)} \\ \mathbf{K}_{\alpha d}^{(e)} & \mathbf{K}_{\alpha\alpha}^{(e)} \end{bmatrix} \begin{Bmatrix} \dot{\mathbf{d}}^{(e)} \\ [\![\dot{\mathbf{u}}]\!]_e \end{Bmatrix} - \begin{Bmatrix} \dot{\mathbf{F}}_{ext}^{(e)} \\ \mathbf{0} \end{Bmatrix} = \begin{Bmatrix} \dot{\mathbf{R}}^{(e)} \\ \dot{\mathbf{r}}^{(e)} \end{Bmatrix} \tag{4.39}$$

with

$$\begin{aligned} \mathbf{K}_{dd}^{(e)} &= \int_{\Omega_e} \mathbf{B}^{(e)^T} \, \mathbf{D} \, \mathbf{B}^{(e)} d\Omega \\ \mathbf{K}_{d\alpha}^{(e)} &= \int_{\Omega_e} \mathbf{B}^{(e)^T} \, \mathbf{D} \, \mathbf{G}^{(e)} d\Omega \\ \mathbf{K}_{\alpha d}^{(e)} &= \int_{\Omega_e} \mathbf{G}^{*(e)} \, \mathbf{D} \, \mathbf{B}^{(e)} d\Omega \\ \mathbf{K}_{\alpha\alpha}^{(e)} &= \int_{\Omega_e} \mathbf{G}^{*(e)} \, \mathbf{D} \, \mathbf{G}^{(e)} d\Omega \end{aligned} \tag{4.40}$$

Remark 33 *The fact of* $\mathbf{G}^{(e)^T} \neq \mathbf{G}^{*(e)}$ *entails that the resulting tangent stiffness matrix of this formulation is non-symmetrical.*

Remark 34 *Due to their elemental support, the modes corresponding to the displacement jumps,* $[[\dot{\mathbf{u}}]]_e$*, can be condensed at element level.*

Remark 35 *It is easy to prove that* $\int_{\Omega_e} \mathbf{G}^{*(e)} d\Omega = \mathbf{0}$*, which ensures the satisfaction of the patch test (see [Simo and Rifai, 1990]).*

In order to express (4.39) in a more compact way, let us define

$$\begin{aligned} \bar{\mathbf{B}}^{(e)} &= \left[\mathbf{B}_1^{(e)}, \ \mathbf{B}_2^{(e)}, \ \mathbf{B}_3^{(e)}, \ \mathbf{B}_4^{(e)}, \ \mathbf{G}^{(e)} \right] \\ \bar{\mathbf{B}}_*^{(e)} &= \left[\mathbf{B}_1^{(e)}, \ \mathbf{B}_2^{(e)}, \ \mathbf{B}_3^{(e)}, \ \mathbf{B}_4^{(e)}, \ \mathbf{G}^{*(e)} \right] \end{aligned} \tag{4.41}$$

and

$$\begin{aligned}\dot{\bar{\mathbf{R}}}^{(e)} &= \left[\ (\dot{\bar{\mathbf{R}}}^{(e)})^T,\ \ \dot{\mathbf{r}}^{(e)^T}\ \right]^T \\ \dot{\bar{\mathbf{F}}}^{(e)}_{ext} &= \left[\ (\dot{\bar{\mathbf{F}}}^{(e)}_{ext})^T,\ \ \mathbf{0}^T\ \right]^T \\ \dot{\bar{\mathbf{d}}}^{(e)} &= \left[\ (\dot{\mathbf{d}}^{(e)})^T\ \ [\![\dot{\mathbf{u}}]\!]^T_e\ \right]^T\end{aligned} \tag{4.42}$$

Then (4.39), can be stated in *B-bar* format [Simo and Hughes, 1998] as

$$\int_{\Omega_e} \bar{\mathbf{B}}^{(e)^T}_* \ \mathbf{D}\ \bar{\mathbf{B}}^{(e)} \dot{\bar{\mathbf{d}}}^{(e)} d\Omega - \dot{\bar{\mathbf{F}}}^{(e)}_{ext} = \dot{\bar{\mathbf{R}}}^{(e)} \tag{4.43}$$

Finally, the global system of equations corresponding to (4.25) is given by

$$\overset{n_{elem}}{\underset{e=1}{\mathcal{A}}} \left[\int_{\Omega_e} \bar{\mathbf{B}}^{(e)^T}_* \ \mathbf{D}\ \bar{\mathbf{B}}^{(e)} \dot{\bar{\mathbf{d}}}^{(e)} d\Omega - \dot{\bar{\mathbf{F}}}^{(e)}_{ext} = 0 \right] \tag{4.44}$$

where $\mathcal{A}$ is the standard assembly operator [Hughes, 1987].

4.3 Symmetric kinematically consistent formulation

For the symmetric kinematically consistent formulation[8], the function space corresponding to the displacement rate field is the same as the one defined for the non-symmetric formulation presented in Section 4.2:

$$\mathcal{V}_{\mathbf{u}} := \mathcal{V}_{\hat{\mathbf{u}}} \oplus \mathcal{V}_{\mathbf{u}'} \tag{4.45}$$

with

$$\mathcal{V}_{\hat{\mathbf{u}}} := \left\{ \hat{\boldsymbol{\eta}} \in [\mathrm{H}^1(\Omega)]^{n_{\dim}} \quad ; \quad \hat{\boldsymbol{\eta}}|_{\Gamma_u} = \dot{\mathbf{u}}^* \right\} \tag{4.46}$$

where $\dot{\mathbf{u}}^*$ stands for the essential boundary conditions prescribed on Γ_u, and

[8] Here we use the term *consistent* (as in [Oliver et al., 2003]) instead of *optimal* (as in [Jirasek, 1998]), because the former seems more appropriate in the context of the functional framework that we use throughout this chapter.

$$\mathcal{V}_{\mathbf{u}'} := \{\boldsymbol{\eta}' = \mathcal{M}_S\,\boldsymbol{\alpha}\ ;\boldsymbol{\alpha}_S \equiv \boldsymbol{\alpha}|_S \in \mathcal{V}_{\boldsymbol{\alpha}}\} \tag{4.47}$$

with $\mathcal{V}_{\boldsymbol{\alpha}}:=[\mathsf{L}_2(\mathcal{S})]^{n_{dim}}$

Nevertheless, this time the function space for the admissible variations of the displacement rate field is

$$\mathcal{V}_{\boldsymbol{\eta}} := \mathcal{V}_{\bar{\boldsymbol{\eta}}} \oplus \mathcal{V}_{\mathbf{u}'} \tag{4.48}$$

with

$$\mathcal{V}_{\bar{\boldsymbol{\eta}}} := \{\bar{\boldsymbol{\eta}} \in [\mathsf{H}^1(\Omega)]^{n_{dim}} \quad ; \quad \bar{\boldsymbol{\eta}}|_{\Gamma_u} = \mathbf{0}\} \tag{4.49}$$

Remark 36 *The spaces $\mathcal{V}_{\mathbf{u}}$ and $\mathcal{V}_{\bar{\boldsymbol{\eta}}}$ only differ in the Dirichlet boundary conditions, which are homogenous for the latter. From this fact, one can foresee the symmetric character of the resulting formulation.*

4.3.1 Continuum Problem

Then the following boundary value problem can be stated:

FIND

$$\dot{\mathbf{u}} \in \mathcal{V}_{\mathbf{u}} \Leftrightarrow \left\{ \begin{array}{l} \dot{\hat{\mathbf{u}}} \in \mathcal{V}_{\hat{\mathbf{u}}} \\ \dot{\mathbf{u}}' \in \mathcal{V}_{\mathbf{u}'} \end{array} \right. \tag{4.50}$$

SUCH THAT

$$\begin{array}{lll} \displaystyle\int_{\Omega\backslash\mathcal{S}} \dot{\Sigma}(\nabla^S\mathbf{u}) : \nabla^S\bar{\boldsymbol{\eta}}\,d\Omega - G_{ext}(\bar{\boldsymbol{\eta}}) = 0 & \forall\bar{\boldsymbol{\eta}} \in \mathcal{V}_{\bar{\boldsymbol{\eta}}} & (a) \\ \displaystyle\int_{\Omega} \dot{\Sigma}(\nabla^S\mathbf{u}) : \nabla^S\boldsymbol{\eta}'\,d\Omega - G_{ext}(\boldsymbol{\eta}') = 0 & \forall\boldsymbol{\eta}' \in \mathcal{V}_{\mathbf{u}'} & (b) \end{array} \tag{4.51}$$

where $G_{ext}(\bullet) := \int_\Omega \dot{\mathbf{b}} \cdot (\bullet)\,d\Omega + \int_{\Gamma_\sigma} \dot{\mathbf{t}}^* \cdot (\bullet)\,d\Gamma$.

On the basis of standard arguments, one can prove that the strong form of (4.51-a) is

$$\begin{array}{lll} \nabla \cdot \dot{\Sigma}(\nabla^S\mathbf{u}) + \dot{\mathbf{b}} = 0 & in\ \Omega\backslash\mathcal{S} & (a) \\ \dot{\Sigma} \cdot \boldsymbol{\nu} = \dot{\mathbf{t}}^* & on\ \Gamma_\sigma & (b) \\ [\![\dot{\Sigma}]\!]_{\Omega\backslash\mathcal{S}} \cdot \mathbf{n} = \mathbf{0} & on\ \mathcal{S} & (c) \end{array} \tag{4.52}$$

With regard to (4.51-b), the following proposition can be stated:

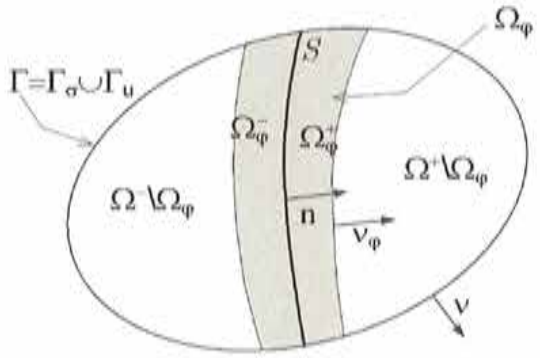

Figure 4.2: Solid with a strong discontinuity interface and surrounded by the domain Ω_φ.

Proposition 1 *Equations (4.12-b) and (4.51-b) are equivalent.*

Proof: This proof is based on the one presented in [Simo and Oliver, 1994].

By definition,

$$\boldsymbol{\eta}' = \mathcal{M}_S \, \boldsymbol{\alpha} \tag{4.53}$$

where, from Section 4.1,

$$\mathcal{M}_S(\mathbf{x}) := H_S - \varphi(\mathbf{x}) \tag{4.54}$$

with $\varphi(\mathbf{x})$ defined in (4.3).

Then, the left hand side of (4.51-b) can be rephrased as

$$\int_{\Omega_\varphi} \dot{\Sigma} : \nabla^S \boldsymbol{\eta}' \, d\Omega - G_{ext}(\boldsymbol{\eta}') = \int_{\Omega_\varphi} \dot{\Sigma} : \nabla^S \boldsymbol{\eta}' \, d\Omega - \int_{\Omega_\varphi} \mathcal{M}_S \, \dot{\mathbf{b}} \cdot \boldsymbol{\alpha} \, d\Omega \tag{4.55}$$

where the fact that $\text{supp}[\mathcal{M}_S] = \Omega_\varphi \subset \Omega$ and the assumption that $\Gamma \cap \bar{\Omega}_\varphi$ is traction free have been used.

From (4.53) and (4.54), we have that

$$\begin{aligned} \nabla^S \boldsymbol{\eta}' &= \nabla^S \mathcal{M}_S \otimes \boldsymbol{\alpha} + \mathcal{M}_S \nabla^S \boldsymbol{\alpha} \\ &= (\delta_S \mathbf{n} \otimes \boldsymbol{\alpha})^S - (\nabla \varphi \otimes \boldsymbol{\alpha})^S + \mathcal{M}_S \nabla^S \boldsymbol{\alpha} \end{aligned} \tag{4.56}$$

Replacing (4.56) into the first term of the right hand side of (4.55) yields

$$\begin{aligned}
&\int_{\Omega_\varphi} \dot{\Sigma} : \nabla^S \boldsymbol{\eta}' \, d\Omega = \\
&\int_{\Omega_\varphi} \dot{\Sigma} : \left[(\delta_S \mathbf{n} \otimes \boldsymbol{\alpha})^S - (\nabla\varphi \otimes \boldsymbol{\alpha})^S + \mathcal{M}_S \nabla^S \boldsymbol{\alpha} \right] d\Omega = \\
&\int_{\Omega_\varphi} \left[\dot{\Sigma} : (\delta_S \mathbf{n} \otimes \boldsymbol{\alpha})^S - \dot{\Sigma} : (\nabla\varphi \otimes \boldsymbol{\alpha})^S + \dot{\Sigma} : \mathcal{M}_S \nabla^S \boldsymbol{\alpha} \right] d\Omega
\end{aligned} \tag{4.57}$$

Let us work with the second term of (4.57). From (4.52-a) and considering the symmetry of $\dot{\Sigma}$, we have

$$\begin{aligned}
&\int_{\Omega_\varphi} \dot{\Sigma} : (\nabla\varphi \otimes \boldsymbol{\alpha}) \, d\Omega = \\
&\int_{\Omega_\varphi} \nabla \cdot (\varphi \dot{\Sigma} \cdot \boldsymbol{\alpha}) d\Omega - \int_{\Omega_\varphi} \varphi \left[(\nabla \cdot \dot{\Sigma}) \cdot \boldsymbol{\alpha} + \dot{\Sigma} : \nabla\boldsymbol{\alpha} \right] d\Omega = \\
&\int_{\partial\Omega_\varphi} \varphi \left[(\dot{\Sigma} \cdot \boldsymbol{\alpha}) \cdot \boldsymbol{\nu}_\varphi \right] d\Gamma + \int_{\Omega_\varphi} \varphi \left[\dot{\mathbf{b}} \cdot \boldsymbol{\alpha} - \dot{\Sigma} : \nabla\boldsymbol{\alpha} \right] d\Omega
\end{aligned} \tag{4.58}$$

where $\partial\Omega_\varphi$ denotes the boundary of Ω_φ, with outward normal $\boldsymbol{\nu}_\varphi$. It is composed of the open sets Γ_φ^+ and Γ_φ^- such that $\partial\Omega_\varphi = \overline{\Gamma_\varphi^+ \cup \Gamma_\varphi^-}$, $\Gamma_\varphi^+ \cap \Gamma_\varphi^- = \emptyset$, $\Gamma_\varphi^+ \subset \Omega^+$, and $\Gamma_\varphi^- \subset \Omega^-$. Moreover, Ω_φ, as said in Section 4.1, is partitioned by $\mathcal{S}$ into $\Omega_\varphi^+ = \Omega_\varphi \cap \Omega^+$ and $\Omega_\varphi^- = \Omega_\varphi \cap \Omega^-$. Thus, considering that, by definition, $\varphi|_{\Gamma_\varphi^+} = 1$ and $\varphi|_{\Gamma_\varphi^-} = 0$, (4.58) can be rewritten as

$$\begin{aligned}
&\int_{\Omega_\varphi} \dot{\Sigma} : (\nabla\varphi \otimes \boldsymbol{\alpha}) \, d\Omega = \\
&\int_{\Gamma_\varphi^+} \left[(\dot{\Sigma} \cdot \boldsymbol{\alpha}) \cdot \boldsymbol{\nu}_\varphi \right] d\Gamma + \int_{\Omega_\varphi} \varphi \left[\dot{\mathbf{b}} \cdot \boldsymbol{\alpha} - \dot{\Sigma} : \nabla\boldsymbol{\alpha} \right] d\Omega
\end{aligned} \tag{4.59}$$

From (4.54) and considering the definition of the Heaviside function, we can write

$$\begin{aligned}
&\int_{\Omega_\varphi} \varphi \left[\dot{\mathbf{b}} \cdot \boldsymbol{\alpha} - \dot{\Sigma} : \nabla\boldsymbol{\alpha} \right] d\Omega = \\
&\int_{\Omega_\varphi^+} \left[\dot{\mathbf{b}} \cdot \boldsymbol{\alpha} - \dot{\Sigma} : \nabla\boldsymbol{\alpha} \right] d\Omega - \int_{\Omega_\varphi} \mathcal{M}_S \left[\dot{\mathbf{b}} \cdot \boldsymbol{\alpha} - \dot{\Sigma} : \nabla\boldsymbol{\alpha} \right] d\Omega
\end{aligned} \tag{4.60}$$

Let us consider the first term of (4.57):

$$\int_{\Omega_\varphi} \dot{\Sigma} : (\delta_S \mathbf{n} \otimes \boldsymbol{\alpha}) d\Omega = \int_S (\dot{\Sigma}_S \cdot \mathbf{n}) \cdot \boldsymbol{\alpha}_S d\Omega \tag{4.61}$$

where the symmetry of $\dot{\Sigma}$ has been considered.

Now, let us substitute, first, (4.60) into (4.59); second, the resulting expression and (4.61) into (4.57), and, finally, into (4.55). This yields

$$\begin{aligned} &\int_{\Omega_\varphi} \dot{\Sigma} : \nabla^S \boldsymbol{\eta}' \, d\Omega - \int_{\Omega_\varphi} \mathcal{M}_S \, \dot{\mathbf{b}} \cdot \boldsymbol{\alpha} \, d\Omega = \\ &\int_S (\dot{\Sigma}_S \cdot \mathbf{n}) \cdot \boldsymbol{\alpha} \, d\Omega - \int_{\Gamma_\varphi^+} (\dot{\Sigma} \cdot \boldsymbol{\alpha}) \cdot \boldsymbol{\nu}_\varphi \, d\Gamma \\ &- \int_{\Omega_\varphi^+} \left[\dot{\mathbf{b}} \cdot \boldsymbol{\alpha} - \dot{\Sigma} : \nabla \boldsymbol{\alpha} \right] \, d\Omega \end{aligned} \tag{4.62}$$

Also, we have that

$$\begin{aligned} \int_{\Omega_\varphi^+} \dot{\Sigma} : \nabla \boldsymbol{\alpha} &= \int_{\Omega_\varphi^+} \nabla \cdot (\dot{\Sigma} \cdot \boldsymbol{\alpha}) - \int_{\Omega_\varphi^+} (\nabla \cdot \dot{\Sigma}) \cdot \boldsymbol{\alpha} \\ = \int_{\Gamma_\varphi^+} (\dot{\Sigma} \cdot \boldsymbol{\alpha}) \cdot \boldsymbol{\nu}_\varphi &- \int_S (\dot{\Sigma}_{\Omega^+} \cdot \boldsymbol{\alpha}_S) \cdot \mathbf{n} + \int_{\Omega_\varphi^+} \dot{\mathbf{b}} \cdot \boldsymbol{\alpha} \end{aligned} \tag{4.63}$$

Finally, substituting (4.63) into the right hand side of (4.62), and considering (4.51-b), we can write

$$\int_S \boldsymbol{\alpha}_S \cdot \left[\dot{\Sigma}_S \cdot \mathbf{n} - \dot{\Sigma}_{\Omega^+} \cdot \mathbf{n} \right] = 0 \quad \forall \boldsymbol{\alpha}_S \in \mathcal{V}_\alpha \tag{4.64}$$

Then proposition (1) follows.

Corollary 2 *The system of variational equations (4.12) and (4.51) are equivalent.*

4.3.2 Finite element discretization

The same finite element approximation for the displacement rate field, $\dot{\mathbf{u}}$, presented in Section 4.2 is adopted here:

$$\dot{\mathbf{u}}^{h^{(e)}} = \underbrace{\Sigma_{i=1}^{i=4} N_i^{(e)}(\mathbf{x})\dot{\mathbf{d}}_i(t)}_{\dot{\hat{\mathbf{u}}}^{h^{(e)}}} + \underbrace{\mathcal{M}_S^{(e)}(\mathbf{x})\,[\![\dot{\mathbf{u}}]\!]_e^h(t)}_{\dot{\mathbf{u}}'^{,h^{(e)}}} \tag{4.65}$$

where $\dot{\hat{\mathbf{u}}}^{h^{(e)}}$ is, again, the standard $\mathcal{C}^0$ elemental approximation of the rate of displacement field, interpolated by the bilinear element shape functions, $N_1^{(e)}$, $N_2^{(e)}$, $N_3^{(e)}$, $N_4^{(e)}$, and parametrized by the nodal values of the displacement rate $\dot{\mathbf{d}}_i(t)$, for $i \in \{1,..,4\}$. The term $\dot{\mathbf{u}}'^{,h^{(e)}}$ resolves, as in the preceding formulation, the jumps in the rate of displacement field in terms of the element-wise constant displacement rate jump $[\![\dot{\mathbf{u}}]\!]_e$, with $\mathcal{M}_S^{(e)}$ defined in (4.16).

Then, the discrete strain rate field at element level reads

$$[\dot{\boldsymbol{\varepsilon}}^h]^{(e)} = \Sigma_{i=1}^{i=4}\,(\nabla N_i^{(e)} \otimes \dot{\mathbf{d}}_i)^S - (\boldsymbol{\nabla}\varphi^{(e)} \otimes [\![\dot{\mathbf{u}}]\!]_e)^S + \mu_S^{(e)}\frac{1}{k}([\![\dot{\mathbf{u}}]\!]_e \otimes \mathbf{n})^S \tag{4.66}$$

Thus, from the finite element approximation of the displacement rate field presented in (4.65), the definition of the following function spaces can be made:

$$\mathcal{V}_{\dot{\mathbf{u}}}^h = \mathcal{V}_{\dot{\hat{\mathbf{u}}}}^h \oplus \mathcal{V}_{\dot{\mathbf{u}}'}^h \tag{4.67}$$

where

$$\begin{array}{l} \mathcal{V}_{\boldsymbol{\alpha}}^h := \left\{\boldsymbol{\alpha}^h;\ \boldsymbol{\alpha}^h(\mathbf{x}) = \boldsymbol{\alpha}_e\ \forall e \in \mathcal{J};\ \ \boldsymbol{\alpha}^h(\mathbf{x}) = 0\ \ \forall e \notin \mathcal{J}\right\} \\ \mathcal{V}_{\hat{\boldsymbol{\eta}}}^h := \left\{\hat{\boldsymbol{\eta}}^h;\ \hat{\boldsymbol{\eta}}^h(\mathbf{x}) = \Sigma_{i=1}^{i=n_{node}} N_i(\mathbf{x})\,\hat{\boldsymbol{\eta}}_i;\ \hat{\boldsymbol{\eta}}_i|_{\Gamma_u} = \dot{\mathbf{u}}^*\right\} \\ \mathcal{V}_{\boldsymbol{\eta}'}^h := \left\{\boldsymbol{\eta}'^{,h};\ \boldsymbol{\eta}'^{,h}(\mathbf{x}) = \Sigma_{e\in\mathcal{J}}\,\mathcal{M}_S^{(e)}(\mathbf{x})\boldsymbol{\alpha}_e\right\} \end{array} \tag{4.68}$$

with $\boldsymbol{\alpha}_e, \boldsymbol{\eta}_i \in \mathbb{R}^2$, and

$$\mathcal{V}_{\boldsymbol{\eta}}^h := \mathcal{V}_{\hat{\boldsymbol{\eta}}}^h \oplus \mathcal{V}_{\boldsymbol{\eta}'}^h \tag{4.69}$$

with

$$\mathcal{V}_{\bar{\boldsymbol{\eta}}}^h := \left\{\bar{\boldsymbol{\eta}}^h;\ \bar{\boldsymbol{\eta}}^h(\mathbf{x}) = \Sigma_{i=1}^{i=n_{node}}\ N_i(\mathbf{x})\,\bar{\boldsymbol{\eta}}_i\quad ;\ \ \bar{\boldsymbol{\eta}}_i|_{\Gamma_u} = 0\right\} \tag{4.70}$$

where $\bar{\boldsymbol{\eta}}_i \in \mathbb{R}^2$.

4.3.3 Discrete symmetric kinematically consistent problem

Now the following discrete problem can be stated:

FIND:

$$\dot{\mathbf{u}}^h \in \mathcal{V}_{\mathbf{u}}^h \Leftrightarrow \left\{ \begin{array}{l} \dot{\hat{\mathbf{u}}}^h \in \mathcal{V}_{\hat{\mathbf{u}}}^h \\ \dot{\mathbf{u}}'^h \in \mathcal{V}_{\mathbf{u}'}^h \end{array} \right. \tag{4.71}$$

SUCH THAT:

$$\begin{array}{ll} \sum_{e=1}^{e=n_{elem}} \int_{\Omega_e} \nabla^S \bar{\boldsymbol{\eta}}^h : \dot{\Sigma}(\dot{\boldsymbol{\varepsilon}}^h) d\Omega \; - G_{ext}(\bar{\boldsymbol{\eta}}^h) = 0 & \forall \bar{\boldsymbol{\eta}}^h \in \mathcal{V}_{\bar{\boldsymbol{\eta}}}^h \\ \Sigma_{e \in \mathcal{J}} \int_{\Omega_e} \nabla^S \boldsymbol{\eta}'^h : \dot{\Sigma} \; d\Omega = 0 & \forall \boldsymbol{\eta}'^h \in \mathcal{V}_{\mathbf{u}'}^h \end{array} \tag{4.72}$$

where $G_{ext}(\boldsymbol{\eta}'^h) \approx 0$ has been assumed.

4.3.4 Matrix representation

The discrete strain field in matrix form is the same as in the non symmetric problem:

$$\{\dot{\bar{\varepsilon}}\}^{(e)} = \mathbf{B}^{(e)} \dot{\mathbf{d}}^{(e)} + \underbrace{\left(\mu_S^{(e)} \frac{1}{k} [\mathbf{n}]^{(e)} - \left[\boldsymbol{\nabla} \varphi^{(e)} \right] \right)}_{=: \mathbf{G}^{(e)}} [\![\dot{\mathbf{u}}]\!]_e \tag{4.73}$$

In this case, the gradient of the displacement rate variations reads

$$\{\nabla^S \boldsymbol{\eta}\} = \mathbf{B}^{(e)} \{\bar{\boldsymbol{\eta}}\}^{(e)} + \mathbf{G}^{(e)} \boldsymbol{\alpha}_e \tag{4.74}$$

Hence, the expression of the incremental residual forces at element level corresponding to (4.72) reads

$$\begin{array}{ll} \dot{\mathbf{R}}^{(e)} := \int_{\Omega_e} \mathbf{B}^{(e)^T} \{\dot{\Sigma}\}^{(e)} \, d\Omega - \dot{\mathbf{F}}_{ext}^{(e)} & (a) \\ \dot{\mathbf{r}}^{(e)} := \int_{\Omega_e} \mathbf{G}^{(e)^T} \{\dot{\Sigma}\}^{(e)} \, d\Omega & (b) \end{array} \tag{4.75}$$

where $\dot{\mathbf{F}}_{ext}^{(e)}$ is the vector of incremental external forces at element level.

Assuming an incrementally linear relation between the strains and the stresses as the one expressed in (4.33), the residual forces (4.75) can be rewritten as

$$\begin{bmatrix} \mathbf{K}_{dd}^{(e)} & \mathbf{K}_{d\alpha}^{(e)} \\ \mathbf{K}_{\alpha d}^{(e)} & \mathbf{K}_{\alpha\alpha}^{(e)} \end{bmatrix} \begin{Bmatrix} \dot{\mathbf{d}}^{(e)} \\ [\![\dot{\mathbf{u}}]\!]_e \end{Bmatrix} - \begin{Bmatrix} \dot{\mathbf{F}}_{ext}^{(e)} \\ 0 \end{Bmatrix} = \begin{Bmatrix} \dot{\mathbf{R}}^{(e)} \\ \dot{\mathbf{r}}^{(e)} \end{Bmatrix} \tag{4.76}$$

with

$$\begin{aligned} \mathbf{K}_{dd}^{(e)} &= \int_{\Omega_e} \mathbf{B}^{(e)^T}\ \mathbf{D}\ \mathbf{B}^{(e)} d\Omega \\ \mathbf{K}_{d\alpha}^{(e)} &= \int_{\Omega_e} \mathbf{B}^{(e)^T}\ \mathbf{D}\ \mathbf{G}^{(e)} d\Omega \\ \mathbf{K}_{\alpha d}^{(e)} &= \int_{\Omega_e} \mathbf{G}^{(e)^T}\ \mathbf{D}\ \mathbf{B}^{(e)} d\Omega \\ \mathbf{K}_{\alpha\alpha}^{(e)} &= \int_{\Omega_e} \mathbf{G}^{(e)^T}\ \mathbf{D}\ \mathbf{G}^{(e)} d\Omega \end{aligned} \tag{4.77}$$

Remark 37 *The resulting tangent stiffness matrix is symmetrical.*

Remark 38 *As in the non-symmetric formulation, due to their elemental support, the modes corresponding to the displacement jumps, $[[\dot{\mathbf{u}}]]_e$, can be condensed at element level.*

Remark 39 *In this formulation* $\int_{\Omega_e} \mathbf{G}^{(e)^T} d\Omega = \mathbf{0}$ does not always hold. *This diminishes the reproducing possibilities of this element: not satisfying the patch test implies that constant stresses cannot always be reproduced, which is the cause of the lack of static optimality suffered by this element.*

Now, let us define

$$\bar{\mathbf{B}}^{(e)} = \left[\ \mathbf{B}_1^{(e)},\ \ \mathbf{B}_2^{(e)},\ \ \mathbf{B}_3^{(e)},\ \ \mathbf{B}_4^{(e)},\ \ \mathbf{G}^{(e)}\ \right] \tag{4.78}$$

and

$$\begin{aligned} \dot{\bar{\mathbf{R}}}^{(e)} &= \left[\ (\dot{\mathbf{R}}^{(e)})^T,\ \ \dot{\mathbf{r}}^{(e)^T}\ \right]^T \\ \dot{\bar{\mathbf{F}}}_{ext}^{(e)} &= \left[\ (\dot{\mathbf{F}}_{ext}^{(e)})^T,\ \ \mathbf{0}^T\ \right]^T \\ \dot{\bar{\mathbf{d}}}^{(e)} &= \left[\ (\dot{\mathbf{d}}^{(e)})^T\ \ [\![\dot{\mathbf{u}}]\!]_e^T\ \right]^T \end{aligned} \tag{4.79}$$

Then , the *B-bar* format of (4.76) is

$$\int_{\Omega_e} \bar{\mathbf{B}}^{(e)T}\, \mathbf{D}\, \bar{\mathbf{B}}^{(e)} \dot{\mathbf{d}}^{(e)} d\Omega - \dot{\bar{\mathbf{F}}}^{(e)}_{ext} = \dot{\bar{\mathbf{R}}}^{(e)} \tag{4.80}$$

Finally, the global system of equations corresponding to (4.72) is given by

$$\overset{n_{elem}}{\underset{e=1}{A}} \left[\int_{\Omega_e} \bar{\mathbf{B}}^{(e)T}\, \mathbf{D}\, \bar{\mathbf{B}}^{(e)} \dot{\mathbf{d}}^{(e)} d\Omega - \dot{\bar{\mathbf{F}}}^{(e)}_{ext} = \mathbf{0} \right] \tag{4.81}$$

4.4 Symmetric assumed enhanced strain approach

This formulation is derived in the context of the assumed enhanced strain method presented in [Simo and Rifai, 1990]. It is based on a three-field variational principle. Let us then assume that, for a given time $t \in \mathbb{R}_+$, the displacement rate field $\dot{\mathbf{u}}(\bullet, t)$:$\Omega \rightarrow \mathbb{R}^{n_{\text{dim}}}$, the admissible variations of the displacement rate field, $\bar{\boldsymbol{\eta}}(\bullet, t)$:$\Omega \rightarrow \mathbb{R}^{n_{\text{dim}}}$, the stress rate field, $\dot{\boldsymbol{\sigma}}(\bullet, t)$:$\Omega \rightarrow \mathbb{S}$, and the assumed enhanced strain rate field, $\dot{\bar{\boldsymbol{\varepsilon}}}(\bullet, t)$:$\Omega \rightarrow \mathbb{S}$ lie on the following function spaces:

$$\mathcal{V}_{\mathbf{u}} := \left\{ \boldsymbol{\eta} \in [\mathsf{H}^1(\Omega)]^{n_{\text{dim}}} \quad ; \quad \boldsymbol{\eta}|_{\Gamma_u} = \dot{\mathbf{u}}^* \right\} \tag{4.82}$$

$$\mathcal{V}_{\eta} := \left\{ \bar{\boldsymbol{\eta}} \in [\mathsf{H}^1(\Omega)]^{n_{\text{dim}}} \quad ; \quad \bar{\boldsymbol{\eta}}|_{\Gamma_u} = 0 \right\} \tag{4.83}$$

$$\mathcal{V}_{\sigma} := \{ \tau; \quad \tau \in \mathsf{L}_2(\Omega; \mathbb{S}); \quad [[\tau]]_S \cdot \mathbf{n} = 0 \} \tag{4.84}$$

where $\mathbb{S}$ denotes, as said before, the space of second order symmetric tensors

$$\mathcal{V}_{\bar{\varepsilon}} := \left\{ \tilde{\boldsymbol{\xi}};\ \bar{\boldsymbol{\xi}} = \bar{\boldsymbol{\xi}} + \delta_S (\boldsymbol{\alpha} \otimes \mathbf{n})^S;\ \bar{\boldsymbol{\xi}} \in \overline{\mathcal{V}}_{\bar{\varepsilon}}\ ;\ \boldsymbol{\alpha}_S \in \mathcal{V}_{\alpha} \right\} \tag{4.85}$$

with $\mathcal{V}_{\bar{\varepsilon}} := \mathsf{L}_2(\Omega; \mathbb{S})$ and $\mathcal{V}_{\alpha}$:=$[\mathsf{L}_2(\mathcal{S})]^{n_{\text{dim}}}$.

Finally, the strain rate field, $\dot{\boldsymbol{\varepsilon}}$:$\Omega \times \mathbb{R}_+ \rightarrow \mathbb{R}^{n_{\text{dim}}}$, is assumed to have the following structure:

$$\dot{\boldsymbol{\varepsilon}}(\mathbf{x}, t) = \nabla \dot{\mathbf{u}}(\mathbf{x}, t) + \dot{\bar{\boldsymbol{\varepsilon}}}(\mathbf{x}, t) \tag{4.86}$$

Remark 40 *Notice that the singular term, $\delta_S(\boldsymbol{\alpha} \otimes \mathbf{n})^S$, of the enhanced strain has the same structure as the singular term of the strain field corresponding to the strong discontinuity kinematics presented in Section 3.2.1.*

Remark 41 *The resulting strain field is not kinematically consistent with the displacement field in the sense that $\dot{\boldsymbol{\varepsilon}}(\mathbf{x}, t) \neq \nabla^S \dot{\mathbf{u}}(\mathbf{x}, t)$.*

4.4.1 Continuum problem

Now the following problem can be stated[9]:

FIND

$$\begin{array}{l} \dot{\mathbf{u}} \in \mathcal{V}_{\mathbf{u}} \\ \dot{\bar{\boldsymbol{\varepsilon}}} \in \mathcal{V}_{\bar{\boldsymbol{\varepsilon}}} \\ \dot{\boldsymbol{\sigma}} \in \mathcal{V}_{\boldsymbol{\sigma}} \end{array} \tag{4.87}$$

SUCH THAT

$$\begin{array}{lll} \displaystyle\int_{\Omega\backslash\mathcal{S}} \dot{\Sigma}(\boldsymbol{\varepsilon}) : \nabla^S \bar{\boldsymbol{\eta}}\, d\Omega - G_{ext} = 0 & \forall \bar{\boldsymbol{\eta}} \in \mathcal{V}_{\bar{\eta}} & (a) \\ \displaystyle\int_{\Omega} \dot{\bar{\boldsymbol{\varepsilon}}} : \boldsymbol{\tau}\, d\Omega = 0 & \forall \boldsymbol{\tau} \in \mathcal{V}_{\boldsymbol{\sigma}} & (b) \\ \displaystyle\int_{\Omega} \left(\dot{\boldsymbol{\sigma}} - \dot{\Sigma}\right) : \bar{\boldsymbol{\xi}}\, d\Omega = 0 & \forall \bar{\boldsymbol{\xi}} \in \mathcal{V}_{\bar{\boldsymbol{\varepsilon}}} & (c) \end{array} \tag{4.88}$$

By using standard arguments, we can prove that the strong form of (4.88-a) is

$$\begin{array}{ll} \nabla \cdot \dot{\Sigma}(\boldsymbol{\varepsilon}) + \dot{\mathbf{b}} = 0 & in\ \Omega\backslash\mathcal{S} \\ \dot{\Sigma} \cdot \boldsymbol{\nu} = \dot{\mathbf{t}}^* & on\ \Gamma_u \\ [\![\dot{\Sigma}]\!]_{\Omega\backslash\mathcal{S}} \cdot \mathbf{n} = 0 & on\ \mathcal{S} \end{array} \tag{4.89}$$

Special care has to be taken with respect to (4.88-b) and (4.88-c) due to the singular term appearing in the expression of the enhanced strain and the enhanced strain variation. For the expressions (4.88-b) and (4.88-c) to make sense, the fact that $[\![\boldsymbol{\tau}]\!]_{\mathcal{S}} \cdot \mathbf{n} = [\![\dot{\boldsymbol{\sigma}}]\!]_{\mathcal{S}} \cdot \mathbf{n} = 0$ is crucial, because it ensures that both $\boldsymbol{\tau}_{\mathcal{S}} \cdot \mathbf{n}$ and $\dot{\boldsymbol{\sigma}}_{\mathcal{S}} \cdot \mathbf{n}$ exist and are bounded. With these concepts in hand we arrive to the strong form of (4.88-b):

$$\dot{\bar{\boldsymbol{\varepsilon}}} = 0 \quad in\ \Omega \tag{4.90}$$

and the strong form of (4.88-c):

$$\dot{\boldsymbol{\sigma}} - \dot{\Sigma} = 0 \quad in\ \Omega \tag{4.91}$$

[9] In [Simo and Rifai, 1990], this variational problem was derived from the Hu-Washizu 3-field variational principle. Here we state it as the weak form of the system of diferential equations 4.6.

4.4.2 Finite element discretization

Consider a finite element discretization of the domain Ω into four-noded finite elements, then the following discrete version of the function spaces 4.82 to 4.85 is proposed:

$$\begin{array}{l} \mathcal{V}_{\mathbf{u}}^h := \left\{ \boldsymbol{\eta}^h;\ \boldsymbol{\eta}^h(\mathbf{x}) = \Sigma_{i=1}^{i=n_{node}}\ N_i(\mathbf{x})\,\boldsymbol{\eta}_i\ ;\ \boldsymbol{\eta}_i|_{\Gamma_u} = \dot{\mathbf{u}}^* \right\} \\ \mathcal{V}_{\bar{\boldsymbol{\eta}}}^h := \left\{ \bar{\boldsymbol{\eta}}^h;\ \bar{\boldsymbol{\eta}}^h(\mathbf{x}) = \Sigma_{i=1}^{i=n_{node}}\ N_i(\mathbf{x})\,\bar{\boldsymbol{\eta}}_i\ ;\ \bar{\boldsymbol{\eta}}_i|_{\Gamma_u} = \mathbf{0} \right\} \\ \mathcal{V}_{\bar{\boldsymbol{\varepsilon}}}^h := \left\{ \bar{\boldsymbol{\xi}}^h;\ \bar{\boldsymbol{\xi}}^h(\mathbf{x}) = \Sigma_{e=1}^{e=n_{elem}} (\mu_S^{(e)} \frac{1}{k} - \frac{l_e}{\Omega_e}) \chi_e(\mathbf{x}) (\boldsymbol{\alpha}_e \otimes \mathbf{n})^S \right\} \\ \mathcal{V}_{\boldsymbol{\sigma}}^h := \left\{ \boldsymbol{\tau}^h;\ \boldsymbol{\tau}^h(\mathbf{x}) = \Sigma_{e=1}^{e=n_{elem}}\ \chi_e(\mathbf{x})\,\boldsymbol{\tau}_e \right\} \end{array} \tag{4.92}$$

where χ_e stands for the characteristic function of Ω_e, i.e.,

$$\chi_e(\mathbf{x}) = \begin{cases} 1 \text{ for } \mathbf{x} \in \Omega_e \\ 0 \text{ otherwise} \end{cases}$$

and $\boldsymbol{\eta}_i, \bar{\boldsymbol{\eta}}_i, \boldsymbol{\alpha}_e \in \mathbb{R}^2$; $\boldsymbol{\tau}_e \in \mathbb{S}$.

Let us now assume that the following *orthogonality* condition between $\mathcal{V}_{\bar{\boldsymbol{\varepsilon}}}^h$ and $\mathcal{V}_{\boldsymbol{\sigma}}^h$ holds[10]:

$$\int_{\Omega_e} \bar{\boldsymbol{\xi}}^h : \boldsymbol{\tau}^h\ d\Omega = 0 \quad \begin{cases} \forall \bar{\boldsymbol{\xi}}^h \in \mathcal{V}_{\bar{\boldsymbol{\varepsilon}}}^h \\ \forall \boldsymbol{\tau}^h \in \mathcal{V}_{\boldsymbol{\sigma}}^h \\ \forall e \in \mathcal{I} \end{cases} \tag{4.93}$$

Remark 42 *Due to the singular term in the enhanced strain rate, we cannot talk about* L_2*−*orthogonality*, as in [Simo and Rifai, 1990], since the integral in the left hand side of (4.93) does not define the* L_2 *inner product, but a duality pairing.*

Then the discrete version of (4.88-b) becomes an identity. Moreover, (4.88-c) can be worked out as follows:

$$\int_\Omega \left[\dot{\boldsymbol{\sigma}}^h - \dot{\Sigma}(\boldsymbol{\varepsilon}^h) \right] : \bar{\boldsymbol{\xi}}\ d\Omega = \underbrace{\int_\Omega \dot{\boldsymbol{\sigma}}^h : \bar{\boldsymbol{\xi}}^h\ d\Omega}_{=0} - \int_\Omega \dot{\Sigma}(\boldsymbol{\varepsilon}^h) : \bar{\boldsymbol{\xi}}^h\ d\Omega = 0 \tag{4.94}$$

which yields

[10] This condition is motivated by the satisfaction of the patch test (see [Simo and Rifai, 1990])

$$\int_{\Omega} \dot{\Sigma}(\dot{\varepsilon}^h) : \bar{\xi}^h d\Omega = 0 \tag{4.95}$$

It is easy to check that $\mathcal{V}_{\bar{\xi}}^h$ fulfills condition (4.93):

$$\begin{aligned} &\textstyle\int_{\Omega} \bar{\xi}^h : \tau^h d\Omega = \sum_{e=1}^{e=n_{elem}} \int_{\Omega_e} (\mu_S^{(e)} \frac{1}{k} - \frac{l_e}{\Omega_e}) \, (\boldsymbol{\alpha}_e \otimes \mathbf{n})^S : \tau_e d\Omega = \\ &\textstyle\sum_{e=1}^{e=n_{elem}} \underbrace{\int_{\Omega_e} (\mu_S^{(e)} \frac{1}{k} - \frac{l_e}{\Omega_e}) \, d\Omega}_{(l_e - l_e) = 0} \, (\boldsymbol{\alpha}_e \otimes \mathbf{n})^S : \tau_e = 0 \end{aligned} \tag{4.96}$$

4.4.3 Discrete Problem

With the above results and definitions in hand, the discrete problem corresponding to (4.98) reduces to

FIND:

$$\begin{aligned} \dot{\mathbf{u}}^h &\in \mathcal{V}_{\mathbf{u}}^h \\ \dot{\bar{\varepsilon}} &\in \mathcal{V}_{\bar{\varepsilon}}^h \end{aligned} \tag{4.97}$$

SUCH THAT:

$$\begin{aligned} &\textstyle\sum_{e=1}^{e=n_{elem}} \int_{\Omega_e} \nabla^S \bar{\eta}^h : \dot{\Sigma}(\dot{\varepsilon}^h) d\Omega \; - G_{ext}(\bar{\eta}^h) = 0 \quad \forall \bar{\eta}^h \in \mathcal{V}_{\bar{\eta}}^h \\ &\textstyle\sum_{e=1}^{e=n_{elem}} \int_{\Omega_e} \dot{\Sigma}(\dot{\varepsilon}^h) : \bar{\xi}^h \; d\Omega = 0 \qquad\qquad\qquad \forall \bar{\xi}^h \in \mathcal{V}_{\bar{\xi}}^h \end{aligned} \tag{4.98}$$

4.4.4 Matrix representation

The discrete strain field in its matrix representation reads

$$\begin{aligned} \{\dot{\bar{\varepsilon}}\}^{(e)} &= \mathbf{B}^{(e)} \dot{\mathbf{d}}^{(e)} + \underbrace{\left(\mu_S^{(e)} \frac{1}{k} - \frac{l_e}{\Omega_e} \right) [\mathbf{n}]^{(e)}}_{=: \mathbf{G}^{(e)}} \boldsymbol{\beta}_e \\ &= \mathbf{B}^{(e)} \dot{\mathbf{d}}^{(e)} + \mathbf{G}_e^{(e)} \boldsymbol{\beta}_e \end{aligned} \tag{4.99}$$

where $\boldsymbol{\beta}_e \in \mathbb{R}^2$.

On the other hand, the matrix form of the strain variations is

$$\begin{aligned} \{\boldsymbol{\xi}\}^{(e)} &= \mathbf{B}^{(e)}\{\bar{\boldsymbol{\eta}}\}^{(e)} + \{\bar{\bar{\boldsymbol{\xi}}}\} \\ &= \mathbf{B}^{(e)}\{\bar{\boldsymbol{\eta}}\}^{(e)} + \mathbf{G}^{(e)}\boldsymbol{\alpha}_e \end{aligned} \tag{4.100}$$

Thus, the following is the expression of the incremental residual forces at element level corresponding to (4.98):

$$\begin{aligned} \dot{\mathbf{R}}^{(e)} &:= \int_{\Omega_e} \mathbf{B}^{(e)^T}\ \{\dot{\Sigma}\}^{(e)}\ d\Omega - \dot{\mathbf{F}}^{(e)}_{ext} \quad (a) \\ \dot{\mathbf{r}}^{(e)} &:= \int_{\Omega_e} \mathbf{G}^{(e)^T}\ \{\dot{\Sigma}\}^{(e)}\ d\Omega \qquad\qquad (b) \end{aligned} \tag{4.101}$$

where $\dot{\mathbf{F}}^{(e)}_{ext}$ is the vector of incremental external forces at element level.

Assuming, again, an incrementally linear constitutive relation as the one expressed in (4.33), the system of equations (4.101), can be rewritten as

$$\begin{bmatrix} \mathbf{K}^{(e)}_{dd} & \mathbf{K}^{(e)}_{d\alpha} \\ \mathbf{K}^{(e)}_{\alpha d} & \mathbf{K}^{(e)}_{\alpha\alpha} \end{bmatrix} \left\{ \begin{array}{c} \dot{\mathbf{d}}^{(e)} \\ \boldsymbol{\beta}_e \end{array} \right\} - \left\{ \begin{array}{c} \dot{\mathbf{F}}^{(e)}_{ext} \\ \mathbf{0} \end{array} \right\} = \left\{ \begin{array}{c} \dot{\mathbf{R}}^{(e)} \\ \dot{\mathbf{r}}^{(e)} \end{array} \right\} \tag{4.102}$$

with

$$\begin{aligned} \mathbf{K}^{(e)}_{dd} &= \int_{\Omega_e} \mathbf{B}^{(e)^T}\ \mathbf{D}\ \mathbf{B}^{(e)} d\Omega \\ \mathbf{K}^{(e)}_{d\alpha} &= \int_{\Omega_e} \mathbf{B}^{(e)^T}\ \mathbf{D}\ \mathbf{G}^{(e)} d\Omega \\ \mathbf{K}^{(e)}_{\alpha d} &= \int_{\Omega_e} \mathbf{G}^{(e)^T}\ \mathbf{D}\ \mathbf{B}^{(e)} d\Omega \\ \mathbf{K}^{(e)}_{\alpha\alpha} &= \int_{\Omega_e} \mathbf{G}^{(e)^T}\ \mathbf{D}\ \mathbf{G}^{(e)} d\Omega \end{aligned} \tag{4.103}$$

Remark 43 *The resulting tangent stiffness matrix is symmetrical.*

Remark 44 *As in the previous formulations, due to their elemental support, the modes corresponding to the displacement jumps, $\boldsymbol{\beta}_e$, can be condensed at element level.*

Remark 45 *In this formulation $\int_{\Omega_e} \mathbf{G}^{(e)} d\Omega = \mathbf{0}$, which is derived directly from the orthogonality condition (4.93) and guarantees the satisfaction of the patch test.*

Remark 46 *The matrix form of the three formulations presented so far (i.e., (4.39), (4.76), and (4.102)) coincide when* $\frac{1}{\Omega_e}\int_{\Omega_e}[\mathbf{n}]^{(e)} = \left[\nabla\varphi^{(e)}\right]$

Now, let us define

$$\bar{\mathbf{B}}^{(e)} = \left[\begin{array}{ccccc} \mathbf{B}_1^{(e)}, & \mathbf{B}_2^{(e)}, & \mathbf{B}_3^{(e)}, & \mathbf{B}_4^{(e)}, & \mathbf{G}^{(e)} \end{array}\right] \tag{4.104}$$

and

$$\begin{array}{l} \dot{\bar{\mathbf{R}}}^{(e)} = \left[\begin{array}{cc} (\dot{\mathbf{R}}^{(e)})^T, & \dot{\mathbf{r}}^{(e)T} \end{array}\right]^T \\ \dot{\bar{\mathbf{F}}}_{ext}^{(e)} = \left[\begin{array}{cc} (\dot{\mathbf{F}}_{ext}^{(e)})^T, & \mathbf{0}^T \end{array}\right]^T \\ \dot{\bar{\mathbf{d}}}^{(e)} = \left[\begin{array}{cc} (\dot{\mathbf{d}}^{(e)})^T & \boldsymbol{\beta}_e^T \end{array}\right]^T \end{array} \tag{4.105}$$

Then, the *B-bar* format of (4.102) is

$$\int_{\Omega_e} \bar{\mathbf{B}}^{(e)T}\ \mathbf{D}\ \bar{\mathbf{B}}^{(e)}\dot{\bar{\mathbf{d}}}^{(e)}d\Omega - \dot{\bar{\mathbf{F}}}_{ext}^{(e)} = \dot{\bar{\mathbf{R}}}^{(e)} \tag{4.106}$$

Finally, the global system of equations corresponding to (4.98), is given by

$$\mathop{A}_{e=1}^{n_{elem}}\left[\int_{\Omega_e} \bar{\mathbf{B}}^{(e)T}\ \mathbf{D}\ \bar{\mathbf{B}}^{(e)}\dot{\bar{\mathbf{d}}}^{(e)}d\Omega - \dot{\bar{\mathbf{F}}}_{ext}^{(e)} = 0\right] \tag{4.107}$$

4.5 The possibility of a self propagating element

So far in this chapter, the formulations of the best known families of elements with embedded discontinuities have been derived from convenient weak statements of the boundary value problem (4.5). In general, the discrete formulations inherit the character of the corresponding continuum formulations. This gives to each of them different characteristics regarding its performance in simulating discontinuities in solids. For instance, the kinematical optimality of the non-symmetric formulation, presented in Section 4.2, and of the symmetric kinematically consistent formulation, presented in Section 4.3, has to do with the consistent way in which the strain field of those formulations is derived from the displacement field. Nevertheless, in the finite element implementation of these formulations, it is necessary to know, for a given element e crossed by the discontinuity line, which nodes lie on Ω^+ and which in Ω^- in order to determine the function $\varphi^{(e)}$, defined in (4.16). This information

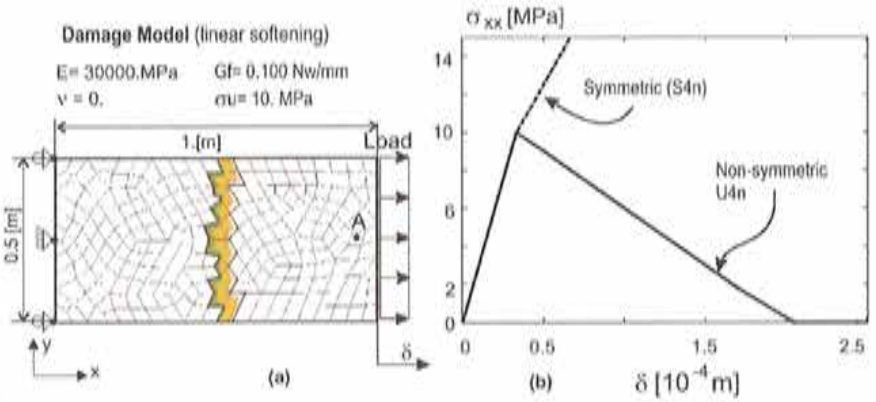

Figure 4.3: Simple traction test: a) geometry, mesh, boudary conditions, and material properties; b) Comparison between the U4n element and the S4n element.

is provided, as mentioned above, by a tracking algorithm, which entails several limitations especially for managing multiple discontinuities. The natural option to get rid of this tracking algorithm seems to be the symmetric assumed enhanced strain based element. Then, the inception and propagation of discontinuities would be determined only by the stress state of the solid through the discontinuous bifurcation analysis studied in Chapter 2. However, the performance of this element is very poor in many cases, due to the appearance of stress locking behavior. We illustrate this through a numerical example.

4.5.1 Stress locking behavior

In order to assess the performance of the symmetric assumed enhanced strain based element described in Section 4.4, a representative numerical simulation is presented here. The non-symmetric element is used as the reference element, due to its statically and kinematically optimal behavior (see [Jirasek, 2000a]).

Based on [Oliver et al., 2003], the following nomenclature is adopted:

- *U4n* for the non-symmetric element
- *S4n* for the symmetric assumed enhanced strain based element

Let us, then, consider the rectangular plate whose dimensions and material properties are shown in Fig. 4.3-a. It is discretized into a non-structured finite element mesh consisting of four noded bilinear elements. The plate is fixed on the left side and uniformly stretched from the right side. The isotropic continuum damage

model presented in Section 2.2. equipped with a linear softening law is employed for modelling its material behavior. It can be shown that the theoretical (exact) discontinuity path describes a straight vertical line crossing the plate from top to bottom. The displacement jump is uniform and only its normal component is different from zero (mode I). Since the stress state is also uniform, the position of the discontinuity line has to be imposed.

The stress vs. displacement curves of both the $U4n$ and $S4n$ element are plotted in Fig. 4.3-b. That figure shows that the $U4n$ element is able to reproduce the theoretical (exact) solution consisting, beyond the peak stress, of a linear softening branch until the total relaxation of the stress is reached. On the other hand, the curve corresponding to the $S4n$ element undergoes a spurious hardening after the theoretical peak stress, causing the stress to reach unphysical levels.

In order to understand this numerical phenomenon, it is important to mention that, based on theoretical reasons, an incrementally linear behavior is algorithmically imposed to $\Omega\backslash\mathcal{S}$ after bifurcation. The stress should, then, unload elastically. However, due to the kinematically inconsistent character of $S4n$, the stress in $\Omega\backslash\mathcal{S}$ grows elastically, which causes the stress locking behavior observed in Fig.4.3-b.

The poor performance of element $S4n$ makes it unsuitable for the numerical modelling of relatively complex problems. Thus, some alternative formulation have to be devised in such a way that the stress locking behavior of $S4n$ is overcome, while keeping its self propagating potentiality.

In the following sections remedies to the stress locking suffered by $S4n$ are presented. In order to motivate them, we first present some comments on the causes of this phenomenon for a parent four noded bilinear element:

- Assuming that $\Omega\backslash\mathcal{S}$ behaves elastically after bifurcation, the following relationship between the strain rate in $\Omega\backslash\mathcal{S}$ and the stress rate holds:

$$\dot{\boldsymbol{\varepsilon}}_{\Omega\backslash\mathcal{S}} = \dot{\tilde{\boldsymbol{\varepsilon}}} = \underbrace{\mathbf{C}^{-1} : \dot{\boldsymbol{\sigma}}}_{\text{elastic strain}} \tag{4.108}$$

  $\mathbf{C}$ is the standard isotropic elastic tensor.

- In the $S4n$ element formulation, the strain rate in $\Omega\backslash\mathcal{S}$ has the following structure:

$$\dot{\boldsymbol{\varepsilon}}^{(e)}_{\Omega\backslash\mathcal{S}} = \underbrace{\nabla^S \dot{\mathbf{u}}^{(e)}}_{\text{linear}} - \underbrace{\frac{l_e}{\Omega_e}(\boldsymbol{\beta}_e \otimes \mathbf{n})^S}_{\text{(enhancement) constant}} \tag{4.109}$$

- Total relaxation of the stress ($\dot{\boldsymbol{\sigma}} = 0$) entails the strain rate being zero ($\dot{\boldsymbol{\varepsilon}}_{\Omega\setminus\mathcal{S}} = 0$) from (4.108). However, the cancellation of the two terms appearing in the right hand side of (4.109) only can occur in the particular case in which $\nabla^S \dot{\mathbf{u}}^{(e)}$ is constant. Therefore, due to its kinematics, this formulation is unable to reproduce this stress state.

The stress locking is, at least partially, explained by the above reasoning. It also suggests two possible remedies:

1) To decrease the polynomial degree of the conforming term.

2) To increase the polynomial degree of the enhancement.

Both possibilities will be explored: the first one by means of the mixed approach proposed in Section 4.6, and the second by means of an assumed strain re-enhancement, proposed in Section 4.7.

4.6 Mixed Approach

Assume that, for a given time $t \in \mathbb{R}_+$, the displacement rate field $\dot{\mathbf{u}}(\bullet, t)$:$\Omega \to \mathbb{R}^{n_{\text{dim}}}$, the admissible variations of the displacement rate field, $\bar{\boldsymbol{\eta}}(\bullet, t)$:$\Omega \to \mathbb{R}^{n_{\text{dim}}}$, the stress rate field, $\dot{\boldsymbol{\sigma}}(\bullet, t)$:$\Omega \to \mathbb{S}$, and the strain rate field, $\dot{\boldsymbol{\varepsilon}}(\bullet, t)$:$\Omega \to \mathbb{S}$ lie on the following function spaces:

$$
\begin{array}{lll}
\mathcal{V}_{\mathbf{u}} := \left\{ \boldsymbol{\eta} \in [\mathsf{H}^1(\Omega)]^{n_{\text{dim}}} \;\; ; \;\; \boldsymbol{\eta}|_{\Gamma_u} = \dot{\mathbf{u}}^* \right\} & (a) & \\
\mathcal{V}_{\bar{\eta}} := \left\{ \bar{\boldsymbol{\eta}} \in [\mathsf{H}^1(\Omega)]^{n_{\text{dim}}} \;\; ; \;\; \bar{\boldsymbol{\eta}}|_{\Gamma_u} = \mathbf{0} \right\} & (b) & \\
\mathcal{V}_{\varepsilon} := \{ \boldsymbol{\xi};\, \boldsymbol{\xi} = \bar{\boldsymbol{\xi}} + \delta_{\mathcal{S}} (\boldsymbol{\alpha} \otimes \mathbf{n})^S \;\; ; \;\; \bar{\boldsymbol{\xi}} \in \mathsf{L}_2(\Omega; \mathbb{S}) \;\; ; \;\; \boldsymbol{\alpha} \in [\mathsf{L}_2(\mathcal{S})]^{n_{\text{dim}}} \} & (c) & (4.110) \\
\mathcal{V}_{\sigma} := \left\{ \boldsymbol{\tau} ; \;\; \boldsymbol{\tau} \in \mathsf{L}_2(\Omega; \mathbb{S}) \;\; ; \;\; [[\boldsymbol{\tau}]]_{\Omega\setminus\mathcal{S}} \cdot \mathbf{n} = [[\boldsymbol{\tau}]]_{\mathcal{S}} \cdot \mathbf{n} = \mathbf{0} \right\} & (d) &
\end{array}
$$

4.6.1 Continuum problem

Now the following three-field variational principle can be stated:

FIND:

$$
\begin{array}{l}
\dot{\mathbf{u}} \in \mathcal{V}_{\mathbf{u}} \\
\dot{\boldsymbol{\varepsilon}} \in \mathcal{V}_{\varepsilon} \\
\dot{\boldsymbol{\sigma}} \in \mathcal{V}_{\sigma}
\end{array}
\tag{4.111}
$$

SUCH THAT

$$
\begin{array}{lll}
\displaystyle\int_{\Omega\setminus\mathcal{S}} \dot{\boldsymbol{\sigma}} : \nabla^S \boldsymbol{\eta} \, d\Omega - G_{ext} = 0 & \forall \bar{\boldsymbol{\eta}} \in \mathcal{V}_{\bar{\eta}} & (a) \\
\displaystyle\int_{\Omega} \left(\dot{\boldsymbol{\varepsilon}} - \nabla^S \dot{\mathbf{u}} \right) : \boldsymbol{\tau} \, d\Omega = 0 & \forall \boldsymbol{\tau} \in \mathcal{V}_{\sigma} & (b) \\
\displaystyle\int_{\Omega} \left(\dot{\boldsymbol{\sigma}} - \dot{\Sigma} \right) : \boldsymbol{\xi} \, d\Omega = 0 & \forall \boldsymbol{\xi} \in \mathcal{V}_{\varepsilon} & (c)
\end{array}
\tag{4.112}
$$

The strong form corresponding to (4.112-a) is

$$\begin{array}{ll} \nabla \cdot \dot{\boldsymbol{\sigma}} + \dot{\mathbf{b}} = \mathbf{0} & in\ \Omega \backslash \mathcal{S} \\ \dot{\boldsymbol{\sigma}} \cdot \boldsymbol{\nu} = \dot{\mathbf{t}} & on\ \Gamma_u \\ [\![\dot{\boldsymbol{\sigma}}]\!]_{\Omega \backslash \mathcal{S}} \cdot \mathbf{n} = \mathbf{0} & on\ \mathcal{S} \end{array} \tag{4.113}$$

and the strong forms of (4.112-b) and (4.112-c) are

$$\dot{\boldsymbol{\varepsilon}} = \nabla^S \dot{\mathbf{u}} \quad in\ \Omega \tag{4.114}$$

$$\dot{\boldsymbol{\sigma}} = \dot{\Sigma} \qquad in\ \Omega \tag{4.115}$$

Thus, equations (4.5-a) to (4.5-e) follow from the variational problem (4.112), whereas (4.5-e) is automatically imposed by the definition of $\mathcal{V}_{\boldsymbol{\sigma}}$.

4.6.2 Finite element discretization

Considering again a discretization of Ω into four-noded bilinear finite elements, the following function spaces are proposed as the discrete version of 4.110:

$$\begin{array}{lll} \mathcal{V}_{\mathbf{u}}^h := \left\{ \boldsymbol{\eta}^h;\ \boldsymbol{\eta}^h(\mathbf{x}) = \Sigma_{i=1}^{i=n_{node}}\ N_i(\mathbf{x})\, \boldsymbol{\eta}_i\ ;\ \boldsymbol{\eta}_i|_{\Gamma_u} = \dot{\mathbf{u}}^* \right\} & (a) \\ \mathcal{V}_{\bar{\boldsymbol{\eta}}}^h := \left\{ \bar{\boldsymbol{\eta}}^h;\ \bar{\boldsymbol{\eta}}^h(\mathbf{x}) = \Sigma_{i=1}^{i=n_{node}}\ N_i(\mathbf{x})\, \bar{\boldsymbol{\eta}}_i\ ;\ \bar{\boldsymbol{\eta}}_i|_{\Gamma_u} = \mathbf{0} \right\} & (b) \\ \mathcal{V}_{\bar{\boldsymbol{\varepsilon}}}^h := \left\{ \boldsymbol{\xi}^h;\ \boldsymbol{\xi}^h(\mathbf{x}) = \Sigma_{e=1}^{e=n_{elem}} \chi_e(\mathbf{x}) \left[\bar{\boldsymbol{\xi}}_e + \mu_S^{(e)} \tfrac{1}{k} (\boldsymbol{\alpha}_e \otimes \mathbf{n})^S \right] \right\} & (c) \\ \mathcal{V}_{\boldsymbol{\sigma}}^h := \left\{ \boldsymbol{\tau}^h;\ \boldsymbol{\tau}^h(\mathbf{x}) = \Sigma_{e=1}^{e=n_{elem}} \chi_e(\mathbf{x})\, \boldsymbol{\tau}_e \right\} & (d) \end{array} \tag{4.116}$$

where

$$\chi_e(\mathbf{x}) := \begin{cases} 1 \text{ for } \mathbf{x} \in \Omega_e \\ 0 \text{ otherwise} \end{cases}$$

and $\boldsymbol{\eta}_i, \bar{\boldsymbol{\eta}}_i, \boldsymbol{\alpha}_e \in \mathbb{R}^2$; $\boldsymbol{\tau}_e, \bar{\boldsymbol{\xi}}_e \in \mathbb{S}$.

4.6.3 Discrete problem

Now the following discrete problem can be stated:

FIND:

$$\begin{array}{ll} \dot{\mathbf{u}}^h \in \mathcal{V}_{\mathbf{u}}^h & (a) \\ \dot{\boldsymbol{\varepsilon}}^h \in \mathcal{V}_{\boldsymbol{\varepsilon}}^h & (b) \\ \dot{\boldsymbol{\sigma}}^h \in \mathcal{V}_{\boldsymbol{\sigma}}^h & (c) \end{array} \tag{4.117}$$

SUCH THAT:

$$\begin{array}{lll} \sum_{e=1}^{e=n_{elem}} \int_{\Omega_e} \dot{\boldsymbol{\sigma}}^h : \nabla^S \bar{\boldsymbol{\eta}}^h \, d\Omega - G_{ext}(\bar{\boldsymbol{\eta}}^h) = 0 & \forall \bar{\boldsymbol{\eta}}^h \in \mathcal{V}_{\bar{\boldsymbol{\eta}}}^h & (a) \\ \sum_{e=1}^{e=n_{elem}} \int_{\Omega_e} \left(\dot{\boldsymbol{\varepsilon}}^h - \nabla^S \dot{\mathbf{u}}^h \right) : \boldsymbol{\tau}^h \, d\Omega = 0 & \forall \boldsymbol{\tau}^h \in \mathcal{V}_{\boldsymbol{\sigma}}^h & (b) \\ \sum_{e=1}^{e=n_{elem}} \int_{\Omega_e} \left(\dot{\boldsymbol{\sigma}}^h - \dot{\Sigma}^h \right) : \boldsymbol{\xi}^h \, d\Omega = 0 & \forall \boldsymbol{\xi}^h \in \mathcal{V}_{\boldsymbol{\varepsilon}}^h & (c) \end{array} \tag{4.118}$$

From equation (4.118-b), it follows that

$$\begin{array}{c} \int_{\Omega_e} \left[\left(\dot{\bar{\boldsymbol{\varepsilon}}}_e + \mu_S^{(e)} \frac{1}{k} (\boldsymbol{\beta}_e \otimes \mathbf{n})^S \right) - \nabla^S \dot{\mathbf{u}}^h \right] : \boldsymbol{\tau}_e \, d\Omega = 0 \\ \forall \boldsymbol{\tau}_e \in \mathbb{S} \; ; \; \forall e \in \mathcal{I} \end{array} \tag{4.119}$$

where $\dot{\boldsymbol{\varepsilon}}^h|_{\Omega_e} = \dot{\bar{\boldsymbol{\varepsilon}}}_e + \mu_S^{(e)} \frac{1}{k} (\boldsymbol{\beta}_e \otimes \mathbf{n})^S$ (with $\dot{\bar{\boldsymbol{\varepsilon}}}_e \in \mathbb{S}$ and $\boldsymbol{\beta}_e \in \mathbb{R}^2$) has been considered. Hence,

$$\Omega_e \dot{\bar{\boldsymbol{\varepsilon}}}_e + l_e (\boldsymbol{\beta}_e \otimes \mathbf{n})^S - \int_{\Omega_e} \nabla^S \dot{\mathbf{u}}^h d\Omega = 0 \quad \forall e \in \mathcal{I} \tag{4.120}$$

solving (4.120) for $\dot{\bar{\boldsymbol{\varepsilon}}}_e$ yields

$$\dot{\bar{\boldsymbol{\varepsilon}}}_e = \underbrace{\frac{1}{\Omega_e} \int_{\Omega_e} \nabla^S \dot{\mathbf{u}}^h d\Omega}_{\overline{\nabla^S \dot{\mathbf{u}}^h}^{(e)}} - \frac{l_e}{\Omega_e} (\boldsymbol{\beta}_e \otimes \mathbf{n})^S \quad \forall e \in \mathcal{I} \tag{4.121}$$

where $\overline{\nabla^S \dot{\mathbf{u}}^h}^{(e)} := \frac{1}{\Omega_e} \int_{\Omega_e} \nabla^S \dot{\mathbf{u}}^h d\Omega$ is the mean value of $\nabla^S \dot{\mathbf{u}}^h$ in Ω_e. Hence,

$$\dot{\boldsymbol{\varepsilon}}^h|_{\Omega_e} = \overline{\nabla^S \dot{\mathbf{u}}^h}^{(e)} + \left(\mu_S^{(e)} \frac{1}{k} - \frac{l_e}{\Omega_e} \right) (\boldsymbol{\beta}_e \otimes \mathbf{n})^S \quad \forall e \in \mathcal{I} \tag{4.122}$$

At element level, we have

$$\int_{\Omega_e} \left(\dot{\boldsymbol{\sigma}}_e - \dot{\Sigma}\right) : \boldsymbol{\xi}^h \, d\Omega =$$
$$\int_{\Omega_e} \left(\dot{\boldsymbol{\sigma}}_e - \dot{\Sigma}\right) : \left[\bar{\boldsymbol{\xi}}_e + \mu_S^{(e)} \frac{1}{k} (\boldsymbol{\alpha}_e \otimes \mathbf{n})^S\right] d\Omega =$$
$$\left(\Omega_e \dot{\boldsymbol{\sigma}}_e - \int_{\Omega_e} \dot{\Sigma} \, d\Omega\right) : \bar{\boldsymbol{\xi}}_e + \left[l_e \left(\dot{\boldsymbol{\sigma}}_e \cdot \mathbf{n}\right) - \int_{\mathcal{S}_e} \dot{\Sigma} \cdot \mathbf{n} d\mathcal{S}\right] \cdot \boldsymbol{\alpha}_e \quad (4.123)$$

From (4.118-c), (4.123) must be null $\forall \bar{\boldsymbol{\xi}}_e \in \mathbb{S}$ and $\forall \boldsymbol{\alpha}_e \in \mathbb{R}^2$. Thus,

$$\begin{aligned} \Omega_e \dot{\boldsymbol{\sigma}}_e - \int_{\Omega_e} \dot{\Sigma} \, d\Omega = 0 \\ l_e \left(\dot{\boldsymbol{\sigma}}_e \cdot \mathbf{n}\right) - \int_{\mathcal{S}_e} \dot{\Sigma} \cdot \mathbf{n} d\mathcal{S} = 0 \end{aligned} \quad (4.124)$$

Defining $\overline{\dot{\Sigma}_{\Omega_e}} := \frac{1}{\Omega_e} \int_{\Omega_e} \dot{\Sigma} \, d\Omega$ and $\overline{\dot{\Sigma}_{\mathcal{S}}} := \frac{1}{l_e} \int_{\mathcal{S}_e} \dot{\Sigma} d\mathcal{S}$, we have

$$\begin{aligned} \dot{\boldsymbol{\sigma}}_e &= \overline{\dot{\Sigma}_{\Omega_e}} \\ \dot{\boldsymbol{\sigma}}_e \cdot \mathbf{n} &= \overline{\dot{\Sigma}_{\mathcal{S}}} \cdot \mathbf{n} \end{aligned} \quad (4.125)$$

which means that (4.118-c) implies

$$\overline{\dot{\Sigma}_{\Omega_e}} \cdot \mathbf{n} = \overline{\dot{\Sigma}_{\mathcal{S}}} \cdot \mathbf{n} \quad \forall e \in \mathcal{J} \quad (4.126)$$

this is the traction continuity stated in terms of the mean values of $\dot{\Sigma}$.

We can rephrase (4.126) in a more convenient format:

$$\frac{1}{l_e} \int_{\mathcal{S}_e} \dot{\Sigma} d\mathcal{S} \cdot \mathbf{n} - \frac{1}{\Omega_e} \int_{\Omega_e} \dot{\Sigma} d\Omega \cdot \mathbf{n} = 0 \quad \forall e \in \mathcal{J} \quad (4.127)$$

and, hence,

$$\int_{\Omega_e} \left(\mu_S^{(e)} \frac{1}{k} - \frac{l_e}{\Omega_e}\right) \dot{\Sigma} \cdot \mathbf{n} \, d\Omega = 0 \quad \forall e \in \mathcal{J} \quad (4.128)$$

On the other hand, from (4.125), we have

$$\int_{\Omega_e} \dot{\boldsymbol{\sigma}}_e : \nabla^S \bar{\boldsymbol{\eta}}^h \, d\Omega - G_{ext} = \overline{\dot{\Sigma}_{\Omega_e}} : \int_{\Omega_e} \nabla^S \bar{\boldsymbol{\eta}}^h \, d\Omega - G_{ext} \tag{4.129}$$

Let us define $\overline{\nabla^S \bar{\boldsymbol{\eta}}^h}^{(e)} := \frac{1}{\Omega_e} \int_{\Omega_e} \nabla^S \bar{\boldsymbol{\eta}}^h d\Omega$. Then,

$$\int_{\Omega_e} \dot{\boldsymbol{\sigma}}_e : \nabla^S \bar{\boldsymbol{\eta}}^h \, d\Omega - G_{ext} = \Omega_e \overline{\dot{\Sigma}_{\Omega_e}} : \overline{\nabla^S \bar{\boldsymbol{\eta}}^h}^{(e)} - G_{ext} \tag{4.130}$$

Finally, considering (4.118-a), the definition of $\overline{\dot{\Sigma}_{\Omega_e}}$, and (4.130), we can state

$$\sum_{e=1}^{e=n_{elem}} \int_{\Omega_e} \dot{\Sigma} : \overline{\nabla^S \bar{\boldsymbol{\eta}}^h}^{(e)} d\Omega - G_{ext} = 0 \quad \forall \bar{\boldsymbol{\eta}}^h \in \mathcal{V}_{\bar{\eta}}^h \tag{4.131}$$

In summary, the system of equations (4.118) is equivalent to

$$\begin{aligned} &\sum_{e=1}^{e=n_{elem}} \int_{\Omega_e} \dot{\Sigma} : \overline{\nabla^S \bar{\boldsymbol{\eta}}^h}^{(e)} d\Omega - G_{ext} = 0 \quad \forall \bar{\boldsymbol{\eta}}^h \in \mathcal{V}_{\bar{\eta}}^h \quad (a) \\ &\int_{\Omega_e} \left(\mu_S^{(e)} \frac{1}{k} - \frac{l_e}{\Omega_e} \right) \dot{\Sigma} \cdot \mathbf{n} \, d\Omega = 0 \qquad \forall e \in \mathcal{J} \quad (b) \end{aligned} \tag{4.132}$$

with the elemental strain rate having the structure stated in (4.122)

$$\dot{\boldsymbol{\varepsilon}}_e \equiv \dot{\boldsymbol{\varepsilon}}^h|_{\Omega_e} = \overline{\nabla^S \dot{\mathbf{u}}^h}^{(e)} + \left(\mu_S^{(e)} \frac{1}{k} - \frac{l_e}{\Omega_e} \right) (\boldsymbol{\beta}_e \otimes \mathbf{n})^S \tag{4.133}$$

Remark 47 *By comparing the expression of the strain rate for this approach ,stated in (4.133), with the strain rate for the assumed enhanced strain based approach, stated in (4.109), we can observe that the enhancement term,* $\left(\mu_S^{(e)} \frac{1}{k} - \frac{l_e}{\Omega_e} \right) (\boldsymbol{\beta}_e \otimes \mathbf{n})^S$, *is the same for both of them. However, in the present approach the term* $\overline{\nabla^S \dot{\mathbf{u}}^h}^{(e)}$ *is element-wise constant, which makes the cancellation of the strain rate possible.*

Remark 48 *The term* $\overline{\nabla^S \dot{\mathbf{u}}^h}^{(e)}$ *can be approximated by the value of* $\nabla^S \dot{\mathbf{u}}^h$ *at the sampling point RSP*[11]*, placed at the centroid of the element. Then, the classical link between mixed elements and reduced integration is recovered in this formulation.*

[11] For non-distorted elements this is not an approximation but an identity

4.6.4 Matrix representation

The discrete strain rate field in its matrix form reads

$$\begin{aligned}\{\dot{\varepsilon}\}^{(e)} &= \mathbf{B}^{(e)}_{RSP}\dot{\mathbf{d}}^{(e)} + \underbrace{\left(\mu_S^{(e)}\frac{1}{k} - \frac{l_e}{\Omega_e}\right)[\mathbf{n}]^{(e)}\boldsymbol{\beta}_e}_{=:\mathbf{G}^{(e)}} \\ &= \mathbf{B}^{(e)}_{RSP}\dot{\mathbf{d}}^{(e)} + \mathbf{G}^{(e)}_e\boldsymbol{\beta}_e \end{aligned} \tag{4.134}$$

where $\boldsymbol{\beta}_e \in \mathbb{R}^2$ and $\mathbf{B}^{(e)}_{RSP}$ is the value of matrix $\mathbf{B}^{(e)}$ at the sampling point RSP.

The matrix representation of the strain rate variations is

$$\{\boldsymbol{\xi}\}^{(e)} = \mathbf{B}^{(e)}_{RSP}\{\bar{\boldsymbol{\eta}}\}^{(e)} + \mathbf{G}^{(e)}\boldsymbol{\alpha}_e \tag{4.135}$$

Then, the incremental residual forces at element level corresponding to (4.132) are

$$\begin{aligned}\dot{\mathbf{R}}^{(e)} &:= \int_{\Omega_e} \mathbf{B}^{(e)^T}_{RSP}\ \{\dot{\Sigma}\}^{(e)}\ d\Omega - \dot{\mathbf{F}}^{(e)}_{ext} \quad (a) \\ \dot{\mathbf{r}}^{(e)} &:= \int_{\Omega_e} \mathbf{G}^{(e)^T}\ \{\dot{\Sigma}\}^{(e)}\ d\Omega \quad (b)\end{aligned} \tag{4.136}$$

where $\dot{\mathbf{F}}^{(e)}_{ext}$ is the vector of incremental external forces at element level.

Considering the incrementally linear constitutive relation expressed in (4.33), the incremental residual forces (4.136) can be rewritten as

$$\begin{bmatrix} \mathbf{K}^{(e)}_{dd} & \mathbf{K}^{(e)}_{d\alpha} \\ \mathbf{K}^{(e)}_{\alpha d} & \mathbf{K}^{(e)}_{\alpha\alpha} \end{bmatrix} \begin{Bmatrix} \dot{\mathbf{d}}^{(e)} \\ \boldsymbol{\beta}_e \end{Bmatrix} - \begin{Bmatrix} \dot{\mathbf{F}}^{(e)}_{ext} \\ 0 \end{Bmatrix} = \begin{Bmatrix} \dot{\mathbf{R}}^{(e)} \\ \dot{\mathbf{r}}^{(e)} \end{Bmatrix} \tag{4.137}$$

with

$$\begin{aligned}\mathbf{K}^{(e)}_{dd} &= \int_{\Omega_e} \mathbf{B}^{(e)^T}_{RSP}\ \mathbf{D}\ \mathbf{B}^{(e)}_{RSP} d\Omega \\ \mathbf{K}^{(e)}_{d\alpha} &= \int_{\Omega_e} \mathbf{B}^{(e)^T}_{RSP}\ \mathbf{D}\ \mathbf{G}^{(e)} d\Omega \\ \mathbf{K}^{(e)}_{\alpha d} &= \int_{\Omega_e} \mathbf{G}^{(e)^T}\ \mathbf{D}\ \mathbf{B}^{(e)}_{RSP} d\Omega \\ \mathbf{K}^{(e)}_{\alpha\alpha} &= \int_{\Omega_e} \mathbf{G}^{(e)^T}\ \mathbf{D}\ \mathbf{G}^{(e)} d\Omega\end{aligned} \tag{4.138}$$

Remark 49 *The tangent stiffness matrix of this formulation is, as expected, also symmetric.*

Let us, now, define

$$\bar{\mathbf{B}}^{(e)} = \left[\mathbf{B}^{(e)}_{RSP}, \mathbf{G}^{(e)}\right] \tag{4.139}$$

and

$$\begin{aligned} \dot{\bar{\mathbf{R}}}^{(e)} &= \left[\begin{array}{cc} (\dot{\mathbf{R}}^{(e)})^T, & \dot{\mathbf{r}}^{(e)^T} \end{array}\right] \\ \dot{\bar{\mathbf{F}}}^{(e)}_{ext} &= \left[\begin{array}{cc} (\dot{\mathbf{F}}^{(e)}_{ext})^T, & \mathbf{0}^T \end{array}\right]^T \\ \dot{\bar{\mathbf{d}}}^{(e)} &= \left[\begin{array}{cc} (\dot{\mathbf{d}}^{(e)})^T & \boldsymbol{\beta}_e^T \end{array}\right]^T \end{aligned} \tag{4.140}$$

With this in hand, the *B-bar* format of (4.137) is

$$\int_{\Omega_e} \bar{\mathbf{B}}^{(e)^T}\, \mathbf{D}\, \bar{\mathbf{B}}^{(e)} \dot{\bar{\mathbf{d}}}^{(e)} d\Omega - \dot{\bar{\mathbf{F}}}^{(e)}_{ext} = \dot{\bar{\mathbf{R}}}^{(e)} \tag{4.141}$$

Finally, the global system of equations corresponding to (4.132), is given by

$$\overset{n_{elem}}{\underset{e=1}{A}} \left[\int_{\Omega_e} \bar{\mathbf{B}}^{(e)^T}\, \mathbf{D}\, \bar{\mathbf{B}}^{(e)} \dot{\bar{\mathbf{d}}}^{(e)} d\Omega - \dot{\bar{\mathbf{F}}}^{(e)}_{ext} = 0\right] \tag{4.142}$$

4.6.5 A note on some implementation aspects

It is well known that the use of reduced integration in four-noded bilinear elements can lead to the appearance of the so-called hour-glass modes. However, the mixed formulation presented in this section is implemented in such a way that the *modifications on the basic element S4n are effective only for the band of elements that captures the discontinuity and only after the time at which this discontinuity appears.* Thus, the elements outside this band behave as the original S4n. Therefore, the elements affected by the reduced integration are restricted to a single band of one element width. This reduces substantially the possible presence of instabilities.

4.7 Assumed strain re-enhancement

To develop this approach, we work on the basis of the formulation of the $S4n$ element described in Section 4.4. We require the present formulation to fulfill the following conditions:

- The orthogonality condition (4.93) :

$$\int_{\Omega_e} \dot{\tilde{\varepsilon}}^h : \tau^h d\Omega = 0 \quad \forall \dot{\tilde{\varepsilon}}^h \in \mathcal{V}_{\dot{\varepsilon}}^h \quad \forall \tau^h \in \mathcal{V}_{\sigma}^h \tag{4.143}$$

- To include linear polynomial terms that contribute to alleviate the stress locking phenomenon.

Having these conditions in mind, the following strain enhancement is proposed:

$$\dot{\tilde{\varepsilon}}^h|_{\Omega_e} \equiv \dot{\tilde{\varepsilon}}_e = \underbrace{(\mu_S^{(e)} \frac{1}{k} - \frac{l_e}{\Omega_e})(\boldsymbol{\beta}_e \otimes \mathbf{n})^S}_{\dot{\tilde{\varepsilon}}_1^{(e)}} + \underbrace{\frac{1}{J} y \mathbf{Y}_e + \frac{1}{J} z \mathbf{Z}_e}_{\dot{\tilde{\varepsilon}}_2^{(e)}} \tag{4.144}$$

where y and z stand for the isoparametric coordinates of the standard four-noded bilinear element, J is the Jacobian of the isoparametric transformation relating differential areas in the regular and isoparametric spaces through

$$d\Omega = J \, dy \, dz \tag{4.145}$$

while $\mathbf{Y}_e$ and $\mathbf{Z}_e$ are two second order element-wise constant tensors whose 2-D matrix (Voigt) representations $\{\mathbf{Y}_e\} = \begin{bmatrix} Y_1 & Y_2 & Y_3 \end{bmatrix}^T$ and $\{\mathbf{Z}_e\} = \begin{bmatrix} Z_1 & Z_2 & Z_3 \end{bmatrix}^T$ are two vectors containing six additional degrees of freedom per element.

Let us analyze expression (4.144): $\dot{\tilde{\varepsilon}}_2^{(e)}$ contains terms of degree one that are included in the structure of the total enhancement, $\dot{\tilde{\varepsilon}}_e$, as a re-enhancement of $\dot{\tilde{\varepsilon}}_1^{(e)}$, which is the basic enhancement already used in element $S4n$. Thus, the first condition required for this formulation is fulfilled. Let us, now, verify if condition two is satisfied:

$$\int_{\Omega_e} \dot{\tilde{\varepsilon}}_1^{(e)} : \tau_e \, d\Omega = \int_{\Omega_e} \left(\mu_S^{(e)} \frac{1}{k} - \frac{l_e}{\Omega_e} \right) (\boldsymbol{\beta}_e \otimes \mathbf{n})^S : \tau_e \, d\Omega =$$
$$\underbrace{\int_{\Omega_e} (\mu_S^{(e)} \frac{1}{k} - \frac{l_e}{\Omega_e}) d\Omega}_{l_e - l_e = 0} (\boldsymbol{\beta}_e \otimes \mathbf{n})^S : \tau_e = 0 \tag{4.146}$$

$$\int_{\Omega_e} \dot{\bar{\boldsymbol{\varepsilon}}}_2^{(e)} : \boldsymbol{\tau}_e d\Omega = \int_{\Omega_e} \frac{1}{J}(y\mathbf{Y}_e + z\mathbf{Z}_e) : \boldsymbol{\tau}_e d\Omega =$$
$$\underbrace{\int_{-1}^{+1}\int_{-1}^{+1} y\, dydz}_{=0}\ \mathbf{Y}_e : \boldsymbol{\tau}_e + \underbrace{\int_{-1}^{+1}\int_{-1}^{+1} z\, dydz}_{=0}\ \mathbf{Z}_e : \boldsymbol{\tau}_e = 0 \qquad (4.147)$$

4.7.1 Matrix representation

Expression (4.144), can be stated in matrix form as

$$\{\dot{\bar{\boldsymbol{\varepsilon}}}\}^{(e)} = \mathbf{B}^{(e)}\dot{\mathbf{d}}^{(e)} + \mathbf{G}^{(e)}\mathbf{b}^{(e)} \qquad (4.148)$$

where

$$\mathbf{G}^{(e)} = \begin{bmatrix} \gamma n_x & 0 & y & 0 & 0 & z & 0 & 0 \\ 0 & \gamma n_y & 0 & y & 0 & 0 & z & 0 \\ \gamma n_y & \gamma n_x & 0 & 0 & y & 0 & 0 & z \end{bmatrix}$$

with $\gamma = \left(\mu_S^{(e)}\frac{1}{k} - \frac{l_s}{\Omega_e}\right)$, and

$$\mathbf{b}^{(e)} = \left[\ \boldsymbol{\beta}_e^T,\ \ \{\mathbf{Y}_e\}^T,\ \ \{\mathbf{Z}_e\}^T\ \right]^T$$

The matrix representation of the strain rate variations is

$$\{\boldsymbol{\xi}\}^{(e)} = \mathbf{B}^{(e)}\{\bar{\boldsymbol{\eta}}\}^{(e)} + \mathbf{G}^{(e)}\mathbf{a}^{(e)} \qquad (4.149)$$

where

$$\mathbf{a}^{(e)} = \left[\ \boldsymbol{\alpha}_e^T,\ \ \{\delta\mathbf{Y}_e\}^T,\ \ \{\delta\mathbf{Z}_e\}^T\ \right]^T$$

with $\delta\mathbf{Y}_e$ and $\delta\mathbf{Z}_e$ being the variations of $\mathbf{Y}_e$ and $\mathbf{Z}_e$, respectively.

The expression of the incremental residual forces at element level is

$$\begin{aligned} \dot{\mathbf{R}}^{(e)} &:= \int_{\Omega_e} \mathbf{B}^{(e)^T}\ \{\dot{\Sigma}\}^{(e)}\ d\Omega - \dot{\mathbf{F}}_{ext}^{(e)} \quad (a) \\ \dot{\mathbf{r}}^{(e)} &:= \int_{\Omega_e} \mathbf{G}^{(e)^T}\ \{\dot{\Sigma}\}^{(e)}\ d\Omega \qquad\qquad (b) \end{aligned} \qquad (4.150)$$

where $\dot{\mathbf{F}}_{ext}^{(e)}$ is the vector of incremental external forces at element level.

Considering the incrementally linear constitutive relation expressed in (4.33), the expression of the residual forces (4.150) can be rephrased as

$$\begin{bmatrix} \mathbf{K}_{dd}^{(e)} & \mathbf{K}_{d\alpha}^{(e)} \\ \mathbf{K}_{\alpha d}^{(e)} & \mathbf{K}_{\alpha\alpha}^{(e)} \end{bmatrix} \begin{Bmatrix} \dot{\mathbf{d}}^{(e)} \\ \mathbf{b}^{(e)} \end{Bmatrix} - \begin{Bmatrix} \dot{\mathbf{F}}_{ext}^{(e)} \\ \mathbf{0} \end{Bmatrix} = \begin{Bmatrix} \dot{\mathbf{R}}^{(e)} \\ \dot{\mathbf{r}}^{(e)} \end{Bmatrix} \tag{4.151}$$

with

$$\begin{aligned} \mathbf{K}_{dd}^{(e)} &= \int_{\Omega_e} \mathbf{B}^{(e)^T}\ \mathbf{D}\ \mathbf{B}^{(e)} d\Omega \\ \mathbf{K}_{d\alpha}^{(e)} &= \int_{\Omega_e} \mathbf{B}^{(e)^T}\ \mathbf{D}\ \mathbf{G}^{(e)} d\Omega \\ \mathbf{K}_{\alpha d}^{(e)} &= \int_{\Omega_e} \mathbf{G}^{(e)^T}\ \mathbf{D}\ \mathbf{B}^{(e)} d\Omega \\ \mathbf{K}_{\alpha\alpha}^{(e)} &= \int_{\Omega_e} \mathbf{G}^{(e)^T}\ \mathbf{D}\ \mathbf{G}^{(e)} d\Omega \end{aligned} \tag{4.152}$$

Remark 50 *Again the resulting tangent stiffness matrix is symmetrical.*

We define now

$$\bar{\mathbf{B}}^{(e)} = \left[\mathbf{B}^{(e)}, \mathbf{G}^{(e)}\right] \tag{4.153}$$

and

$$\begin{aligned} \dot{\bar{\mathbf{R}}}^{(e)} &= \left[\ (\dot{\mathbf{R}}^{(e)})^T,\ \ \dot{\mathbf{r}}^{(e)^T}\ \right] \\ \dot{\bar{\mathbf{F}}}_{ext}^{(e)} &= \left[\ (\dot{\mathbf{F}}_{ext}^{(e)})^T,\ \ \mathbf{0}^T\ \right]^T \\ \dot{\bar{\mathbf{d}}}^{(e)} &= \left[\ (\dot{\mathbf{d}}^{(e)})^T\ \ \mathbf{b}^{(e)^T}\ \right]^T \end{aligned} \tag{4.154}$$

The *B-bar* format of (4.151) is, then,

$$\int_{\Omega_e} \bar{\mathbf{B}}^{(e)^T}\ \mathbf{D}\ \bar{\mathbf{B}}^{(e)} \dot{\bar{\mathbf{d}}}^{(e)} d\Omega - \dot{\bar{\mathbf{F}}}_{ext}^{(e)} = \dot{\bar{\mathbf{R}}}^{(e)} \tag{4.155}$$

The global system of equations is given by

$$\overset{n_{elem}}{\underset{e=1}{A}} \left[\int_{\Omega_e} \bar{\mathbf{B}}^{(e)^T}\ \mathbf{D}\ \bar{\mathbf{B}}^{(e)} \dot{\bar{\mathbf{d}}}^{(e)} d\Omega - \dot{\bar{\mathbf{F}}}_{ext}^{(e)} = \mathbf{0} \right] \tag{4.156}$$

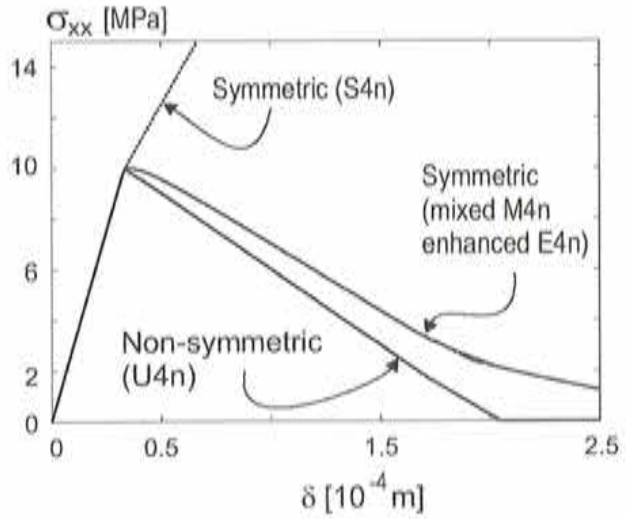

Figure 4.4: Simple traction test: comparison of several elements with embedded discontinuities.

4.7.2 A note on some implementation aspects

The re-enhancement proposed in this section does not fullfil the so-called stability condition[Simo and Rifai, 1990]: $\mathcal{V}_{\tilde{g}}^h \cap \nabla^s \mathcal{V}_{\mathbf{u}}^h = \{0\}$. Nevertheless, as in the mixed formulation presented in Section 4.6, the implementation of this element was performed in such a way that the *re-enhancement is activated only for the band of elements that captures the discontinuity and only after the discontinuous bifurcation time*. Again the modified elements are restricted to a band of one element width and the possibilities for the appearance of instabilities are negligible.

4.8 Performance Assessment

Based, again, on [Oliver et al., 2003], the following nomenclature is adopted:

- *M4n* for the mixed element presented in Section 4.6.
- *E4n* for the re-enhanced element presented in Section 4.7.

The test of Section 4.5.1 and Fig. 4.3 is now repeated using the modified elements *M4n* and *E4n*. The results, again in terms of $\sigma_{xx} - \delta$ curves, are presented in Fig. 4.4 as well as the ones obtained with the original element *S4n* and the exact result (*U4n*).

The reduction in the stress-locking effect obtained with the new elements is dramatic (additional numerical results with comparative analyses of the elements treated here can be found in [Oliver et al., 2003]). However, the performance of element $U4n$ is still better. Further development of the strategies presented in Sections 4.6 and 4.7 is perhaps necessary. Nevertheless, the possibility of modifications in the spirit of $M4n$ seems limited, whereas further enhancement in the spirit of $E4n$ can lead to very cumbersome formulations.

One of the main motivations for exploring the possibility of a self-propagating element is that it would permit to dispense with the tracking algorithm, which constitutes the major drawback of element $U4n$. However, the use of this element still seems highly desirable, due to its excellent performance. Then, the idea of trying to devise an efficient tracking algorithm that allows to simulate complex problems (multiple discontinuity paths, for instance) emerges as an especially interesting research line. In order to attain this goal, the next chapter is devoted to studying these tracking strategies.

Chapter 5

Tracking strategies

In the previous chapters some of the ingredients needed for the numerical simulation of strong discontinuities in solids have been laid out. Chapter 2 dealt with the necessary conditions for the appearance of localization bands. The kinematics of strong discontinuities and the implications of its adoption in the context of continuum constitutive modelling were studied in Chapter 3. Then, in Chapter 4, a group of finite element formulations that allow for capturing strong discontinuities within an element domain were analyzed. However, the very important issue of the inception and propagation of such discontinuities has not been tackled yet. In an ideal scenario all the information necessary for managing the initiation and propagation of a discontinuity path should come from the discontinuous bifurcation analysis. Nevertheless, in numerical simulations and, particularly, in the case of the non-symmetric formulation studied in Section 4.2, the use of a tracking algorithm [Oliver, 1996b] is also necessary. These algorithms are devised to predict and capture the geometrical position of a discontinuity path inside a body or, more specifically, inside every element crossed by that discontinuity.

The strategies to track discontinuity paths in solids are studied in this chapter. In Section 5.1 a motivation for the necessity of tracking algorithms is made. Section 5.2 describes the general characteristics of a tracking strategy and describes the groups in which such strategies can be classified. A heat-conduction-like problem is proposed as a way to compute implicitly all the possible discontinuity lines in a solid for a given time in Section 5.3. In Section 5.4, the performance of this methodology is assessed through some representative numerical simulations. Finally, the concept of an *exclusion zone* is motivated and explained in Section 5.5.

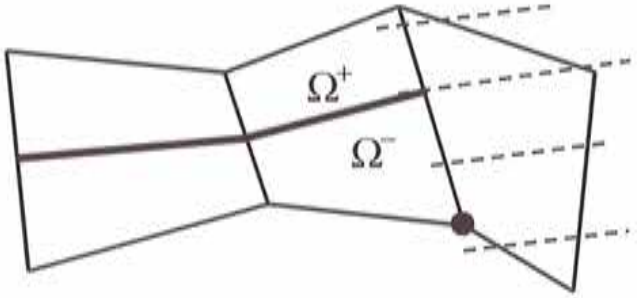

Figure 5.1: Tracing a discontinuity path in a patch of elements.

5.1 Motivation

Consider a body Ω containing a discontinuity line $\mathcal{S}$, which splits Ω into Ω^+ and Ω^-, discretized into a finite element mesh consisting of four-noded quadrilaterals. Consider, also, the open domain Ω_e corresponding to an element e crossed by $\mathcal{S}$, which partitions Ω_e into $\Omega_e^+ \subset \Omega^+$ and $\Omega_e^- \subset \Omega^-$. Remember from Section 4.2.2., the expression, at element level, of the finite element interpolation of the displacement rate corresponding to the nonsymmetric formulation:

$$\dot{\mathbf{u}}^{h^{(e)}}(\mathbf{x},t) = \Sigma_{i=1}^{i=4}\, N_i^{(e)}(\mathbf{x})\dot{\mathbf{d}}_i(t) + \mathcal{M}_{\mathcal{S}}^{(e)}(\mathbf{x})\,[[\dot{\mathbf{u}}]]_e(t) \tag{5.1}$$

Let us focus on the second term of the right hand side of (5.1), which is the term that captures the displacement jump, and more specifically in

$$\mathcal{M}_{\mathcal{S}}^{(e)} := H_{\mathcal{S}}^{(e)}(\mathbf{x}) - \varphi^{(e)} \tag{5.2}$$

$H_{\mathcal{S}}^{(e)}$ is the Heaviside function acting on the elemental discontinuity line ($\mathcal{S}_e = \Omega_e \cap \mathcal{S}$), i.e.,

$$H_{\mathcal{S}}^{(e)}(\mathbf{x}) = \begin{cases} 1 & \forall \mathbf{x} \in \Omega_e^+ \\ 0 & \forall \mathbf{x} \in \Omega_e^- \end{cases} \tag{5.3}$$

and

$$\varphi^{(e)} = \Sigma_{i^+=1}^{n_e^+} N_{i^+} \tag{5.4}$$

where n_e^+ stands for the number of nodes of element e lying on $\overline{\Omega}_e^+$ and N_{i^+} denotes the shape function corresponding to node $i^+ \in \overline{\Omega}_e^+$.

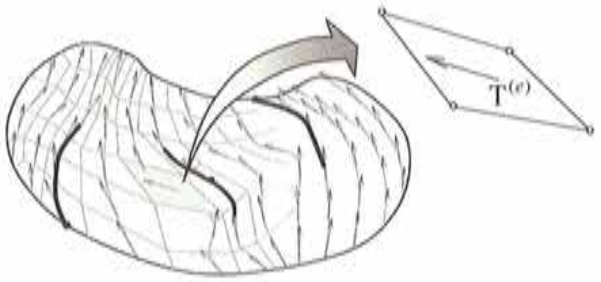

Figure 5.2: Propagation vector field.

As said in Section 4.2.2., the discontinuous bifurcation analysis corresponding to an element is performed in a single sampling point placed at the centroid of that element, which we named RSP. Thus, we know when an element undergoes localization and the direction of the corresponding localization band, but we do not know its position within the element. However, in order to determine $\mathcal{M}_{\mathcal{S}}^{(e)}$, we need to know which nodes lie in $\overline{\Omega}_e^+$. If we consider one single element, the position of $\mathcal{S}_e$ can be fixed arbitrarily; however, when the fact that a discontinuity, in general, passes through several elements is taken into account, we have to be more careful. The reason is the following: suppose that a node belongs to two elements crossed by the discontinuity and suppose that for one of those elements that node lies on $\overline{\Omega}_e^+$, then it cannot be in $\overline{\Omega}_e^-$ for the other element and vice versa. In a way, this means that, somehow, the discontinuity path has to be continuous across elements. This continuity is understood in the sense that a node has to unambiguously be either in Ω^+ or in Ω^-. This fact is illustrated in Fig. 5.1, where a patch of elements is considered. The continuous line indicates the part of a discontinuity that has already developed. Some possible options to trace the discontinuity for an element that has bifurcated for the first time are indicated by parallel dotted lines. The node which is signaled with a dot could lie in Ω^+ and Ω^- at the same time if some continuity of the discontinuity path is not enforced. Hence, the necessity of an algorithm that guarantees the alignment of the elemental discontinuity interfaces belonging to the same discontinuity path becomes apparent.

5.2 Tracking strong discontinuities

In order to track the evolution through time of a strong discontinuity $\mathcal{S}$ in a solid Ω, we need to have the following information:

1. *A failure criterion.* It tell us when a material point becomes part of disconti-

nuity line. A simple example of such criteria is the initiation of the inelastic regime [Wells and Sluys, 2000]. The singularity of the acoustic tensor, derived in Chapter 2 in the context of the discontinuous bifurcation analysis, is an example of a more rigorous, from the Continuum Mechanics standpoint, failure criterion.

2. *A direction of propagation.* This direction can be determined from empirical considerations, for instance, the direction orthogonal to the maximum tensile stress. Again the discontinuous bifurcation analysis can be used to get this information as done in Section 2.3. for an isotropic continuum damage model.

We assume here that this information is available for every material point of the solid at any time of the analysis.

Remark 51 *Regarding the direction of propagation, this assumption implies the existence of a vector field with values* $\mathbf{T}(\mathbf{x},t)$ *(see Fig. 5.2), defined for all* $\mathbf{x} \in \Omega$ *and for all* t *belonging to the analysis time interval, signaling the direction in which the propagation of a discontinuity path having its tip at* $\mathbf{x}$ *would occur if the failure criterion were met at time* t *for that material point. In two-dimensional cases this vector field is defined by an angle; for instance, the critical angle obtained by means of the discontinuous bifurcation analysis in Section 2.3.*

Remark 52 *In the discrete BVP, the information for tracking a discontinuity is taken from representative points discretely distributed. For the finite element discretization presented in Section 4.2.2, this information is available at each sampling point RSP, placed at the centroid of every element.*

In [Oliver et al., 2002c] a classification of the existing type of tracking strategies was presented. They were divided into *local strategies* and *global strategies*. We describe them in the following two subsections.

5.2.1 Local tracking

In this type of strategies, the alignment of an elemental discontinuity line is only enforced explicitly with respect to its neighbor elements.

Consider a two-dimensional body Ω discretized into a finite element mesh and the set of material lines, hereafter called *possible discontinuity lines*, $\{S_i\}$ whose tangent vector, for time t, at every point $\mathbf{x} \in \Omega$ is $\mathbf{T}(\mathbf{x},t)$. Any discontinuity path appearing at a given time t of an incremental loading process has to coincide with one of these lines. Let us now describe schematically how a local algorithm works.

The determination of a possible discontinuity line S_i can be performed through the following geometrical algorithm (see Fig. 5.3) at element level:

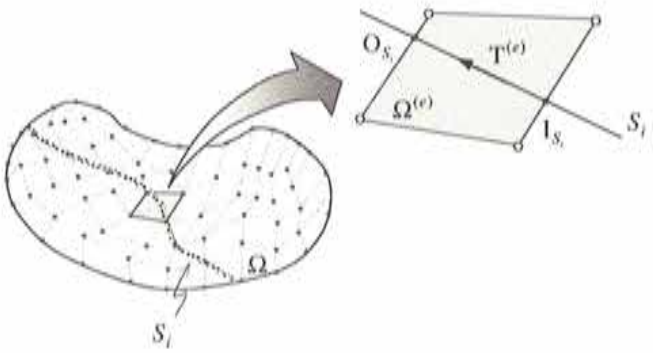

Figure 5.3: Local tracking.

DATA:	Input point of the possible discontinuity line I_{S_i}. Propagation direction $\mathbf{T}^{(e)}$.
ACTIONS:	
1)	Trace a line in the direction of $\mathbf{T}^{(e)}$ passing through I_{S_i}.
2)	Find the intersected output point O_{S_i}.
3)	Consider the geometrical position of O_{S_i} as the input tracking point I_{S_i} for the neighbour element $e+1$.

(5.5)

Remark 53 *This algorithm requires handling a* side-connectivity array *indicating those elements that share sides with a given one.*

It is clear that, for some element, called root element (r_i), crossed by S_i, the discontinuity input point I_{S_i} has to be arbitrarily fixed. In practice, only some of these possible discontinuity lines S_i are traced. When only a single line S_i is considered, the root element is the first bifurcated element. In this case the algorithm is very simple and robust. However, as the number of possible discontinuity lines increases, this algorithm can become extremely cumbersome.

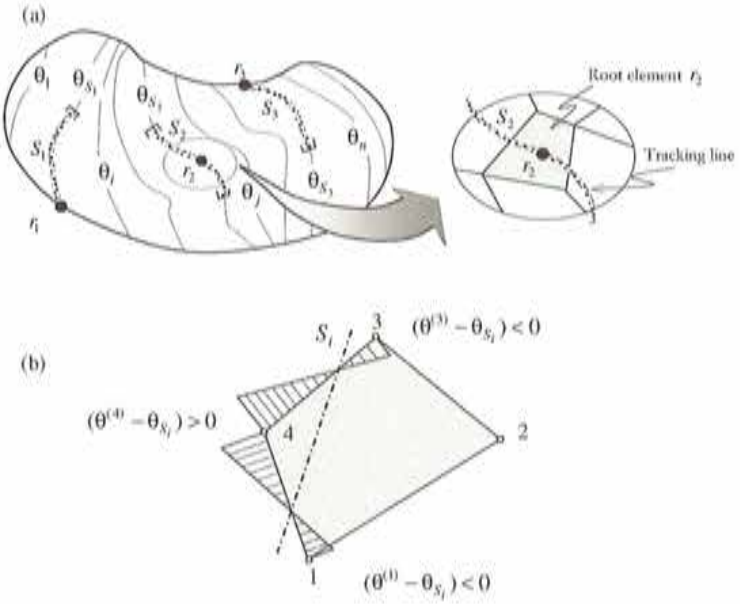

Figure 5.4: Global tracking.

5.2.2 Global tracking

Here, all the possible discontinuity lines S_i are implicitly traced. Since, by construction, at every point $\mathbf{x}$ of the possible discontinuity lines S_i, its tangent has the same direction as the propagation vector $\mathbf{T}(\mathbf{x},t)$, then S_i are the members of the family of curves enveloping the vector field $\mathbf{T}$. Therefore, the construction of the envelopes implicitly supplies all the possible discontinuity lines at time t. Assume that these envelopes can be described by a scalar field with values $\theta(\mathbf{x})$ whose *level contours* define all the possible discontinuity lines as (see Fig. 5.4)

$$S_i := \{\mathbf{x} \in \Omega \,;\, \theta(\mathbf{x}) = \theta_{S_i}\} \tag{5.6}$$

where θ_{S_i} is a constant that acts as the "label" of the possible discontinuity line S_i.

In Section 5.3, a methodology for the construction of the scalar field θ based on solving a heat-conduction-like BVP is presented. The solution of the corresponding finite element BVP provides the nodal values of θ^h (the finite element approximation of θ).

With this information in hand, the algorithm for tracing, at element level, possible discontinuity lines at a given time t of an incremental loading process can be

schematically described by the two following steps:

1. *Identify the possible discontinuity line label corresponding to the root elements.* The position of the possible discontinuity line can be arbitrarily fixed in every root element r_i. A possible choice is to consider that the discontinuity path passes through its centroid $\mathbf{x}_0$ (see Fig. 5.4-a). Consequently, the corresponding temperature level is the average of the nodal values of θ for this root element:

$$\theta_{S_i} = \frac{1}{n} \sum_{k=1}^{n} \theta^{(k)} \tag{5.7}$$

where n stands for the number of nodes of the element (i.e.: $n = 3$, for linear triangles and $n = 4$ for linear quadrilaterals). Then, as said before, the constant θ_{S_i} is the label corresponding to line S_i.

2. *Determine the position of the possible discontinuity line inside a given element.* Once the nodal values $\theta^{(k)}$ and the possible discontinuity line labels θ_{S_i} are known, the position of S_i inside a given element e can be determined through the following algorithm (see Fig. 5.4-b):

DATA:	Nodal values of θ at element e: $\theta^{(k)}$. Label of the possible discontinuity line: θ_{S_i}.
ACTIONS:	
1)	Determine the sides involving a change of sign of $(\theta^{(k)} - \theta_{S_i})$ at their vertices.
2)	For every one of these sides compute the position of S_i through linear interpolation.

(5.8)

Remark 54 *Notice that no information from the neighbor elements is required in the preceding algorithm. This fact can be exploited for implementation purposes.*

To determine the root elements at a given time t, one has to verify for each possible root element that it is not crossed by the discontinuity line of another root element. In order to guarantee this, one needs the concept of *active discontinuity line*. We say that one of the possible discontinuity lines S_i is *active* when it crosses at least one bifurcated element. Then, when an element bifurcates, two possibilities arise:

- If the element is crossed by a line S_i that is already active, the algorithm in (5.8) is applied to that element.
- Otherwise, the element is considered a root element and the possible discontinuity line passing through its centroid becomes active.

5.3 Enveloping of the propagation vector field

In this section, we present a procedure to compute the envelopes of the vector field $\mathbf{T}$ defined on a two-dimensional domain Ω. We assume that $\mathbf{T}$ is a unit vector field, i.e.:

$$\mathbf{T} \cdot \mathbf{T} = \|\mathbf{T}\|^2 = 1 \qquad in\ \Omega \tag{5.9}$$

whose sense is considered to be non-relevant. Our aim is to obtain an scalar field with values $\theta(\mathbf{x})$ whose level lines are the envelopes of $\mathbf{T}$. By definition (5.6), each level line has to fulfill the following condition:

$$\theta(\mathbf{x}) = \theta_{S_i} \qquad in\ S_i \tag{5.10}$$

where θ_{S_i} is a constant. Then, since the set $\{S_i\}$ is the family of envelopes of the field $\mathbf{T}$, the following equation can be stated:

$$\frac{\partial \theta}{\partial T} = \mathbf{T} \cdot \nabla\theta = \nabla\theta \cdot \mathbf{T} = 0 \qquad in\ \Omega \tag{5.11}$$

where $\frac{\partial \theta}{\partial T}$ stands for the directional derivative of θ in the direction of $\mathbf{T}$.

5.3.1 Heat-conduction-like problem

Solving equation (5.11) with appropriate boundary conditions would provide field θ. However, this formulation has some inconveniences. The first one has to do with the boundary conditions: one needs to prescribe a value θ_{S_i}, for each line S_i. Notice that we are not interested in having some specific label for a given S_i, but in having any distinguishable θ_{S_i} for every S_i. Then prescribing all the labels would entail unnecessary complications. Moreover, expressing (5.11) in weak form would lead to a non-symmetric formulation whose discrete version could be inconvenient for its implementation in a non-linear finite element code. With these arguments in mind, we propose here a heat-conduction like problem that allows to solve (5.11).

Considering (5.11), we can write

$$\begin{aligned} &\mathbf{T}\frac{\partial \theta}{\partial T} = (\mathbf{T} \otimes \mathbf{T}) \cdot \nabla\theta = \mathbb{K} \cdot \nabla\boldsymbol{\theta} \\ &\mathbb{K} := \mathbf{T} \otimes \mathbf{T} \end{aligned} \tag{5.12}$$

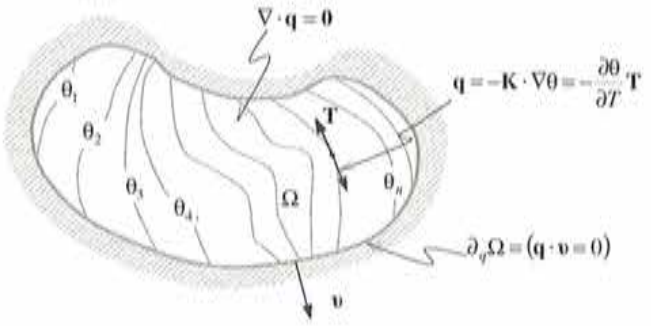

Figure 5.5: Heat-conduction-like boundary value problem.

Let us define

$$\mathbf{q} := -\mathbb{K} \cdot \nabla\boldsymbol{\theta} \tag{5.13}$$

With the above definitions in hand, let us state the following boundary value problem:

$$\begin{array}{lll} \text{FIND} : \theta & & \\ \text{SUCH THAT} & & \\ \nabla \cdot \mathbf{q} = 0 & in\ \Omega & (a) \\ \mathbf{q} = -\mathbb{K} \cdot \nabla\theta = -\mathbf{T}\frac{\partial\theta}{\partial T} & in\ \Omega & (b) \\ \mathbf{q} \cdot \boldsymbol{\nu} = (\boldsymbol{\nu} \cdot \mathbf{T})\frac{\partial\theta}{\partial T} = 0 & on\ \partial_q\Omega & (c) \\ \theta = \theta^* & on\ \partial_\theta\Omega & (d) \end{array} \tag{5.14}$$

where $\boldsymbol{\nu}$ is the outward normal to the boundary $\partial\Omega$, which is composed of $\partial_q\Omega$ and $\partial_\theta\Omega$ such that $\overline{\partial_q\Omega \cup \partial_\theta\Omega} = \partial\Omega$ and $\partial_q\Omega \cap \partial_\theta\Omega = \emptyset$.

It is easy to see that, with appropriate Dirichlet boundary conditions, if (5.11) holds for some θ, this θ is a solution of (5.14). Then, a solution of (5.14) can provide us the envelopes of the vector field $\mathbf{T}$.

Problem (5.14) can be regarded as a steady-state heat conduction BVP in Ω (see Fig. 5.5), for the case of no internal heat sources and null heat flux input ($\mathbf{q} \cdot \boldsymbol{\nu} = 0$) on the boundary $\partial_q\Omega$ (adiabatic boundary). Thus, θ plays the role of the temperature field, $\mathbf{q}$ is the conduction flux vector and $\mathbb{K}$ is a anisotropic thermal conductivity tensor that varies from point to point and whose matrix representation, for two dimensional cases, is

$$[\mathbb{K}(\mathbf{T}(\mathbf{x}))] = [\mathbf{T} \otimes \mathbf{T}] = \begin{bmatrix} T_x^2 & T_xT_y \\ T_xT_y & T_y^2 \end{bmatrix} \tag{5.15}$$

Remark 55 *Notice that* $\mathbb{K}(\mathbf{T}) = \mathbb{K}(-\mathbf{T})$*) and, as one would expect, the solution of problem (5.14) is only affected by the direction of the vector field* $\mathbf{T}$ *and not by its sense.*

Weak form and uniqueness

Let us define the following function spaces

$$\begin{aligned} \mathcal{V}_\theta &:= \left\{\theta \ ; \ \tfrac{\partial\theta}{\partial T} \in \mathsf{L}_2(\Omega), \ \ \theta|_{\partial_\theta\Omega} = \theta^*\right\} \\ \mathcal{V}_{\delta\theta} &:= \left\{\delta\theta \ ; \ \tfrac{\partial(\delta\theta)}{\partial T} \in \mathsf{L}_2(\Omega), \ \ \delta\theta|_{\partial_\theta\Omega} = 0\right\} \end{aligned} \tag{5.16}$$

Now we can write the following BVP in weak form:

$$\begin{array}{l} \text{FIND} : \theta \in \mathcal{V}_\theta \\ \text{SUCH THAT} \\ \int_\Omega \nabla\delta\theta \cdot \mathbb{K} \cdot \nabla\theta \ d\Omega = 0 \qquad \forall\delta\theta \in \mathcal{V}_{\delta\theta} \end{array} \tag{5.17}$$

By standard calculations, one can prove that this problem is the weak form of (5.14).

Remark 56 *Considering the definition of* $\mathbb{K}$*, the weak equation in (5.17) can be rephrased as* $\int_\Omega \frac{\partial(\delta\theta)}{\partial T}\frac{\partial\theta}{\partial T} \ d\Omega = 0$*. Then it is easy to see that a function* θ *fulfilling the condition* $\frac{\partial\theta}{\partial T} = 0$ *in* Ω *is a solution of (5.17).*

In order to prove uniqueness of the BVP (5.17), $\mathbb{K}$ must be an elliptic operator ([Reddy, 1998]), which means that all its eigenvalues must be positive. However, by definition (see (5.15)), it is a rank-one tensor, having, therefore, for the two-dimensional case, one null eigenvalue.

Remark 57 *The lack of uniqueness of (5.17) can be understood by the fact that the value of the directional derivative* $\frac{\partial\theta}{\partial n} := \nabla\theta \cdot \mathbf{n}$*, where* $\mathbf{n}$ *is orthogonal to* $\mathbf{T}$*, in the problems (5.14) and (5.17) is not determined; thus, the behavior of the solutions of those problems in the direction of* $\mathbf{n}$ *is undefined.*

With the above arguments on mind, let us propose the following modification of tensor $\mathbb{K}$:

$$\mathbb{K}_\epsilon := \mathbf{T} \otimes \mathbf{T} + \epsilon\mathbf{1} \tag{5.18}$$

where ϵ is a small positive constant having, in the context of the present heat-conduction-like problem, the meaning of a fictitious isotropic conductivity. For practical purposes, it has to be small enough to ensure meaningful solutions of (5.17).

Remark 58 *Definition (5.18) guarantees the positive definiteness of* $\mathbb{K}_\epsilon$.

By substituting $\mathbb{K}_\epsilon$ for $\mathbb{K}$ in the BVP (5.17), uniqueness is guaranteed.

Finite element formulation

Consider a discretization of Ω into a finite element mesh, with n_{elem} elements and n_{node} nodes. The following finite element approximation of the temperature field is adopted:

$$\theta^h(\mathbf{x}) = \Sigma_{i=1}^{i=n_{node}} \; N_i\theta_i = \mathbf{N}^T\boldsymbol{\theta} \tag{5.19}$$

with

$$\begin{aligned} \mathbf{N} &:= [N_1, ..., N_{n_{node}}]^T \\ \boldsymbol{\theta} &:= [\theta_1, ..., \theta_{n_{node}}]^T \end{aligned}$$

Then the following finite element spaces can be defined:

$$\begin{aligned} \mathcal{V}_\theta^h &:= \left\{\theta^h;\;\; \theta^h(\mathbf{x}) = \Sigma_{i=1}^{i=n_{node}} \; N_i\theta_i;\;\; \theta|_{\partial_\theta\Omega} = \theta^*\right\} \\ \mathcal{V}_{\delta\theta}^h &:= \left\{\delta\theta^h;\;\; \delta\theta^h(\mathbf{x}) = \Sigma_{i=1}^{i=n_{node}} \; N_i\theta_i;\;\; \theta|_{\partial_\theta\Omega} = 0\right\} \end{aligned} \tag{5.20}$$

The discrete counterpart of the continuum problem (5.17) reads

$$\begin{aligned} &\text{FIND} : \theta^h \in \mathcal{V}_\theta^h \\ &\text{SUCH THAT} \\ &\textstyle\int_\Omega \nabla\delta\theta^h \cdot \mathbb{K}_\epsilon \cdot \nabla\theta^h \; d\Omega = 0 \qquad \forall\delta\theta^h \in \mathcal{V}_{\delta\theta}^h \end{aligned} \tag{5.21}$$

Let us set

$$[\nabla\mathbf{N}] := \left[\begin{array}{c} [\partial_x N_1, ..., \partial_x N_{n_{node}}] \\ [\partial_y N_1, ..., \partial_y N_{n_{node}}] \end{array}\right] \tag{5.22}$$

Thus, from (5.21), the following system of equations can be obtained by means of a standard procedure:

$$\int_\Omega [\nabla\mathbf{N}]^T \, [\mathbb{K}_\epsilon] \, [\nabla\mathbf{N}] \;\; \boldsymbol{\theta} \; d\Omega = 0 \tag{5.23}$$

Defining

$$\mathbf{K} := \int_{\Omega} [\nabla \mathbf{N}]^T [\mathbb{K}_\epsilon] [\nabla \mathbf{N}] \, d\Omega \tag{5.24}$$

the system of equations (5.23) can be rephrased as

$$\mathbf{K}\boldsymbol{\theta} = 0 \tag{5.25}$$

Remark 59 *The rank of* $\mathbf{K}$ *is* $n_{node} - 1$ *before the prescription of the Dirichlet boundary conditions. Consequently, prescribing the temperature for one node of the boundary would be enough to have a unique solution for the above system of equations. However, in order to preclude solutions of the type* θ *=constant in* Ω*, the temperature has to be prescribed in at least two nodes.*

Remark 60 *This methodology can be easily implemented in a non-linear finite element code equipped with a thermal analysis module.*

Extension to three dimensions

The extension of the above formulation to three-dimensional settings is straightforward. Consider the vector fields $\mathbf{S}$ and $\mathbf{T}$ defined for every point of the domain Ω at a given time t, such that $\mathbf{S}(\mathbf{x},t)$ and $\mathbf{T}(\mathbf{x},t)$ define the tangent plane to a *possible discontinuity surface* S_i at $(\mathbf{x},t)$. Assume that the family of surfaces $\{S_i\}$ enveloping both vector fields, $\mathbf{S}$ and $\mathbf{T}$, at the same time can be described by a scalar (temperature-like) field with values $\theta(\mathbf{x})$ such that the surfaces

$$S_i := \{\mathbf{x} \in \Omega \, ; \, \theta(\mathbf{x}) = \theta_{S_i}\} \tag{5.26}$$

for all the meaningful values of θ_{S_i}, are tangent at each point $\mathbf{x} \in \Omega$ to the vectors $\mathbf{S}$ and $\mathbf{T}$. Then, the following conditions must hold:

$$\left.\begin{array}{l} \mathbf{S}\cdot\nabla\theta = \nabla\theta \cdot \mathbf{S} = \frac{\partial\theta}{\partial S} = 0 \\ \mathbf{T}\cdot\nabla\theta = \nabla\theta \cdot \mathbf{T} = \frac{\partial\theta}{\partial T} = 0 \end{array}\right\} \quad in \ \Omega \tag{5.27}$$

Remark 61 *Let* $\mathbf{n}$ *be the unit vector field, defined at every point of the domain* Ω *at a given time* t*, such that* $\mathbf{n}(\mathbf{x},t)$ *determines the direction normal to the tangent plane to a tracking surface* S_i *at* $(\mathbf{x},t)$*. Then,* $\mathbf{S}$ *and* $\mathbf{T}$ *must satisfy*

$$\mathbf{S} \cdot \mathbf{n} = \mathbf{T} \cdot \mathbf{n} = 0 \quad in \ \Omega \tag{5.28}$$

With appropriate boundary conditions, the solution of problem (5.27) is also a solution of the following heat-conduction-like problem:

$$\begin{array}{lll}
\text{FIND} : \theta & & \\
\text{SUCH THAT} & & \\
\nabla\cdot\mathbf{q} = 0 & in\ \Omega & (a) \\
\mathbf{q} = -\mathbb{K}\cdot\nabla\boldsymbol{\theta} = -\mathbf{S}\frac{\partial\theta}{\partial S} - \mathbf{T}\frac{\partial\theta}{\partial T} & in\ \Omega & (b) \\
\mathbf{q}\cdot\boldsymbol{\nu} = (\boldsymbol{\nu}\cdot\mathbf{S})\frac{\partial\theta}{\partial S} + (\boldsymbol{\nu}\cdot\mathbf{T})\frac{\partial\theta}{\partial T} = 0 & on\ \partial_q\Omega & (c) \\
\theta = \theta^* & on\ \partial_\theta\Omega & (d)
\end{array} \tag{5.29}$$

where the anisotropic conductivity tensor $\mathbb{K}$ is given by

$$\mathbb{K}(\mathbf{S}(\mathbf{x}), \mathbf{T}(\mathbf{x})) = \mathbf{S}\otimes\mathbf{S} + \mathbf{T}\otimes\mathbf{T} \tag{5.30}$$

and the introduction of an artificial isotropic conductivity ϵ leads to

$$\mathbb{K}_\epsilon = \mathbf{S}\otimes\mathbf{S} + \mathbf{T}\otimes\mathbf{T} + \epsilon\mathbf{1} \tag{5.31}$$

We can arrive to the finite element discretization of (5.29) in a way analogous to that used for the two dimensional case. Again, the temperature-like variable, θ, have to be prescribed at, at least, two points to obtain meaningful solutions. Once the temperature field θ^h is determined at every node of the finite element mesh, an element level algorithm, the straightforward extension of the one presented in Section 5.2.2 to three-dimensional cases, allows to determine the exact position of the discontinuity path inside every element.

Remark 62 *Although in the present work no numerical simulation in three-dimensional settings is tackled and the thermal analogy presented in this section is mainly used to render possible the simulation of multiple discontinuities, it must be said that the possibilities of this formulation to overcome some of the problems arising in the propagation of discontinuities in three dimensions seem enormous*

5.4 Representative numerical simulations

The performance of the heat-conduction-like model presented in Section 5.3 is assessed through the set of illustrative simulations shown in Fig. 5.6. A square domain discretized into the unstructured finite element mesh of quadrilaterals shown in Fig. 5.6-a is considered. Fig. 5.6-b to 5.6-d show different vector fields (left) and the corresponding contours of iso-temperatures (right) obtained with that model. For

every case, the two nodal points at which temperatures were prescribed are indicated. It is worth noting that, regardless of the character of the vector field, the envelopes are precisely captured even if their direction changes abruptly (see Fig. 5.6-d).

The simulations presented in Fig. 5.6 were done for $\epsilon = 0$ and for $\epsilon = 10^{-5}$ obtaining almost identical results. For the simulations with $\epsilon = 0$, no ill-conditioning of the stiffness matrix was observed. This can be explained by the fact that the use of a non-structured mesh introduces some constraints regarding the continuity of the possible solutions in the direction orthogonal to the tracking lines S_i. In the case of structured meshes with nodes aligned with the tracking lines, ill-conditioning of the stiffness matrix may occur, and the use of $\epsilon \neq 0$ is mandatory. Thus, based on the fact that small values of ϵ do not perturb significantly the solution, the use of $\epsilon \neq 0$ seems always recommendable.

5.5 Exclusion Zone

The simulation of the evolution of multiple discontinuity lines by means of the nonsymmetric formulation presented in Section 4.2 becomes feasible when a *global tracking* algorithm is available. However, some precautions have to be taken. For instance, some discontinuity lines can activate spuriously. This happens when there is a region near a crack tip where the stress state is very similar for all its material points. Then, due to numerical errors, some elements within this region can bifurcate spuriously. In order to circumvent this, we propose the creation of an *exclusion zone* surrounding a discontinuity line[1].

We will call *consolidated discontinuity line*, $\mathcal{S}_i \subset S_i$, a material line consisting of all the bifurcated points belonging to a discontinuity line S_i. As said before, when the domain Ω is discretized into a finite element mesh, the bifurcation analysis is performed at certain sampling points discretely distributed. Assume that those sampling points are placed at the centroid of every element. Consider that $\mathbf{x}_e$ denotes the sampling point corresponding to a non-bifurcated element e, $\mathbf{x}_{\mathcal{S}_i}$ stands for a sampling point belonging to an element crossed by the consolidated discontinuity line $\mathcal{S}_i$, and $d_{\mathcal{S}_i}$ is a positive constant named *exclusion distance* of $\mathcal{S}_i$, then the definition of the exclusion zone corresponding to $\mathcal{S}_i$ is the following:

$$\mathbb{H}_{\mathcal{S}_i} := \left\{ \mathbf{x}_e \in \Omega \; ; \; \min_{\mathbf{x}_{\mathcal{S}_i} \in \mathcal{S}_i} \|\mathbf{x}_e - \mathbf{x}_{\mathcal{S}_i}\| \leq d_{\mathcal{S}_i} \text{ and } \Omega_e \cap S_i = \emptyset \right\} \tag{5.32}$$

[1] A concept similar to what we call *exclusion zone* here can be found in [Alfaiate et al., 2002].

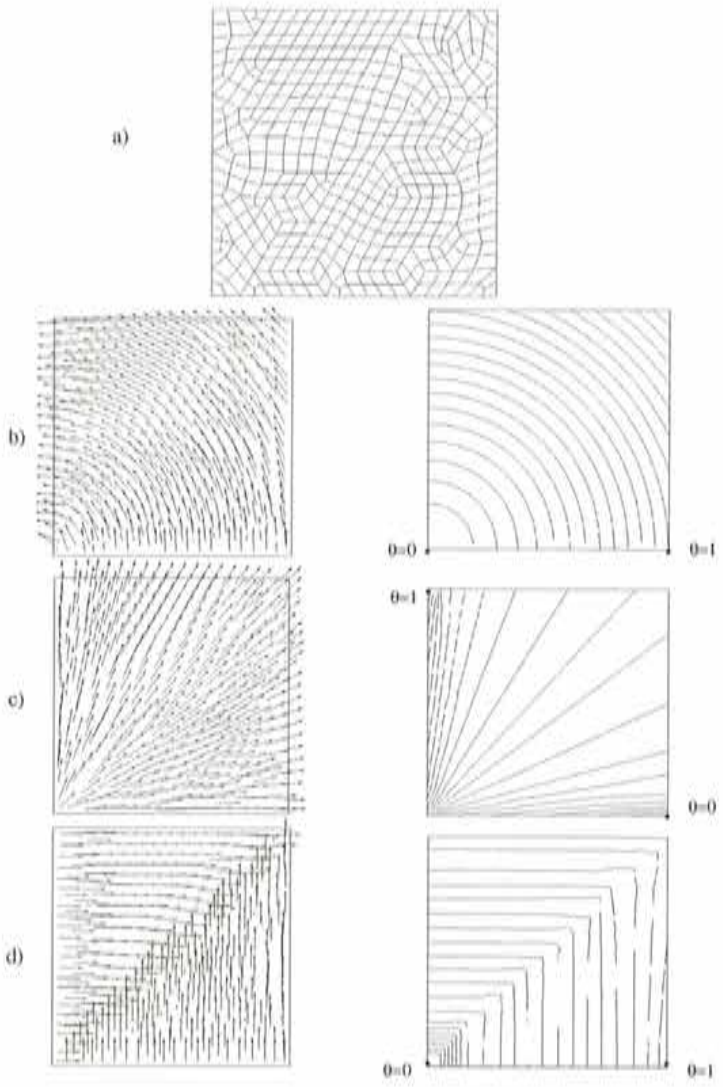

Figure 5.6: Numerical tests.

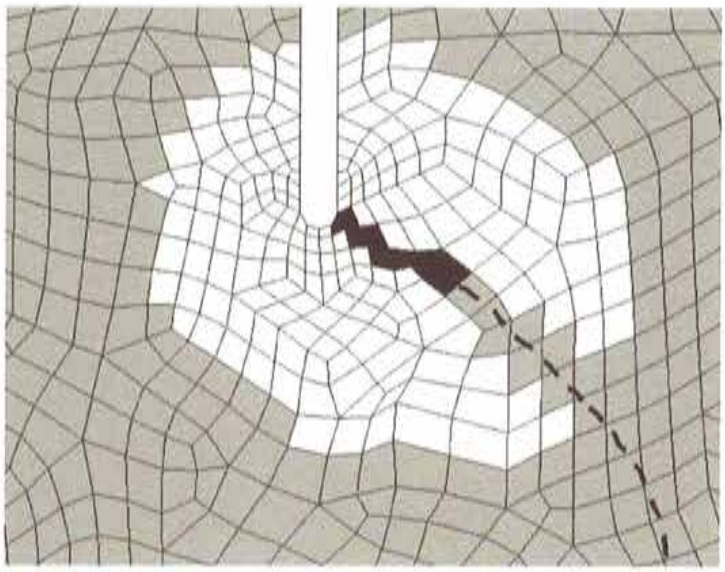

Figure 5.7: Exclusion zone.

Fig. 5.7 shows the exclusion zone of a consolidated discontinuity for a given finite element mesh. The elements belonging to the exclusion zone are depicted in white, while the elements crossed by the consolidated discontinuity line are colored in black. The dotted line indicates the part of the discontinuity line that has not been consolidated yet.

Now, at a given time t, an element e will be allowed to bifurcate if at least one of the following conditions is fulfilled:

1. Element e does not belong to the exclusion zone of any consolidated discontinuity line $\mathcal{S}_i$.

2. Element e is crossed by a possible discontinuity line S_i that is already active (i.e. S_i crosses at least one bifurcated element).

Chapter 6

Stability and uniqueness issues

The numerical simulation of complex problems involving strain localization requires the use of robust algorithms that allow for the description of their highly non-linear behavior. Adequate control techniques and sophisticated continuation methods are necessary to obtain the global equilibrium path throughout a loading process. Even in the case of using these tools, the eventual appearance of bifurcation points can lead to no convergence of the overall incremental iterative scheme (a Newton-Raphson scheme, for instance).

Furthermore, although the nonsymmetric finite element formulation presented in Section 4.2. has been successfully used for the simulation of strong discontinuities (see, e.g., [Oliver et al., 2002a]), some questions about its robustness have arised lately. In [Jirasek, 2000b], an element level uniqueness condition was derived. There, it was argued that not satisfying this condition would result in a loss of robustness of the numerical model used.

In this chapter, the inclusion of an artificial numerical damping as a remedy for the above mentioned problems is motivated and studied. The approach adopted is different from the one in [Jirasek, 2000b]. The possible element level instabilities are regarded as a controllability problem related to the "brittleness" of the element. Section 6.1 is devoted to studying these instabilities for the nonsymmetric formulation presented in Section 4.2.4. Then, an artificial damping term is added to the virtual work principle equation as a remedy in Section 6.2. Some of the most relevant consequences of doing this are analyzed

6.1 Element level instabilities

The study of eventual element level instabilities of a discrete BVP based on the non-symmetric formulation presented in Section 4.2. is tackled here. From Section 4.2.4, the matrix expression of the incremental residual forces at element level is

$$\begin{bmatrix} \mathbf{K}_{dd}^{(e)} & \mathbf{K}_{d\alpha}^{(e)} \\ \mathbf{K}_{\alpha d}^{(e)} & \mathbf{K}_{\alpha\alpha}^{(e)} \end{bmatrix} \begin{Bmatrix} \dot{\mathbf{d}}^{(e)} \\ [\![\dot{\mathbf{u}}]\!]^{(e)} \end{Bmatrix} - \begin{Bmatrix} \dot{\mathbf{F}}_{ext}^{(e)} \\ 0 \end{Bmatrix} = \begin{Bmatrix} \dot{\mathbf{R}}^{(e)} \\ \dot{\mathbf{r}}^{(e)} \end{Bmatrix} \tag{6.1}$$

with

$$\begin{aligned} \mathbf{K}_{dd}^{(e)} &= \int_{\Omega_e} \mathbf{B}^{(e)^T}\, \mathbf{D}\, \mathbf{B}^{(e)} d\Omega \\ \mathbf{K}_{d\alpha}^{(e)} &= \int_{\Omega_e} \mathbf{B}^{(e)^T}\, \mathbf{D}\, \mathbf{G}^{(e)} d\Omega \\ \mathbf{K}_{\alpha d}^{(e)} &= \int_{\Omega_e} \mathbf{G}^{*(e)}\, \mathbf{D}\, \mathbf{B}^{(e)} d\Omega \\ \mathbf{K}_{\alpha\alpha}^{(e)} &= \int_{\Omega_e} \mathbf{G}^{*(e)}\, \mathbf{D}\, \mathbf{G}^{(e)} d\Omega \end{aligned} \tag{6.2}$$

Let us focus on the expression of the element level residual forces corresponding to the displacement jumps stated in (6.1):

$$\dot{\mathbf{r}}^{(e)} = \mathbf{K}_{\alpha d}^{(e)} \dot{\mathbf{d}}^{(e)} + \mathbf{K}_{\alpha\alpha}^{(e)} [\![\dot{\mathbf{u}}]\!]^{(e)} = 0 \tag{6.3}$$

Equation (6.3) can be regarded as a control problem in which $\mathbf{K}_{\alpha d}^{(e)} \dot{\mathbf{d}}^{(e)}$ is the control variable and $[\![\dot{\mathbf{u}}]\!]^{(e)}$ is the state variable. In such a context, the singularity of $\mathbf{K}_{\alpha\alpha}^{(e)}$ will correspond to a critical point. In light of this, let us study the structure of $\mathbf{K}_{\alpha\alpha}^{(e)}$. Remember from Section 4.2.4, the definition of $\mathbf{G}^{*(e)}$ and $\mathbf{G}_e$:

$$\mathbf{G}^{*(e)} = (\mu_S^{(e)} \frac{1}{k} - \frac{l_e}{\Omega_e}) [\mathbf{n}]^{(e)^T} \tag{6.4}$$

$$\mathbf{G}^{(e)} = \mu_S^{(e)} \frac{1}{k} [\mathbf{n}]^{(e)} - [\nabla \varphi^{(e)}] \tag{6.5}$$

From (6.2), 6.5, and 6.4, we obtain

$$\mathbf{K}_{\alpha\alpha}^{(e)} = \int_{\Omega_e} \left[\frac{\mu_S^{(e)}}{k} [\mathbf{n}]^{(e)^T} - \frac{l_e}{\Omega_e} [\mathbf{n}]^{(e)^T} \right] \mathbf{D} \left[\frac{\mu_S^{(e)}}{k} [\mathbf{n}]^{(e)} - [\nabla \varphi^{(e)}] \right] d\Omega \tag{6.6}$$

Since $\mathbf{D}_S = \mathcal{O}(k)$ and $\mathbf{D}_{\Omega_e \setminus S_e} = \mathbf{D}_{el}$ (the elastic constitutive matrix), expression (6.6) can be rephrased as

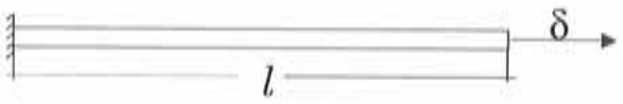

Figure 6.1: One-dimensional bar subjected to tension.

$$\mathbf{K}_{\alpha\alpha}^{(e)} = \int_{\mathcal{S}_e} \left[\mathbf{Q}^d\right] d\mathcal{S} + \frac{l_e}{\Omega_e} \int_{\Omega_e \setminus \mathcal{S}_e} [\mathbf{n}]^{(e)^T} \mathbf{D}_{el} \left[\nabla \varphi^{(e)}\right] d\Omega \tag{6.7}$$

where $\left[\mathbf{Q}^d\right]$ is the matrix representation of the acoustic tensor (which can be identified with the constitutive tangent operator of the induced discrete, or cohesive, law).

It is worth noting that matrix $\left[\mathbf{Q}^d\right]$ is not positive definite, which implies that, for $\mathbf{K}_{\alpha\alpha}^{(e)}$ to be positive definite, the second term of (6.7) has to be positive definite. If $\left[\nabla \varphi^{(e)}\right]$ and $[\mathbf{n}]^{(e)}$ are proportional, the positive definiteness of the second term of (6.7) is guaranteed by the positive definiteness of the elastic matrix $\mathbf{D}_{el}$. In the case of $\left[\nabla \varphi^{(e)}\right]$ and $[\mathbf{n}]^{(e)}$ being orthogonal in the scalar product induced by $\mathbf{D}_{el}$, the second term of (6.7) is equal to zero and $\mathbf{K}_{\alpha\alpha}^{(e)} = \int_{\mathcal{S}_e} \left[\mathbf{Q}^d\right] d\mathcal{S}$.

The importance of the definiteness of $\mathbf{K}_{\alpha\alpha}^{(e)}$ can be explained by the fact that passing for a critical point can be related to loosing positive definiteness. This is illustrated in the next subsection by a one-dimensional example and then related with the *brittleness* of the element

6.1.1 One dimensional example

Consider the one-dimensional bar of Fig. 6.1 discretized into one linear finite element. Then we have that (6.7) reduces to

$$K_{\alpha\alpha}^{(e)} = E\bar{H} + \int_{\Omega_e} \frac{1}{l} E \frac{1}{l} d\Omega = E\bar{H} + \frac{E}{l} \tag{6.8}$$

where $E\bar{H}$ is the value of the discrete tangent modulus acting on point $\mathcal{S}$. We also have

$$K_{\alpha d}^{(e)} = \int_{\Omega_e} -\frac{1}{l} E \left[\begin{array}{cc} \partial_x N_1 & \partial_x N_2 \end{array}\right] d\Omega = \int_{\Omega_e} -\frac{1}{l} E \left[\begin{array}{cc} -\frac{1}{l} & \frac{1}{l} \end{array}\right] d\Omega \tag{6.9}$$

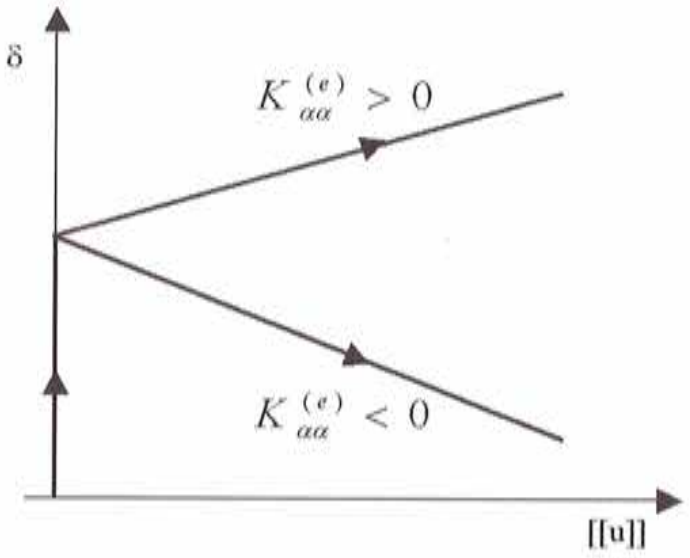

Figure 6.2: Nodal displacement vs. elemental jump in a one dimensional element.

Then we can write (6.3) as follows

$$\left(\int_{\Omega_e} -\frac{1}{l} E \begin{bmatrix} -\frac{1}{l} & \frac{1}{l} \end{bmatrix} d\Omega\right) \begin{Bmatrix} \dot{d}_1 \\ \dot{d}_2 \end{Bmatrix} + \left[E\bar{H} + \frac{E}{l}\right] [\![\dot{u}]\!]^{(e)} = 0 \tag{6.10}$$

As indicated in Fig. 6.1, $\dot{d}_1$=0 and $\dot{d}_2 = \dot{\delta}$. Then, solving (6.10) for $[\![\dot{u}]\!]^{(e)}$ yields

$$[\![\dot{u}]\!]^{(e)} = \underbrace{\frac{1}{E\bar{H} + \frac{E}{l}}}_{\mathbf{K}^{(e)}_{\alpha\alpha}} \left(\frac{1}{l} E\dot{\delta}\right) \tag{6.11}$$

An schematic picture of the prescribed displacement vs. the displacement jump ($\delta - [\![u]\!]^{(e)}$) curve for this case is shown in Fig. 6.2. Before bifurcation, $\dot{\delta} > 0$ while $[\![\dot{u}]\!]^{(e)} = 0$, so that one can consider that $K^{(e)}_{\alpha\alpha}$ is "infinitely positive", i.e., rigid. Consider the case of $K^{(e)}_{\alpha\alpha} < 0$ after bifurcation, a positive rate of the prescribed displacement entails a negative rate of the element jump (see Figure 6.2). For $K^{(e)}_{\alpha\alpha}$ to change of sign, the existence of a critical point in between is necessary. Thus, from (6.11) the condition, in this one-dimensional case, to avoid the appearance of element level critical points is

$$l \leq \frac{1}{H} \tag{6.12}$$

Remark 63 *The brittleness of the element is related to condition (6.12). For this one-dimensional case, it depends on the element size and on the intrinsic softening parameter.*

Remark 64 *For higher dimensional cases and for other constitutive models, the positive definiteness of* $\mathbf{K}_{\alpha\alpha}^{(e)}$ *can be established as a sufficient condition to ensure the absence of element level critical points for (6.3). The effects of these element level critical points in the global problem remain to be studied. Thus, the spirit of the strategy presented in the next section is to preclude element level critical points in order to avoid the possibility of numerical instabilities caused by them.*

6.2 Artificial damping term

In this section, a strategy to overcome the element level critical points in problems undergoing strong discontinuities is proposed. It is based on adding a regularizing damping term to the weak form of the momentum balance equation. Though the main motivation for this strategy is to solve the stability problems identified in the preceding section, an important uniqueness result regarding the continuum BVP is also obtained.

Consider the body Ω with boundary $\Gamma = \overline{\Gamma_{\boldsymbol{\sigma}} \cup \Gamma_{\mathbf{u}}}$ (fulfilling $\Gamma_{\boldsymbol{\sigma}} \cap \Gamma_{\mathbf{u}} = \emptyset$) and the discontinuity interface $\mathcal{S} \subset \Omega$. Let us adopt the strong discontinuity kinematics presented in Section 3.21. For any time t, the following variational equation must hold:

$$\int_{\Omega} \nabla^S \boldsymbol{\eta} : \boldsymbol{\sigma} \, d\Omega + G_{ext}(\boldsymbol{\eta}) = 0 \qquad \forall \boldsymbol{\eta} \in \mathcal{V}_{\eta} \tag{6.13}$$

where $G_{ext}(\boldsymbol{\eta}) := \int_{\Omega \setminus \mathcal{S}} \mathbf{b} \cdot \boldsymbol{\eta} \, d\Omega + \int_{\Gamma_{\sigma}} \mathbf{t}^* \cdot \boldsymbol{\eta} \, d\Gamma$.(with $\mathbf{b}$ being the body force density and $\mathbf{t}^*$ the traction prescribed on boundary Γ_{σ}) and $\mathcal{V}_{\eta}$ is the space of (kinematically) admissible displacement variations. From Section 4.3, we have that the elements of $\mathcal{V}_{\eta}$ have the following structure:

$$\boldsymbol{\eta} = \bar{\boldsymbol{\eta}} + \mathcal{M}_{\mathcal{S}} \, \boldsymbol{\alpha}$$

$\bar{\boldsymbol{\eta}} \in \mathcal{V}_{\bar{\eta}}$ and $\boldsymbol{\alpha} \in \mathcal{V}_{\alpha}$.

Remark 65 *Based on the linearity of both the gradient operator and the integral, it is easy to prove that the rate form of equation (6.13) is equivalent to the rate form of the system of variational equations (4.51) and, therefore, to (4.12).*

With these concepts in hand, the following modification to (6.13) is proposed:

$$\int_{\mathcal{S}} \boldsymbol{\alpha} \cdot (\bar{\mu}\mathbf{1}) \cdot [\![\dot{\mathbf{u}}]\!] d\mathcal{S} + \int_{\Omega} \nabla^S \boldsymbol{\eta} : \boldsymbol{\sigma} d\Omega + G_{ext}(\boldsymbol{\eta}) = 0 \qquad \forall \boldsymbol{\eta} \in \mathcal{V}_\eta \tag{6.14}$$

where $\bar{\mu}$ is damping-like parameter acting in $\mathcal{S}$ such that when $\bar{\mu} \to 0$, equation (6.14) approximates (6.13).

Now the following proposition can be stated:

Proposition 3 *Equation (6.14) has a unique solution if* $\bar{\mu}>0$.

Proof: Let us assume that, for a given time t, two solutions for (6.14), $[\![\dot{\mathbf{u}}]\!]_1$ and $[\![\dot{\mathbf{u}}]\!]_2$, exist. Setting $\Delta[\![\dot{\mathbf{u}}]\!] := [\![\dot{\mathbf{u}}]\!]_2 - [\![\dot{\mathbf{u}}]\!]_1$, then, since at bifurcation time $\Delta\boldsymbol{\sigma} := \boldsymbol{\sigma}_2 - \boldsymbol{\sigma}_1 = 0$,

$$\int_{\mathcal{S}} \boldsymbol{\alpha} \cdot (\bar{\mu}\mathbf{1}) \cdot \Delta[\![\dot{\mathbf{u}}]\!] d\mathcal{S} = 0 \qquad \forall \boldsymbol{\alpha} \in \mathcal{V}_\alpha \tag{6.15}$$

must hold. Since by definition, $\Delta[\![\dot{\mathbf{u}}]\!] \in \mathcal{V}_\alpha$, equation (6.15) must hold for $\boldsymbol{\alpha} = \Delta[\![\dot{\mathbf{u}}]\!]$, i.e.,

$$\int_{\mathcal{S}} \Delta[\![\dot{\mathbf{u}}]\!] \cdot (\bar{\mu}\mathbf{1}) \cdot \Delta[\![\dot{\mathbf{u}}]\!] d\mathcal{S} = 0 \tag{6.16}$$

Provided that $\bar{\mu} > 0$, equation (6.16) implies that $\Delta[\![\dot{\mathbf{u}}]\!] = 0$. Which contradicts the assumption of loss of uniqueness and so proposition 3 follows.

6.2.1 Discrete version of the problem

By standard procedures one can easily arrive to the discrete version of (6.14) at element level. Due to the fact that the added damping acts exclusively within the discontinuity interface, only the part of the residual forces corresponding to the inner traction continuity equation (i.e., the part of the residual forces whose rate is $\dot{\mathbf{r}}^{(e)}$ in (6.1)) needs to be modified:

$$\mathbf{r}_{\bar{\mu}}^{(e)} := \int_{\mathcal{S}_e} \bar{\mu}\, [\![\dot{\mathbf{u}}]\!]^{(e)}\, d\mathcal{S} + \int_{\Omega_e} \mathbf{G}^{*(e)}\, \boldsymbol{\sigma} d\Omega = 0 \tag{6.17}$$

Consider, now, the discretization of the time interval of interest

$$[t_0, t_N] = \bigcup_{n=0}^{N-1} [t_n, t_{n+1}] \tag{6.18}$$

Let us focus on a typical interval $[t_n, t_{n+1}]$; then the following approximation for $[\![\dot{\mathbf{u}}]\!]^{(e)}$ is proposed:

$$[\![\dot{\mathbf{u}}]\!]^{(e)}_{n+1} \approx \frac{[\![\mathbf{u}]\!]^{(e)}_{n+1} - [\![\mathbf{u}]\!]^{(e)}_{n}}{\Delta t} \tag{6.19}$$

with $\Delta t := t_{n+1} - t_n$. Thus, we can write

$$\mathbf{r}^{(e)}_{n+1} := \int_{\mathcal{S}_e} \bar{\mu}\, \frac{[\![\mathbf{u}]\!]^{(e)}_{n+1} - [\![\mathbf{u}]\!]^{(e)}_{n}}{\Delta t}\, d\mathcal{S} + \int_{\Omega_e} \mathbf{G}^{*(e)}\, \boldsymbol{\sigma}_{n+1}\, d\Omega = \mathbf{0} \tag{6.20}$$

which corresponds to a backward Euler integration of (6.17) in time. Hence, considering (6.1), a modified $\mathbf{K}^{(e)}_{\alpha\alpha}$ is obtained:

$$\begin{aligned} \hat{\mathbf{K}}^{(e)}_{\alpha\alpha} \;&:=\; \frac{d\mathbf{r}^{(e)}_{n+1}\left([\![\mathbf{u}]\!]^{(e)}_{n+1}\right)}{d[\![\mathbf{u}]\!]^{(e)}_{n+1}} = \int_{\mathcal{S}_e} \frac{\bar{\mu}}{\Delta t}\mathbf{1}\, d\mathcal{S} + \int_{\Omega_e} \mathbf{G}^{*(e)}\, \mathbf{D}\, \mathbf{G}^{(e)}\, d\Omega \\ &= \int_{\mathcal{S}_e} \frac{\bar{\mu}}{\Delta t}\mathbf{1}\, d\mathcal{S} + \mathbf{K}^{(e)}_{\alpha\alpha} \end{aligned} \tag{6.21}$$

Matrix $\hat{\mathbf{K}}^{(e)}_{\alpha\alpha}$ is then equal to the original $\mathbf{K}^{(e)}_{\alpha\alpha}$ plus a damping matrix, which depends on the damping-like parameter $\bar{\mu}$ and on Δt. Thus, the damping parameter $\bar{\mu}$ can be chosen in such a way that the positive definiteness of $\hat{\mathbf{K}}^{(e)}_{\alpha\alpha}$ is guaranteed. Let $\xi_{\max}(\bullet)$, $\xi_{\min}(\bullet)$, and $\xi(\bullet)$ denote the maximum, the minimum, and an arbitrary eigenvalue of a square matrix $(\bullet)$, respectively. Since the following condition holds (Bromwich bounds):

$$\xi_{\min}\left[\left(\hat{\mathbf{K}}^{(e)}_{\alpha\alpha}\right)^S\right] \leq \xi(\hat{\mathbf{K}}^{(e)}_{\alpha\alpha}) \leq \xi_{\max}\left[\left(\hat{\mathbf{K}}^{(e)}_{\alpha\alpha}\right)^S\right]$$

then a sufficient condition for $\hat{\mathbf{K}}^{(e)}_{\alpha\alpha}$ to be positive definite is

$$\xi_{\min}\left[\left(\mathbf{K}_{\alpha\alpha}^{(e)}\right)^{S}\right]+\frac{\bar{\mu}}{\Delta t}\geq 0 \tag{6.22}$$

Hence, a critical value for the time increment can be computed:

$$\Delta t_{crit}=\frac{\bar{\mu}}{\left|\xi_{\min}\left[\left(\hat{\mathbf{K}}_{\alpha\alpha}^{(e)}\right)^{S}\right]\right|} \tag{6.23}$$

Remark 66 *The positive definiteness of $\hat{\mathbf{K}}_{\alpha\alpha}^{(e)}$ precludes the appearance of the element level critical points studied in the preceding section*

Remark 67 *A significant increase on the robustness of the global incremental - iterative algorithm is to be expected with the addition of damping, not only because it precludes element level critical points, but also due to the smoothing effect that it usually has on tracing the equilibrium path and to the uniqueness*[1] *of the incremental problem stated in proposition 3.*

6.2.2 Implementation aspects

The implementation of the proposed strategies requires changes, only at element level, on $\mathbf{K}_{\alpha\alpha}^{(e)}$ to obtain $\hat{\mathbf{K}}_{\alpha\alpha}^{(e)}$, as indicated in (6.21), and on the residual forces, as indicated in (6.20).

Furthermore, the result given in (6.23) can be used to compute the time step size, Δt, to be used by the overall incremental-iterative scheme as

$$\Delta t=\min_{e\in\mathcal{I}}\left\{\frac{\bar{\mu}}{\left|\xi_{\min}\left[\left(\mathbf{K}_{\alpha\alpha}^{(e)}\right)^{S}\right]\right|}\right\} \tag{6.24}$$

where $\mathcal{I}=\{1,\ldots,n_{elem}\}$.

Remark 68 *Since the analyses carried out in the present work only consider the quasistatic problem with rate independent behavior, when we talk about time, we mean* pseudo-time. *For instance, in the case in which an arc-length control is used (see Appendix A), the pseudo-time can be identified with the arc-length.*

[1] Here, only uniqueness of the continuum problem was proved and bifurcation of the discrete problem might occur if the time-step size is greater than some critical value. However, the use of large enough values of $\bar{\mu}$ will make that possibility very improbable

In order to optimize the performance of an algorithm based on (6.24), it is convenient to vary conveniently the value of the variable considered as the pseudo-time (e.g., the arc-length), increasing it when $\mathbf{K}_{\alpha\alpha}^{(e)}$ is positive definite for every element, and setting it to the value obtained by (6.24) when $\mathbf{K}_{\alpha\alpha}^{(e)}$ loses positive-definiteness for at least some element.

Chapter 7

Numerical Examples

In this chapter, some numerical examples are presented in order to apply the concepts and techniques developed throughout the present work to the numerical simulation of problems in which strong discontinuities appear. To check the possibilities of those concepts and techniques in the modelling of complex two-dimensional examples undergoing multiple cracking is the main aim here.

All the simulations presented in this chapter were run in the non-linear multipurpose finite element program COMET (COupled Mechanical and Thermal analysis, [Cervera et al., 2001]) developed in CIMNE (International Center for Numerical Methods in Engineering). The pre and post-processing was carried out in GiD also developed in CIMNE.

Before presenting them, some general characteristics of the numerical simulations reported in this chapter have to be laid out:

- The nonsymmetric formulation of finite elements with embedded discontinuities presented in Section 4.3, which has proven to be the most efficient, is used for all the simulations.

- A variant of the isotropic continuum damage model presented in Section 2.2 is employed in all the examples. It is characterized for allowing damage only for tension in the principal stresses. We will call it, from now on, *tension-only damage model*. In order to briefly explain it, let us define the positive part of the stress tensor as follows:

$$\boldsymbol{\sigma}^{+} := \sum_{k=1}^{n_{\text{dim}}} \langle \sigma_i \rangle \, \mathbf{p}_i \otimes \mathbf{p}_i \tag{7.1}$$

  where $\langle \bullet \rangle$ are the Macaulay brackets, σ_i stands for the principal stresses, and $\mathbf{p}_i$ for the principal stress directions. Now, we can define the damage function

of this model:

$$f(\boldsymbol{\sigma}^+, \boldsymbol{\sigma}, q) := \sqrt{\boldsymbol{\sigma}^+ : \mathbf{C}^{-1} : \boldsymbol{\sigma}} - q \tag{7.2}$$

The rest of ingredients of this constitutive model are the same as in the isotropic damage model from Section 2.2.

- For most of the examples presented here, tracing the equilibrium path is by no means trivial. Thus, the use of continuation techniques has been unavoidable. In general, the normal updated strategy has been employed, together with an algorithm that enlarges and reduces the length of the step according to a defined-by-the-user ideal number of iterations (see Appendix A).

The remaining of this chapter is organized as follows. One of the classical four points bending tests with one notch is studied in Section 7.1. First, a comparison of several meshes to check convergence upon refinement and to assess the performance of triangular and quadrilateral meshes is made. Then, the appearance of several crack lines is allowed for a quadrilateral mesh and the corresponding results are analyzed and compared with experimental results. Section 7.2 presents the simulation of a double-notched four points bending test. Two main crack lines are expected to activate, but other crack lines are allowed to appear. Their evolution through the loading process is studied and a comparison with experimental results is presented. In Section 7.3, a rectangular plate with two geometrical imperfections submitted to tension is modelled. The purpose of those imperfections is to trigger two (dominant) bands of localization. Then, the evolution of those bands through the loading process is analyzed. The effect of brittleness and the necessity of good continuation techniques is remarked, as well as the convergence to the original problem when the artificial damping tends to zero. The simulation of one of the tests in [Nooru-Mohamed, 1992] is tackled in Section 7.4. Again, two dominant cracks appear, but they are not the only ones allowed to activate. Finally, in Section 7.5, a reinforced specimen is modelled. The reinforcement helps the appearance of several discontinuities that activate and arrest through the loading process. The effect of refinement will be also analyzed.

7.1 Four points bending test with one notch

One of the classical four point bending tests reported in [Arrea and Ingraffea, 1982] is simulated in this section. Some of the features of the numerical simulation of strain localization by means of the strong discontinuity approach are studied through this benchmark test. First, a study of the performance of various quadrilateral and triangular meshes is made. For this comparison,

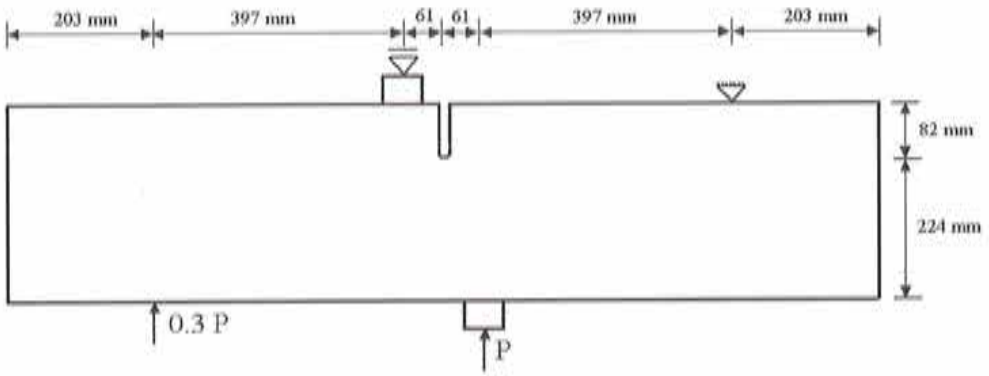

Figure 7.1: Single notched four points bending test: geometry and boundary conditions.

only one discontinuity line (the main one) is allowed to appear. Afterwards, the possibility of the appearance of several discontinuities is considered.

7.1.1 Comparative analysis of the performance of various meshes

Here we assess the performance of triangular and quadrilateral meshes and their convergence upon refinement through the classical four points bending test allowing the activation of only one discontinuity line (a local tracking strategy was used). Comparison with experimental data will be delayed until Section 7.1.2 where the activation of several discontinuities is allowed. The dimensions and boundary conditions applied to the beam can be seen in Fig. 7.1. The tension-only damage model was used, considering the following material properties: $E = 2.4 \cdot 10^{10}$ Pa, $\sigma_u = 2.8 \cdot 10^6$ Pa, ν =0.18, and $G_f = 100$ N/m. The plane stress case was adopted and a thickness $t = 0.156$ m was considered. The quadrilateral and the triangular meshes employed are shown in Fig. 7.2 and Fig 7.3 respectively. In the same figures, the nomenclature employed to refer to each mesh is also presented.

Fig. 7.4 shows a comparison between the general response curves obtained with both triangular and quadrilateral meshes. The triangular meshes have curves that tend asymptotically to total relaxation of load P. However, for quadrilaterals, negative values of P are observed, and it is seen that the global response is more brittle than the one obtained with triangles. Convergence upon refinement is observed both in triangles and in quadrilaterals. The structural brittleness in the behavior of the quadrilateral meshes tend to disappear with refinement. It is also observed

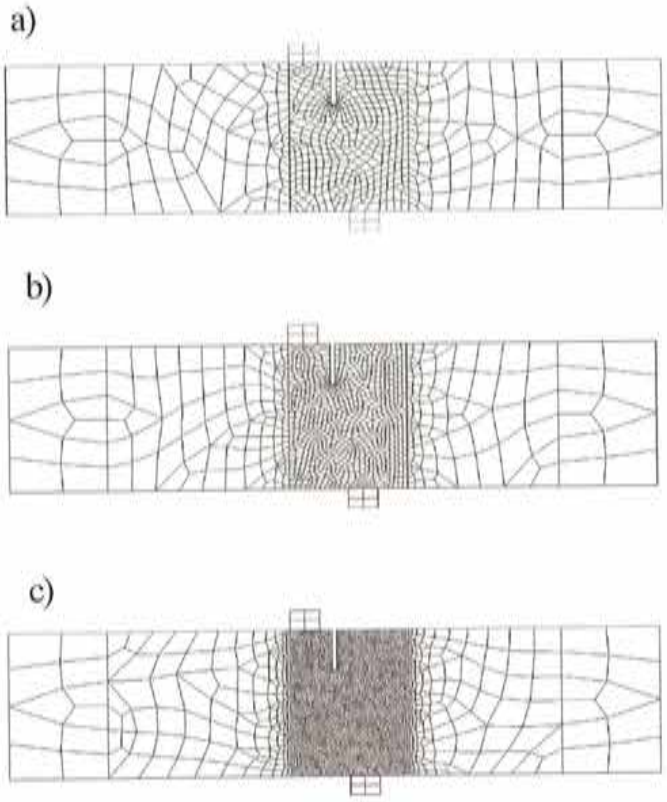

Figure 7.2: Quadrilateral meshes: a) 643 nodes (Q643), b) 1123 nodes (Q1123), c) 3881 (Q3881).

that convergence with regard to the late stages of the postcritical behavior is faster in triangles than in quadrilaterals. However, convergence regarding the prediction of the peak load and the early stages of the postcritical behavior is attained fast for both triangles and quadrilaterals.

The resulting discontinuity paths for all the meshes are shown in Fig. 7.5. They are similar for all the meshes considered.

7.1.2 Simulation of several discontinuities

Despite the structural brittleness exhibited by quadrilateral meshes, they are used in the remaining simulations presented in this chapter. This choice can be justified by several reasons. The first of them is that numerical examples with triangular meshes can be find elsewhere in the literature (see, for instance, [Oliver et al., 2002a]) and

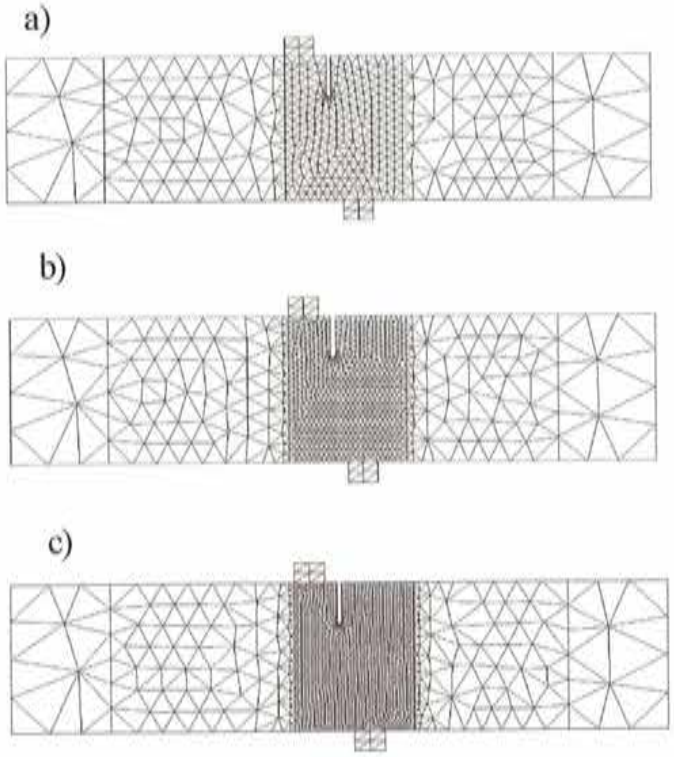

Figure 7.3: Triangular meshes: a) 441 nodes (T441), b) 1042 nodes (T1042), c) 1544 nodes (T1544).

that, therefore, a deeper knowledge about the performance of quadrilaterals is necessary. Moreover, the above mentioned brittle behavior of quadrilaterals occurs in advanced stages of the loading process, where, in general, experimental data is not available. The fact that quadrilaterals have the advantage of better capturing the stress state of the solid in the elastic regime, which contributes to get a more accurate tracking of discontinuity paths, has also been considered.

For this simulation, the quadrilateral mesh in Fig. 7.6 was used. A global tracking strategy was made use of and the appearance of more than one discontinuity line was allowed. Some algorithmic damping and an exclusion zone of 5 cm were applied in order to help convergence of the iterative scheme (Newton-Raphson). The updated normal plane method was the continuation technique employed.

In Fig. 7.7-a the exclusion zone corresponding to that step is shown. The possible discontinuity lines for an intermediate step in the loading process can be observed in Fig. 7.7-b.

Fig. 7.8 indicates the loading stages at which the pictures in Fig. 7.9 were taken.

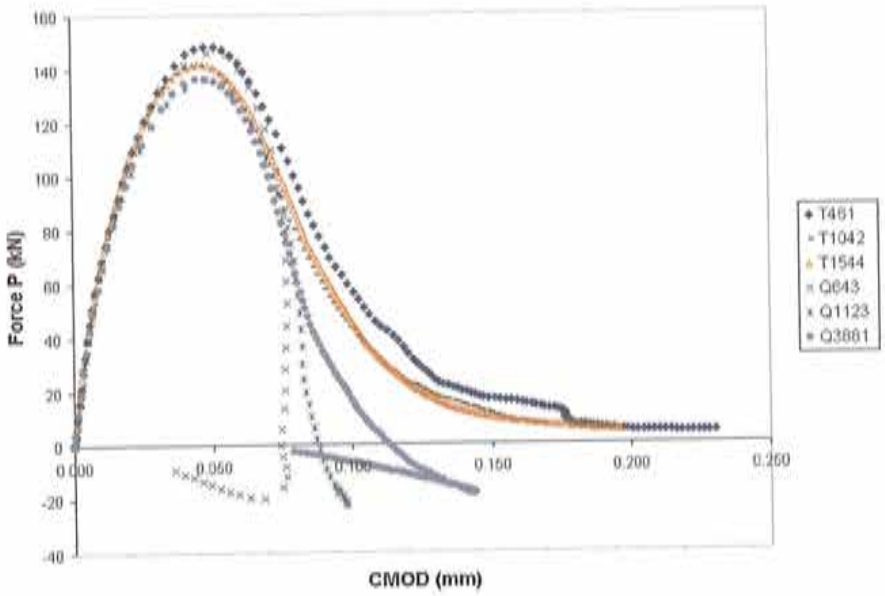

Figure 7.4: Single notched four points bending test: comparison of the global response of several meshes.

Fig. 7.9-a and Fig. 7.9-b show the elements in inelastic loading for an early and an intermediate loading step, respectively. The main crack, emanating from the notch, reported elsewhere (see, for instance, [Arrea and Ingraffea, 1982]) is observed, but other cracks do also appear. However, at later stages these cracks arrest and close (see Fig. 7.9-c) leaving the main crack as the only one which remains open. The presence of algorithmic damping was observed to help convergence of the iterative scheme significantly. This can be explained by the fact that new crack lines are activated, which entails a process of crack opening and closure, until the main crack dominates. Moreover, as the number of crack lines allowed to open increases, so does the risk of element level numerical instabilities. Thus, the manifold beneficial effect of the artificial damping is likely to have played a crucial role.

A comparison between the numerical simulation curve and the experimental envelope of the global response in terms of force P and the Crack Mouth Opening Displacement (CMOD) of the notch is shown in Fig. 7.10. Again a brittle behavior in the postcritical phase of the late stages of the loading process is observed. However, a good agreement regarding the peak load and the early stages of the postcritical part of the response curve is obtained.

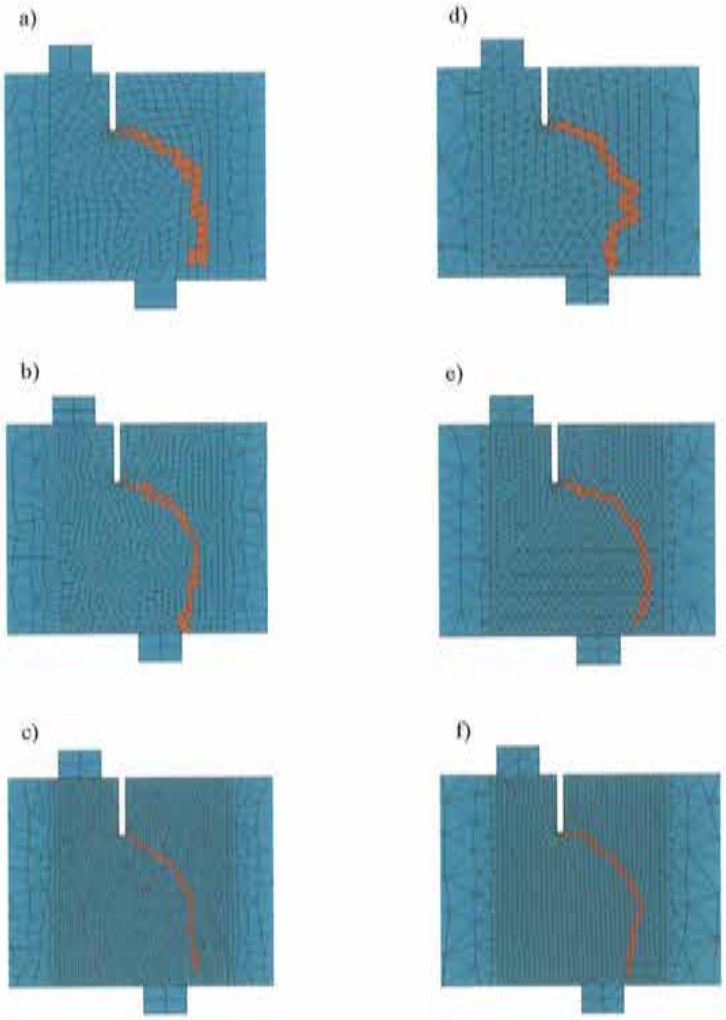

Figure 7.5: Single notched four points bending test: crack path at final stages of the loading process for different meshes: a) Q643 b) Q1123, c) Q3881, d) T441, e) T1042, f) T1544.

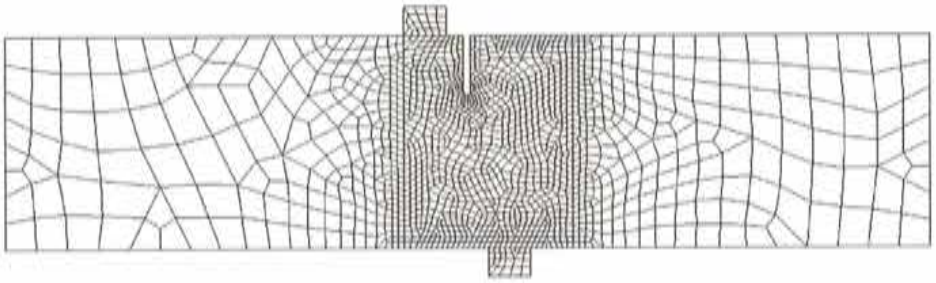

Figure 7.6: Single notched four points beam: mesh.

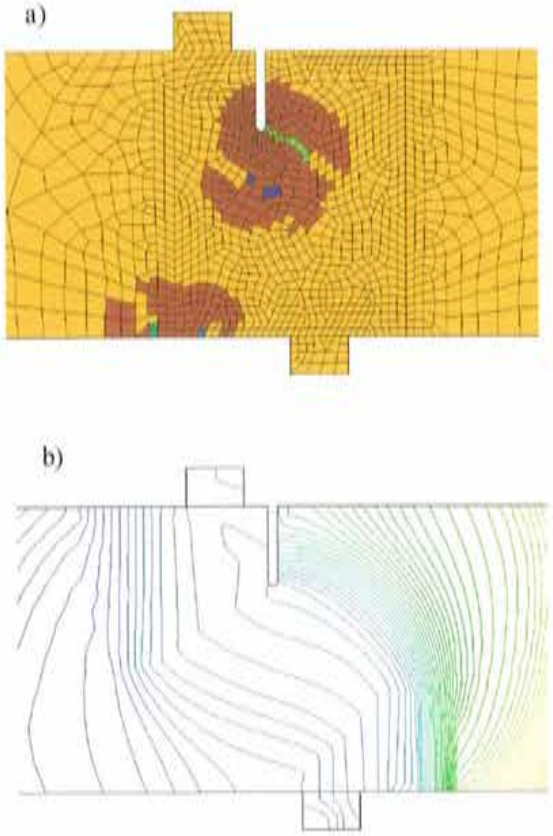

Figure 7.7: Single notched four points bending test a) Exclusion zone (elements in dark brown), b)Possible discontinuity lines.

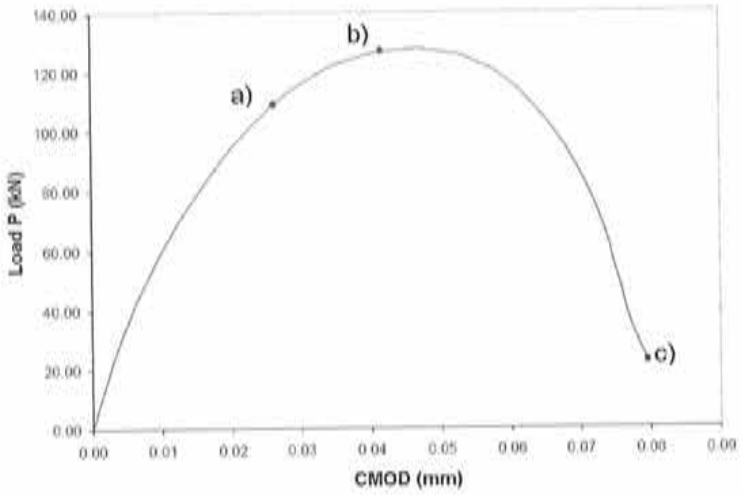

Figure 7.8: Single notched four points bending test: global response curve indicating the loading levels at which pictures of the cracking state are taken.

7.2 Four points bending test with two notches

In this section, one of the four point bending tests reported by ([Bocca et al., 1990]) is modelled. The mesh employed, the dimensions, the applied loads, and constraints are shown in Fig. 7.11. Also a schematic diagram of the experiment is presented in presented in Fig. 7.12.

The tension-only damage model was used. The material properties are the following: $E = 2.7 \cdot 10^{10}$ Pa, $\sigma_u = 2.0 \cdot 10^6$ Pa, ν =0.18, and $G_f = 100$ N/m. The plane stress case was adopted and a thickness $t = 0.1$ m was considered. A global tracking strategy was used and an exclusion zone of 5 cm. was applied. The updated normal plane strategy was employed.

The exclusion zone in an intermediate loading stage is shown in Fig 7.13-a. In Fig. 7.13-b, the possible discontinuity lines for the same time step can be seen. In both figures the central symmetry of the solution in this intermediate step can clearly be seen.

The loading stages at which the pictures in Fig. 7.15 were taken are indicated in Fig. 7.14. Figure 7.15-a shows the elements in inelastic loading in an early loading stage. Two main cracks, emanating from the notches, can be observed at this early loading stage. Other cracks also activate in an intermediate stage (see Fig. 7.15-b) distributed in a symmetric configuration. However, at certain point of the loading process, the symmetry is broken, as shown in Fig. 7.15-c, and only one of the main cracks remains open until the final loading stages, whereas the others arrest. This is

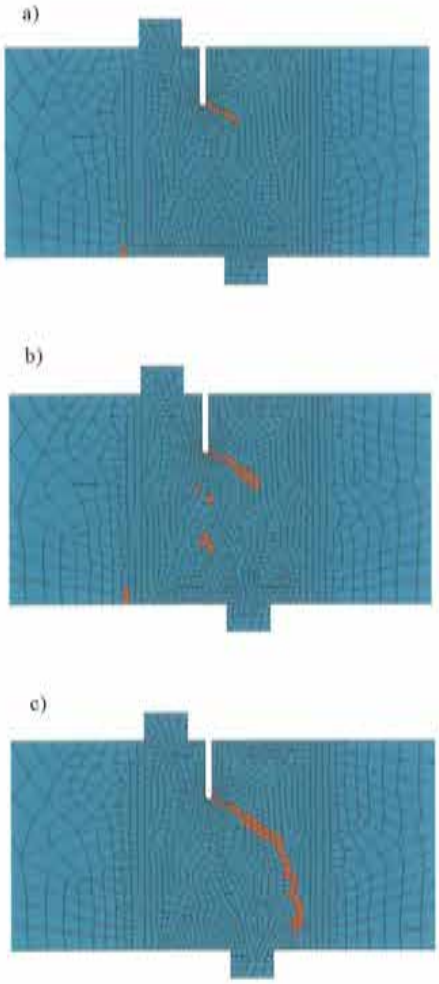

Figure 7.9: Single notched four points bending test: zones of inelastic loading for increasing steps of the loading process.

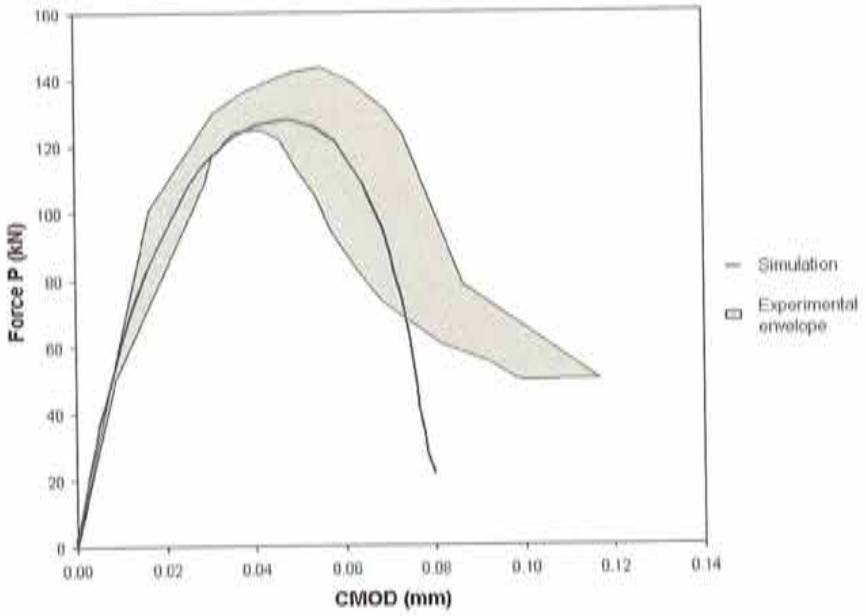

Figure 7.10: Single notched four points bending test: comparison with experimental results.

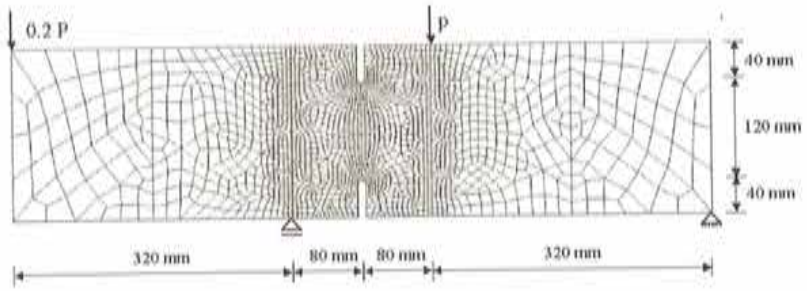

Figure 7.11: Double notched four points bending test: mesh and boundary conditions.

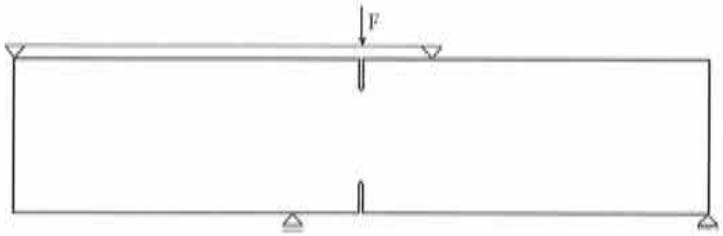

Figure 7.12: Double notched four points beam: schematical diagram of the applied loads in the experimental test.

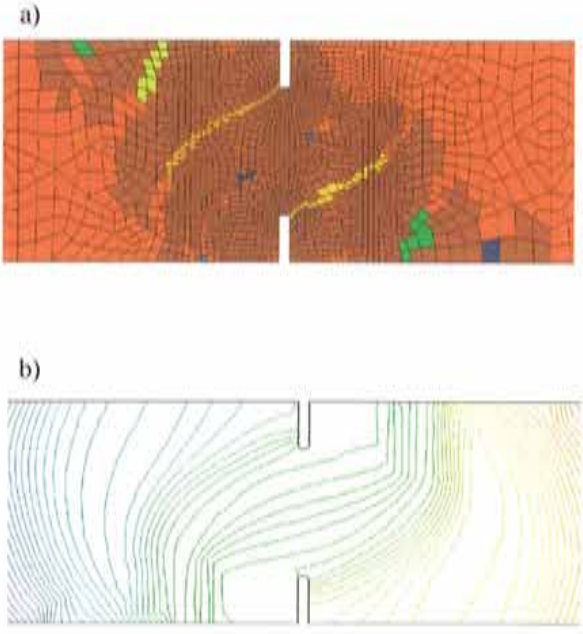

Figure 7.13: Double notched four points bending test: a) exclusion zone (elements in dark brown); b) Possible discontinuity lines.

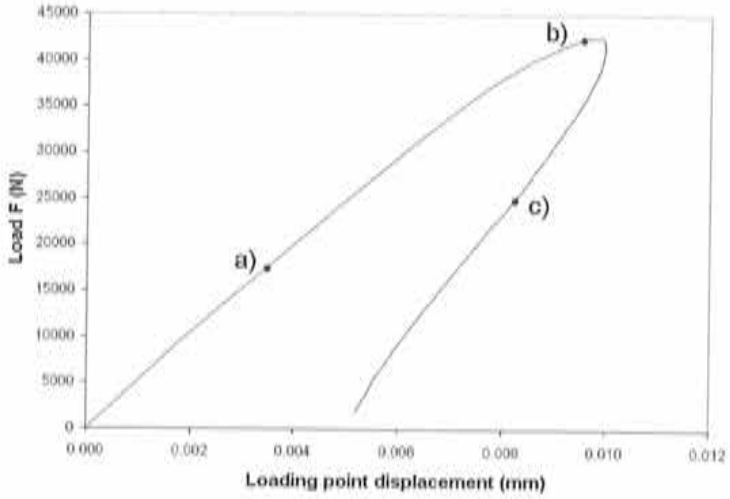

Figure 7.14: Double notched four points bending test: global response curve indicating the loading levels at which pictures of the cracking state are taken.

to be expected since the opening of only one crack seems the less dissipative option.

It is important to say that the presence of a certain exclusion zone was crucial to attain convergence. This can be explained by the fact that there are regions at which the stress state is very similar for all their material points, which entails that some elements can bifurcate spuriously.

A comparison between the experimental envelope and the numerical simulation curve of the global response expressed in terms of load F (see Fig 7.12) and the displacement at its point of application is shown in Fig 7.16.

7.3 Rectangular plate with two geometrical imperfections

This test is based on one presented in [Diez et al., 2000]. The dimensions of the specimen, the boundary conditions and the mesh employed are shown in Fig. 7.17. The two circular imperfections are intended to trigger the appearance of localization. The tension-only model was used. This example was run considering two materials: a brittle one and a more ductile one. For both the plane strain case was considered. The material properties used for the brittle material are $E = 3 \cdot 10^6$ Pa, $\sigma_u = 1 \cdot 10^3$ Pa, ν =0.3, $G_f = 0.01$ N/m. An exclusion zone of 4 mm was used.

Fig. 7.19-a shows the possible discontinuity lines obtained by the procedure explained in Chapter 5 for an intermediate step in the loading process. In Fig.

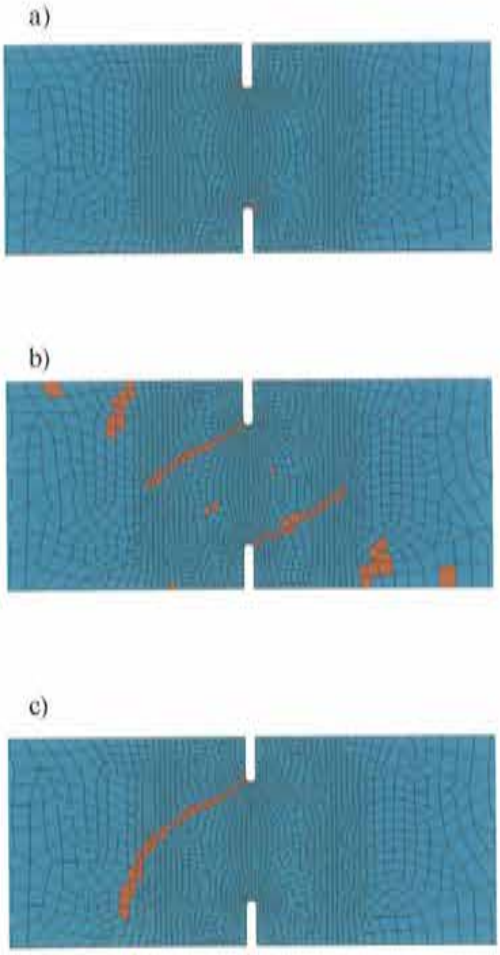

Figure 7.15: Double notched four points bending test: zones in inelastic loading for increasing stages.

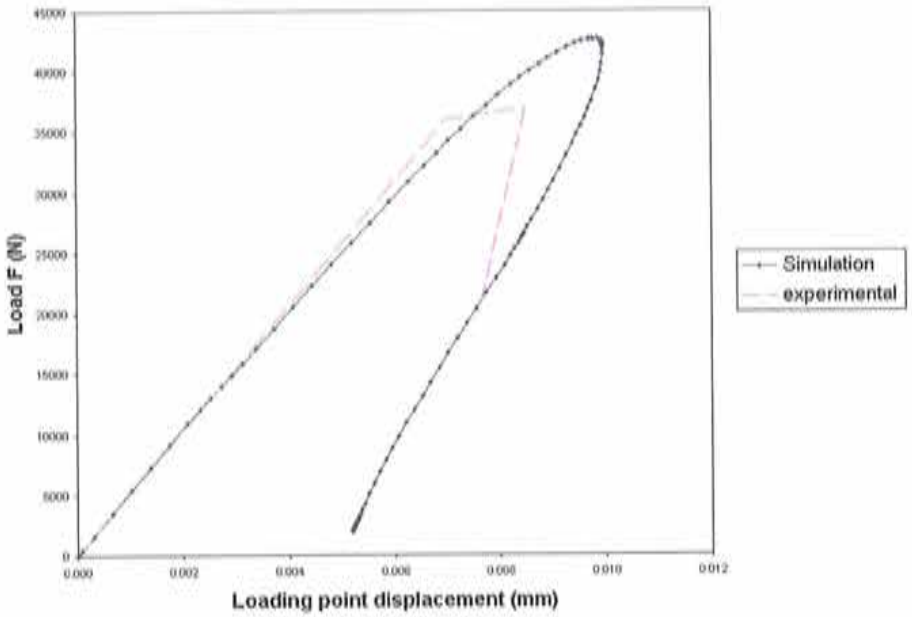

Figure 7.16: Double notched four points bending test: comparison with experimental results.

7.19-b the exclusion zone for that same step is also shown.

In Fig. 7.18 the global response curves (stress xx vs. displacement) of the brittle material with some artificial damping and without it are presented. Both curves are very similar, which shows convergence of the solution with damping to the one without it. The updated normal plane method was used as the continuation technique to follow the equilibrium path and so it was possible to trace the snap backs observed in the curve. Fig 7.18 also shows the points in the global response curve at which the pictures of the cracking state in Fig. 7.20 were taken.

In Fig. 7.20 the evolution of the discontinuity lines is shown. Two discontinuity lines appear at the initial stages. Then, at some point, one of them starts arresting. At final stages only one of them remains open.

For a new run, the fracture energy was changed to $G_f = 0.1$ N/m, obtaining a more ductile material. No exclusion zone was applied, and as a consequence some artificial damping was needed to help convergence of the iterative scheme.

Fig. 7.21 shows the global response of the specimen, indicating also the points in the curve corresponding to the pictures of the cracking state presented in Fig. 7.22. No snap backs appear, as can be expected considering the ductility of the material. The elements in inelastic loading can be seen in Fig. 7.22. Again two main localization bands appear, but now the appearance of other cracks can be

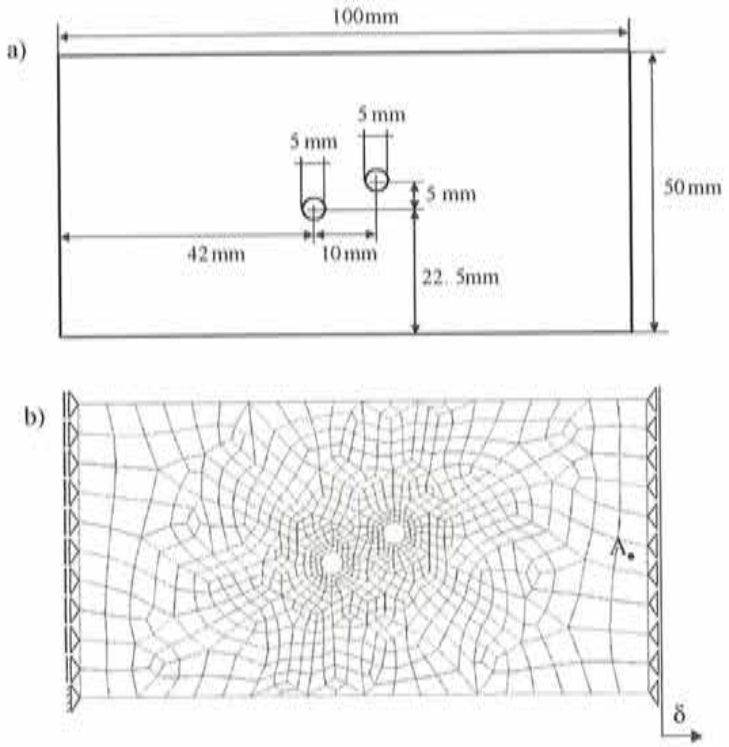

Figure 7.17: Plate with two geometrical imperfections: a) geometry, b) mesh and boundary conditions.

observed. The ductility or the material favors the appearance of various cracks (remember, also, that no exclusion zone was applied). However, at final stages one single crack remains open as seen in Figs. 7.22-g and 7.22-h. It is important to notice that these last two figures correspond to the points in the descending branch of the curve in Fig. 7.21.

7.4 Mixed mode test

One of the double-edge notched concrete specimens tested by [Nooru-Mohamed, 1992] is simulated in this section. The specimen simulated here is the one reported in [Nechnech, 2000]. Experimental data will be taken from that reference. Fig. 7.23 shows the geometry and the applied loads. The steel testing apparatus bonded to the concrete specimen in the experimental test was simulated by a region of elastic elements having Young modulus much higher than the one of concrete and placed along the top and the upper left edges. The mesh employed is

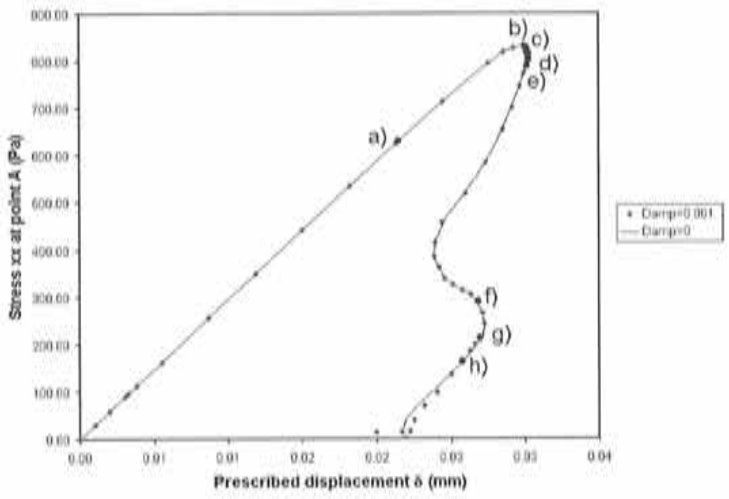

Figure 7.18: Plate with two geometrical imperfections (brittle material): general response curve indicating the loading levels at which pictures of the cracking state will be taken.

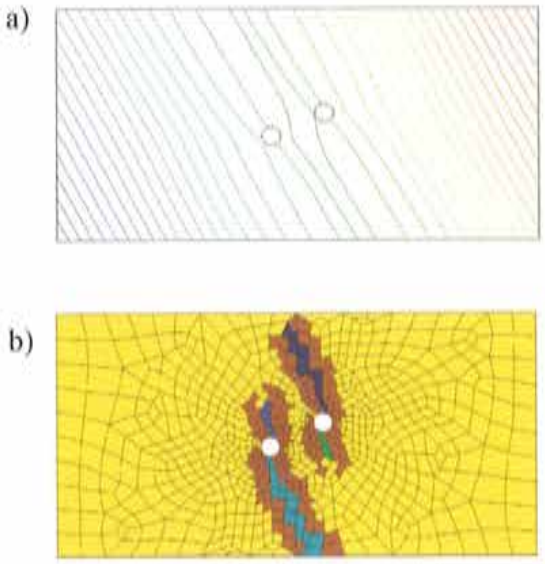

Figure 7.19: Plate with two geometrical imperfections: a) discontinuity lines, b) exclusion zone (elements in dark brown).

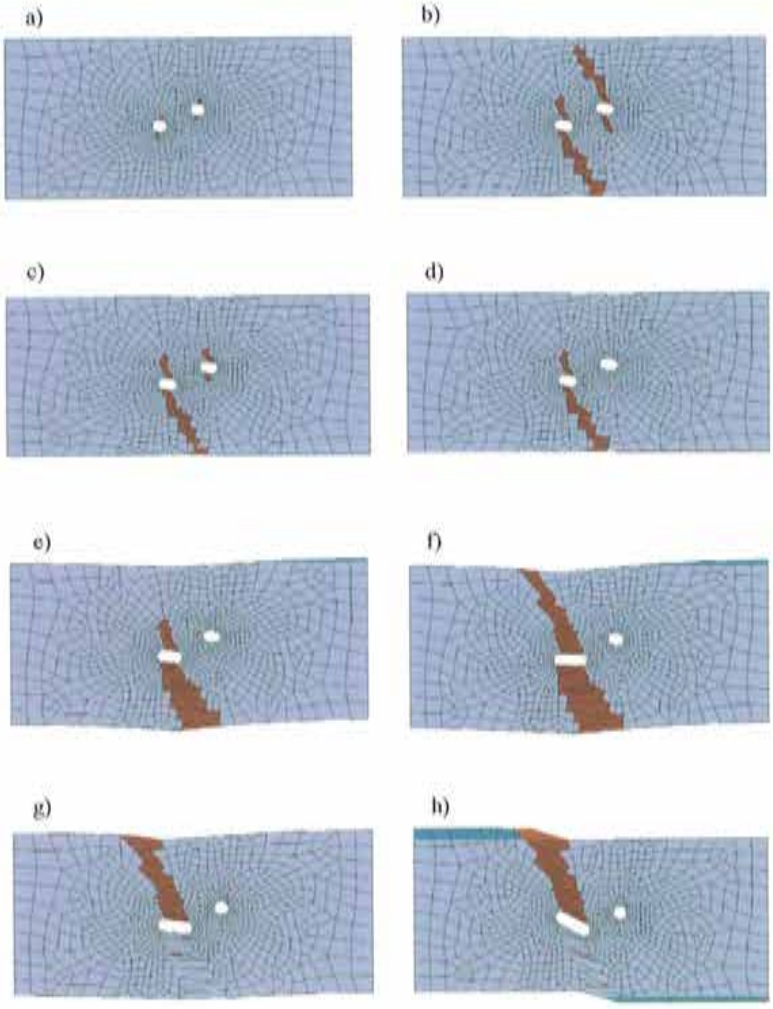

Figure 7.20: Plate with two geometrical imperfections (brittle material): elements in inelastic loading for increasing stages.

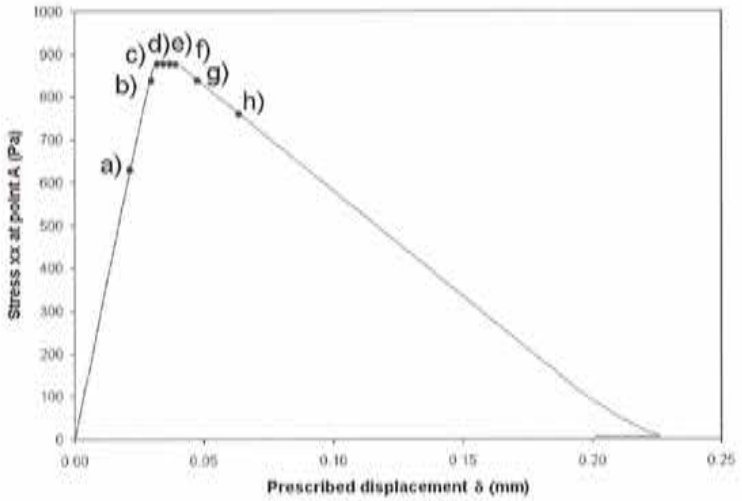

Figure 7.21: Plate with two geometrical imperfections (ductile material): global response curve indicating the loading levels at which pictures of the cracking state will be taken.

shown in Fig. 7.24.

The horizontal load illustrated in Fig. 7.23 was kept constant during the experimental test with a value $P_h = 5$ kN. To simulate this, the nodes on the upper left side of the mesh were subjected to monotonically increasing horizontal forces until their sum reached 5 kN. Then, these forces were kept constant during the rest of the simulation, whereas monotonically increasing displacements were imposed in the nodes on the top of the mesh.

Again the tension-only model was used to simulate the behavior of concrete, however the principal stress direction was used as the propagation vector. The following material properties were considered: $E = 3.2 \cdot 10^{10}$ Pa, $\sigma_u = 2.6 \cdot 10^6$ Pa, ν =0.2, and $G_f = 110$ N/m. The plane stress case was adopted and a thickness $t =$ 0.05 m was considered. Some algorithmic damping was added to help convergence of the iterative procedure.

Fig. 7.25-a shows the exclusion zone for an intermediate loading stage, while Fig 7.25-b shows the discontinuity lines obtained by the global tracking algorithm employed for the same time step.

In Fig. 7.27, a sequence of the deformation and the evolution of cracking is shown by means of pictures corresponding to the points in the curve of Fig. 7.26. Notice how the solutions in the early stages are symmetrical, coinciding with the points in the ascending branch of curve 7.26. Two main cracks, emanating from the notches, develop, but at a given time, coinciding with the beginning of the descending branch of the curve in Fig. 7.26, one of them arrests.

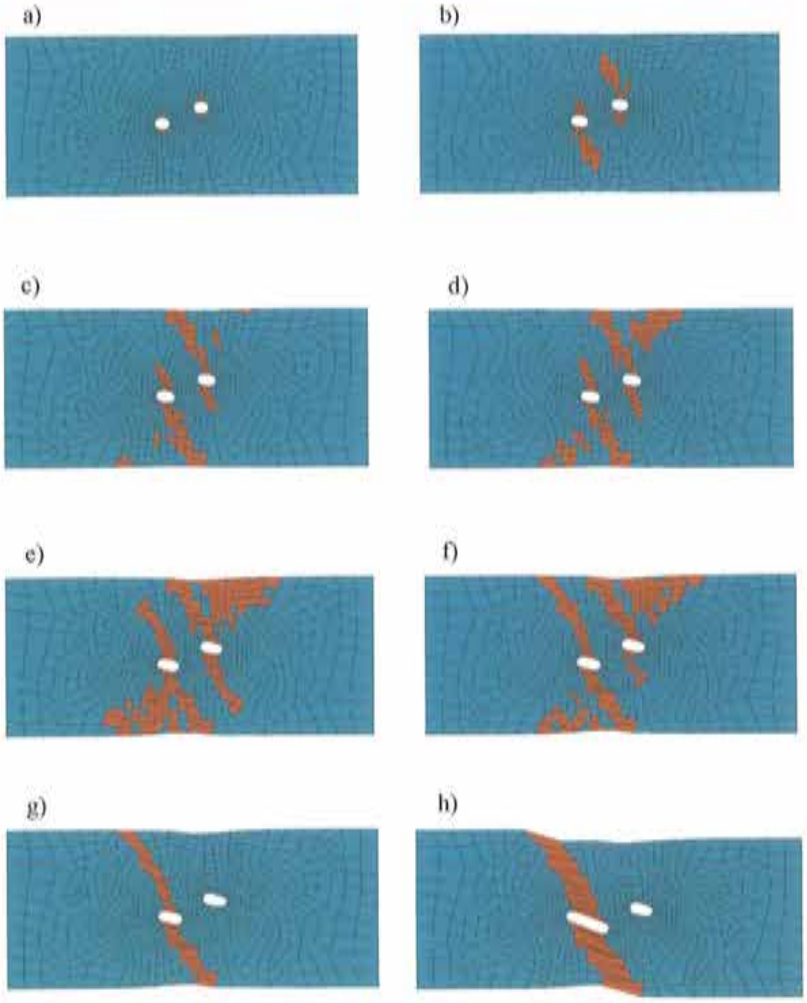

Figure 7.22: Plate with two geometrical imperfections (ductile material): elements in inelastic loading for increasing stages.

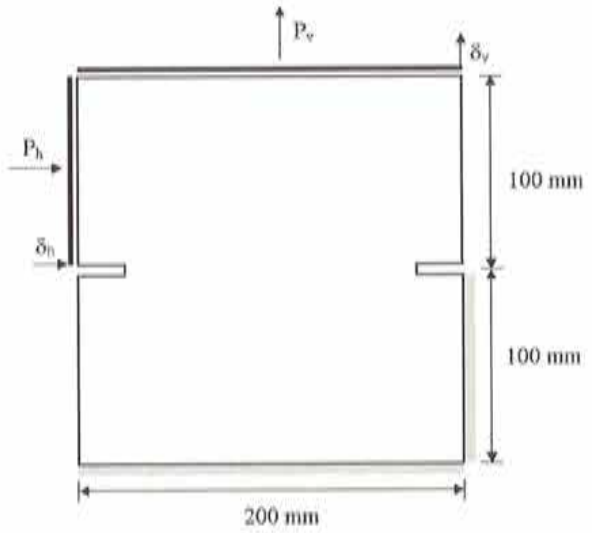

Figure 7.23: Mixed mode test: geometry and boundary conditions.

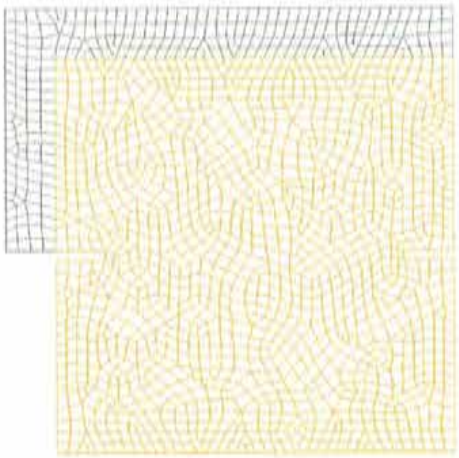

Figure 7.24: Mixed mode test: mesh.

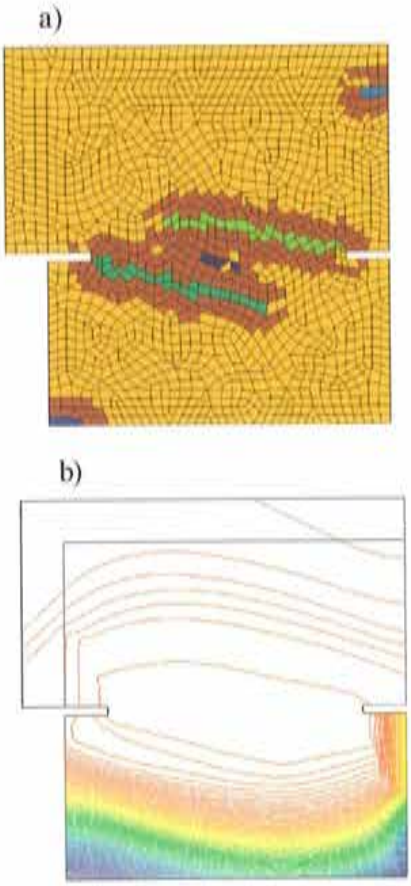

Figure 7.25: Mixed mode test: a) exclusion zone (elements in dark brown), b)discontiuity lines.

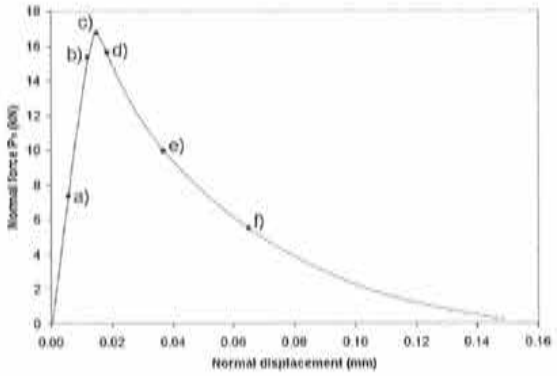

Figure 7.26: Mixed mode test: global response curve indicating the loading levels at which pictures of the cracking state will be taken.

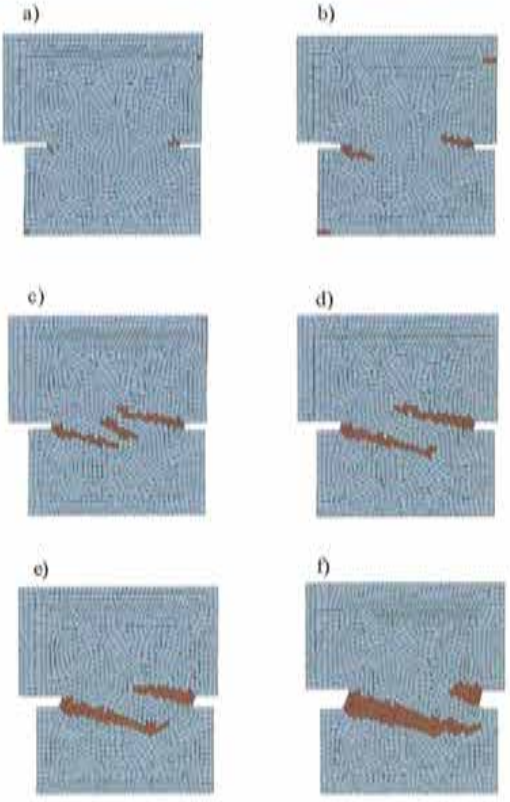

Figure 7.27: Mixed mode test: elements in inelastic loading for increasing stages.

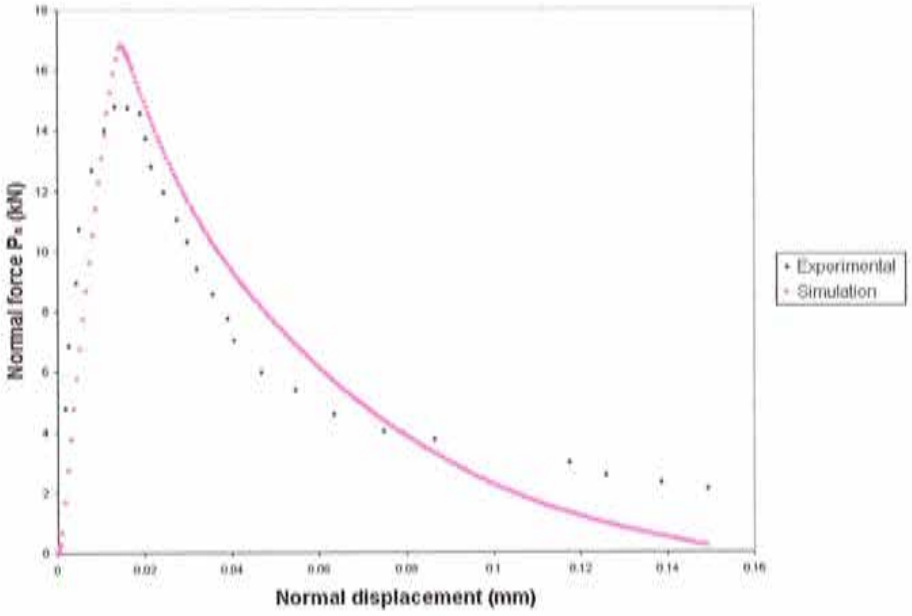

Figure 7.28: Mixed mode test: global response curves of the experimental test and of the numerical simulation.

A comparison between the simulation and the experimental ([Nechnech, 2000]) curves of the global response in terms of the normal force P_n and the normal displacement δ_n is shown in Fig. 7.28.

7.5 Tension pull reinforced specimen

A tension pull test applied to a reinforced specimen is simulated in this section. This test was inspired by a similar one presented in ([Rots, 1988]). In the simulation presented here, the plane strain case is considered, while in the one in Rots the axisymmetric case was used. The dimensions and loads applied to the specimen are shown in Fig. 7.29. Two meshes were used and are shown in Fig. 7.30. The tension-only damage model was used for the concrete matrix, considering the following material properties: $E = 2.5 \cdot 10^{10}$ Pa, $\sigma_u = 3 \cdot 10^6$ Pa, ν =0.18, and $G_f = 25$ N/m. The reinforcement was modelled as an elastic material having the following material properties: $E = 2.14 \cdot 10^{11}$ Pa, ν =0.3. To model the interface between concrete and reinforcement, a region of one element width governed by a J2 perfectly plastic constitutive model was placed, having as material properties $E = 2.14 \cdot 10^{11}$ Pa, $\sigma_u = 3 \cdot 10^6$ Pa, ν =0.3.

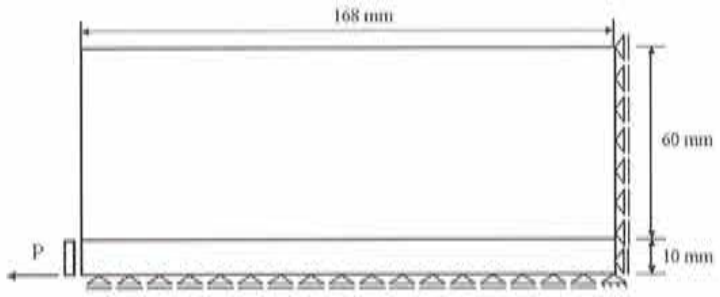

Figure 7.29: Tension pull specimen: geometry.

Fig. 7.31 shows a comparison between the global response curves of the two meshes considered. The global response is expressed in terms of the applied force and the corresponding displacement on node A (see Fig. 7.30-a) for the coarse mesh and on node B (see Fig. 7.30-b) for the fine mesh. Very sharp snap backs can be observed. The use of the algorithmic damping is crucial to be able to run these examples, due both to the smoothness that it gives to the tracing of the equilibrium path and to the fact that it precludes an eventual loss of uniqueness.

The presence of reinforcement favors the appearance of several discontinuity lines. A picture of the exclusion zone for the coarse mesh at an intermediate loading stage is shown in Fig 7.32-a, while in Fig. 7.32-b the discontinuity lines at

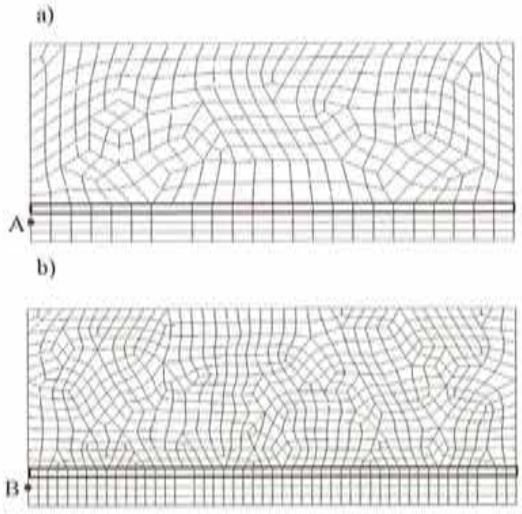

Figure 7.30: Tension pull specimen: a) coarse mesh, b) fine mesh.

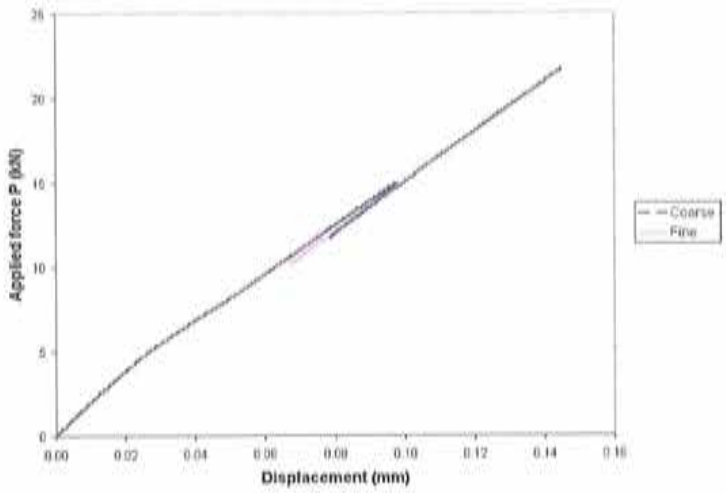

Figure 7.31: Tension pull specimen: comparison between coarse and fine mesh.

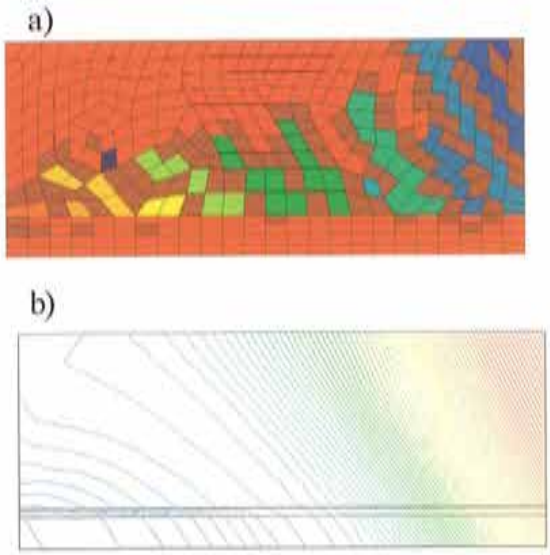

Figure 7.32: Tension pull specimen (coarse mesh): a) exclusion zone (elements in dark brown), b) discontinuity lines.

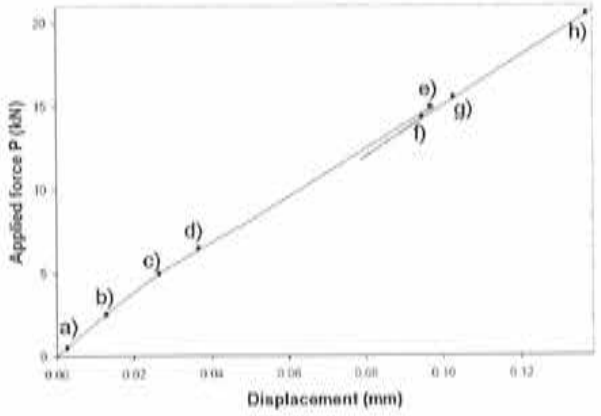

Figure 7.33: Tension pull specimen (coarse mesh): global response curve indicating the loading levels at which pictures of the cracking state will be taken.

that stage are shown.

Again considering the coarse mesh, the points on the global response curve corresponding to the pictures of the cracking state shown in Fig. 7.34 are illustrated in Fig. 7.33. The progress of cracking along time (for the coarse mesh) can be described as follows. First, the interface between concrete and reinforcement undergoes progressive plastic yielding (as shown in Figs. 7.34-a and 7.34-b). Then, the opening of multiple cracks in the concrete matrix is observed (Fig. 7.34-c). Most of them are secondary cracking. However, Figs. 7.34-d and 7.34-e show how some primary cracking becomes apparent. The snap-backs in Fig. 7.33 are reflected in the distribution of cracking shown in Fig. 7.34-f. There, much of the secondary cracking arrest and close while the main crack remains open. Finally, due to the effect of the reinforcement, the secondary cracking opens again as seen in Figs. 7.34-g and 7.34-h.

The exclusion zone and the possible discontinuity lines for an intermediate stage of the loading process when the fine mesh is employed are shown in Fig. 7.35. A different exclusion zone from the one used for the coarse mesh is applied.

The propagation and arrest of crack lines can be seen in Fig 7.37 for the fine mesh. The points of the equilibrium path to which the pictures in that figure correspond are illustrated in Fig. 7.36. Though the distribution of the secondary cracking seems to be ruled by the mesh and by the size of the exclusion zone, the main cracks are very similar to the ones observed in the coarse mesh.

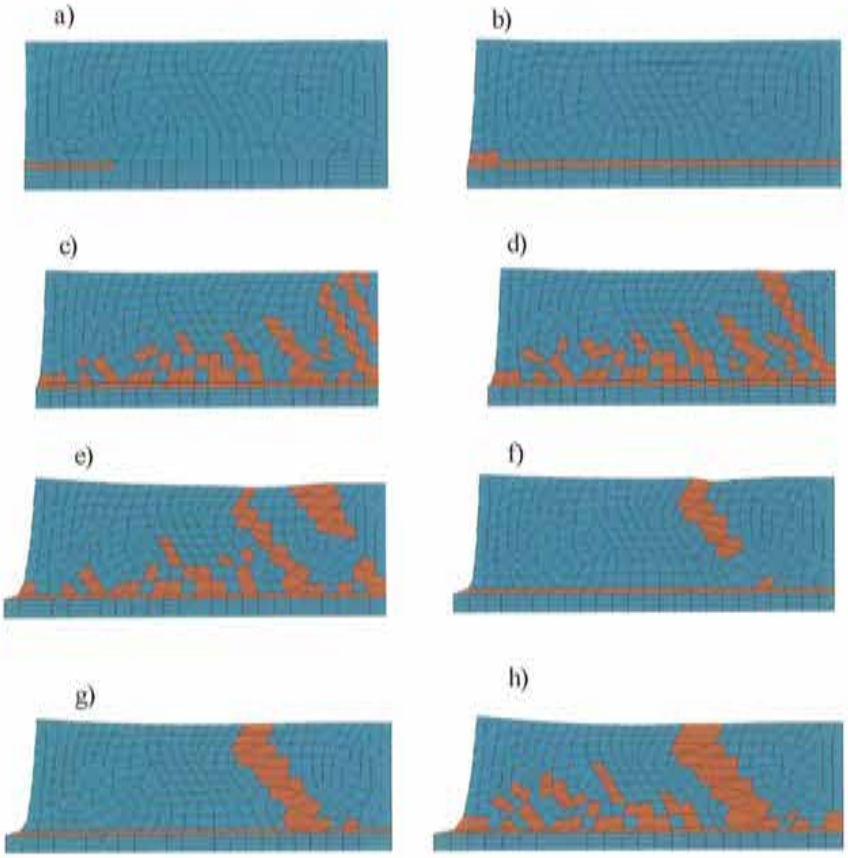

Figure 7.34: Tension pull specimen (coarse mesh): elements in inelastic loading for increasing stages.

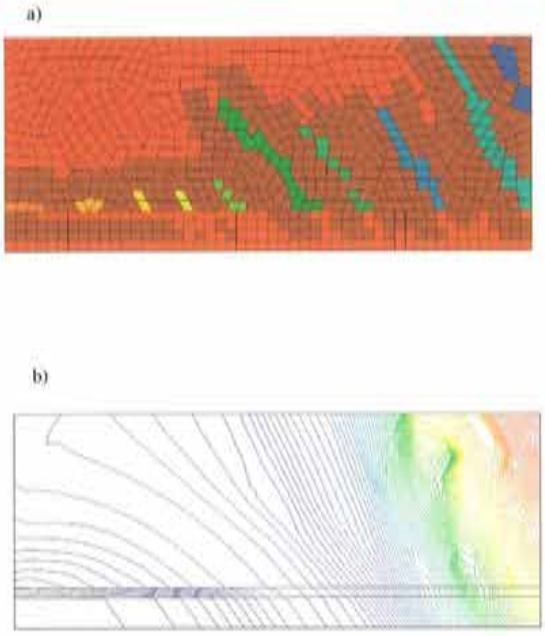

Figure 7.35: Tension pull specimen (fine mesh): a) exclusion zone (elements in dark brown), b) discontinuity lines.

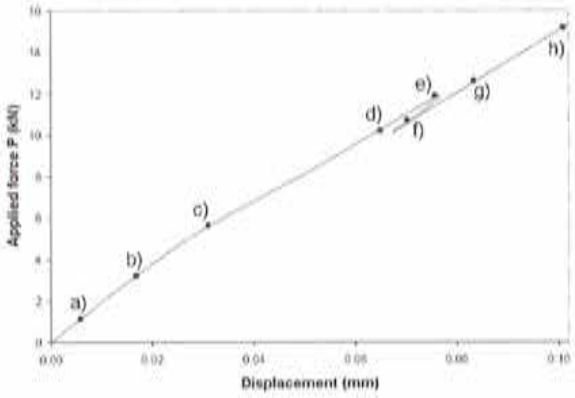

Figure 7.36: Tension pull specimen (fine mesh): global response curve indicating the loading levels at which pictures of the cracking state will be taken.

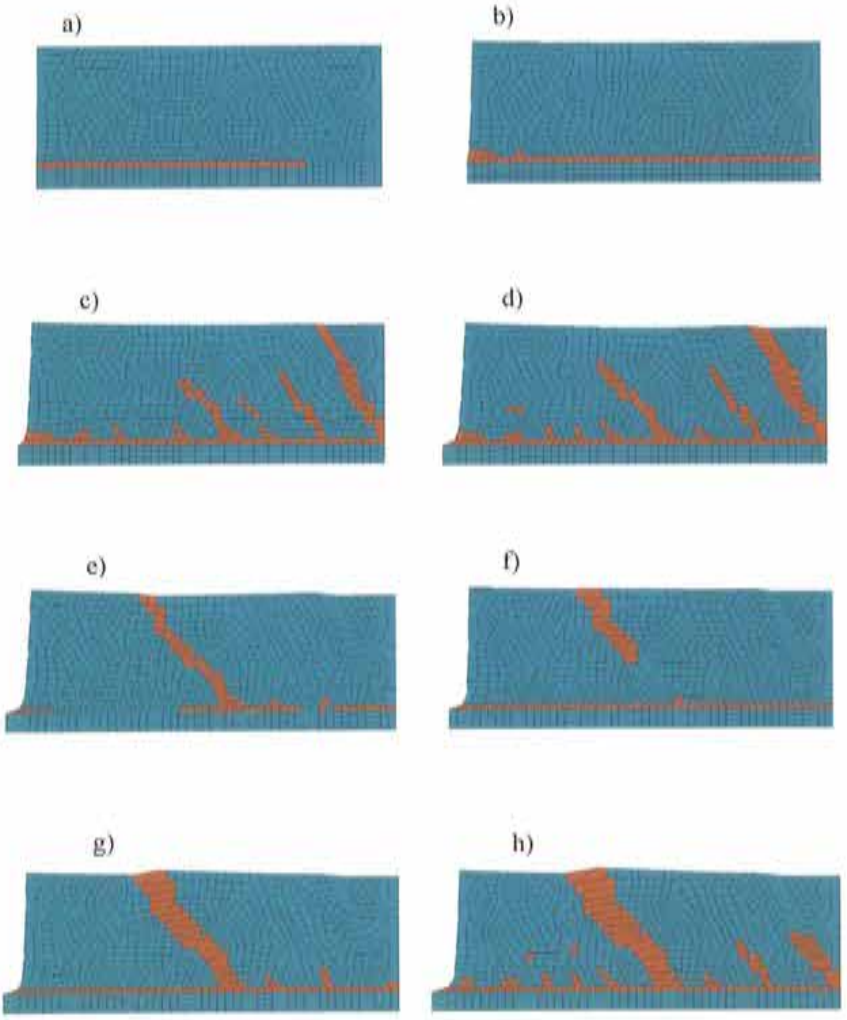

Figure 7.37: Tension pull specimen (fine mesh): elements in inelastic loading for increasing stages of the loading process.

Chapter 8

Conclusions and future developments

Throughout this monograph, different aspects of the modelling of strain localization in two-dimensional solids in a strong discontinuity setting have been studied. The main aim was to contribute to the numerical simulation of the postcritical behavior of structures by a continuum strong discontinuity approach. To attain this, the theoretical basis of the approach adopted was analyzed, identifying the following as its most relevant features:

- It is fully consistent with classical continuum constitutive modelling and no resorting to any kind of alternative continuum (generalized continua) has been employed.

- In the spirit of remaining within the context of Continuum Mechanics, the classical discontinuous bifurcation analysis was adopted as the proper framework to determine the inception and the propagation direction of a discontinuity interface.

- The mathematical conditions that make it possible to use continuum constitutive models in combination with the strong discontinuity kinematics were derived in the context of the so-called Strong Discontinuity Analysis. Perhaps, the most interesting result of this analysis is the fact that the use of continuum constitutive models plus the strong discontinuity kinematics naturally lead to projected discrete constitutive models acting in the discontinuity interface.

The numerical counterpart of the mathematical model summarized above, can be, at least roughly, described by the following characteristics:

- The numerical implementation has been performed keeping the continuum format of the strong discontinuity approach. This is mainly reflected in the fact that no discrete (cohesive) constitutive model has been explicitly implemented.
- The numerical discretization of BVP's involving strong discontinuities has been tackled by means of finite elements with embedded discontinuities. A multifield approach was adopted to derive different formulations.
- In case of using the nonsymmetric formulation of elements with embedded discontinuities, some tracking strategy, based on the information obtained from the discontinuous bifurcation analysis, is necessary. These strategies were studied in this work and two main groups were identified: local and global (or overall) ones.
- The nonsymmetric formulation may lead to instabilities at element level having to do with the "brittleness" of that element. This might be a source of numerical problems.

8.1 Conclusions

Within the context of the analytical and the numerical models summarized above, the following conclusions can be extracted from this work:

- The modelling of strong discontinuities can consistently be carried out in a continuum format in an efficient way from the computational point of view. No discrete traction-separation relationship needs to be implemented explicitly.
- Within the context of a multifield BVP, the way in which the variational problem is stated can naturally lead to different finite element formulations.
- Although the nonsymmetric formulation entails the necessity of a tracking algorithm, its performance is clearly superior to that of other formulations of finite elements with embedded discontinuities. Specifically, the statically consistent formulation, which could (in principle) be the ideal candidate for a self-propagating element, has a major drawback: it suffers from stress locking. Even in the case of employing certain techniques to overcome this pathology (as far as assessed in this monograph), the performance of the nonsymmetric formulation is overwhelmingly superior.
- If the nonsymmetric element is to be used for the simulation of multiple discontinuities, an efficient tracking algorithm becomes necessary. The fact that

global tracking strategies provide information about all the possible discontinuity lines at every time step makes them specially appealing for handling several discontinuities. Thus, an efficient algorithm for multi-cracking can naturally be devised from the overall tracking concept.

- The numerical simulation of strong discontinuities in solids can lead to very complex problems that require special techniques to stabilize them and to properly trace the corresponding equilibrium path.

8.2 Main contributions

In this work some contributions to the modelling of strong discontinuities in solids have been made. The most important are the following:

- A systematic review of the theoretical fundamentals of the Strong Discontinuity Approach has been presented.

- A very general framework to derive different formulations of finite elements with embedded discontinuities based on the multi-field statement of the governing equations of a BVP with strong discontinuities has been proposed.

- Two variations of the symmetric assumed-enhanced-strain based element have been proposed to alleviate its stress locking effect. One of them was based on a mixed approach, whereas the other was based on a re-enhancement of the basic element.

- An overall tracking strategy based on a heat-conduction-like BVP was devised. This thermal analogy, besides profiting the structure of standard non-linear thermo-mechanical finite element codes, provides physical insight that helps understand some characteristics of this strategy.

- An algorithm to manage several discontinuities based on the overall tracking strategy mentioned above was developed.

- In order to preclude some possible instabilities, an artificial damping term was added to the principle of virtual work equation. This added damping also precludes any eventual loss of uniqueness of the BVP and can help to obtain a smoother tracing of the equilibrium path.

8.3 Future work

Based on the work developed in this monograph, the following lines of future research are proposed:

- The implementation of the heat-conduction-like algorithm for three-dimensional settings.
- The development of continuation techniques that take into account the possible numerical instabilities coming from "brittle" elements.
- The study of the influence of this "element brittleness" in the global problem.
- A rigorous study of eventual bifurcation points in the equilibrium path due to the presence of multiple discontinuity interfaces.
- Further comparative analyses of embedded elements based on linear triangles and bilinear quadrilaterals as well as on other possible parent elements.
- A detailed comparison, based on theoretical analyses and on numerical results, between elements with embedded discontinuities (elemental enrichment) and partition of unity based formulations (nodal enrichment).

Appendix A

Tracing the equilibrium path

When complex problems in nonlinear structural analysis are tackled, tracing the overall response in terms of load vs. deflection curves can turn out to be an especially complicated task. In the case of material nonlinearities and, specifically, when constitutive models with strain softening (which can lead to the appearance of strain localization) are employed, the need of continuation techniques that allow for a correct tracing of the equilibrium path becomes apparent. This is even more critical when phenomena such as the presence of multiple localization bands (which in the case of the Strong Discontinuity Approach implies multiple discontinuity lines) have to be modelled.

Here we present a brief review of the best known continuation techniques and discuss their most relevant features. For a more complete account of this subject the reader is referred to [Crisfield, 1998].

A.1 Residual forces equation

The equations resulting from a finite element discretization of a boundary value problem undergoing material nonlinearities can be expressed as a *residual forces equation* (see, for instance, [Felippa, 2001]):

$$\mathbf{r}(\mathbf{u}, \lambda) = \mathbf{F}_{int}(\mathbf{u}) - \lambda \mathbf{q} = 0 \tag{A.1}$$

where $\mathbf{r}(\mathbf{u}, \lambda) \in \mathbb{R}^n$ is the so-called *residual forces vector*, $\mathbf{F}_{int}(\mathbf{u}) \in \mathbb{R}^n$ stands for the *internal forces vector* and $\mathbf{q} \in \mathbb{R}^n$ denotes the *external load vector*. In this context, the nodal displacement vector, $\mathbf{u} \in \mathbb{R}^n$, is the *state variable*, while λ is the *control*

parameter, which defines the loading level. Consider the following $\mathbb{R}^{n+1}$ vector:

$$\mathbf{w} := \left\{ \begin{array}{c} \mathbf{u} \\ \lambda \end{array} \right\}$$

which will be termed, from now on, *generalized displacement vector*. Then we can define the **equilibrium path** as the locus of points $\mathbf{w}$ in the generalized displacement space for which $\mathbf{r}(\mathbf{w}) = \mathbf{0}$.

Remark 69 *The residual forces equation (A.1) constitutes a system of n nonlinear equations, whose unknowns are, in principle, the displacements* $\mathbf{u}$.

Remark 70 *Only the case of* proportional loading *has been considered in (A.1).*

A.2 Predictor-corrector algorithms

One way to solve the system of nonlinear equations (A.1) is by means of the so-called predictor-corrector (or incremental-iterative) algorithms. The first step is to split the loading process up into increments. At every increment i, a prediction on the value of the displacement vector, $\mathbf{u}$, for a given increment of the loading level (characterized by an increment of the control parameter, $\Delta\lambda_i^0$) is computed as follows:

$$\mathbf{u}_i^0 = \mathbf{u}_{i-1} + \Delta\mathbf{u}_i^0 \tag{A.2}$$

with

$$\Delta\mathbf{u}_i^0 = (\mathbf{K}_{i-1})^{-1}\Delta\lambda_i^0\mathbf{q} \tag{A.3}$$

Matrix $\mathbf{K}_{i-1}^{-1}$ can be computed as

$$\mathbf{K}_{i-1} = \left.\frac{\partial\mathbf{r}}{\partial\mathbf{u}}\right|_{\mathbf{u}_{i-1}} \tag{A.4}$$

In general, when the value obtained by (A.2) is substituted into the expression of the residual forces (A.1), we obtain that

$$\mathbf{r}(\mathbf{u}_i^0, \lambda_i^0) \neq \mathbf{0} \tag{A.5}$$

with $\lambda_i^0 = \lambda_{i-1} + \Delta\lambda_i^0$. Then, we say that the residual forces are *unbalanced* and a correction phase to *balance* them becomes necessary. Every correction (iteration) k to the displacement vector is computed as

$$\mathbf{u}_i^k = \mathbf{u}_{i-1} + \Delta\mathbf{u}_i^k \tag{A.6}$$

and is characterized by an *iterative displacement*, $\delta\mathbf{u}^k = \Delta\mathbf{u}_i^k - \Delta\mathbf{u}_i^{k-1}$, and by an *iterative control parameter*, $\delta\lambda^k = \Delta\lambda_i^k - \Delta\lambda_i^{k-1}$. The value of the displacement vector obtained by (A.6) is then replaced in the residual forces expression (A.1) until some convergence criterion is fulfilled.

There are several ways to perform the correction phase. Perhaps the most simple is to keep the control parameter λ_i constant during the whole increment i, which entails that $\delta\lambda_i^k = 0$. Then the iterative displacement can be computed as

$$\delta\mathbf{u}_i^k = (\mathbf{K}_i^k)^{-1}\mathbf{r}_i^{k-1} \tag{A.7}$$

where $\mathbf{r}_i^{k-1} := \mathbf{r}(\mathbf{u}_i^{k-1}, \lambda_i^{k-1})$. If, for instance,

$$\mathbf{K}_i^k = \left.\frac{\partial \mathbf{r}}{\partial \mathbf{u}}\right|_{\mathbf{u}_i^{k-1}} \tag{A.8}$$

where $\mathbf{K}_i^k$ is the so-called tangent-stiffness matrix, then we arrive to the classical Newton-Raphson method. Of course, other alternatives can be chosen, such as using the same stiffness matrix for the whole increment, and then we arrive at a modified Newton-Raphson strategy.

The above described strategy in which the control parameter λ_i remains constant along the increment is known as *load control* (see Fig. (A.1-a)). It is a very efficient technique in many cases. However, it can lead to some instabilities or to the case where it is impossible to find a point in the equilibrium path for a given loading level . These problems commonly appear in the modelling of structures undergoing strain softening. Therefore, alternative strategies have to be used.

Remark 71 *Special care has to be taken when bifurcation points exist. In such a case no continuation technique is enough to ensure a correct tracing of the equilibrium path.*

A.3 Continuation methods

When load control is not enough to trace the equilibrium path of a loading process, then more sophisticated techniques are necessary. These techniques are known as *continuation methods*. We present some of them in this section.

A.3.1 Arc-length method

As mentioned above, load control fails in some cases in which the imposed loading level is not feasible. Therefore, to make sure that the loading level can be reached

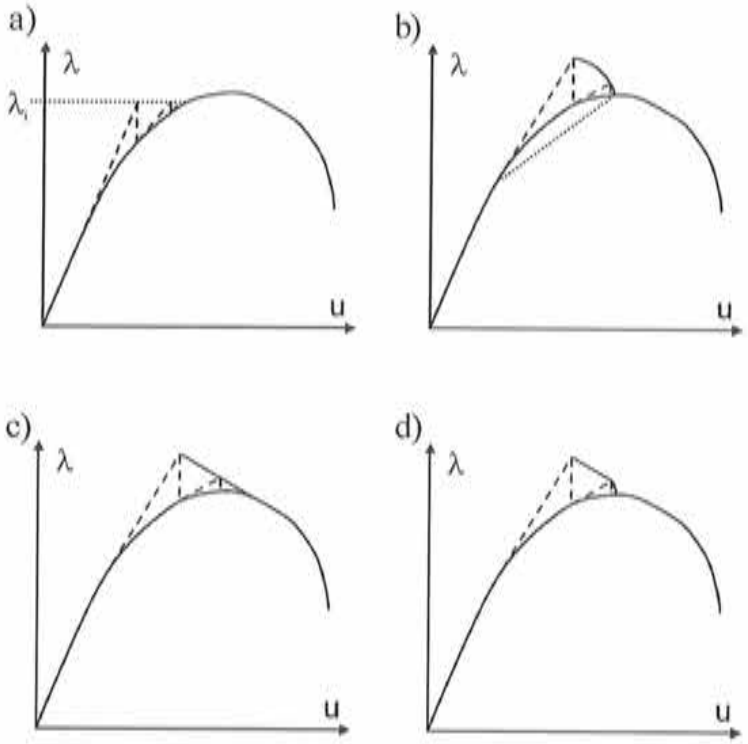

Figure A.1: Continuation methods: a) load control, b) arc-length method, c) normal plane, d) updated normal plane.

by the equilibrium path, it seems logical to consider the control parameter λ as an additional unknown, which requires the addition of another equation to the nonlinear system (A.1). One way to get this additional equation is defining a hyper-sphere with radius Δl in the general displacement space (see Fig. A.1-b) as follows:

$$(\Delta \mathbf{u}_i^k)^T \Delta \mathbf{u}_i^k + (\alpha \Delta \lambda_i^k)^2 = \Delta l^2 \tag{A.9}$$

where α is a scaling parameter. Equation (A.9) can be regarded as a constraint on the values of the generalized displacements. The combination of this constraint with the predictor-corrector algorithm presented in the preceding section gives rise to the so-called *arc-length method* or *spherical control*.

A.3.2 Normal and updated normal plane

A simpler option is to define a hyper-plane orthogonal to the prediction $(\Delta\mathbf{u}_i^0, \lambda_i^0)$ to act as a constraint to the generalized displacement vector (see Fig. (A.1-c)):

$$(\Delta\mathbf{u}_i^0)^T \delta\mathbf{u}_i^k + \alpha^2 \Delta\lambda_i^0 \delta\lambda_i^k = 0 \tag{A.10}$$

Equation (A.10) leads to the so-called *normal plane* strategy.

Better performance than with normal plane can be obtained by updating the normal hyperplane at each iteration (see Fig. (A.1-d)) as follows:

$$(\Delta\mathbf{u}_i^{k-1})^T \delta\mathbf{u}_i^k + \alpha^2 \Delta\lambda_i^{k-1} \delta\lambda_i^k = 0 \tag{A.11}$$

giving rise to the so-called *updated normal plane* strategy

Remark 72 *The direct addition of any of the equations (A.9), (A.10) or (A.11) to the nonlinear system (A.6) would lead to an augmented tangent stiffness matrix that would be neither symmetric nor banded.*

Remark 73 *In cases in which the dimension of the generalized displacement space is big enough (i.e., in most of the practical cases), the scaling parameter α can be set to zero without losing robustness . When this is done for the arc-length method, we arrive at the so-called 'cylindrical control' ([Crisfield, 1998]).*

A.3.3 Implementation Aspects

The most common way of implementing the continuation methods described above is not based on directly adding the corresponding constraint equation. In order to keep the logic and the data structure of a standard nonlinear finite element code, in which load control is implemented, it is common to split every correction into two:

$$\delta\mathbf{u}_i^k = \delta_I\mathbf{u}_i^k + \delta\lambda_i^k \delta_{II}\mathbf{u}_i^k \tag{A.12}$$

where $\delta_I\mathbf{u}_i^k$ is computed as

$$\delta_I\mathbf{u}_i^k = (\mathbf{K}_i^k)^{-1}\mathbf{r}_i^{k-1} \tag{A.13}$$

and $\delta_{II}\mathbf{u}_i^k$ as

$$\delta_{II}\mathbf{u}_i^k = (\mathbf{K}_i^k)^{-1}\mathbf{q} \tag{A.14}$$

Substituting (A.13) and (A.14) into (A.6), then into (A.9), and, finally, solving for $\delta\lambda_i^k$ yields

$$\delta\lambda_i^k = c_1(\delta\lambda_i^k)^2 + c_2\delta\lambda_i^k + c_3 \tag{A.15}$$

where

$$\begin{aligned} c_1 &= (\delta_{II}\mathbf{u}_i^k)^T\delta_{II}\mathbf{u}_i^k \\ c_2 &= 2(\Delta\mathbf{u}_i^{k-1} + \delta_I\mathbf{u}_i^k)^T\delta_{II}\mathbf{u}_i^k \\ c_3 &= (\Delta\mathbf{u}_i^{k-1} + \delta_I\mathbf{u}_i^k)^T(\Delta\mathbf{u}_i^{k-1} + \delta_I\mathbf{u}_i^k) \end{aligned}$$

With a similar procedure, we can arrive to expressions for $\delta\lambda_i^k$ in the normal plane strategy,

$$\delta\lambda_i^k = -\frac{(\Delta\mathbf{u}_i^0)^T\delta_I\mathbf{u}_i^k}{(\Delta\mathbf{u}_i^0)^T\delta_{II}\mathbf{u}_i^k + \alpha^2\Delta\lambda_i^0} \tag{A.16}$$

and for the updated normal plane strategy,

$$\delta\lambda_i^k = -\frac{(\Delta\mathbf{u}_i^{k-1})^T\delta_I\mathbf{u}_i^k}{(\Delta\mathbf{u}_i^{k-1})^T\delta_{II}\mathbf{u}_i^k + \alpha^2\Delta\lambda_i^{k-1}} \tag{A.17}$$

Loading level of the prediction

Since, in the continuation methods presented above, the control parameter λ has been added as a new unknown, it seems logical that its predictive incremental value $\Delta\lambda_i^0$ also has to be computed, not prescribed. One way to achieve this is to use an arc-length type constraint for the prediction:

$$(\Delta\mathbf{u}_i^0)^T\Delta\mathbf{u}_i^0 + (\alpha\Delta\lambda_i^0)^2 = \Delta l^2 \tag{A.18}$$

Let us define

$$\mathbf{v}_i := (\mathbf{K}_{i-1})^{-1}\mathbf{q} \tag{A.19}$$

Then from (A.3) and (A.18), one obtains

$$\Delta\lambda_i^0 = \pm\sqrt{\frac{\Delta l^2}{(\mathbf{v}_i)^T\mathbf{v}_i + \alpha^2}} \tag{A.20}$$

The issue of how to choose the most convenient sign in expression (A.20) is by no means trivial for complex problems. Here, we present a simple criterion that can

be very efficient. It is based on requiring that the external work release be positive, i.e.,

$$\Delta W = \mathbf{q}^T \Delta \mathbf{u}_i^0 = \Delta \lambda_i^0 \mathbf{q}^T \mathbf{v}_i > 0 \tag{A.21}$$

In order to optimize the performance of any of the continuation techniques reviewed here, it seems logical that the length of an increment, Δl, should vary automatically, based on some criterion that reduces it in the parts of the equilibrium path that are highly non-linear. A heuristic way of estimating the degree of non-linearity of some part of the equilibrium path is by means of the number of iterations needed to attain convergence of the iterative procedure. Thus, the following expression for Δl, intended to maintain the number of iterations almost constant for every increment i, can be used:

$$\Delta l_i = \Delta l_{i-1} \sqrt{\frac{I_d}{I_{i-1}}}$$

where Δl_{i-1} is the length of the last converged increment, I_{i-1} is the number of iterations needed for convergence in increment $i-1$, and I_d is a defined-by-the-user ideal number of iterations.

Appendix B

Nodal Enrichment

There are problems in continuum mechanics for which the resolution provided by the standard finite element method seems not to be satisfactory. In some of these problems, there are qualitative features of the solution that are known a priori. However, it happens very often that this information cannot be introduced via standard finite element shape functions. This is the case of strain localization. If one assumes the space of bounded deformations $BD(\Omega)$ (see [Temam, 1983]) as the proper function space for problems in which constitutive models with strain softening are involved, as proposed in [Simo et al., 1993], then jumps in the displacement field need to be modelled. Many formulations have been devised in order to enrich the standard finite element approximation to optimally capture these displacement jumps. They can be classified into two basic groups: elemental enrichment and nodal enrichment. The former has been extensively described in Chapter 4 under the name of finite elements with embedded discontinuities[1]; the latter is briefly reviewed in this appendix.

B.1 Motivation

Consider the problem of a body Ω crossed by a discontinuity $\mathcal{S}$, which partitions Ω into Ω^- and Ω^+. The boundary of Ω consists of two disjoint subsets Γ_σ and Γ_u, the former being the part of the boundary on which tractions are prescribed, and the latter, the part of the boundary in which displacements are prescribed. In Chapter 4, two ways of stating the strong discontinuity kinematics corresponding to such a

[1] As mentioned before, although the author does not see any reason to restrict this term to formulations based on elemental enrichment, this is a common practice in the literature that we have adopted in this thesis.

problem are presented:

$$\dot{\mathbf{u}}(\mathbf{x},t) = \dot{\hat{\mathbf{u}}}(\mathbf{x},t) + H_S\,[\![\dot{\mathbf{u}}]\!](\mathbf{x},t) \tag{B.1}$$

and

$$\dot{\mathbf{u}}(\mathbf{x},t) = \dot{\hat{\mathbf{u}}}(\mathbf{x},t) + \mathcal{M}_S(\mathbf{x})\,[\![\dot{\mathbf{u}}]\!](\mathbf{x},t) \tag{B.2}$$

with

$$\dot{\hat{\mathbf{u}}}(\mathbf{x},t) := \dot{\hat{\mathbf{u}}}(\mathbf{x},t) + [\![\dot{\mathbf{u}}]\!](\mathbf{x},t)\varphi(\mathbf{x}) \tag{B.3}$$

φ being a smooth function such that, for a certain subdomain $\Omega_\varphi \subset \Omega$ containing the discontinuity line $\mathcal{S}$ (i.e. $\Omega_\varphi \supset \mathcal{S}$),

$$\varphi(\mathbf{x}) = \begin{cases} 1 & \forall \mathbf{x} \in \Omega^+ \backslash \Omega_\varphi \\ 0 & \forall \mathbf{x} \in \Omega^- \backslash \Omega_\varphi \end{cases} \tag{B.4}$$

From (B.1), (B.2), and (B.3), we can derive that

$$\mathcal{M}_S(\mathbf{x}) = H_S - \varphi(\mathbf{x}) \tag{B.5}$$

Remark 74 *Notice that supp*$[\mathcal{M}_S]$=Ω_φ.

One of the motivations to use (B.2) instead of (B.1) in Chapter 4 is the fact that the former avoids having to prescribe Dirichlet type boundary condition for $[\![\dot{\mathbf{u}}]\!]$. However, there are other ways to achieve this. For instance, one could require that $[\![\dot{\mathbf{u}}]\!]$ have local support around the discontinuity $\mathcal{S}$, as shown in Fig. B.1. This can be done by considering an open domain $\Omega_{[\dot{\mathbf{u}}]} \subset \Omega$, partitioned by $\mathcal{S}$ into $\Omega^+_{[\dot{\mathbf{u}}]} = \Omega_{[\dot{\mathbf{u}}]} \cap \Omega^+$ and $\Omega^-_{[\dot{\mathbf{u}}]} = \Omega_{[\dot{\mathbf{u}}]} \cap \Omega^-$, such that $\partial\Omega_{[\dot{\mathbf{u}}]} \cap \Gamma_u = \emptyset$ and $[\![\dot{\mathbf{u}}]\!]|_{\Omega\backslash\Omega_{[\dot{\mathbf{u}}]}} = 0$.

Based on the above considerations, let us propose the following finite element discretization of (B.1) into four-noded quadrilaterals for an element crossed by the discontinuity:

$$\dot{\mathbf{u}}^{h^{(e)}}(\mathbf{x},t) = \underbrace{\textstyle\sum_{i=1}^{i=4} N_i^{(e)}(\mathbf{x})\dot{\mathbf{d}}_i(t)}_{\dot{\hat{\mathbf{u}}}^{h^{(e)}}} + H_S \underbrace{\left(\textstyle\sum_{i=1}^{i=4} N_i^{(e)}(\mathbf{x})\,\dot{\mathbf{a}}_i(t)\right)}_{[[\dot{\mathbf{u}}]]^{h^{(e)}}} \tag{B.6}$$

where $\left\{N_i^{(e)}\right\}_{i=1}^{4}$ are the standard shape functions of the bilinear quadrilateral. From (B.6), it is clear that the support of $[[\dot{\mathbf{u}}]]^h$ goes beyond the domain of the elements crossed by the discontinuity, due to the fact that standard finite element shape functions are involved in its definition. Thus, this kind of enrichment is associated to the shape functions whose support are intersected by a discontinuity line; hence its name: *nodal enrichment*. A rigorous way to state this type of enrichment, based on the partition of unity concept, is presented in the next section.

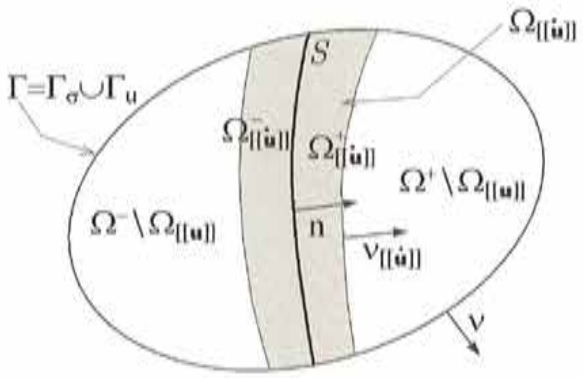

Figure B.1: Solid with a strong discontinuity.

B.2 Partition of unity method

The concept of partition of unity was first applied to enrich the standard finite element approximation in [Melenk and Babuska, 1996], giving rise to the so-called Partition of Unity Finite Element Method (PUFEM). In [Moes et al., 1999], this concept was applied to capturing jumps in the displacement field within the context of Linear Fracture Mechanics and was given the name of Extended Finite Elements (X-FEM). Later, [Wells and Sluys, 2001] employed this formulation to model strong discontinuities in cohesive surfaces.

A very general expression for the partition of unity based enrichment of an scalar field u reads:

$$u^h(\mathbf{x}) = \sum_{i\in\mathcal{K}} \phi_i(\mathbf{x}) \left(a_i + \sum_{j=1}^{n^{enr}} b_{ji} c_j(\mathbf{x}) \right) \tag{B.7}$$

where $\mathcal{K} := \{1, ..., n_{node}\}$, a_i and b_{ji} are nodal degrees of freedom, n^{enr} stands for the number of enrichment functions, c_j are the enrichment functions, and ϕ_i are some functions fulfilling the partition of unity property, i.e.,

$$\sum_{i=1}^{n_{node}} \phi_i(\mathbf{x}) = 1 \quad \forall \mathbf{x} \in \Omega \tag{B.8}$$

Remark 75 *As it is well known, standard finite element shape functions N_i fulfill the partition of unity property stated in (B.8).*

Remark 76 *The enrichment functions c_j can, in principle, vary from node to node.*

Now, let us use expression (B.7) to approximate (B.1), by taking $\phi_i(\mathbf{x}) = N_i(\mathbf{x})$ and $c_j(\mathbf{x}) = H_S$:

$$\dot{\mathbf{u}}^h(\mathbf{x},t) = \underbrace{\sum_{i\in\mathcal{K}} N_i(\mathbf{x})\dot{\mathbf{d}}_i(t)}_{\dot{\mathbf{u}}^h} + H_S \underbrace{\sum_{i\in\mathcal{N}} N_i(\mathbf{x})\dot{\mathbf{a}}_i(t)}_{[\![\dot{\mathbf{u}}]\!]^h} \tag{B.9}$$

$\mathcal{N}$ is the set of nodes whose support is split up into two by the discontinuity $\mathcal{S}$.

Remark 77 *Expression (B.9) is clearly the extension of (B.6) from an element domain to the whole solid Ω.*

Remark 78 *The definition of $\mathcal{N}$ is consistent with the requirement of $\Omega_{[\![\dot{\mathbf{u}}]\!]}$ having local support around $\mathcal{S}$.*

B.3 Variational formulation

Here, we state the variational form of the BVP corresponding to a solid Ω crossed by a discontinuity $\mathcal{S}$ in a format convenient for its discretization using (B.9). The equivalence with the strong form of the BVP will also be shown, emphasizing the fact that the inner traction continuity equation (characteristic of problems involving strong discontinuities) can be readily derived from the principle of virtual work if one adopts the kinematics stated in (B.1).

The principle of virtual work expressed in rates (principle of virtual power) reads:

$$\int_\Omega \dot{\boldsymbol{\sigma}} : \nabla^S \boldsymbol{\eta}\, d\Omega - G_{ext}(\boldsymbol{\eta}) \;\; = 0 \quad \forall \boldsymbol{\eta} \in \mathcal{V}_\eta \tag{B.10}$$

where $\mathcal{V}_\eta$ is the space of admissible variations of the displacement rate, whose typical element has the following structure:

$$\boldsymbol{\eta} = \bar{\boldsymbol{\eta}} + H_S\, \boldsymbol{\alpha} \tag{B.11}$$

$\bar{\boldsymbol{\eta}}$, $\boldsymbol{\alpha}$ being two smooth functions fulfilling $\bar{\boldsymbol{\eta}}|_{\Gamma_u} = 0$ and $\boldsymbol{\alpha}|_{\Omega\setminus\Omega_{[\![\dot{\mathbf{u}}]\!]}} = 0$, respectively, and

$$G_{ext}(\bullet) := \int_\Omega \dot{\mathbf{b}} \cdot (\bullet)\, d\Omega + \int_{\Gamma_\sigma} \dot{\mathbf{t}}^* \cdot (\bullet)\, d\Gamma \tag{B.12}$$

In light of (B.11), equation (B.10) can be rewritten as

$$\begin{aligned} &\int_{\Omega} \dot{\boldsymbol{\sigma}} : \nabla^S \bar{\boldsymbol{\eta}}\, d\Omega - G_{ext}(\bar{\boldsymbol{\eta}}) = 0 && \forall \bar{\boldsymbol{\eta}} \in \mathcal{V}_{\bar{\eta}} \quad (a) \\ &\int_{\Omega} \dot{\boldsymbol{\sigma}} : \left[\nabla^S (H_S\, \boldsymbol{\alpha})\right] d\Omega - G_{ext}(H_S\, \boldsymbol{\alpha}) = 0 && \forall \boldsymbol{\alpha} \in \mathcal{V}_{\alpha} \quad (b) \end{aligned} \tag{B.13}$$

By using standard arguments, we can show that the strong form of (B.13-a) is

$$\begin{aligned} &\nabla \cdot \dot{\boldsymbol{\sigma}} + \dot{\mathbf{b}} = 0 && in\ \Omega \backslash \mathcal{S} \quad (a) \\ &\dot{\boldsymbol{\sigma}} \cdot \boldsymbol{\nu} = \dot{\mathbf{t}}^* && on\ \Gamma_\sigma \quad (b) \\ &(\dot{\boldsymbol{\sigma}}_{\Omega^+} - \dot{\boldsymbol{\sigma}}_{\Omega^-}) \cdot \mathbf{n} = 0 && on\ \mathcal{S} \quad (c) \end{aligned} \tag{B.14}$$

Let us now work with (B.13-b). We have that

$$\nabla^S (H_S\, \boldsymbol{\alpha}) = (\delta_S \mathbf{n} \otimes \boldsymbol{\alpha})^S + (H_S\, \nabla \boldsymbol{\alpha})^S \tag{B.15}$$

Substituting (B.15) into (B.13-b) yields

$$\int_{\Omega} \dot{\boldsymbol{\sigma}} : (\delta_S \mathbf{n} \otimes \boldsymbol{\alpha})^S d\Omega + \int_{\Omega} \dot{\boldsymbol{\sigma}} : (H_S\, \nabla \boldsymbol{\alpha})^S d\Omega - G_{ext}(H_S\, \boldsymbol{\alpha}) = 0 \tag{B.16}$$

$\forall \boldsymbol{\alpha} \in \mathcal{V}_{\alpha}$.

Since $\boldsymbol{\alpha}|_{\Omega \backslash \Omega_{[\dot{\mathbf{u}}]}} = 0$ by definition, the left hand side of B.16 can be rewritten as

$$\int_{\mathcal{S}} \mathbf{n} \cdot \dot{\boldsymbol{\sigma}}_{\mathcal{S}} \cdot \boldsymbol{\alpha} d\mathcal{S} + \int_{\Omega^+_{[\dot{\mathbf{u}}]}} \dot{\boldsymbol{\sigma}} : \nabla \boldsymbol{\alpha} d\Omega - \int_{\Omega^+_{[\dot{\mathbf{u}}]}} \dot{\mathbf{b}} \cdot \boldsymbol{\alpha}\, d\Omega - \int_{\Gamma_\sigma \cap \partial\Omega^+_{[\dot{\mathbf{u}}]}} \dot{\mathbf{t}}^* \cdot \boldsymbol{\alpha}\, d\Gamma \tag{B.17}$$

where $\partial\Omega^+_{[\dot{\mathbf{u}}]}$ stands for the boundary of $\Omega^+_{[\dot{\mathbf{u}}]}$. We have that

$$\begin{aligned} \int_{\Omega^+_{[\dot{\mathbf{u}}]}} \dot{\boldsymbol{\sigma}} \ : \ \nabla \boldsymbol{\alpha} d\Omega &= \int_{\Omega^+_{[\dot{\mathbf{u}}]}} \nabla \cdot (\dot{\boldsymbol{\sigma}} \cdot \boldsymbol{\alpha})\, d\Omega - \int_{\Omega^+_{[\dot{\mathbf{u}}]}} (\nabla \cdot \dot{\boldsymbol{\sigma}}) \cdot \boldsymbol{\alpha} d\Omega \\ &= \int_{\partial\Omega^+_{[\dot{\mathbf{u}}]}} \boldsymbol{\nu}_{[\dot{\mathbf{u}}]} \cdot (\dot{\boldsymbol{\sigma}} \cdot \boldsymbol{\alpha})\, d\Gamma - \int_{\Omega^+_{[\dot{\mathbf{u}}]}} (\nabla \cdot \dot{\boldsymbol{\sigma}}) \cdot \boldsymbol{\alpha} d\Omega \end{aligned} \tag{B.18}$$

$\boldsymbol{\nu}_{[\dot{\mathbf{u}}]}$ being the outward normal to $\partial\Omega^+_{[\dot{\mathbf{u}}]}$ (see Fig.(B.1)). Substituting (B.18) in B.17

and considering (B.14-a), we obtain

$$\begin{aligned}
&\int_{\mathcal{S}} \mathbf{n}\cdot\dot{\boldsymbol{\sigma}}_{\mathcal{S}}\cdot\boldsymbol{\alpha}d\mathcal{S} + \int_{\partial\Omega^{+}_{[\![\dot{\mathbf{u}}]\!]}} \boldsymbol{\nu}_{[\![\dot{\mathbf{u}}]\!]}\cdot(\dot{\boldsymbol{\sigma}}\cdot\boldsymbol{\alpha})\,d\Gamma \\
&\underbrace{-\int_{\Omega^{+}_{[\![\dot{\mathbf{u}}]\!]}} (\nabla\cdot\dot{\boldsymbol{\sigma}})\cdot\boldsymbol{\alpha}d\Omega - \int_{\Omega^{+}_{[\![\dot{\mathbf{u}}]\!]}} \dot{\mathbf{b}}\cdot\boldsymbol{\alpha}\,d\Omega}_{=0} \\
&-\int_{\Gamma_{\sigma}\cap\partial\Omega^{+}_{[\![\dot{\mathbf{u}}]\!]}} \dot{\mathbf{t}}^{*}\cdot\boldsymbol{\alpha}\,d\Gamma \\
=\ &\int_{\mathcal{S}} \mathbf{n}\cdot\dot{\boldsymbol{\sigma}}_{\mathcal{S}}\cdot\boldsymbol{\alpha}d\mathcal{S} + \int_{\partial\Omega^{+}_{[\![\dot{\mathbf{u}}]\!]}} \boldsymbol{\nu}_{[\![\dot{\mathbf{u}}]\!]}\cdot(\dot{\boldsymbol{\sigma}}\cdot\boldsymbol{\alpha})\,d\Gamma \\
&-\int_{\Gamma_{\sigma}\cap\partial\Omega^{+}_{[\![\dot{\mathbf{u}}]\!]}} \dot{\mathbf{t}}^{*}\cdot\boldsymbol{\alpha}\,d\Gamma
\end{aligned} \tag{B.19}$$

Notice that $\partial\Omega^{+}_{[\![\dot{\mathbf{u}}]\!]}$ can be partitioned into $(\partial\Omega_{[\![\dot{\mathbf{u}}]\!]}\cap\Omega^{+})$, $(\Gamma_{\sigma}\cap\partial\Omega^{+}_{[\![\dot{\mathbf{u}}]\!]})$, and $\mathcal{S}$. Thus, since $\boldsymbol{\alpha}|_{\partial\Omega_{[\![\dot{\mathbf{u}}]\!]}\cap\Omega^{+}}=\mathbf{0}$, then

$$\int_{\partial\Omega^{+}_{[\![\dot{\mathbf{u}}]\!]}} \boldsymbol{\nu}_{[\![\dot{\mathbf{u}}]\!]}\cdot(\dot{\boldsymbol{\sigma}}\cdot\boldsymbol{\alpha})\,d\Gamma = -\int_{\mathcal{S}} \mathbf{n}\cdot\dot{\boldsymbol{\sigma}}_{\Omega^{+}}\cdot\boldsymbol{\alpha}d\mathcal{S} + \int_{\Gamma_{\sigma}\cap\partial\Omega^{+}_{[\![\dot{\mathbf{u}}]\!]}} (\boldsymbol{\nu}\cdot\dot{\boldsymbol{\sigma}})\cdot\boldsymbol{\alpha}d\Gamma \tag{B.20}$$

Now, replacing (B.20) into (B.19) and considering (B.14-b), one obtains

$$\begin{aligned}
&\int_{\mathcal{S}} \mathbf{n}\cdot\dot{\boldsymbol{\sigma}}_{\mathcal{S}}\cdot\boldsymbol{\alpha}d\mathcal{S} - \int_{\mathcal{S}} \mathbf{n}\cdot\dot{\boldsymbol{\sigma}}_{\Omega^{+}}\cdot\boldsymbol{\alpha}d\mathcal{S} \\
&\underbrace{+\int_{\Gamma_{\sigma}\cap\partial\Omega^{+}_{[\![\dot{\mathbf{u}}]\!]}} (\boldsymbol{\nu}\cdot\dot{\boldsymbol{\sigma}})\cdot\boldsymbol{\alpha}d\Gamma - \int_{\Gamma_{\sigma}\cap\partial\Omega^{+}_{[\![\dot{\mathbf{u}}]\!]}} \dot{\mathbf{t}}^{*}\cdot\boldsymbol{\alpha}\,d\Gamma}_{0}
\end{aligned}$$

Finally, we arrive at

$$\int_{\mathcal{S}} (\mathbf{n}\cdot\dot{\boldsymbol{\sigma}}_{\mathcal{S}} - \mathbf{n}\cdot\dot{\boldsymbol{\sigma}}_{\Omega^{+}})\cdot\boldsymbol{\alpha}d\mathcal{S} = 0 \tag{B.21}$$

By standard arguments, the so-called inner traction continuity is obtained from (B.21):

$$\mathbf{n}\cdot\dot{\boldsymbol{\sigma}}_{\mathcal{S}} - \mathbf{n}\cdot\dot{\boldsymbol{\sigma}}_{\Omega^{+}} = 0 \tag{B.22}$$

B.4 Finite element discretization

Expression (B.9) can be rewritten in matrix form as

$$\dot{\mathbf{u}}^h = \mathbf{N}^T \dot{\mathbf{d}} + \mathit{II}_S \mathbf{N}_{\mathcal{N}}^T \dot{\mathbf{a}} \tag{B.23}$$

with

$$\mathbf{N} = \left\{ \begin{array}{c} \mathbf{N}_1 \\ \vdots \\ \mathbf{N}_i \\ \vdots \\ \mathbf{N}_{n^{node}} \end{array} \right\}; \quad \dot{\mathbf{d}} = \left\{ \begin{array}{c} \dot{\mathbf{d}}_1 \\ \vdots \\ \dot{\mathbf{d}}_i \\ \vdots \\ \dot{\mathbf{d}}_{n^{node}} \end{array} \right\}; \quad \dot{\mathbf{a}} = \left\{ \begin{array}{c} \dot{\mathbf{a}}_1 \\ \vdots \\ \dot{\mathbf{a}}_i \\ \vdots \\ \dot{\mathbf{a}}_{n^{node}} \end{array} \right\} \tag{B.24}$$

$\mathbf{N}_i$ being, for 2-D,

$$\mathbf{N}_i = N_i \mathbf{1} = N_i \begin{bmatrix} 1 & 0 \\ 0 & 1 \end{bmatrix}$$

and

$$\mathbf{N}_{\mathcal{N}} = \left\{ \begin{array}{c} \gamma_1 \mathbf{1} \\ \vdots \\ \gamma_i \mathbf{1} \\ \vdots \\ \gamma_{n^{node}} \mathbf{1} \end{array} \right\} \quad \gamma_i \equiv \left\{ \begin{array}{ll} N_i & \text{for } i \in \mathcal{N} \\ 0 & \text{for } i \notin \mathcal{N} \end{array} \right. \tag{B.25}$$

The strain can be computed as

$$\left\{ \dot{\boldsymbol{\varepsilon}}^h \right\} = \left\{ \nabla^S \dot{\mathbf{u}}^h \right\} = \mathbf{L} \dot{\mathbf{u}}^h \tag{B.26}$$

where the operator $\mathbf{L}$ has the following expression for two-dimensional cases:

$$\mathbf{L} := \begin{bmatrix} \partial_x(\bullet) & 0 \\ 0 & \partial_y(\bullet) \\ \partial_y(\bullet) & \partial_x(\bullet) \end{bmatrix} \tag{B.27}$$

Let us define

$$\mathbf{B} := \mathbf{L}\mathbf{N}^T \quad \text{and} \quad \mathbf{B}_{\mathcal{N}} := \mathbf{L}\mathbf{N}_{\mathcal{N}}^T \tag{B.28}$$

Then (B.26) can be rewritten as

$$\left\{\dot{\varepsilon}^h\right\} = \mathbf{B}\dot{\mathbf{d}} + H_S\mathbf{B}_{\mathcal{N}}\dot{\mathbf{a}} + \delta_S\,[\mathbf{n}]\,\mathbf{N}_{\mathcal{N}}^T\dot{\mathbf{a}} \tag{B.29}$$

with

$$[\mathbf{n}] = \begin{bmatrix} n_x & 0 \\ 0 & n_y \\ n_y & n_x \end{bmatrix} \tag{B.30}$$

Analogously, we have

$$\left\{\nabla^S\boldsymbol{\eta}^h\right\} = \underbrace{\mathbf{B}\,\delta\dot{\mathbf{d}}}_{\left\{\nabla^S\bar{\eta}^h\right\}} + \underbrace{H_S\mathbf{B}_{\mathcal{N}}\,\delta\dot{\mathbf{a}} + \delta_S\,[\mathbf{n}]\,\mathbf{N}_{\mathcal{N}}^T\,\delta\dot{\mathbf{a}}}_{\left\{\nabla^S(H_S\,\alpha)^h\right\}} \tag{B.31}$$

where $\delta\dot{\mathbf{d}}$ and $\delta\dot{\mathbf{a}}$ are the admissible variations of $\dot{\mathbf{d}}$ and $\dot{\mathbf{a}}$, respectively. Assume that the stresses rate can be expressed as

$$\left\{\dot{\boldsymbol{\sigma}}^h\right\} = \mathbf{D}\;\left\{\dot{\varepsilon}^h\right\} \tag{B.32}$$

$\mathbf{D}$ being the matrix version of the constitutive tangent operator[2]. Let us define

$$\mathbf{G}_{\mathcal{N}} := H_S\mathbf{B}_{\mathcal{N}} + \delta_S\,[\mathbf{n}]\,\mathbf{N}_{\mathcal{N}}^T \tag{B.33}$$

Substituting (B.32), (B.31), and (B.33) into (B.13) yields:

$$\begin{aligned} &\int_\Omega \delta\dot{\mathbf{d}}^T\mathbf{B}^T\mathbf{D}\left\{\dot{\varepsilon}^{\mathbf{h}}\right\}d\Omega - G_{ext}(\mathbf{N}^T\delta\dot{\mathbf{d}}) \;= 0 \qquad (a) \\ &\int_\Omega \delta\dot{\mathbf{a}}^T\mathbf{G}_{\mathcal{N}}^T\mathbf{D}\left\{\dot{\varepsilon}^{\mathbf{h}}\right\}d\Omega - G_{ext}(H_S\mathbf{N}_{\mathcal{N}}^T\delta\dot{\mathbf{a}})\,d\Omega = 0 \qquad (b) \end{aligned} \tag{B.34}$$

$\forall\delta\dot{\mathbf{d}} \in \mathbb{R}^{n^{node}}$ and $\forall\delta\dot{\mathbf{a}} \in \mathbb{R}^{n^{node}}$. By considering (B.29) and (B.33), the system of variational equations (B.34) leads to the following system of algebraic equations:

$$\begin{bmatrix} \mathbf{K}_{dd} & \mathbf{K}_{da} \\ \mathbf{K}_{ad} & \mathbf{K}_{aa} \end{bmatrix} \begin{Bmatrix} \dot{\mathbf{d}} \\ \dot{\mathbf{a}} \end{Bmatrix} = \begin{Bmatrix} \dot{\mathbf{F}}_{ext} \\ \dot{\mathbf{f}}_{ext}^{\mathcal{N}} \end{Bmatrix} \tag{B.35}$$

with

[2]Remember that, from the Strong Discontinuity Analysis presented in Chapter 3, matrix $\mathbf{D}_S = \mathcal{O}(h)$ with $h \to 0$.

$$\begin{aligned}
\mathbf{K}_{dd} &= \int_{\Omega} \mathbf{B}^T\ \mathbf{D}\ \mathbf{B} d\Omega \\
\mathbf{K}_{da} &= \int_{\Omega} \mathbf{B}^T\ \mathbf{D}\ \mathbf{G}_{\mathcal{N}} d\Omega \\
\mathbf{K}_{ad} &= \int_{\Omega} \mathbf{G}_{\mathcal{N}}^T\ \mathbf{D}\ \mathbf{B} d\Omega \\
\mathbf{K}_{aa} &= \int_{\Omega} \mathbf{G}_{\mathcal{N}}^T\ \mathbf{D}\ \mathbf{G}_{\mathcal{N}} d\Omega
\end{aligned} \tag{B.36}$$

Remark 79 *For the integrals (B.36) to make sense, it is important that the Strong Discontinuity Analysis presented in Chapter 3 is taken into account for* $\mathbf{D}|_S$.

Remark 80 *The resulting system of equations is symmetric.*

Remark 81 *The enrichment degrees of freedom cannot be condensed at element level as in the elemental approach presented in Chapter 4.*

Remark 82 *From a computational point of view the determination of the set of elements that have to be enriched,* $\mathcal{N}$*, can significantly increase the implementation effort needed for this approach.*

Remark 83 *The resulting finite element interpolation is conforming. As a consequence, the approximation of a discontinuity interface will be continuous across the boundaries of the elements.*

B.5 Some final comments

At this point a comparison between nodal and elemental enrichment seems unavoidable. It is clear that the conforming character of the former gives it some reproducing advantage over the latter. However, the nodal enrichment formulation has two major drawbacks: the implementation effort and the mandatory increase in the number of degrees of freedom that it entails. Moreover, although the conforming character of this approximation gives it a better reproducing performance from the kinematical point of view, it is not clear what happens with respect to the imposition of the inner traction continuity. Consider, for instance, that in the case of linear triangles, when the nonsymmetric formulation for elements with embedded discontinuities is used, the inner traction continuity condition can be imposed in strong form. Clearly, this is not possible for nodal enrichment, which implies that some kind of refinement is necessary in order to get a better performance from the statical point of view.

Regrettably, no comparison based on numerical experiments between the elemental and the nodal enrichment is available. For the time being, the author cannot see any conclusive reason to prefer one approach over the other.

Bibliography

[Alfaiate et al., 2002] Alfaiate, J., Wells, G., and Sluys, L. (2002). On the use of embedded discontinuity elements with crack path continuity for mode-i and mixed-mode fracture. *Engineering Fracture Mechanics*, (69):661–686.

[Armero and Garikipati, 1996] Armero, F. and Garikipati, K. (1996). An analysis of strong discontinuities in multiplicative finite strain plasticity and their relation with the numerical simulation of strain localization in solids. *Int.J. Solids and Structures*, 33(20–22):2863–2885.

[Arrea and Ingraffea, 1982] Arrea, M. and Ingraffea, A. (1982). Mixed-mode crack propagation in mortar and concrete. Technical report. Report 81-13, Dept. Struct. Eng., cornell Univ. New York.

[Barenblatt, 1962] Barenblatt (1962). The mathematical theory of equilibrium cracks in brittle fracture. *Advances in Applied Mechanics*, 7:55–129.

[Bazant, 1983] Bazant, Z. (1983). Crack band theory for fracture of concrete. *Materiaux et Constructions*, (93):155–177.

[Belytschko et al., 2001] Belytschko, T., Moes, N., Usui, S., and Parimi, C. (2001). Arbitrary discontinuities in finite elements. *Int. J. Numer. Meth. Engng.*, (50):993–1013.

[Bocca et al., 1990] Bocca, P., Carpintieri, A., and Valente, S. (1990). Size effect in the mixed mode crack propagation: softening and snap-back analysis. *Engineering Fracture Mechanics*, 35(1/2/3):159–170.

[Cervera et al., 2001] Cervera, M., Agelet de Saracibar, C., and Chiumenti, M. (2001). *COMET: a multipurpose finite element code for numerical analysis in solid mechanics,* User's Guide . CIMNE, Barcelona.

[Crisfield, 1998] Crisfield, M. A. (1998). *Non-linear Finite Element Analysis of Solids and Structures, Volume 1: Essentials.* John Wiley & Sons.

[de Borst and Mulhaus, 1992] de Borst, R. and Mulhaus, H. (1992). Gradient dependent plasticity: formulation and algorithmic aspects. *Int. Journ. Num. Meth. Engng.*, 35:521–539.

[Diez et al., 2000] Diez, P., Arroyo, M., and Huerta, A. (2000). Adaptivity based on error estimation for viscoplastic softening materials. *Mechanics of Cohesive-frictional materials*, 5:87–112.

[Dugdale, 1960] Dugdale, D. (1960). Yielding of steel sheets containing slits. *Journal of the Mechanics and Physics of Solids*, 8:100–108.

[Dvorkin et al., 1990] Dvorkin, E., Cuitino, A., and Gioia, G. (1990). Finite elements with displacement embedded localization lines insensitive to mesh size and distortions. *Int.J.Num.Meth.Engng.*, 30:541–564.

[Elices et al., 2002] Elices, M., Guinea, G., J.Gomez, and Planas, J. (2002). The cohesive zone model: advantages, limitations and challenges. *Engineering Fracture Mechanics*, (69):137–163.

[Felippa, 2001] Felippa, C. (Fall, 2001). *Nonlinear Finite Element Methods.* Lecture Notes, University of Colorado at Boulder. url: http://caswww.colorado.edu/courses.d/NFEM.d/Home.html.

[Garikipati and Hughes, 2000] Garikipati, K. and Hughes, T. (2000). A variational multiscale approach to strain localization for multidimensional problems. *Comput. Methods Appl. Mech. Engrg.*, (188):39–60.

[Gurtin, 1981] Gurtin, M. E. (1981). *An introduction to Continuum Mechanics.* Academic Press, London, UK.

[Hill, 1962] Hill, R. (1962). Acceleration waves in solids. *Journal Mech. Phys. Solids*, 16:1–10.

[Hillerborg et al., 1976] Hillerborg, A., Modeer, M., and Petersson, P. (1976). Analysis of crack formation and crack growth in concrete by means of fracture mechanics and finite elements. *Cement and Concrete Research*, 6:773–782.

[Hughes, 1995] Hughes, T. (1995). Multiscale phenomena: Green's functions, the dirichlet-to-neumann formulation, subgrid scale models, bubles and the origins of stabilized methods. *Comput. Methods Appl. Mech. Engrg.*, 127:387–401.

[Hughes, 1987] Hughes, T. J. R. (1987). *The Finite Element Method. Linear Static and Dynamic Finite Element Analysis.* Prentice Hall, Englewood Cliffs, New Jersey.

[Jirasek, 2000a] Jirasek, M. (2000a). Comparative study on finite elements with embedded discontinuities. *Comput. Methods Appl. Mech. Engrg.*, (188):307–330.

[Jirasek, 1998] Jirasek, M. (April 1998). Finite elements with embedde cracks. Technical report. LSC Laboratoire de Méc. des Struct. et Milieux Continus, École Pol. Fed. Lausanne, Internal Report 98/01.

[Jirasek, 2000b] Jirasek, M. (Barcelona, 2000b). Conditions of uniqueness for finite elements with embedded cracks. In *Proceeding of the Sixth International conference in Computational Plasticity, CD-ROM.*

[Klisinski et al., 1991] Klisinski, M., Runesson, K., and Sture, S. (1991). Finite element with inner softening band. *J. Eng. Mech., ASCE*, 117:575–587.

[Knap and Ortiz, 2001] Knap, J. and Ortiz, M. (2001). An analysis of the quasicontinuum method. *Journal of the Mechanics and Physics of Solids*, 49:1899–1923.

[Larsson et al., 1999] Larsson, R., Steinmann, P., and Runesson, K. (1999). Finite element embedded localization band for finite strain plasticity based on a regularized strong discontinuity. *Mech. Cohes.-Frict. Mater.*, (4):171–194.

[Lemaitre, 1996] Lemaitre, J. (1996). *A course on Damage Mechanics*, Second Edition. Springer-Verlag.

[Melenk and Babuska, 1996] Melenk, J. and Babuska, I. (1996). The partition of unity finite element method: Basic theory and applications. *Comp. Meth. Appl. Mech. Eng.*, 39:289–314.

[Moes et al., 1999] Moes, N., Dolbow, J., and Belytschko, T. (1999). A finite element method for crack growth without remeshing. *Int. Journ. Num. Meth. Engng.*, 46:131–150.

[Nechnech, 2000] Nechnech, W. (2000). *Contribution a l'etude numerique du comportement du beton et des structures en beton arme soumises a des sollicitacions thermiques et mecaniques couplees.* Doctoral Thesis, Institut National des Sciences appliques de Lyon. url: http://csidoc.insa-lyon.fr/these/2000/nechnech/index.html.

[Nooru-Mohamed, 1992] Nooru-Mohamed, N. (1992). Mixed mode fracture of concrete, *Ph.D. Thesis.* Delft University of Technology.

[Ogden, 1984] Ogden, R. W. (1984). *Non-Linear Elastic Deformations.* Dover Publications, Mineola, New York.

[Oliver, 1989] Oliver, J. (1989). A consistent characteristic length for smeared cracking models. *Int.J.Num.Meth.Engng.*, 28:461–474.

[Oliver, 1996a] Oliver, J. (1996a). Modeling strong discontinuities in solid mechanics via strain softening constitutive equations. Part 1: Fundamentals. *Int.J.Num.Meth.Engng.*, 39(21):3575–3600.

[Oliver, 1996b] Oliver, J. (1996b). Modeling strong discontinuities in solid mechanics via strain softening constitutive equations. Part 2: Numerical simulation. *Int.J.Num.Meth.Engng.*, 39(21):3601–3623.

[Oliver, 2000] Oliver, J. (2000). On the discrete constitutive models induced by strong discontinuity kinematics and continuum constitutive equations. *International Journal Solids and Structures*, 37:7207–7229.

[Oliver et al., 1997] Oliver, J., Cervera, M., and Manzoli, O. (1997). On the use of J2 plasticity models for the simulation of 2D strong discontinuities in solids. In Owen, D., Onate, E., and Hinton, E., editors, *Proc. Int. Conf. on Computational Plasticity*, pages 38–55, Barcelona (Spain). C.I.M.N.E.

[Oliver et al., 1998] Oliver, J., Cervera, M., and Manzoli, O. (1998). On the use of strain-softening models for the simulation of strong discontinuities in solids, in: *Material Instabilities in Solids*, edited by R. de Borst and E. van der Giessen, chapter 8, pages 107–123. John Wiley & Sons Ltd.

[Oliver et al., 1999] Oliver, J., Cervera, M., and Manzoli, O. (1999). Strong discontinuities and continuum plasticity models: The strong discontinuity approach. *International Journal of Plasticity*, 15(3):319–351.

[Oliver et al., 1990] Oliver, J., Cervera, M., Oller, S., and Lubliner, J. (1990). Isotropic damage models and smeared crack analysis of concrete. In et al., N. B., editor, *Proc. SCI-C Computer Aided Analysis and Design of Concrete Structures*, pages 945–957.

[Oliver et al., 2002a] Oliver, J., Huespe, A., Pulido, M., and Chaves, E. (2002a). From continuum mechanics to fracture mechanics: the strong discontinuity approach. *Engineering Fracture Mechanics*, 69(2):113–136.

[Oliver et al., 2002b] Oliver, J., Huespe, A., Pulido, M., and Samaniego, E. (2002b). On the strong discontinuity approach in finite deformation settings. *In press. Int. J. Numer. Meth. Engng.*

[Oliver et al., 2003] Oliver, J., Huespe, A., and Samaniego, E. (2003). A study on finite elements for capturing strong discontinuities. *In press. Int. J. Numer. Meth. Engng.*

[Oliver et al., 2002c] Oliver, J., Huespe, A., Samaniego, E., and Chaves, E. (2002c). On strategies for tracking strong discontinuities in computational failure mechanics. In Mang, H., Rammerstorfer, F., and Eberhardsteiner, J., editors, *Proceedings of the Fifth World Congress on Computational Mechanics (WCCM V)*. Vienna University of Technology, Austria, url: http://wccm.tuwien.ac.at.

[Ortiz et al., 1987] Ortiz, M., Leroy, Y., and Needleman, A. (1987). A finite element method for localized failure analysis. *Comp.Meth.Appl.Mech.Eng.*, 61:189–214.

[Ottosen and Runesson, 1991] Ottosen, N. and Runesson, K. (1991). Properties of discontinuous bifurcation solutions in elasto-plasticity. *Int. J. Solids and Structures*, 27(4):401–421.

[Pjaudier-Cabot and Bazant, 1997] Pjaudier-Cabot, G. and Bazant, Z. (1997). Nonlocal damage theory. *J. Eng. Mech., ASCE*, 113:1512–1533.

[Rashid, 1968] Rashid, Y. (1968). Analysis of prestressed concrete pressure vessels. *Nucl. Eng. Des.*, 7:773–782.

[Reddy, 1998] Reddy, B. D. (1998). *Introductory Functional Analysis. With Applications to Boundary Value Problems and Finite Elements.* Springer, New York.

[Rice and Rudnicki, 1980] Rice, J. and Rudnicki, J. (1980). A note on some features of the theory of localization of deformation. *Int. J. Solids Structures*, 16:597–605.

[Rots, 1988] Rots, J. G. (1988). Computational Modeling of Concrete Fractures, *Ph.D. Thesis.* Delft University of Technology.

[Runesson et al., 1991] Runesson, K., Ottosen, N. S., and Peric, D. (1991). Discontinuous bifurcations of elastic-plastic solutions at plane stress and plane strain. *Int. J. of Plasticity*, 7:99–121.

[Simo and Hughes, 1998] Simo, J. and Hughes, T. (1998). *Computational Inelasticity.* Springer.

[Simo and Ju, 1987] Simo, J. and Ju, J. (1987). Stress and strain based continuum damage models: I formulation. *International Journal Solids and Structures*, 15:821–840.

[Simo and Oliver, 1994] Simo, J. and Oliver, J. (1994). A new approach to the analysis and simulation of strong discontinuities. In et al., Z. B., editor, *Fracture and Damage in Quasi-brittle Structures*, pages 25–39. E & FN Spon.

[Simo et al., 1993] Simo, J., Oliver, J., and Armero, F. (1993). An analysis of strong discontinuities induced by strain-softening in rate-independent inelastic solids. *Computational Mechanics*, 12:277–296.

[Simo and Rifai, 1990] Simo, J. and Rifai, S. (1990). A class of mixed assumed strain methods and the method of incompatible modes. *Int. Journ. Num. Meth. Engng.*, 29:1595–1638.

[Sluys, 1992] Sluys, L. (1992). Wave propagation localization and dispersion in softening solids, *Ph.D. Thesis*. Delft University of Technology.

[Spencer, 2002] Spencer, B. (2002). Finite Elements with Embedded Discontinuities for Modelling reinforced concrete Members, *Ph.D. Thesis*. University of Colorado, Boulder.

[Steinmann, 1999] Steinmann, P. (1999). A finite element formulation for strong discontinuities in fluid saturated porous media. *Mech. Cohes.-Fricl. Mater.*, (4):133–152.

[Temam, 1983] Temam, R. (1983). *Problemes Mathematiques en Plasticite*. Collection Methodes Mathematiques de l'Informatique, Gauthier-Villard, Paris, France.

[Vardoulakis, 1989] Vardoulakis, I. (1989). Shear banding and liquefaction in granular materials on the basis of cosserat continuum. *Ingeneur-Archiv*, 59:106–113.

[Wells and Sluys, 2000] Wells, G. and Sluys, L. (2000). Application of embedded discontinuities for softening solids. *Engineering Fracture Mechanics*, (65):263–281.

[Wells and Sluys, 2001] Wells, G. and Sluys, L. (2001). A new method for modelling cohesive cracks using finite elements. *Int. J. Numer. Meth. Engng*, (50):2667–2682.